NASA Contractor Report 4082

Ground and Flight Test Results of a Total Main Rotor Isolation System

Dennis R. Halwes

CONTRACT NAS1-16969
JULY 1987

NASA

NASA Contractor Report 4082

Ground and Flight Test Results of a Total Main Rotor Isolation System

Dennis R. Halwes
Bell Helicopter Textron Inc.
Fort Worth, Texas

Prepared for
Langley Research Center
under Contract NAS1-16969

National Aeronautics
and Space Administration

**Scientific and Technical
Information Office**

1987

Table of Contents

Table of Contents (Concluded)

List of Figures

List of Figures (Concluded)

List of Tables

List of Symbols and Abbreviations

DAVI	Dynamic Anti-Vibration Isolator
deg/s^2	Degrees per Second Squared
DOF	Degree of Freedom
F/A	Fore and Aft
FWD	Forward
g	Acceleration of Gravity at Earth's Surface
GR	Ground Run
GW	Gross Weight
IFR	Instrument Flight Rules
IGE	In Ground Effect
IRIS	Improved Rotor Isolation System
Kn, Kts	Knot, Knots
L	Lateral
LIVE	Liquid Inertia Vibration Eliminator
MIL-SPEC	Military Specification
MMH/FH	Maintenance Man-Hours Per Flight-Hour
M/R	Main Rotor
N/A	Not Applicable
P	Pitch
R	Roll
SAVITAD	System to Alleviate Vibration Independent of Tuning and Damping
SCAS	Stability and Control Augmentation System
T/B	Tail Boom
TRIS	Total Rotor Isolation System
V	Vertical
V_{cal}	Calibrated Airspeed
V_H	Maximum Continuous Power Airspeed
V_{ne}	Velocity to Never Exceed
Y	Yaw
4/rev	Four per Revolution

TOTAL ROTOR ISOLATION SYSTEM (TRIS)

D. R. Halwes
Bell Helicopter Textron Inc.

SUMMARY

Airframe vibrations can have an adverse effect on airframe life, electronic equipment life, aircrew fatigue and comfort, and, in many cases, helicopter performance. As a consequence, methods for reducing helicopter vibration levels have been an important research area for many years.

Previous antiresonant isolation concepts developed to isolate the fuselage from the main rotor oscillatory forces such as Kaman's DAVI, Boeing-Vertol's IRIS, and Bell's nodal beam never achieved the Army's goals of less than 0.05 g's vibration levels. In 1979, the Army funded a research program that resulted in the development of a Total Rotor Isolation System by Bell Helicopter Textron, Inc.

To determine the effectiveness of the Total Rotor Isolation System (TRIS) in reducing helicopter vibrations, a flight verification study was conducted at Bell's Flight Research Center in Arlington, Texas. The objective was to demonstrate a 90% (or greater) isolation of the helicopter fuselage from the forces and moments generated by the rotor hub at 4/rev, the blade passage frequency, or 26.26 Hz in the case of the Bell 206LM. The flight test was the final phase of a three-phase program performed by Bell under a NASA Langley Research Center contract with funding by the U.S. Army Aerostructures Directorate. The flight test data of the testbed aircraft indicate that the program objectives have been surpassed. The 4/rev vibration levels at the pilot's seat were suppressed below 0.056g throughout the transition flight regime (from hover to forward flight) with its inherently high vibration potential.

The results of flight tests to date indicate the vibration levels from the rotor hub to the pilot's seat were reduced by 95%, and this was achieved

at a considerable weight savings over traditional antiresonant isolation concepts. In addition, the TRIS installation was designed with a decoupled control system and has shown a significant improvement in aircraft flying qualities. The improvement was such that it permitted the trimmed aircraft to be flown "hands-off" for a significant period of time, over 90 seconds. This improvement in flying qualities was further investigated under BHTI IR&D. In conclusion, the TRIS program and the flight tests have demonstrated a system that greatly reduces vibration levels of a current-generation helicopter, the Bell 206LM, while improving the flying qualities to a point where stability augmentation is no longer a requirement.

INTRODUCTION

The vibrations inherent in helicopters cause many undesirable effects, including helicopter crew fatigue, resulting in decreased proficiency; unacceptable passenger comfort; poor component and system equipment lives; lower avionics reliability, resulting in increased operating cost; and, in the case of severe vibrations, limited operational envelopes.

The Drive for Lower Vibration Levels

Vibration reduction has been a major goal of the rotary wing community since the helicopter's inception. In the 1940s and 1950s, helicopters using first-generation main-rotor-shaft isolation systems exceeded the MIL-SPEC n/rev vibration levels of 0.15g, and many had vibration levels over 0.5g during transition. During the 1960s, second-generation designs (with focal pylons) were generally able to meet the 0.15g requirement in cruise flight, but not during transition. In the 1970s, the military, recognizing the adverse effects of vibrations and desiring a more stable weapons platform, reduced the MIL-SPEC acceptable levels of the predominant rotor harmonic (n/rev) g-levels from 0.15g at cruise speed to 0.05g. The third-generation isolation-type systems, including Boeing-Vertol's IRIS, Kaman's DAVI, and Bell's nodal beam, were designed to meet this requirement, but failed. In addition, the weight penalties imposed by these systems, or a combination

thereof, varied from 2% to 3% (more in some cases) of the helicopter's design gross weight. Even the current state-of-the-art Army helicopters, Sikorsky's UH-60 Blackhawk and McDonnell Douglas' AH-64 Apache, never met the 0.05g vibration criterion during competition, and the criterion was later raised to 0.1 g's.

The military was not alone in its demands for lower vibration levels. Commercial operators, particularly those conducting long flights to offshore oil rigs or ambulance runs, also demanded lower vibration levels in aircraft. In addition, helicopter users have also demanded new objectives for high-speed performance, higher payloads, improved maneuverability, and increased agility. These new goals have led to new rotor designs, including rigid, articulated or soft inplane with large hinge offsets, and teetering rotors with added hub springs. All of these changes have tended to increase weight and generate higher excitation shears and/or moments.

Programs Leading to TRIS

With the overall objective of meeting the Army's MIL-SPEC vibration objective and reducing the helicopter's overall weight, the U.S. Army's Aerostructures Directorate (then the Army's Structures Laboratory), located at NASA's Langley Research Center, issued a request for proposal in 1979 for the "analysis of the feasibility of a six-degree-of-freedom isolation system," which was phase one of this program. Under a NASA/Army contract, Bell Helicopter Textron completed the analysis and was subsequently awarded a follow-on contract for the "Design, Analysis, Fabrication, and Bench Testing of a Total Main Rotor Isolation System," which is documented in Reference 1. The results of the bench test were so promising that in 1984 a contract was awarded for a program to install the system on a Bell Model 206LM helicopter and then conduct ground and flight tests on the aircraft. This report covers the results of that ground and flight test program.

Objective of TRIS Program

The objective of the program was to establish the requirements, preliminary design, and verification procedures for TRIS at n/rev. Total main rotor isolation at n/rev is considered to be such that there is no more than 5% response at any point on a theoretical rigid body fuselage due to any main rotor shaft load at the blade passage frequency. This is equivalent to 95% isolation or reduction in vibration levels. With this requirement of 95% isolation on a rigid-body analytical model, it was the program objective to demonstrate that 90% isolation could be achieved on a flexible fuselage in the ground vibration test.

Approach

The TRIS isolation system discussed in this report extends the previously limited isolation applications to all six degrees of freedom while significantly reducing the weight penalty. The system achieves the objective and can be universally applied to all rotor systems. The Liquid Inertia Vibration Eliminator (LIVE) isolation element used in the system has demonstrated a 98% isolation efficiency in laboratory tests. This element also reduces weight by a significant factor, while providing a number of other important advantages.

LIVE - THE BASIC ISOLATION UNIT OF TRIS

In 1972, research was begun at Bell on the use of the hydraulic cylinder concept as an isolation system. Hydraulic fluid was used in two concentric cylinders with differential areas to amplify the motion of a tungsten piston being used as a tuning weight. This concept progressed to a very compact system using a high-density, low-viscosity liquid (mercury) as both the "hydraulic fluid" and the tuning weight. This system, called LIVE, is shown in a cross-section schematic in Figure 1.

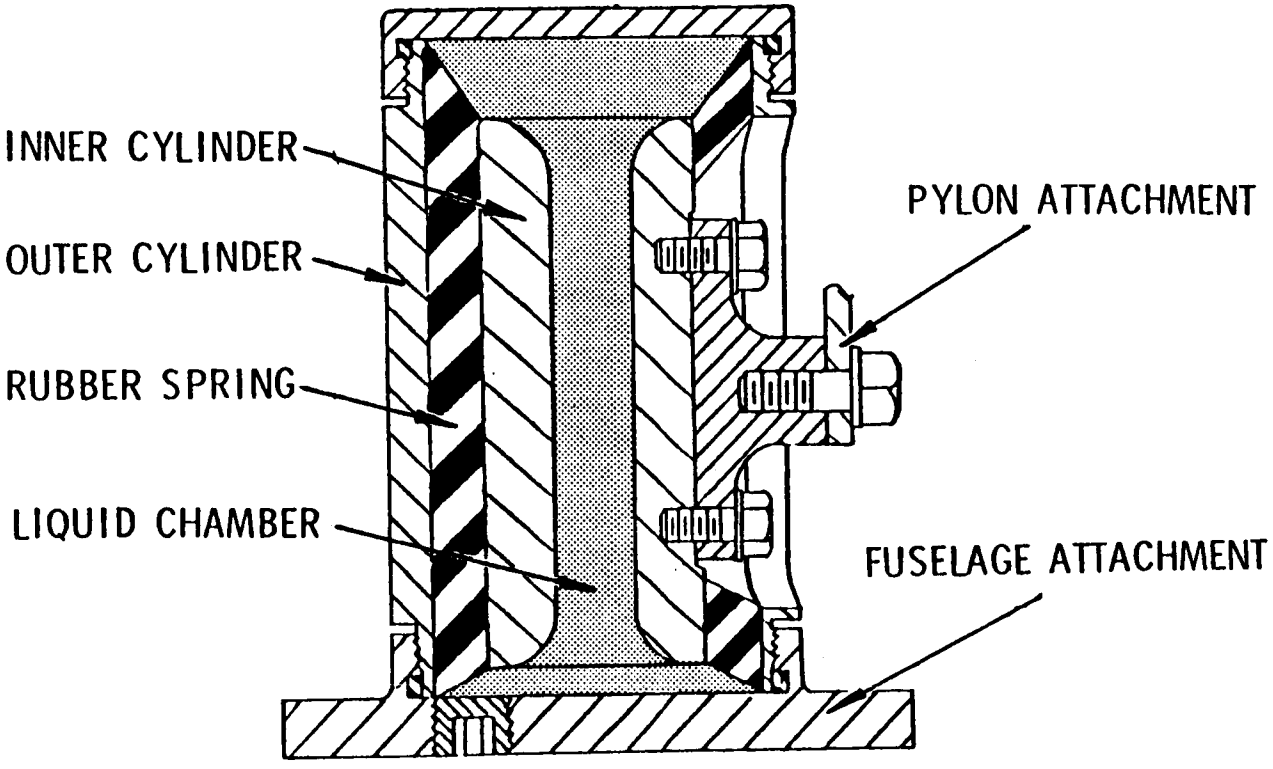

Figure 1. LIVE System Internal Design

As shown in the schematic, an inner cylinder is bonded to an outer cylinder with a layer of elastomer, as in a coaxial bushing elastomer spring. Cavities at the top and bottom are enclosed, creating reservoirs for the "hydraulic fluid." The inner cylinder is attached to the transmission, and the outer cylinder is attached to the fuselage. The hole or "tuning port" through the inner cylinder connects the upper and lower reservoirs.

Theoretically, the mechanics of a classical pinned-pinned link is such that only axial loads can be transmitted; no moments can be input through the pinned ends. If a LIVE unit is mounted within a link and tuned to isolate the blade passage frequency, then no oscillatory loads at the blade passage frequency (n/rev), in any direction, will be transmitted through the link. By attaching the pylon to the fuselage with six pinned-pinned links employing spherical bearings at each end and containing LIVE isolator units (in any configuration that is statically stable in all six degrees of freedom), and with no other attachments, every attachment link will isolate the blade passage frequency and no oscillatory loads will be transmitted from any degree of freedom at the hub.

A representative LIVE isolator link for the six degree-of-freedom application is shown in the cross-section view of Figure 2. The inner cylinder is attached to the pylon, and the outer cylinder is attached to the fuselage. The two cylinders are bonded to the elastomer that fills the annulus between them. This elastomer (working in shear) acts as a spring that supports and reacts to the static and dynamic loads placed on the isolator. Pressurized liquid mercury fills the center port in the inner cylinder and both cavities at the ends of the isolators. No air space remains in the isolators.

In operation, the liquid mercury oscillates within the LIVE units, and isolation is achieved when the force due to pressure created by the motion of the mercury cancels the spring force due to the displacement of the elastomer.

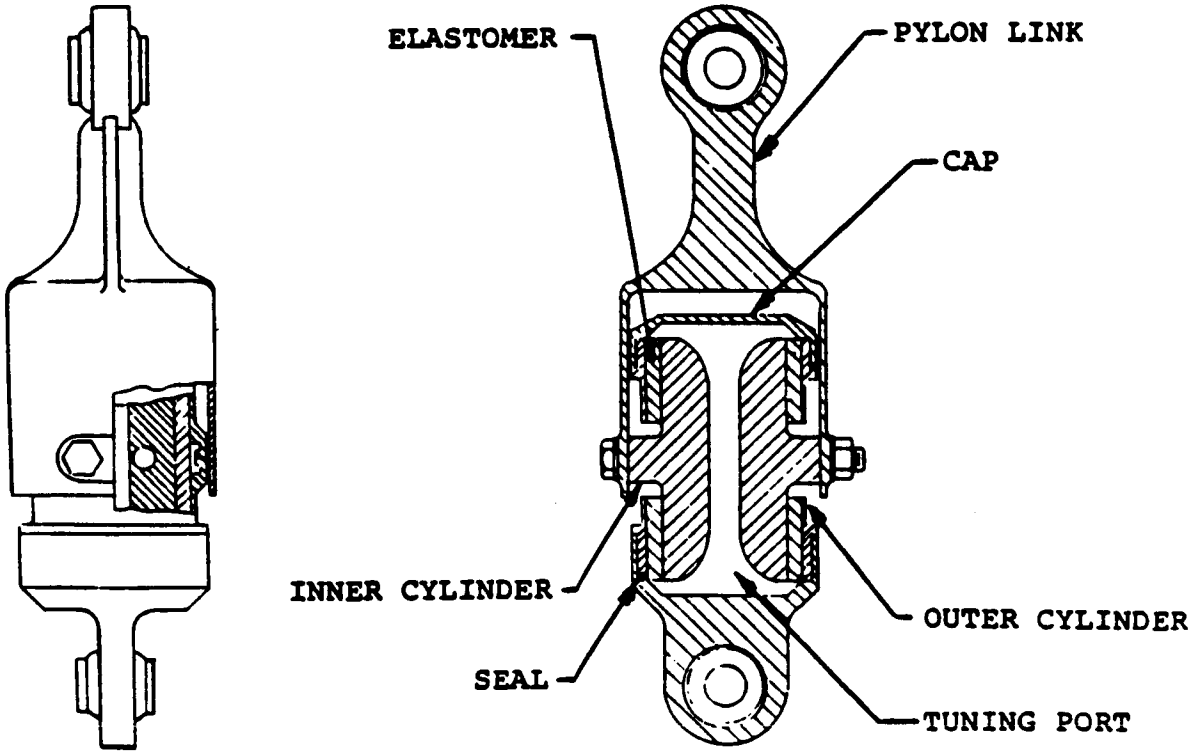

Figure 2. Cut-Away View of Pinned-Pinned LIVE Link.

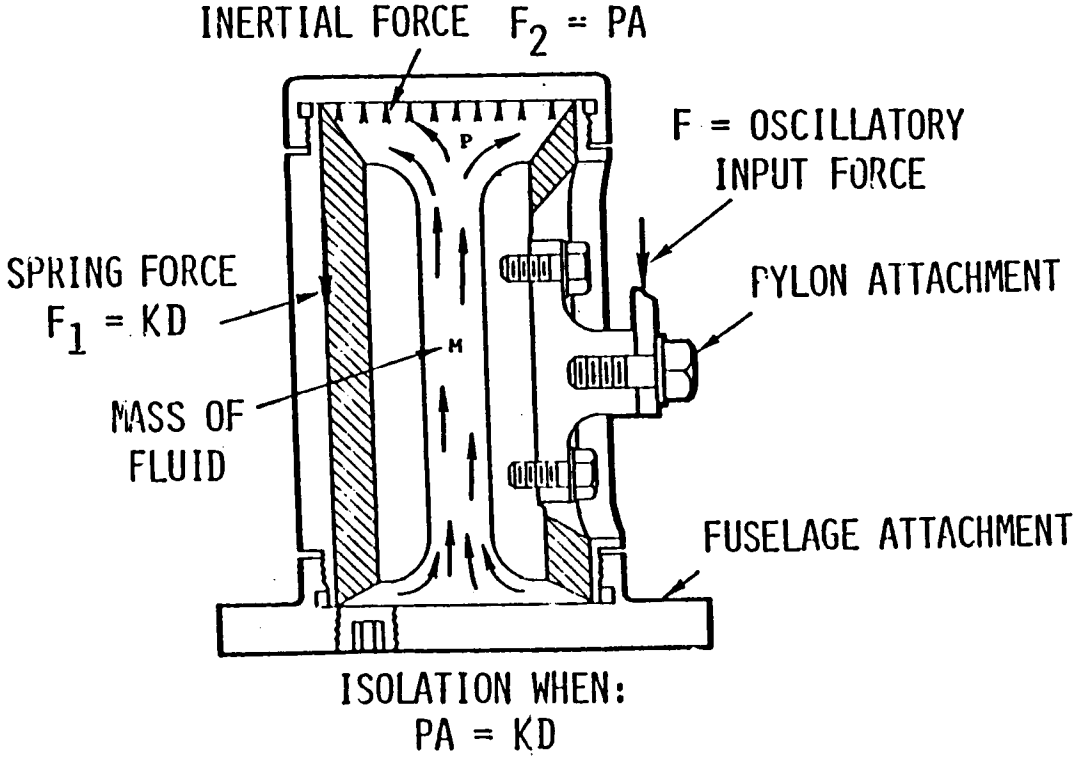

Figure 3. Isolation Principle of LIVE.

This action is shown in Figure 3. By altering the spring rate and port diameter, the LIVE units can be tuned to isolate the desired blade-passage frequency. This six degree-of-freedom system has been named the Total Rotor Isolation System, or TRIS.

DESCRIPTION OF TEST HELICOPTER

The baseline helicopter selected for the purpose of establishing by analysis and test, the specific isolation system performance, risk, weight impact, and system integration, was the Bell Model 206LM, serial number 45269 (Figure 4), a derivative of ther two-bladed Model 206L. The Model 206LM is an 1814-kg class turbine engine helicopter with a four-bladed, soft-in-plane, flexbeam rotor system. An impedance controlled pylon isolation system had been installed on the Model 206LM, and is referred to in this report as the Soft Pylon Isolation System.

The isolation system selected for the baseline helicopter is a modification of the six LIVE unit system using the LIVE units in a pinned-pinned link configuration.

Analysis

Predesign drawings were produced that showed a design installation of the LIVE units with no modification to the transmission or the helicopter fuselage structure. This installation can be seen in Figure 5. A NASTRAN model of this geometry was constructed and tuned for optimum isolation, pylon and mast modal placement, static motions, and drive shaft coupling angles. The NASTRAN model had a rigid fuselage and the fully flexible pylon of the 206LM. The effective mass and inertia of the rotor at 4/rev from the Myklestad analysis were included at the hub. This method gives very good results at 4/rev, but will produce some error in natural frequency determination at any other frequency. This work is detailed in Reference 1.

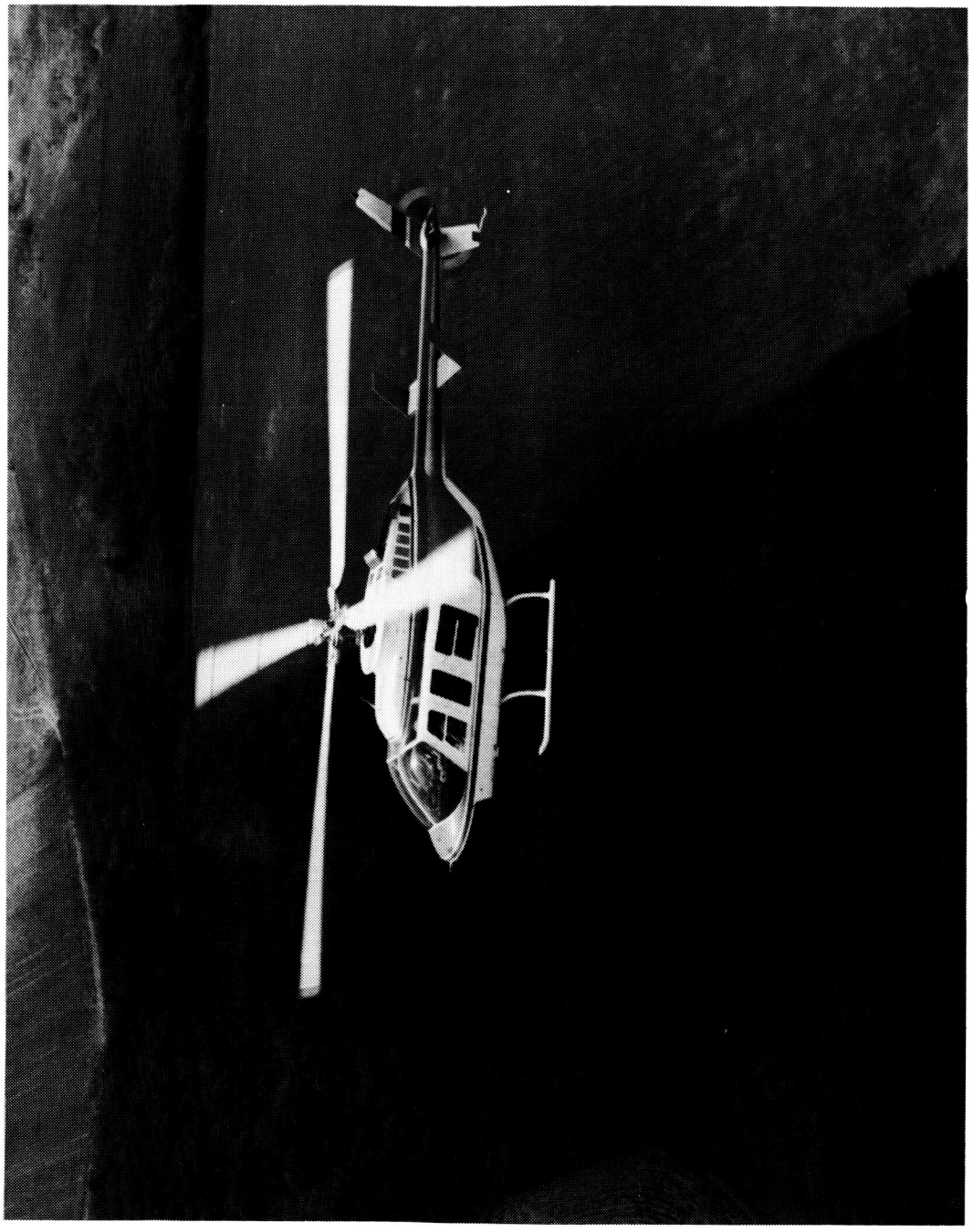

Figure 4. Bell Model 206LM Total Rotor Isolation System Helicopter

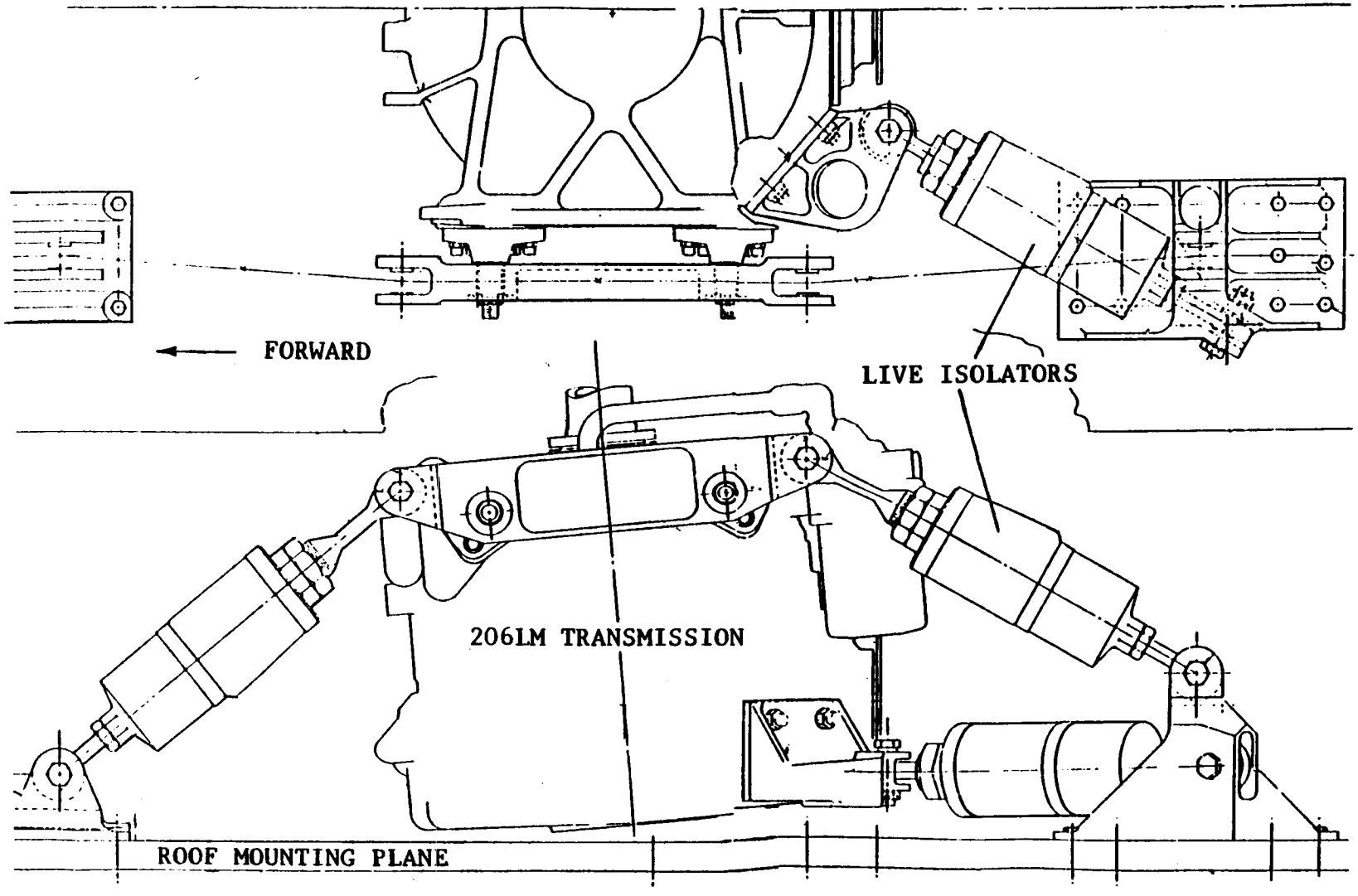

Figure 5. Installation of Six Degree-of-Freedom Isolation System on Helicopter

Modifications for TRIS Installation

After the isolators were retuned (Reference 1) individually, they were installed on the baseline helicopter. This required the following modifications to the aircraft:

a. Removal of the existing pylon mounting system.

b. Installation of the six degree-of-freedom isolation system.

c. A cutout in the engine air intake cowling to clear aft LIVE units.

d. A relocation of transmission oil filter/reservoir to the roof to clear left aft LIVE unit.

e. Installation of different main rotor control bellcranks and supports to decouple rotor inputs from pylon motions.

These changes are depicted in the following Bell drawings:

206-830-319	6DOF M/R Pylon Installation
654-010-400	654 M/R Controls Installation
Engineering Order 654B-72	654 Main Rotor Controls Modification

The isolation system installation can be seen in Figures 6 through 10. A complete drawing list and a parts breakdown are on file at the Arlington Flight Research Center.

Additional configuration items required for conversion from the Model 206L to the Model 206LM are the following:

a. A fixed (nonmovable) horizontal stabilizer trim tab.

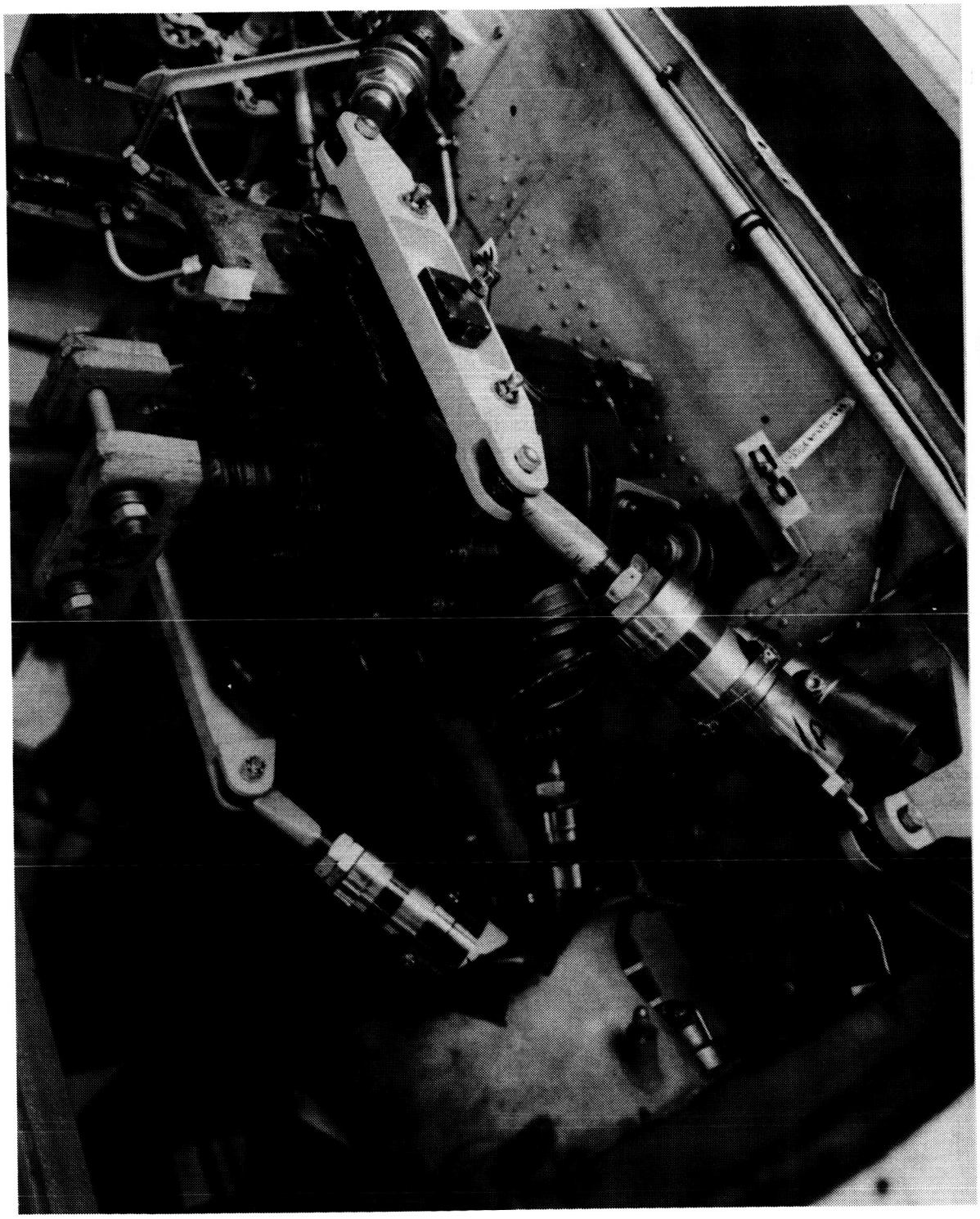

Figure 6. TRIS Installation on Bench Test Transmission for Shake Test

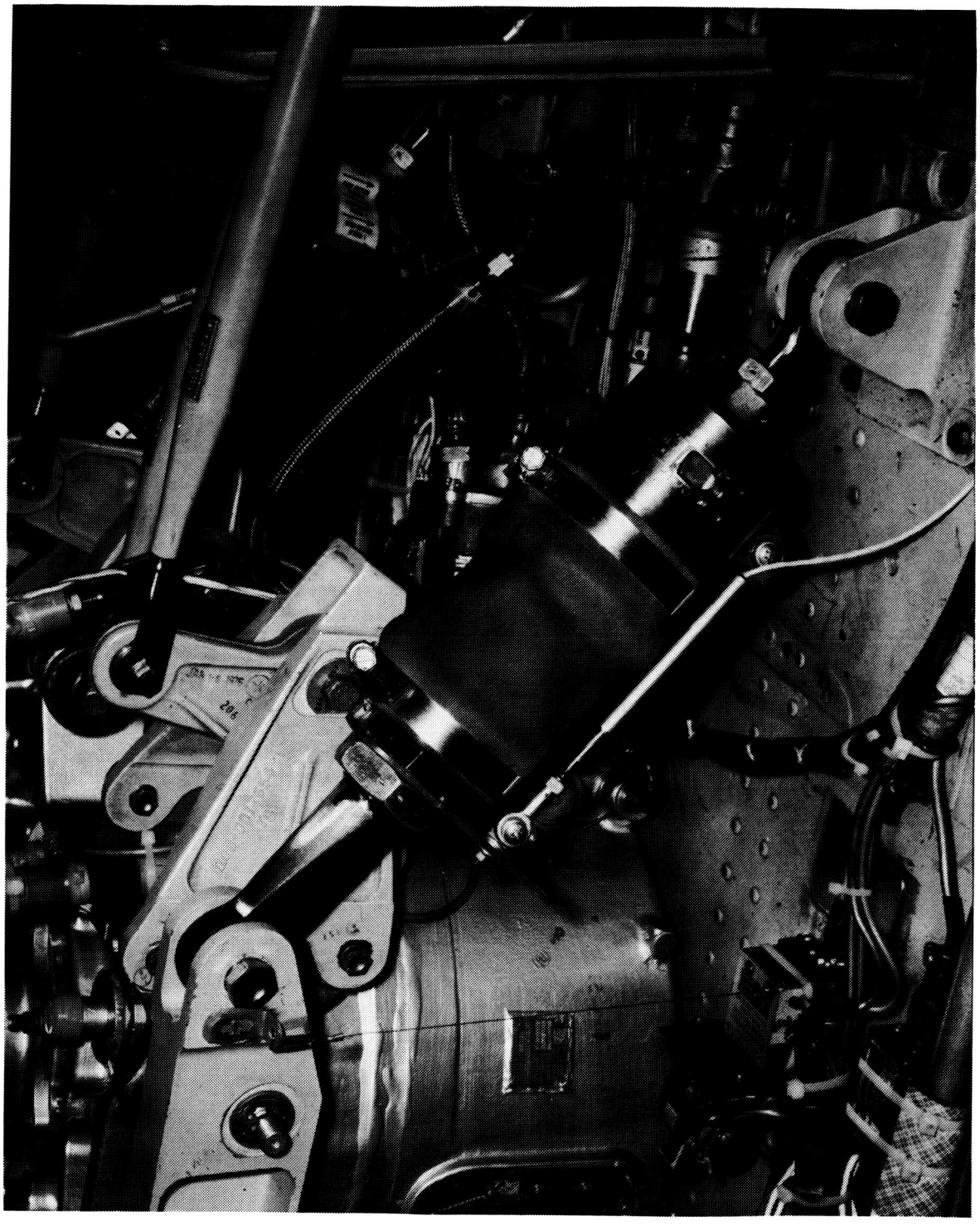

Figure 7. Right Forward LIVE Isolator Installation for Flight Test

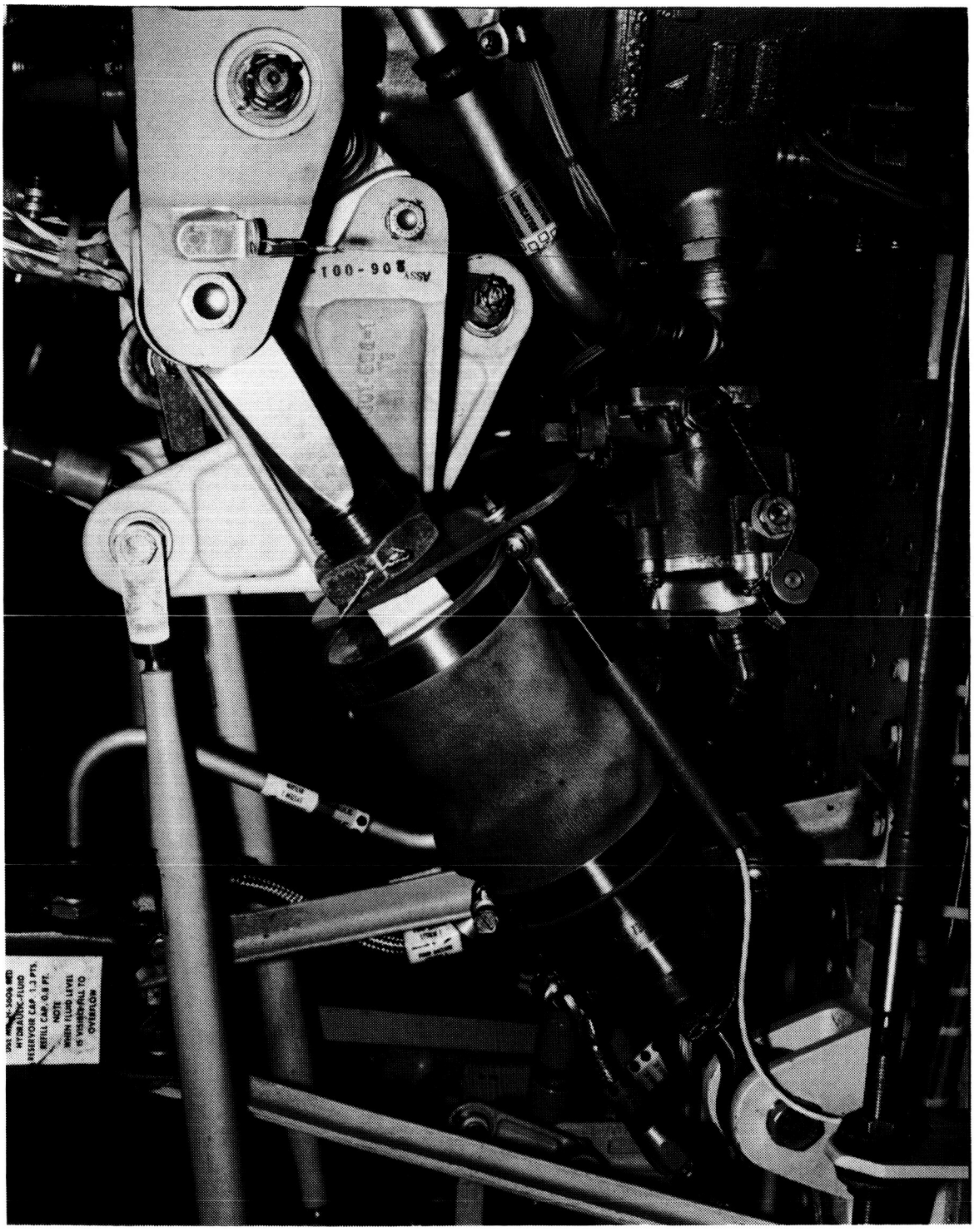

Figure 8. Right Aft LIVE Isolator Installation for Flight Test

Figure 9. Lower Right Aft LIVE Isolator Installation for Flight Test

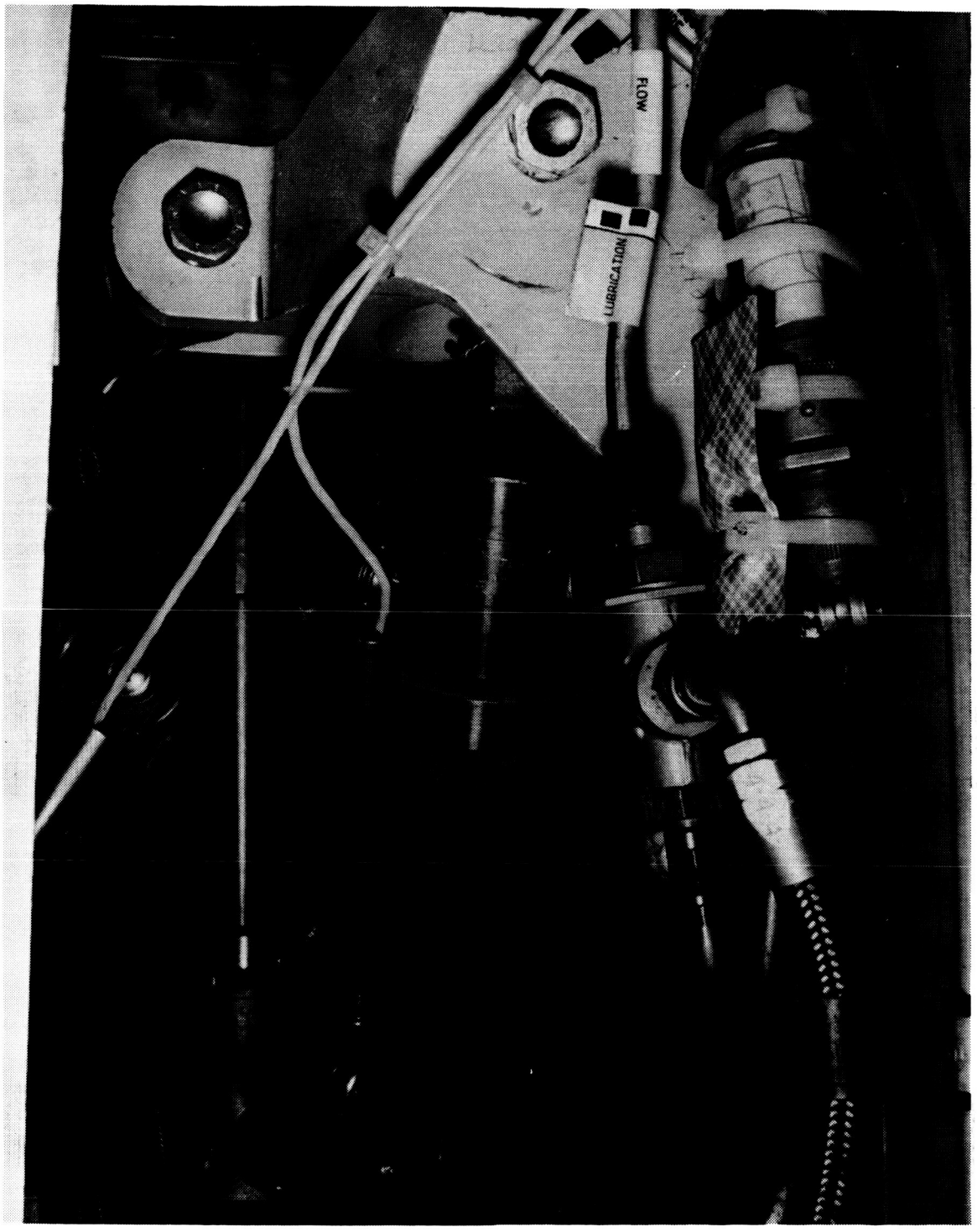

Figure 10. Lower Left Aft LIVE Installation for Flight Test

b. A 206-801-301 cyclic mixing bellcrank in the main rotor control system.

c. Horizontal stabilizer leading edge slats not previously used on the 206LM helicopter.

d. A 206LM landing gear assembly without crosstube fairings.

The above items were significant to the aircraft's handling qualities.

AIRCRAFT SHAKE TEST

The next phase of the program was to perform a shake test in each of the six degrees of freedom. This test would determine the isolation efficiency achieved and the natural frequencies and damping of the primary pylon modes for comparison to the NASTRAN analysis. In addition, tests were required to determine the frequency and damping parameters for calculations of the ground and air resonance stability margins.

Since this test would expose the transmission to very high oscillatory loads without rotation or torque applied to gears and bearings, a bench test transmission was used to avoid damage to flightworthy parts. The swashplate and pylon-mounted controls were simulated by the installation of lead weights at the proper locations to accurately represent the pylon dynamics.

Figure 6 shows photographs of the isolation system installation used during the shake test.

Excitation

Three different systems were used for hub excitation. A single 1500-lb capacity electromagnetic shaker was used for hub vertical, lateral, and longitudinal shear inputs; two 1500-lb electromagnetic shakers were operated out of phase for hub yaw moment input; and a rotary hydraulic shaker was used

for hub pitch and roll moment inputs. The excitation setup hardware can be seen in Figures 11 through 14.

For each excitation degree-of-freedom, sweeps were made with the full hub weight to determine the placement of pylon and fuselage natural frequencies and the approximate shape and frequency placement of the isolation valley. In addition, frequency dwells at various load levels with and without the hub weight at 1/rev, 4/rev, and 8/rev were made to determine the isolation efficiency and load linearity of the isolation system. Load levels up to 800 lb in shear and 5000 in-lb in moment were applied to the hub.

Instrumentation

The instrumentation used for the shake test are listed in Table I. The accelerometer locations are indicated in Figure 15, and Figures 16 through 25 are photographs of their installations. An array of nine accelerometers at the hub (Figure 26) and another array of six accelerometers near the fuselage cg (Figure 27) were used to measure the input and response at each of the six degrees of freedom. These accelerometer arrays were the primary transducers used to determine the percentage of isolation achieved by TRIS and to determine if the system met the 90% isolation criteria of the contract statement of work. The accelerometer measurements were used to calculate the percentage of isolation in the six degrees of freedom in the following manner:

a. For the translation directions, the response of the two accelerometers, with their sensitive axis in the same direction, were averaged to determine the response of the point halfway between them.

b. For the rotational directions, the response of the two accelerometers, with their sensitive axis in a plane perpendicular to the axis of rotation, were subtracted, one from the other, divided by the distance between them, and then converted to units of

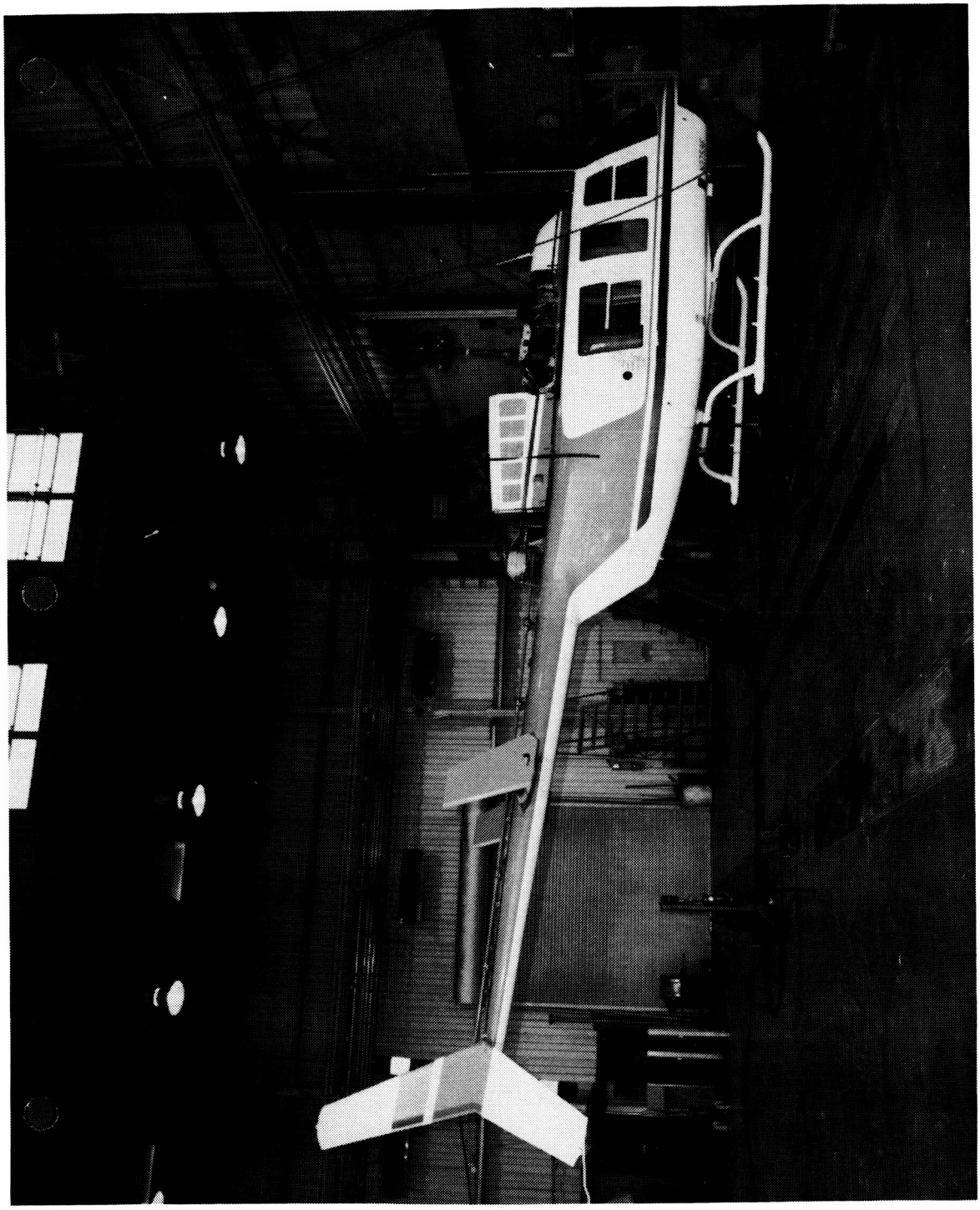

Figure 11. Vertical Shear Hardware for Shake Test

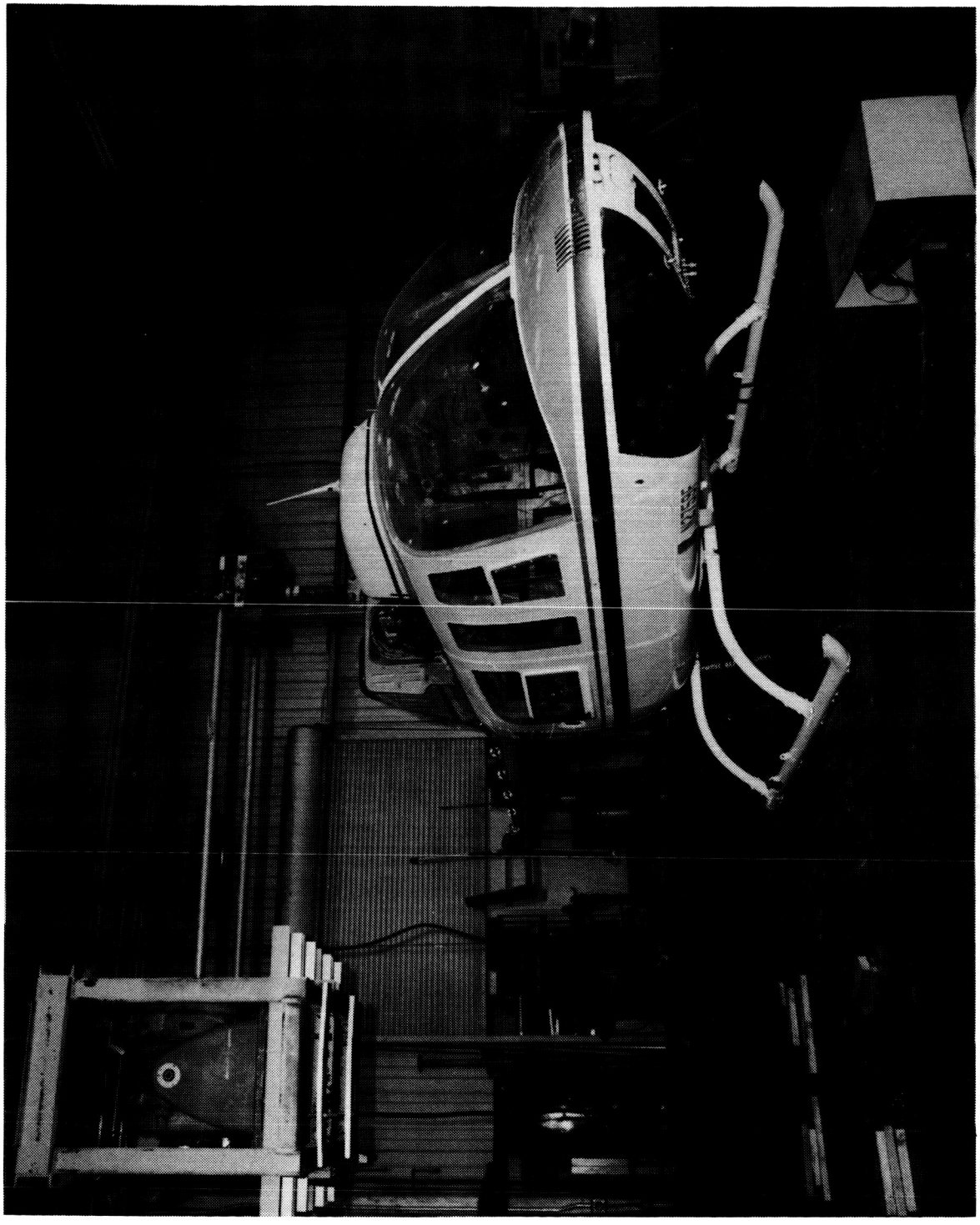

Figure 12. Yaw Moment Excitation Hardware for Shake Test

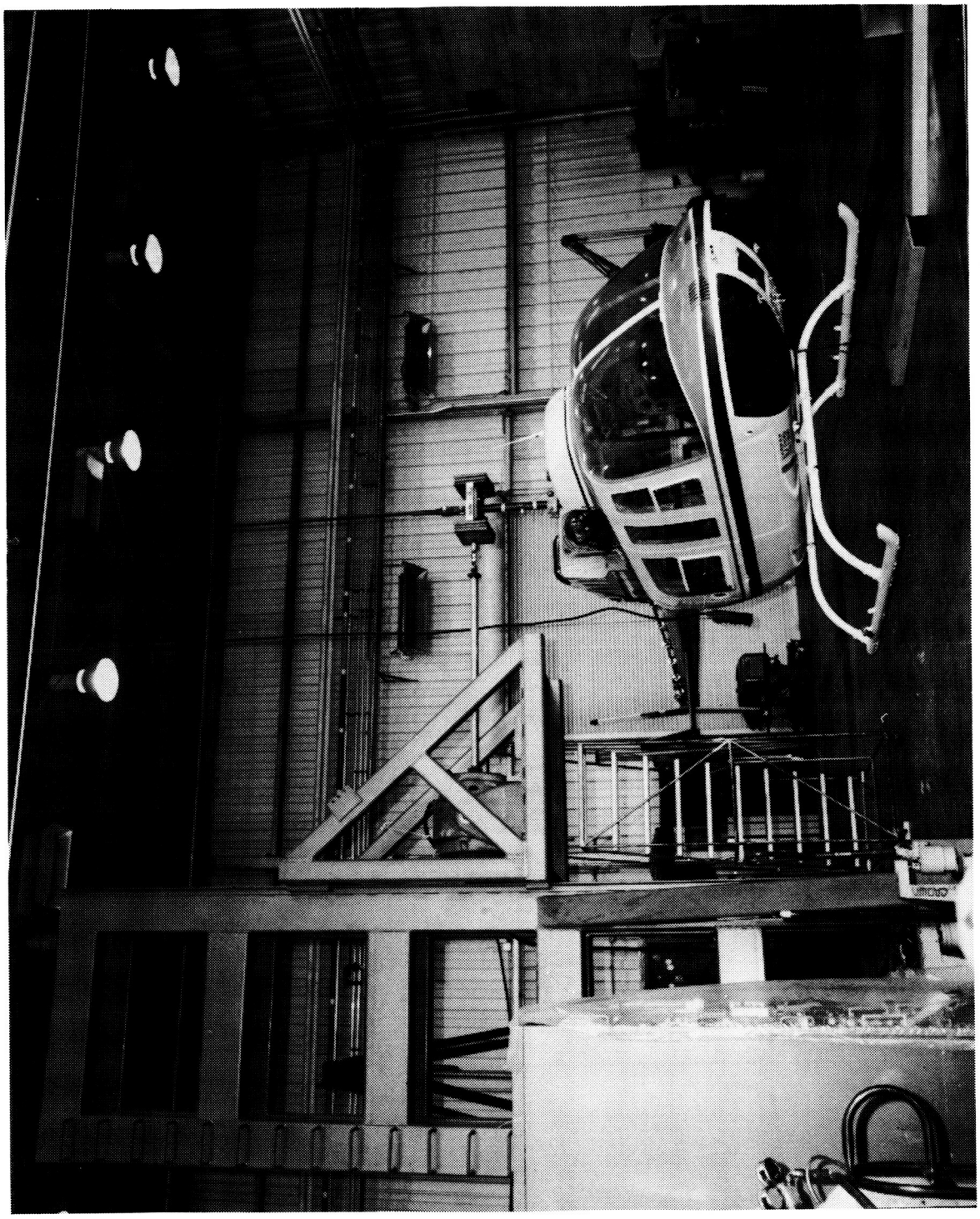

Figure 13. Lateral Shear Excitation Hardware for Shake Test

Figure 14. Pitch Moment Excitation Hardware for Shake Test

Table I. Instrumentation List for Shake Test

DESCRIPTION	VERTICAL	LATERAL	F/A	PITCH	ROLL	YAW
PILOT SEAT VERTICAL	X	X	X	X	X	X
PILOT SEAT LATERAL	X	X	X	X	X	X
COPILOT SEAT VERTICAL	X	X	X	X	X	X
RIGHT AFT SEAT VERTICAL	X	X	X	X	X	X
AFT SEAT LATERAL	X	X	X	X	X	X
LEFT AFT SEAT VERTICAL	X	X	X	X	X	X
AFT SEAT F/A	X	X	X	X	X	X
HUB FORWARD VERTICAL			X	X		
HUB AFT VERTICAL			X	X		
HUB RIGHT VERTICAL		X			X	
HUB LEFT VERTICAL		X			X	
HUB CENTERLINE VERTICAL	X					X
HUB CENTERLINE F/A			X	X		
HUB FORWARD LATERAL						X
HUB AFT LATERAL						X
HUB CENTERLINE LATERAL		X			X	
HUB PITCH			X	X		
HUB ROLL		X			X	
HUB YAW						X
CG VERTICAL	X					
CG LATERAL		X			X	X
CG F/A			X	X		
CG PITCH			X	X		
CG ROLL		X			X	
CG YAW						X
FORWARD TRANSMISSION LATERAL	X	X	X	X	X	X
TRANSMISSION F/A	X	X	X	X	X	X
ELEVATOR VERTICAL	X	X	X	X	X	X
ELEVATOR LATERAL	X	X	X	X	X	X
90 DEGREE GEARBOX VERTICAL	X	X	X	X	X	X
90 DEGREE GEARBOX LATERAL	X	X	X	X	X	X

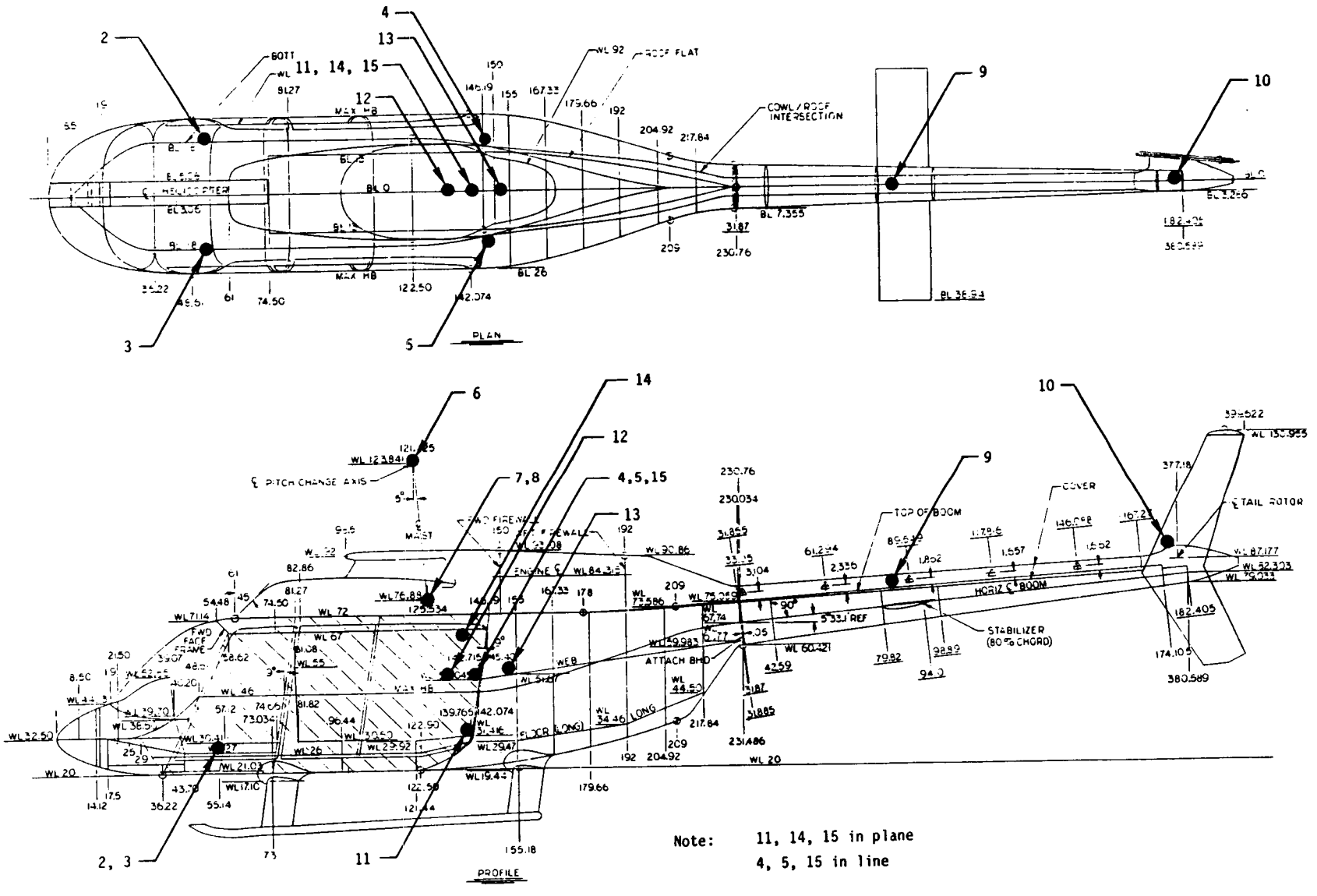

Figure 15. Accelerometer Locations for Shake Test and Flight Test

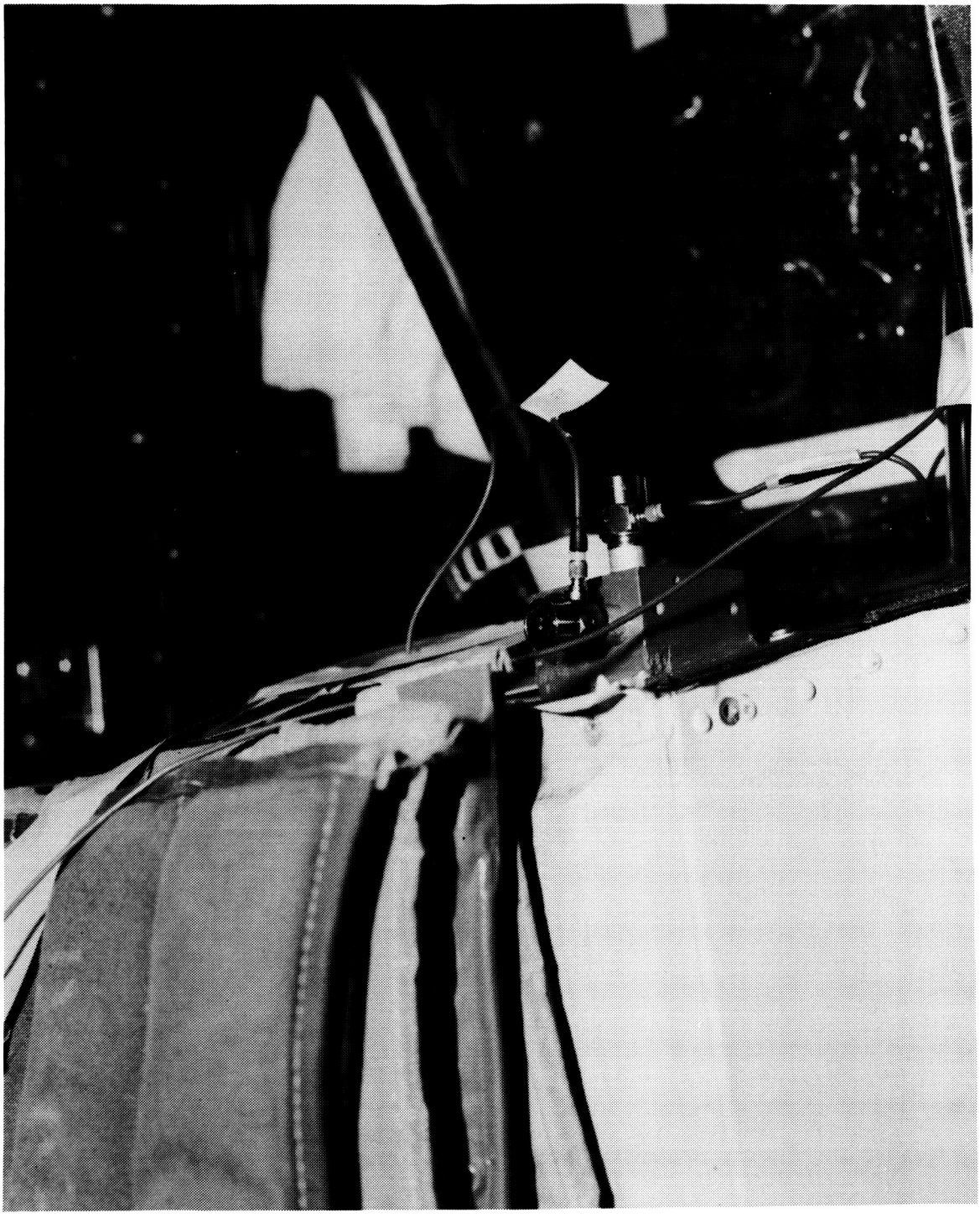

Figure 16. Pilot Seat Triaxial Accelerometer Location

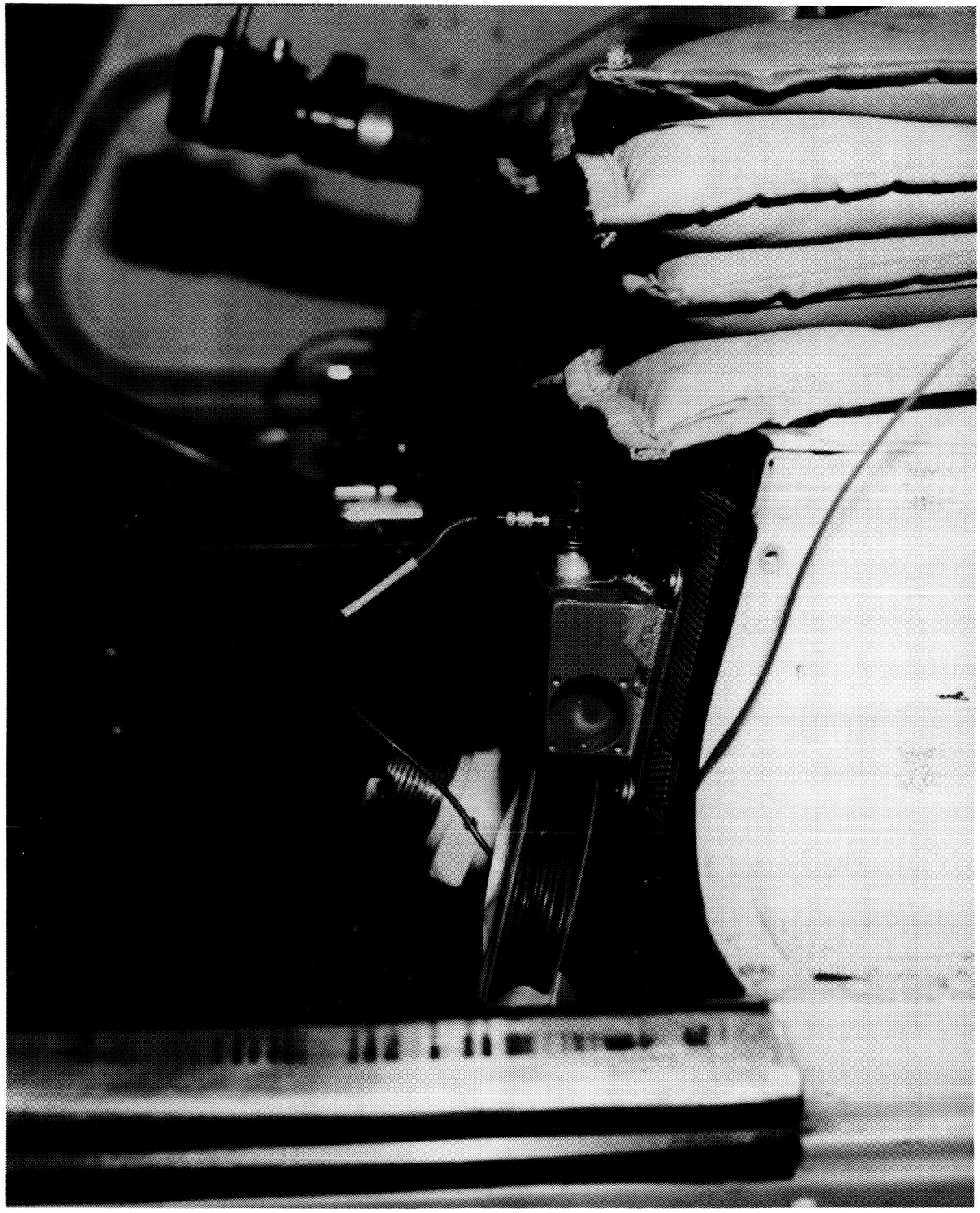

Figure 17. Co-pilot Seat Accelerometer Location for Shake Test

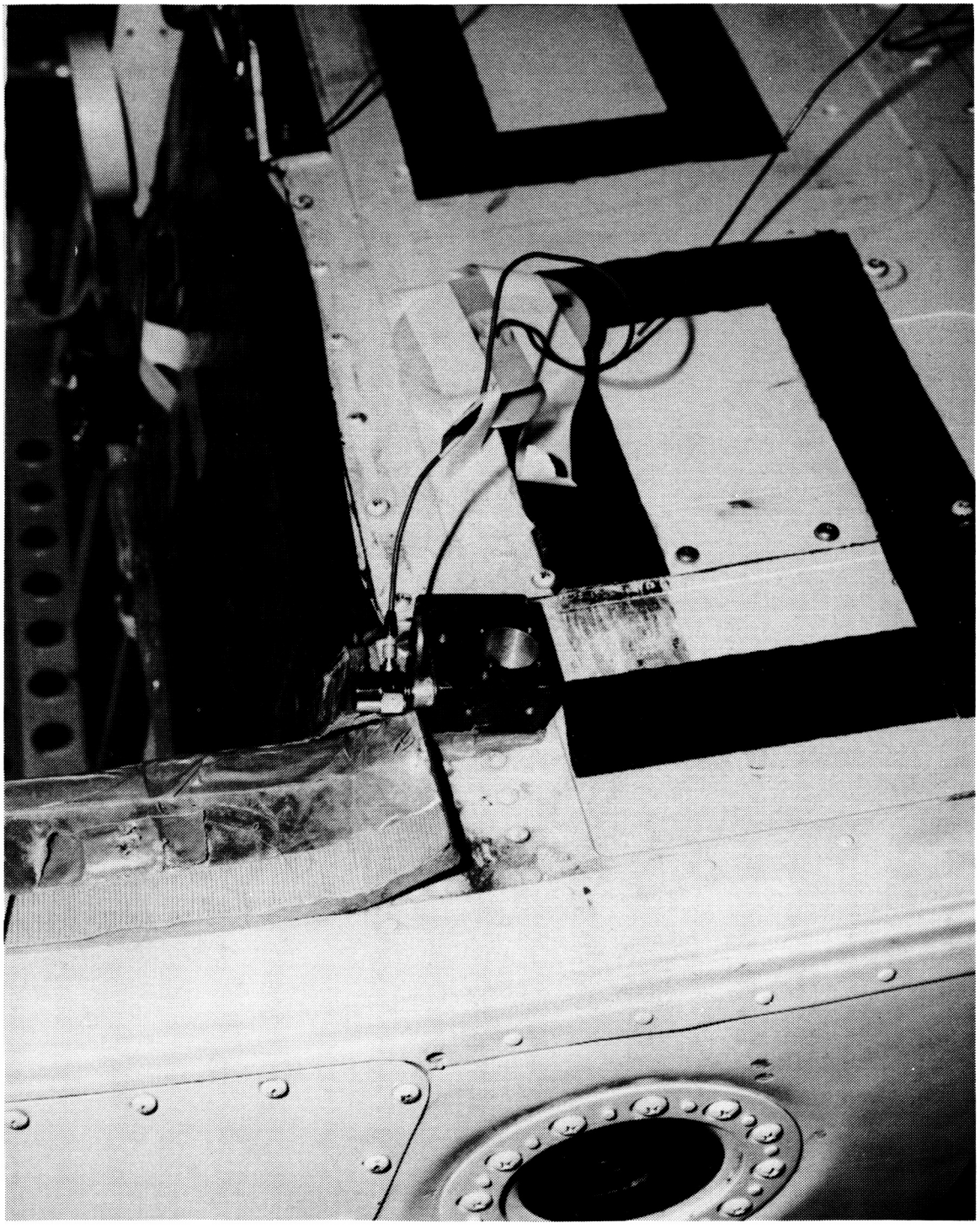

Figure 18. Aft Cabin Seat Vertical Accelerometer

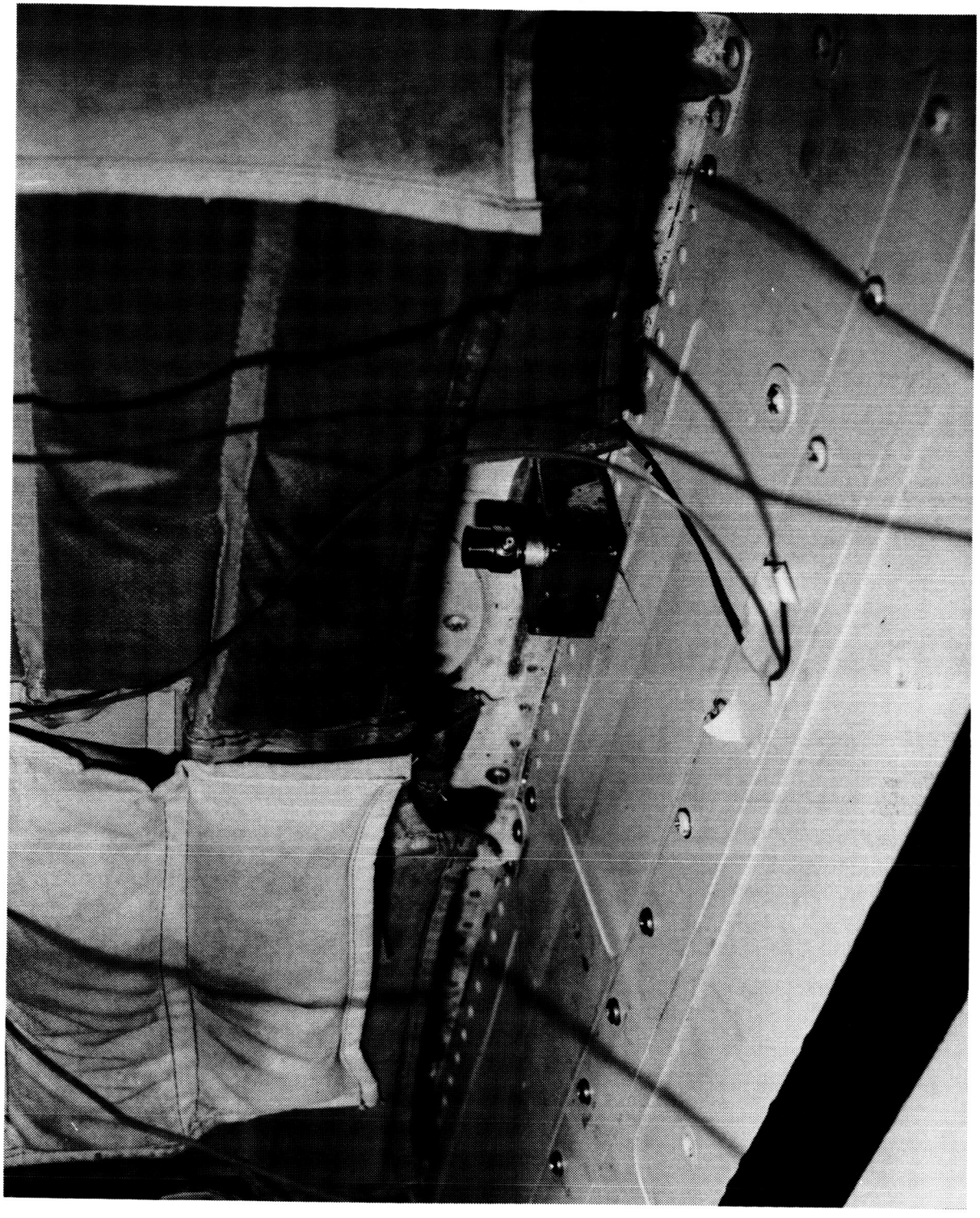

Figure 19. Aft Cabin Seat Fore/Aft Accelerometer

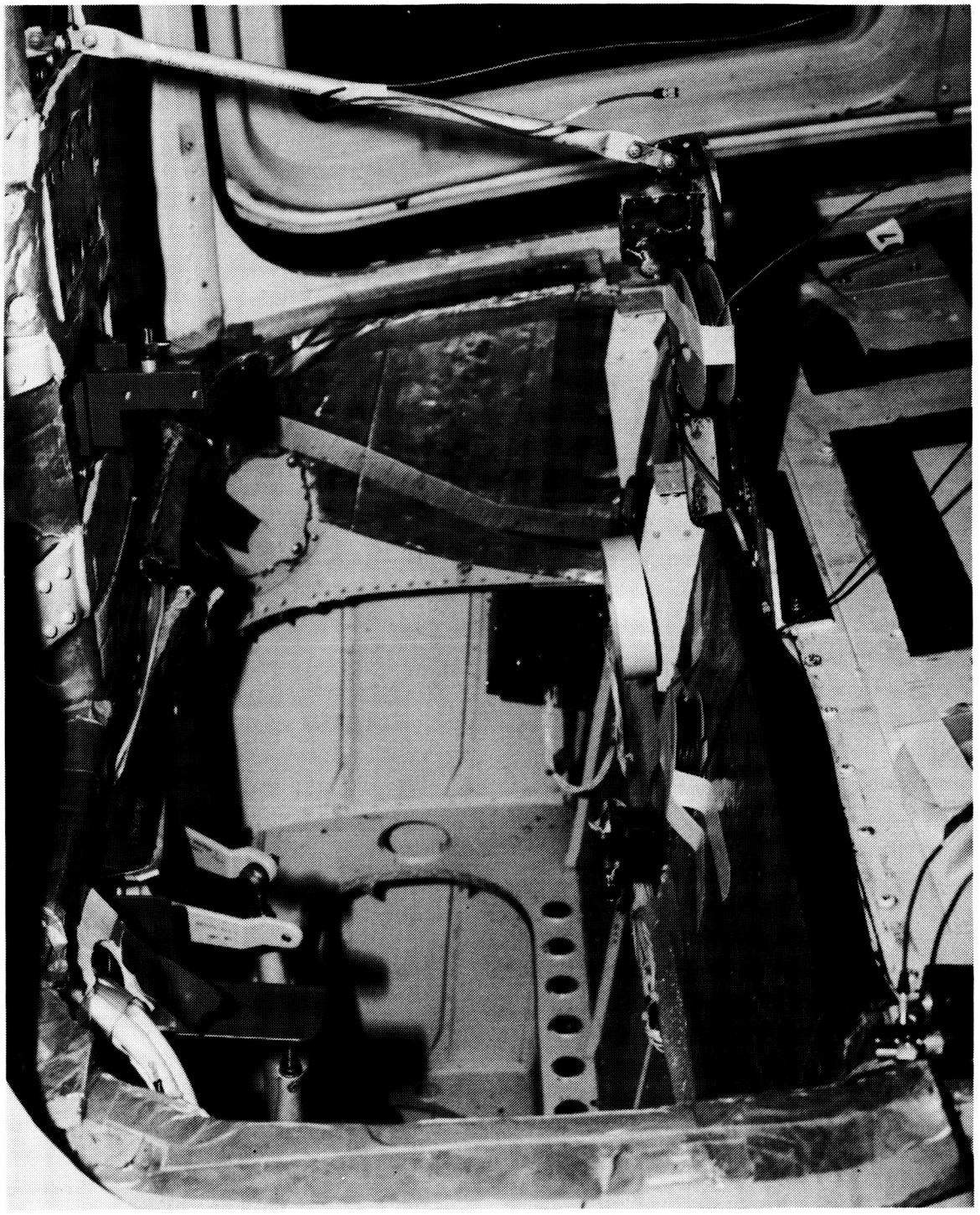

Figure 20. Accelerometers Used to Define CG Response

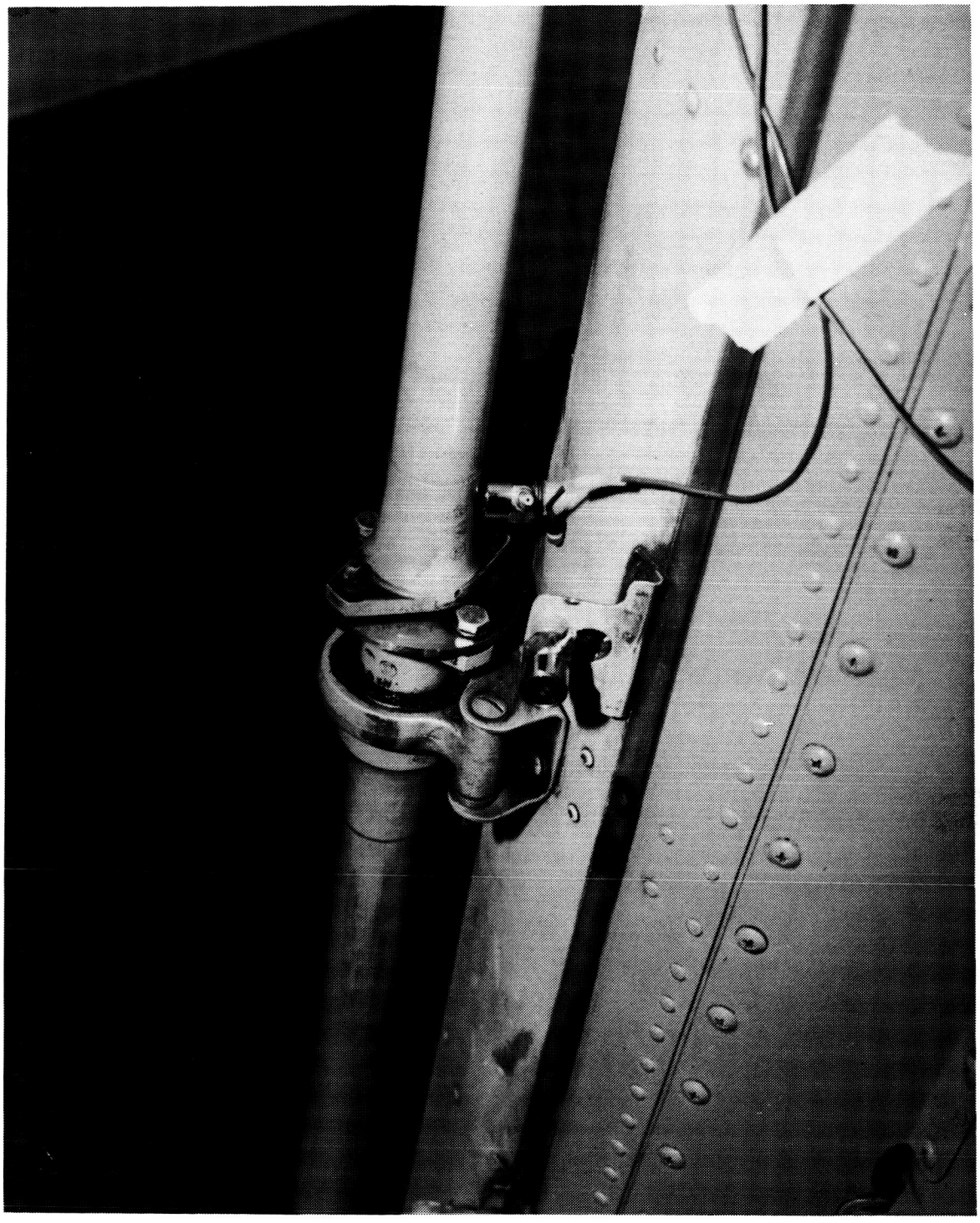

Figure 21. Vertical and Lateral Accelerometers at Elevator Centerline

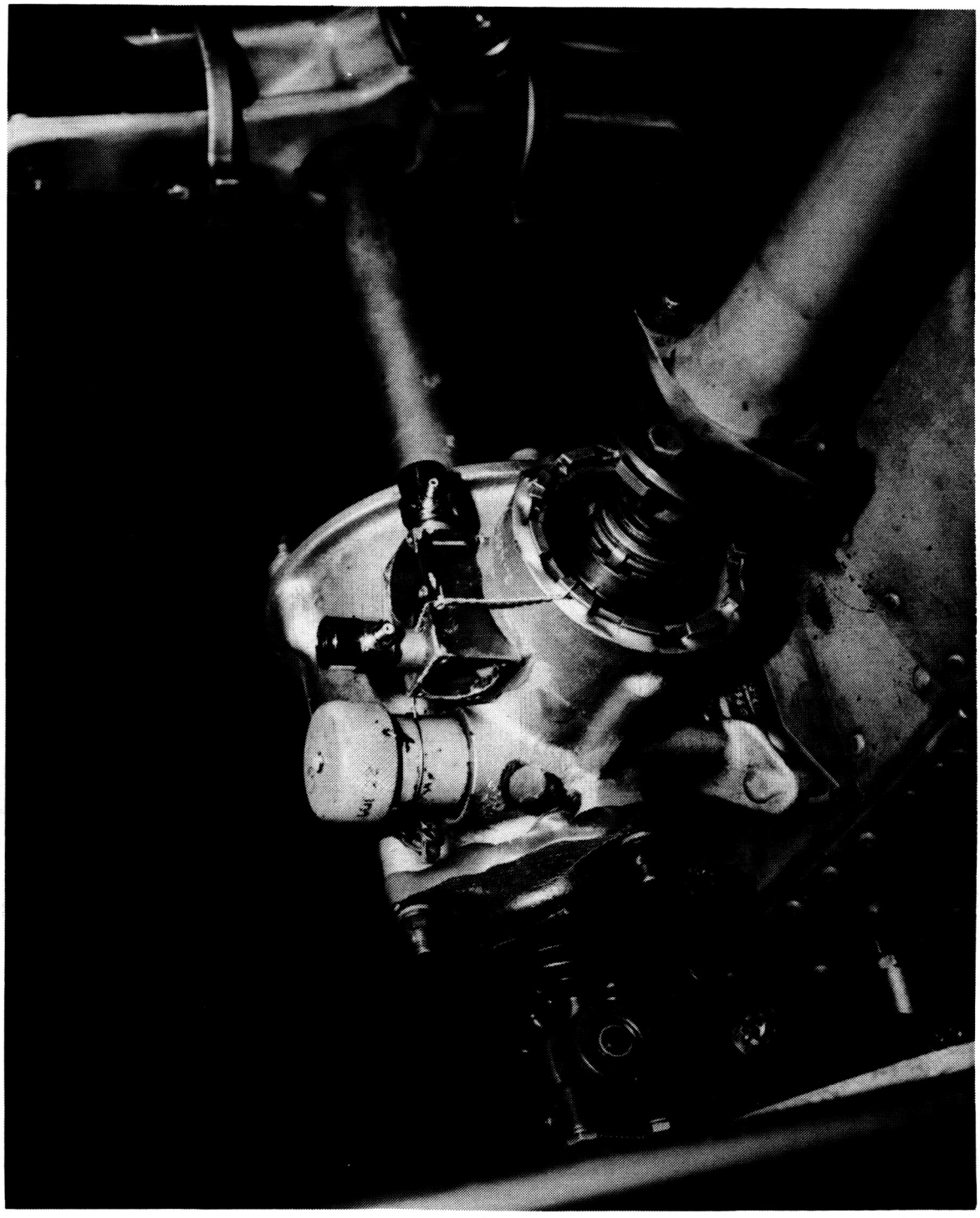

Figure 22. Vertical and Lateral Accelerometers at Tail Rotor Gearbox

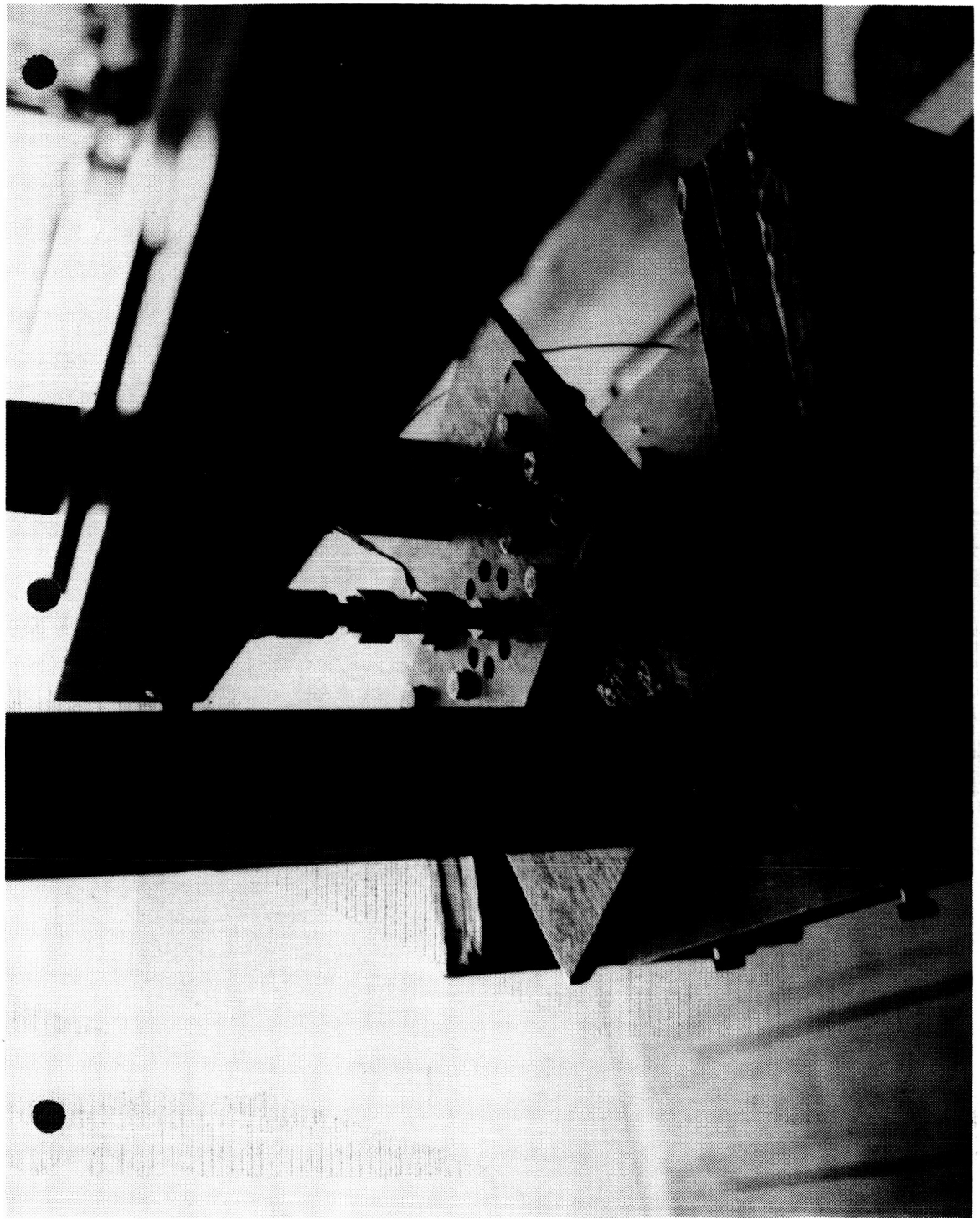

Figure 23. Force Impedance Head Installation for Vertical Shake Test

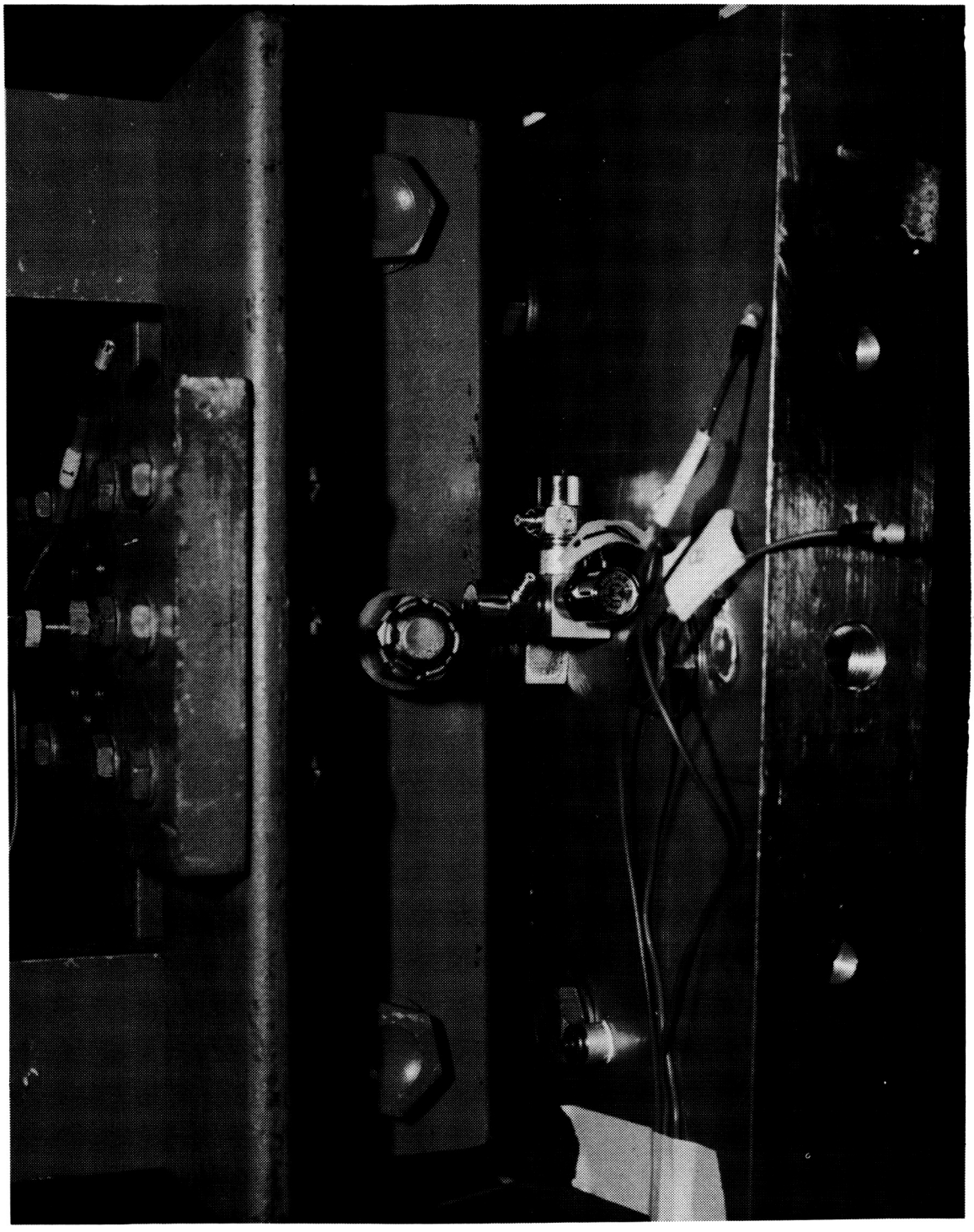

Figure 24. Hub Triaxial Accelerometers for Vertical Shake Test

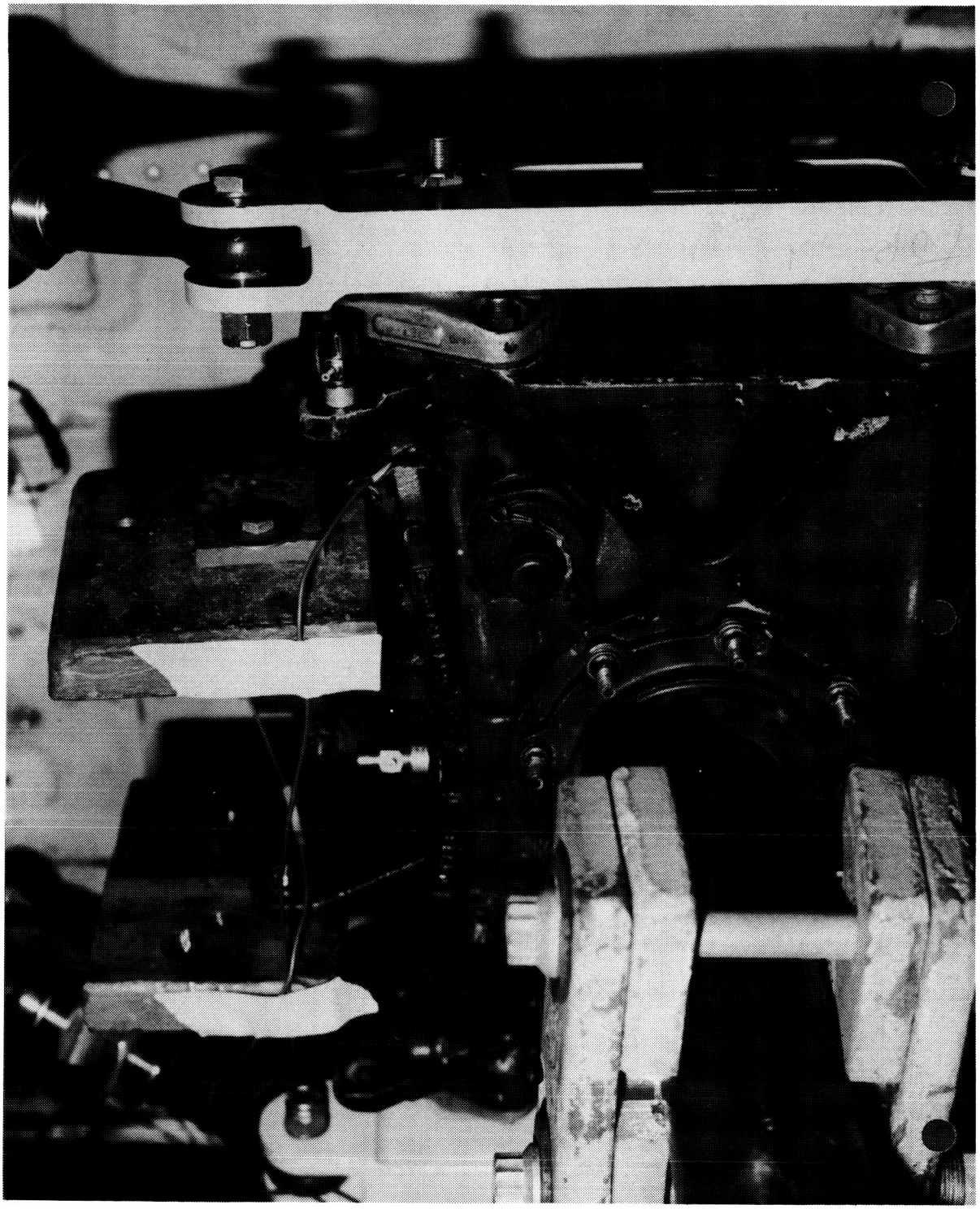

Figure 25. Transmission Accelerometer Location for Shake Test

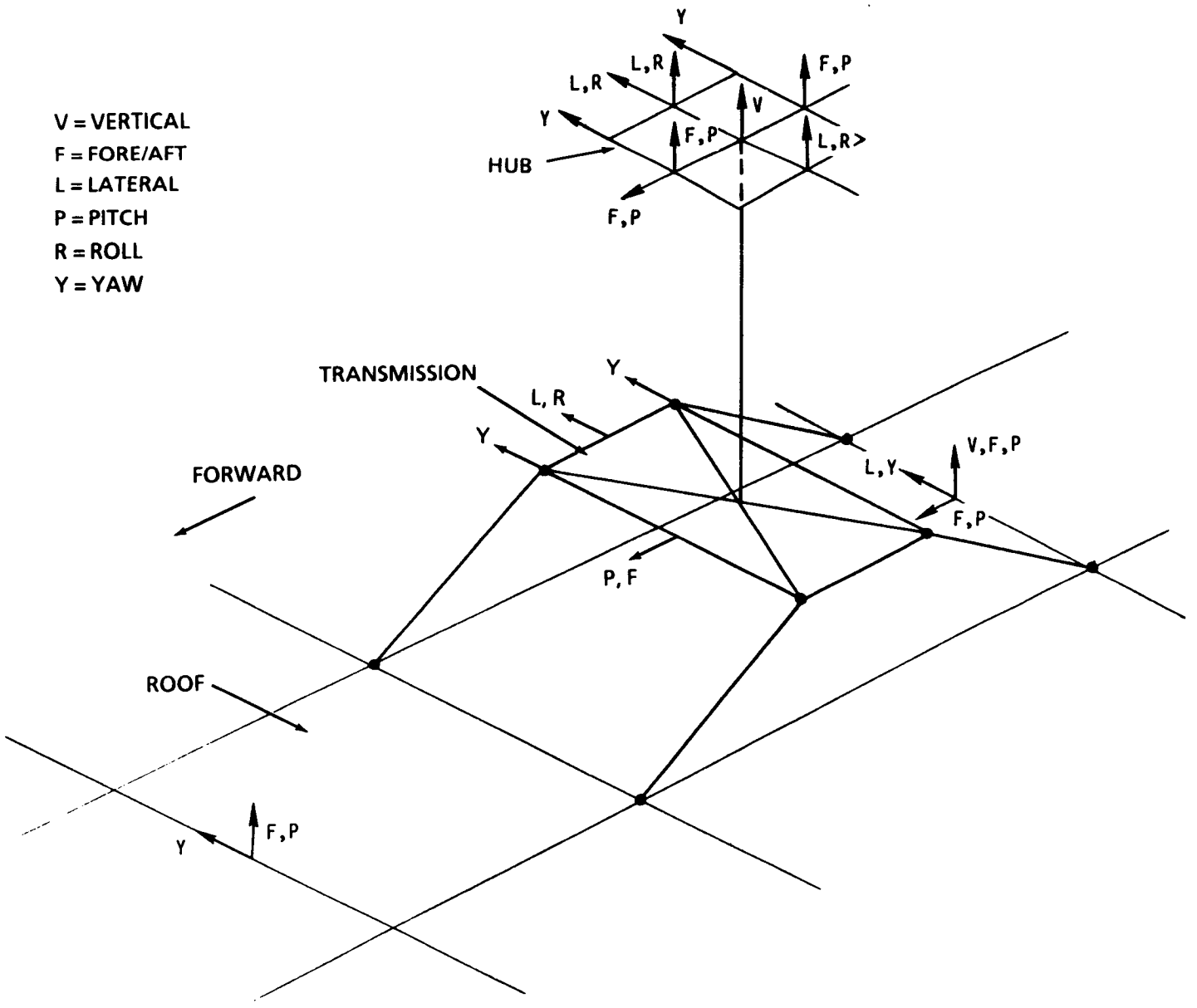

Figure 26. Accelerometer Locations on Hub and Roof During Shake Test

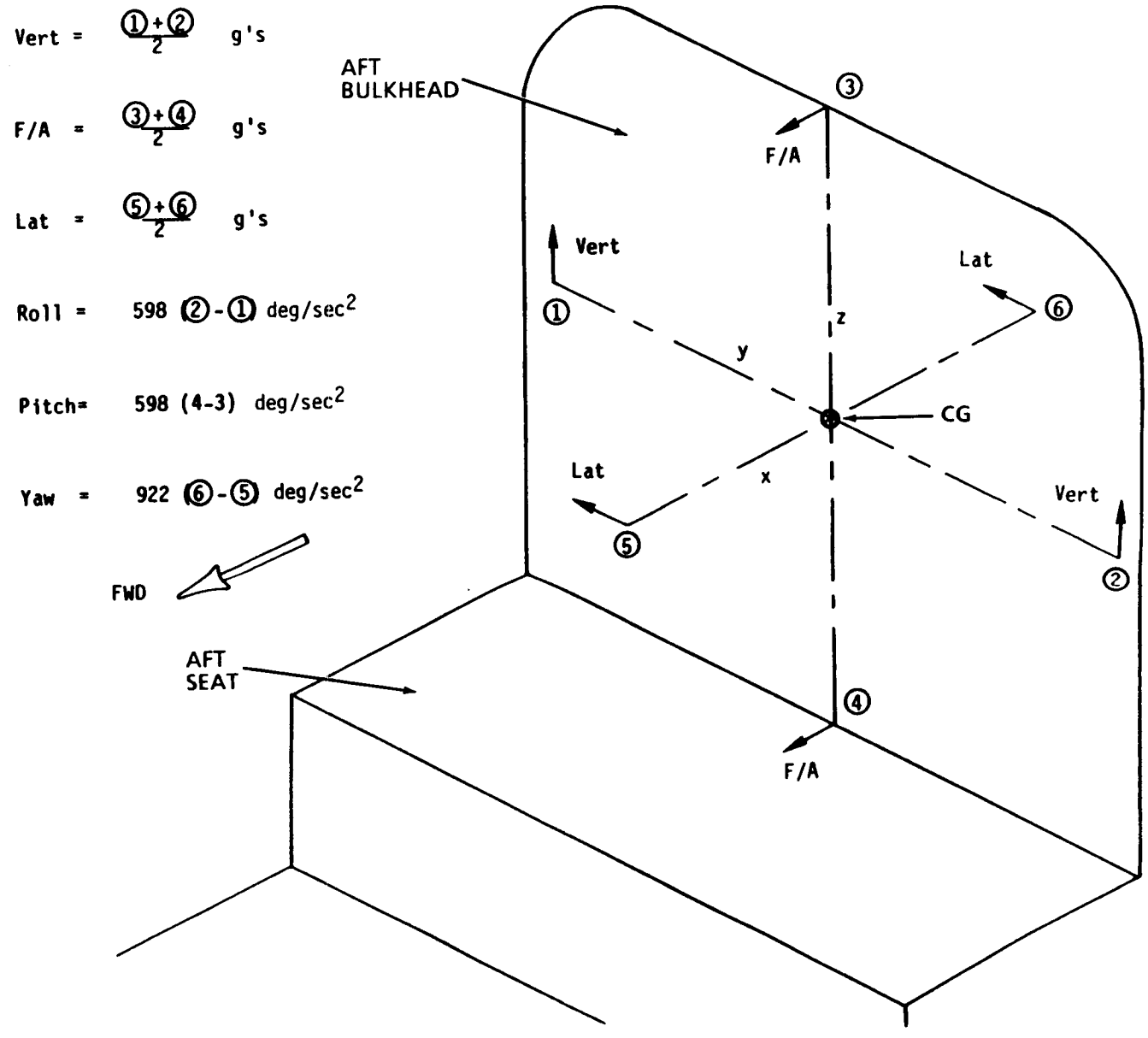

Figure 27. Accelerometer Locations Used to Define CG Response in Shake Test

deg/s^2. This calculation yields the rotational response of the structure halfway between the two accelerometers.

These calculations were performed by computer on both the sine and cosine components of the response so that correct phase and magnitude were maintained between the two accelerometers. In addition to the above accelerometers, accelerometers were located at each of the crew seats, each of the aft passenger seat locations, the elevator, and the 90° tailrotor gearbox.

Transfer Functions

Transfer functions were acquired on all accelerometers for each degree of freedom. These transfer functions were used with a Bell modal analysis computer program to define the natural frequencies of the pylon and the fuselage. A summary of the natural frequencies is given in Table II.

Mode shapes of the pylon pitch and roll modes were generated to determine the waterline of the nodes on the transmission. These transmission node locations had to be determined to ensure that pylon control coupling could not cause an instability (see discussion under **Pylon Control Coupling,** page 12).

The major transfer functions (all seat and cg locations) are presented in Appendix A, Figures A1 through A53. These plots show that the isolation valley at 4/rev (26.3 Hz) occurs in each accelerometer, and for each excitation degree of freedom. Table II shows good frequency separation between 4/rev and all pylon and most fuselage modes, although for this project no attempt was made to change the fuselage modes from the standard 206L fuselage.

Table II. Natural Frequencies of TRIS Installation on 206LM

DESCRIPTION	FREQUENCY
PYLON PITCH	7.22
PYLON ROLL	5.24
TAIL BOOM LATERAL	7.50
TAIL BOOM VERTICAL	5.82
TAIL BOOM TORSIONAL	24.0
TRANSMISSION VERTICAL	13.8
TRANSMISSION LATERAL	16.2
TRANSMISSION FORE/AFT	19.1
TRANSMISSION YAW	18.3
SECOND FUSELAGE VERTICAL	21.4
SECOND FUSELAGE LATERAL	20.2
FORE/AFT MAST BENDING	32.1
LATERAL MAST BENDING	34.6
ELEVATOR VERTICAL BENDING	15.2
VERTICAL FIN LATERAL BENDING	31.8

4/Rev Forced Response

For a more accurate measurement of the TRIS response at 4/rev, forced response data were acquired by exciting the aircraft with a constant 4/rev sine wave. This part of the test was performed two ways: one, with no hub weight so that the hub and airframe response would equal the inflight response for the same hub load measured between the rotor hub and the top of the mast; and two, with a 4/rev impedance hub mass so the responses would compare to the NASTRAN model. By measuring the hub response in g's or deg/s^2 and ratioing it to the cg response in the same units, a measure of the isolation systems transmissibility was calculated. The 4/rev forced response data for the maximum hub load from each accelerometer located at the hub, cg, and cabin seats are presented in Table III. A broad range of hub loads in each degree of freedom was measured to determine linearity. The ratio of hub load to accelerometer response was calculated from these data and is shown in Table IV.

Hub and fuselage cg response data from these tables are plotted in Figures 28 through 39 for each degree of freedom. The cg response scale is one-tenth that of the hub response scale. This dual scale was selected in order to show at a glance whether or not the 90% isolation criterion had been met. If the curve for the cg response falls below the curve for the hub response, that degree of freedom achieved 90% isolation; but if the cg curve is above the hub curve, then the 90% isolation criterion was not achieved. These plots show that all responses met the 90% isolation criterion with the exception of the cg fore/aft response to a hub fore/aft shear at low force levels, although at high force levels well over 90% isolation was achieved.

It was found during the detailed data analysis after the test that one of the hub vertical accelerometers used to calculate hub rotational roll response was not working properly during the roll excitation test. For this reason, hub roll was calculated with the data from only one accelerometer; the other

Table III. Forced Response at 4/Rev for Maximum Hub Load

LOCATION		VERTICAL	YAW	PITCH	F/A	ROLL	LATERAL
PILOT SEAT VERTICAL	MAG	0.0047	0.0094	0.0095	0.0086	0.0081	0.0034
	PHASE	147.54	-43.81	86.71	103.11	-65.42	14.44
PILOT SEAT LATERAL	MAG	0.0188	0.0195	0.0075	0.0065	0.0204	0.0150
	PHASE	-158.27	-36.0	-16.68	-117.10	-167.25	-133.10
CO-PILOT SEAT VERTICAL	MAG	0.0089	0.0197	0.0154	0.0127	0.0115	0.0102
	PHASE	-6.71	100.15	111.73	91.62	21.65	-11.73
RIGHT AFT SEAT VERTICAL	MAG	0.0855	0.0135	0.0242	0.0345	0.0018	0.0027
	PHASE	36.55	119.62	40.10	7.90	-132.73	68.29
AFT SEAT LATERAL	MAG	0.0079	0.0085	0.0040	0.0005	0.0140	0.0041
	PHASE	12.70	170.82	156.30	80.43	69.75	-163.12
LEFT AFT SEAT VERTICAL	MAG	0.0757	0.0144	0.029	0.032	0.0112	0.0095
	PHASE	29.42	133.21	63.67	16.46	96.21	-144.62
HUB (TRANSLATIONAL)	MAG	2.04	0.0622	0.8474	2.63	0.8213	2.940
	PHASE	-26.14	61.68	-65.38	-109.25	144.36	-104.46
AFT SEAT F/A	MAG	0.0998	0.0172	0.0205	0.0318	0.0027	0.0056
	PHASE	31.79	126.87	22.4	-10.21	153.21	-145.97
CG	MAG	0.0804	3.86	33.46	0.0245	7.41	0.0055
	PHASE	33.20	-39.76	26.17	-177.89	90.05	166.90
HUB (ROTATIONAL)	MAG	-	1907	505.36	-	463.3	-
	PHASE	-	55.75	154.75	-	-9.13	-
LOAD	MAG	787.9	3099	3844	210.6	4190	215.7
	PHASE	158.6	155.3	-52.0	77.7	-22.0	78.9

Table IV. Transfer Function Ratio for Maximum Hub Loads

LOCATION		VERTICAL g's/in-lb×10-3	YAW g's/in-lb×10-3	PITCH g's/in-lb×10-3	F/A g's/in-lb×10-3	ROLL g's/in-lb×10-3	LATERAL g's/in-lb×10-3
PILOT SEAT VERTICAL	RATIO	0.00597	0.0033	0.00247	0.0408	0.0193	0.0158
	PHASE	11.1	161	139	25.4	43.2	64.5
PILOT SEAT LATERAL	RATIO	0.0239	0.0063	0.00195	0.0308	0.0487	0.0695
	PHASE	43.1	168.7	35.3	165	145	148
CO-PILOT SEAT VERTICAL	RATIO	0.0113	0.0063	0.00401	0.0603	0.0274	0.0473
	PHASE	165	55.2	164	13.9	43.7	90.6
RIGHT AFT SEAT VERTICAL	RATIO	0.109	0.0044	0.00630	0.164	0.0043	0.0125
	PHASE	122	35.7	92.1	69.8	110	10.6
AFT SEAT LATERAL	RATIO	0.0100	0.0027	0.00104	0.00237	0.0334	0.0190
	PHASE	146	15.5	152	2.73	91.8	118
LEFT AFT SEAT VERTICAL	RATIO	0.0961	0.0046	0.00754	0.152	0.0267	0.0440
	PHASE	129	22.1	116	61.2	118	136
HUB (TRANSLATIONAL)	RATIO	2.59	0.020	0.220	12.5	1.96	13.6
	PHASE	175	93.62	13.4	173	166	176
AFT SEAT F/A	RATIO	0.127	0.0055	0.00533	0.151	0.0064	0.0259
	PHASE	127	28.4	74.4	87.9	175	135
CG	RATIO	0.102	1.245	8.70	0.116	17.6	0.0255
	PHASE	125.4	165	78.2	104	112	88.0
HUB (ROTATIONAL)	RATIO	-	615.36	131	-	1106	-
	PHASE	-	99.6	153	-	12.87	-

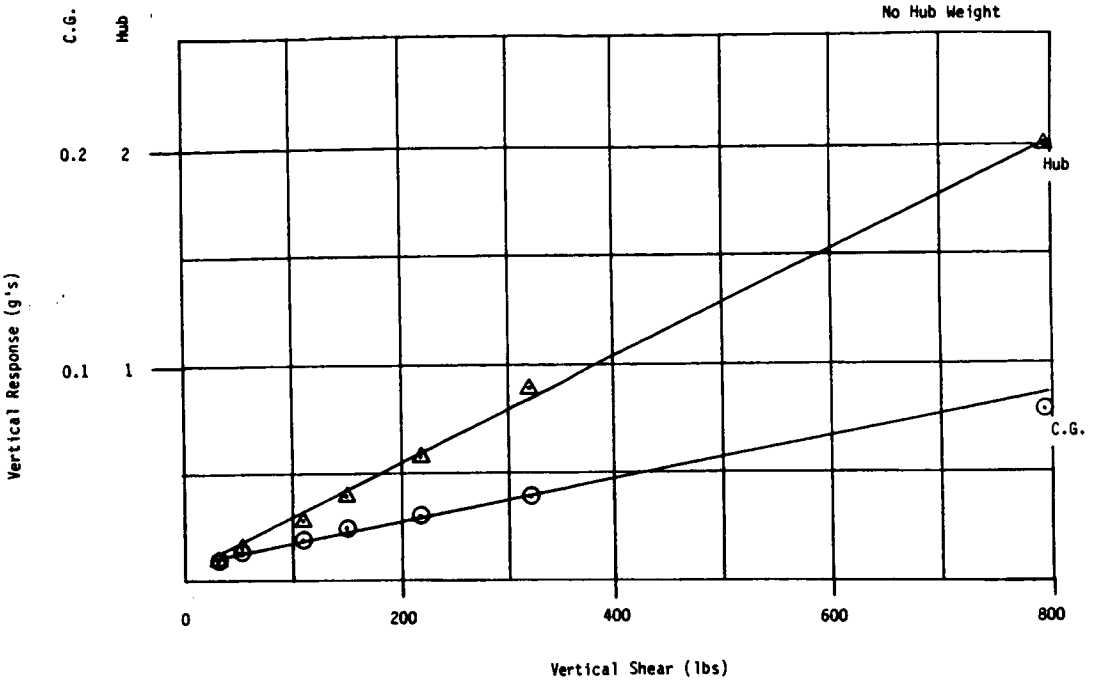

Figure 28. Fuselage Vertical Response to Vertical Hub Shear

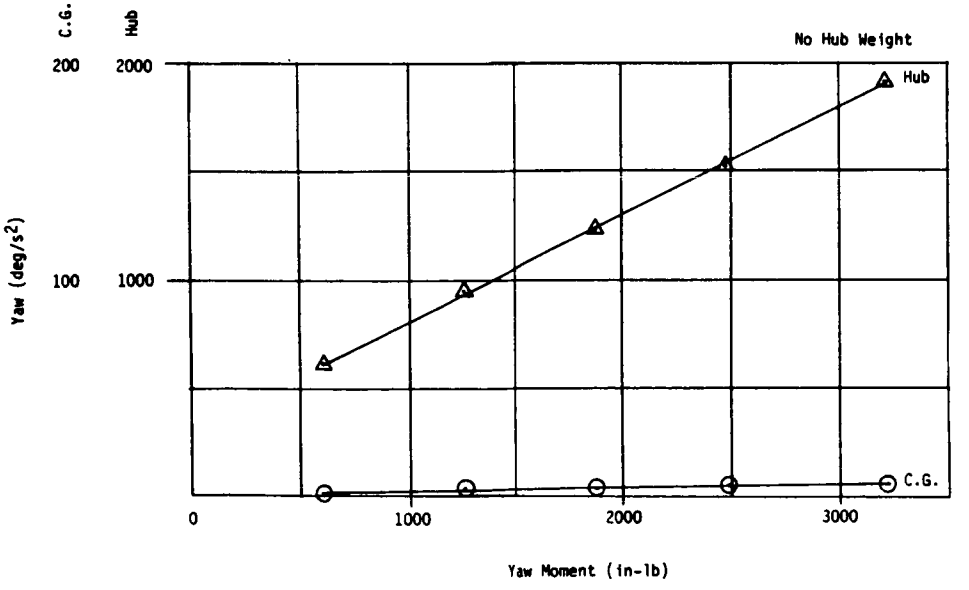

Figure 29. Fuselage Yaw Response to Yaw Hub Moment

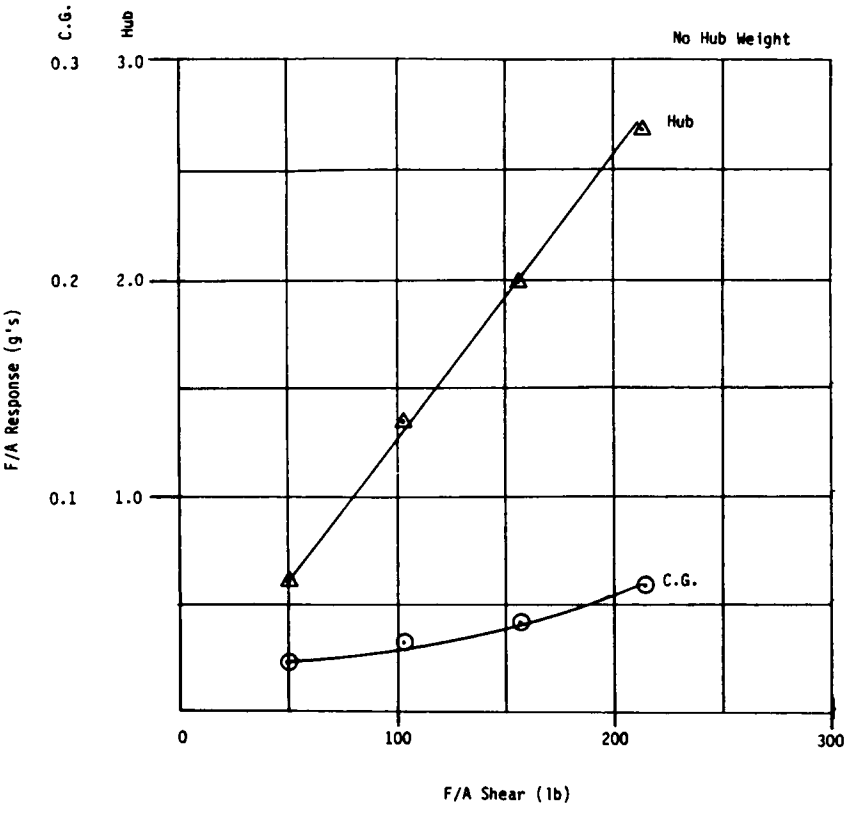

Figure 30. Fuselage F/A Response to F/A Hub Shear

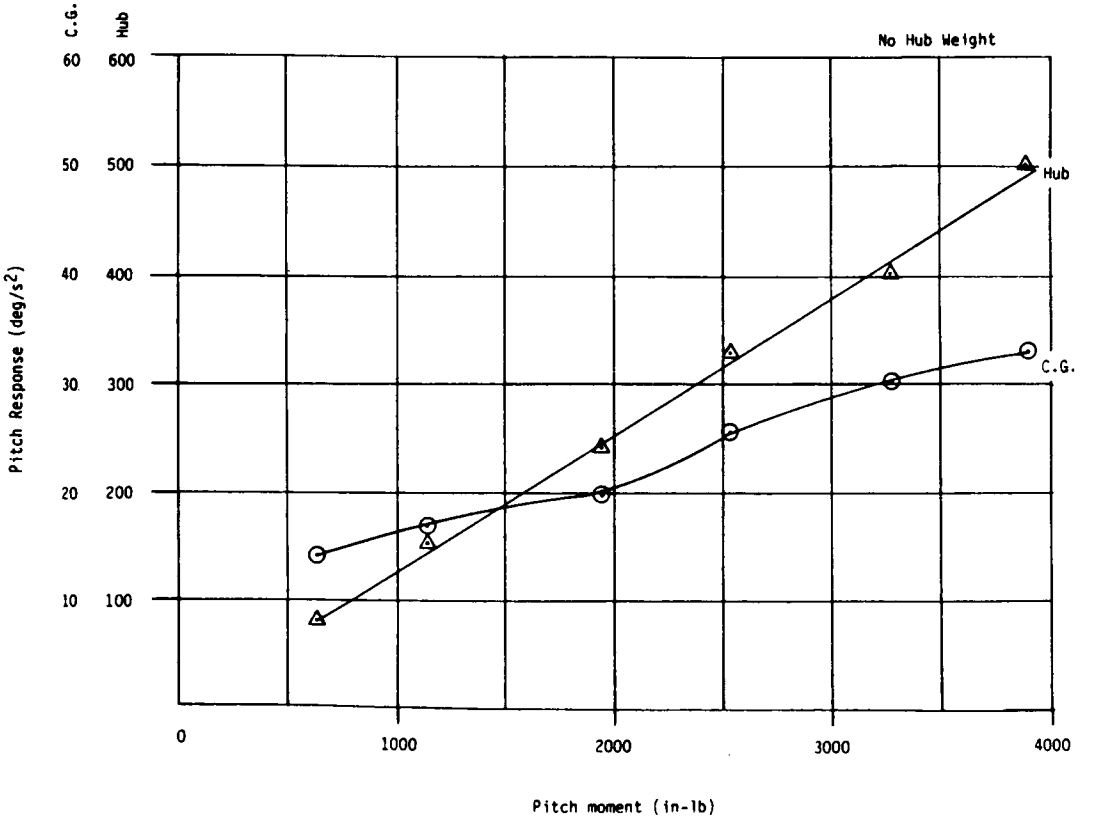

Figure 31. Fuselage Pitch Response to Pitch Hub Moment

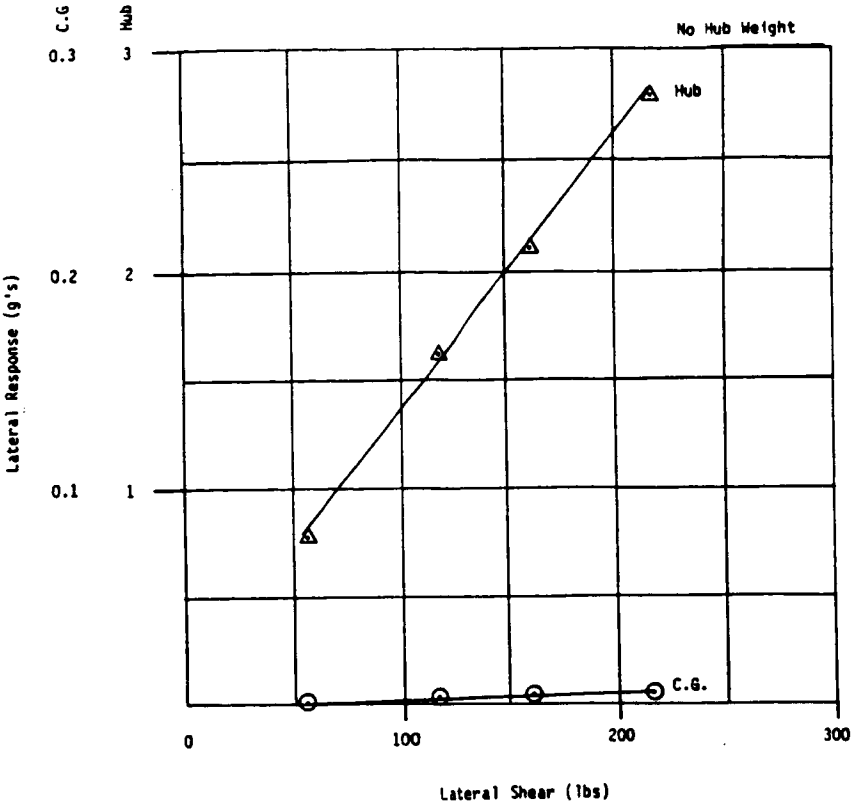

Figure 32. Fuselage Lateral Response to Lateral Hub Shear

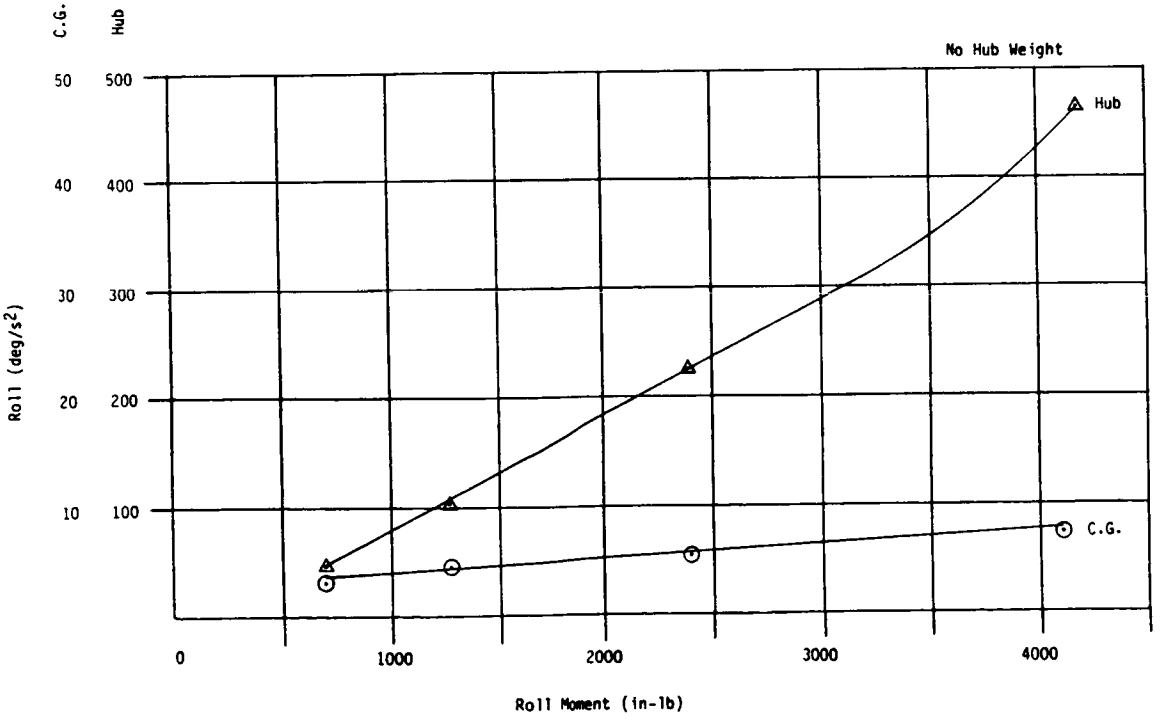

Figure 33. Fuselage Roll Response to Roll Hub Moment

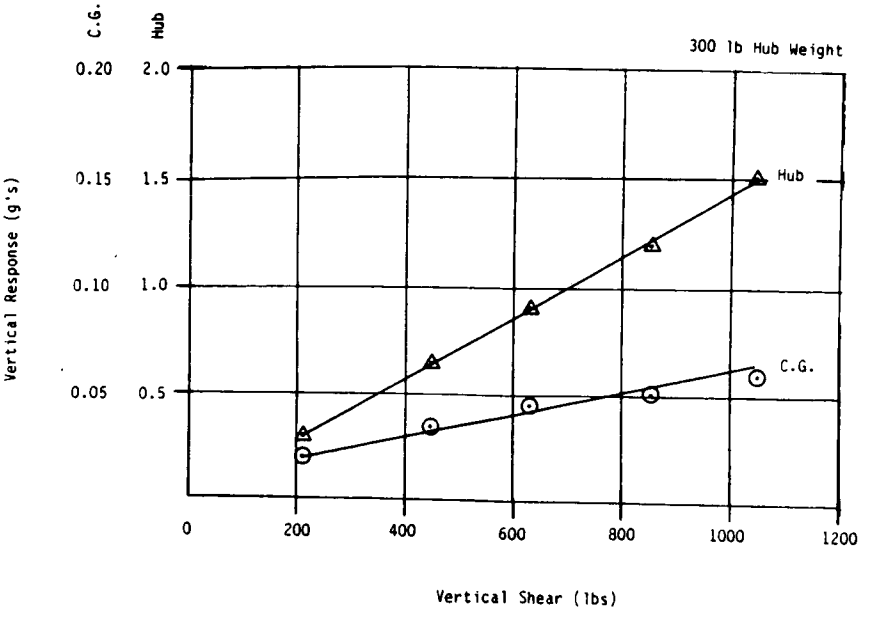

Figure 34. Fuselage Vertical Response to Vertical Hub Shear

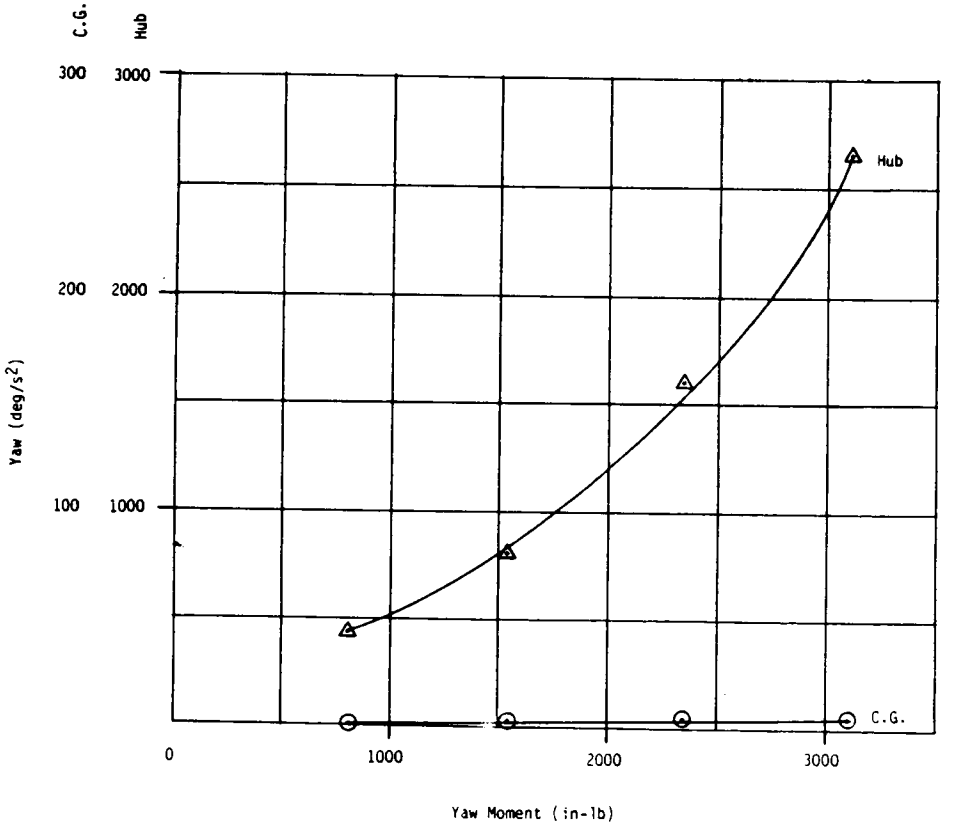

Figure 35. Fuselage Yaw Response to Yaw Hub Moment

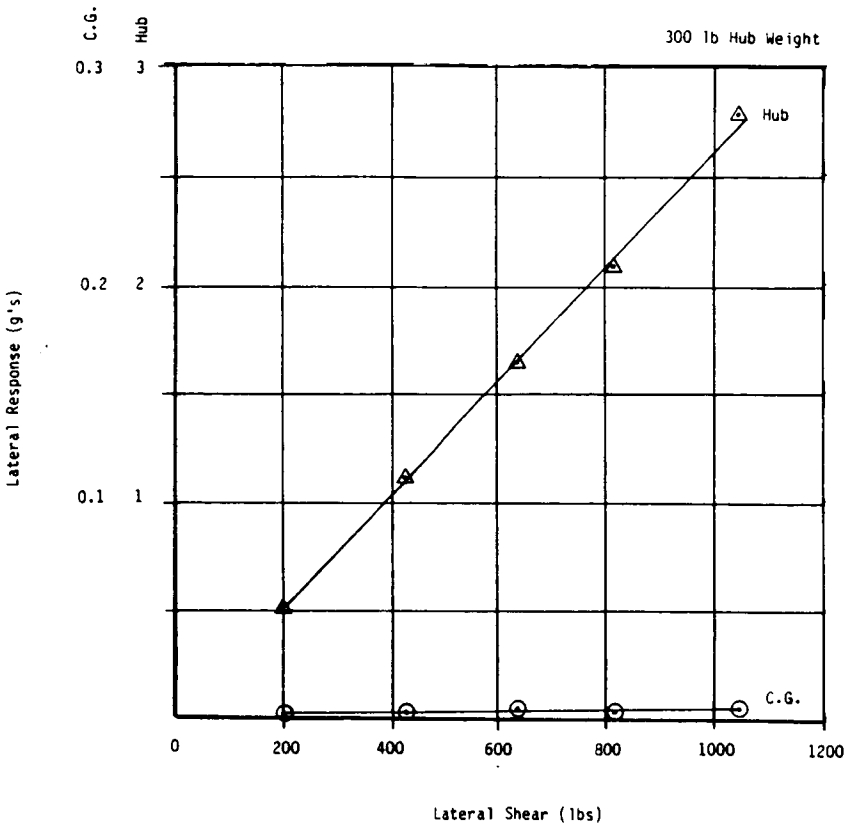

Figure 36. Fuselage Lateral Response to Lateral Hub Shear

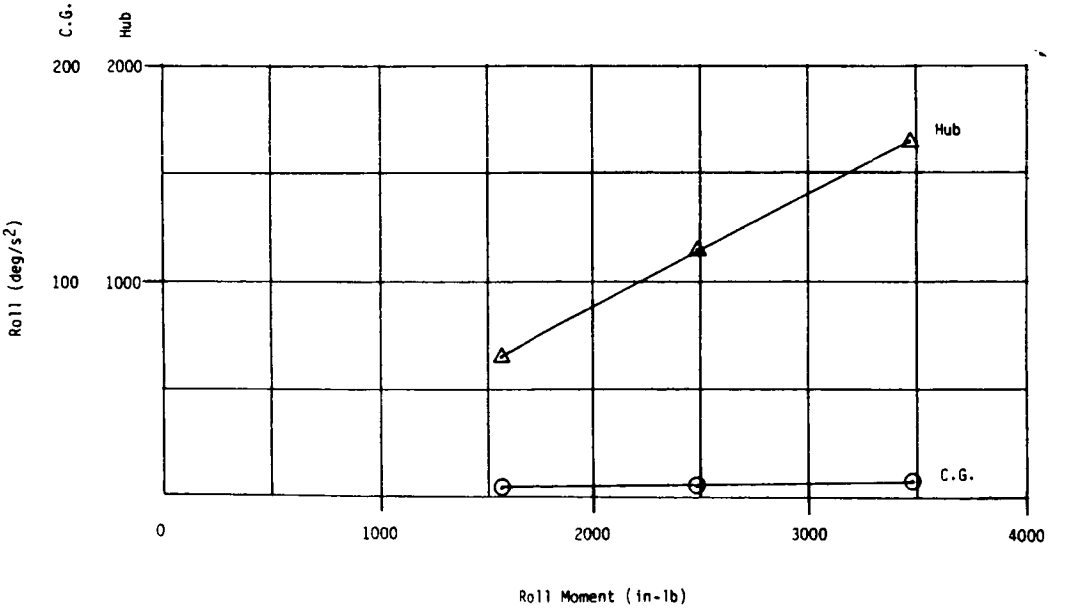

Figure 37. Fuselage Roll Response to Roll Hub Moment

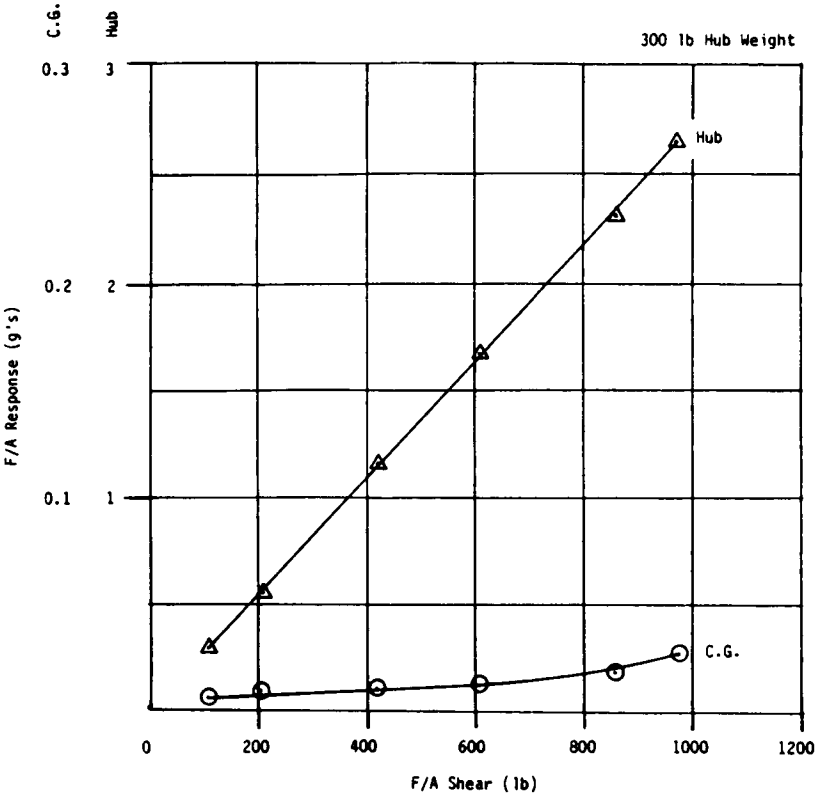

Figure 38. Fuselage F/A Response to F/A Hub Shear

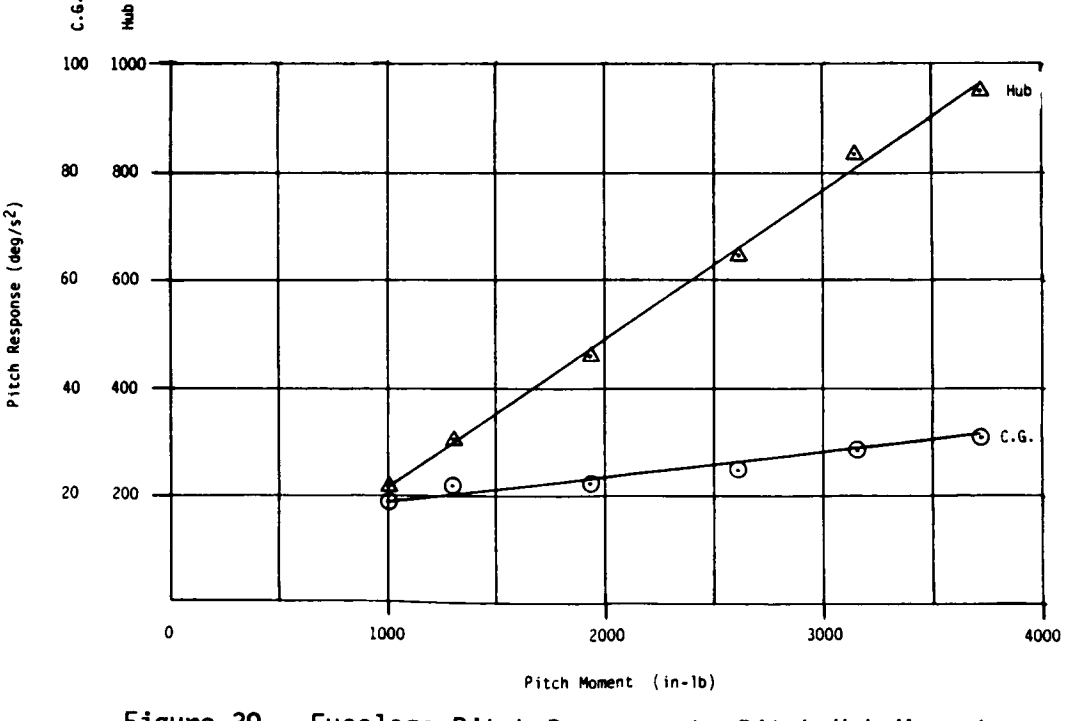

Figure 39. Fuselage Pitch Response to Pitch Hub Moment

accelerometer was assumed to be equal in magnitude but 180° out of phase. This assumption was based on the fact that the hub accelerometers should show only roll and lateral response, and the two vertical accelerometers used for the pitch test did have this relationship. The very low response levels in the cg roll and the very high percentage of isolation achieved in the hub lateral shear test both indicate that roll isolation was well over 90%.

GROUND RESONANCE VIBRATION TEST

In order to ensure aeromechanical stability margins, a ground resonance shake test was performed at the completion of the six degree-of-freedom vibration tests. The results of this test (the frequencies, damping, and mode shapes) were used to update the ground and air resonance stability models (Bell computer program DNAW01). The frequency and damping information acquired in this test is shown in Table V. The results of the stability analysis are shown in Figures 40 through 43.

These figures show that greater than 1.6% damping is expected under all ground and flight conditions. This analysis showed enough margin of safety that the ground run could proceed with these plots used as a guide line as to what to expect at various rpm and collective settings.

Pylon Control Coupling

For aeroelastic stability, it is necessary to minimize any possible main rotor control coupling that may be due to pylon motions. If there were a closed loop control input feedback that responded to pylon motion, an aeroelastic stability problem could occur at the pylon pitch or roll modes. The six degree-of-freedom isolation system spring rates and isolator angles and attachment points were selected, in part, to create a node in the pylon pitch and roll mode shapes at a specific waterline. This waterline is the same as the waterline in which the three main rotor control input tube axes

Table V. Natural Frequencies and Damping From Vibration Test

NATURAL FREQUENCY	HUB G's	HERTZ	DAMPING %	
PITCH PENDULUM MODE		0.45		
ROLL PENDULUM MODE		1.11		
T/B VERTICAL (IN AIR)		5.61	2.8	
PYLON PITCH (IN AIR)	0.6	7.00	2.2	
PYLON PITCH (IN AIR)	0.08	7.22	1.8	
PYLON PITCH (IN AIR)	0.01	7.29	1.7	
PYLON ROLL (IN AIR)	0.45	5.05	3.2	
PYLON ROLL (IN AIR)	0.19	5.13	3.2	
PYLON ROLL (IN AIR)	0.023	5.24	2.9	
FUSELAGE ROLL (ON GROUND)	0.13	1.56	8.1	
FUSELAGE ROLL (ON GROUND)	0.033	1.68	7.2	
FUSELAGE ROLL (ON GROUND)	0.0063	1.82	6.9	
FUSELAGE PITCH (ON GROUND)	0.28	1.37	10.5	(SCRUBBING SKID TUBES)
FUSELAGE PITCH (ON GROUND)	0.062	1.75	5.1	
FUSELAGE PITCH (ON GROUND)	0.042	1.83	3.7	
FUSELAGE PITCH (ON GROUND)	0.026	1.87	3.4	
FUSELAGE PITCH (ON GROUND)	0.018	1.89	3.3	
T/B VERTICAL (ON GROUND)	0.039	4.06	6.6	
T/B VERTICAL (ON GROUND)	0.0068	4.25	1.3	
PYLON PITCH (ON GROUND)	0.032	6.95	7.5	
PYLON PITCH (ON GROUND)	0.018	6.56	7.4	
PYLON ROLL (ON GROUND)	0.029	4.55	14.1	
PYLON ROLL (ON GROUND)	0.0069	5.05	16.2	

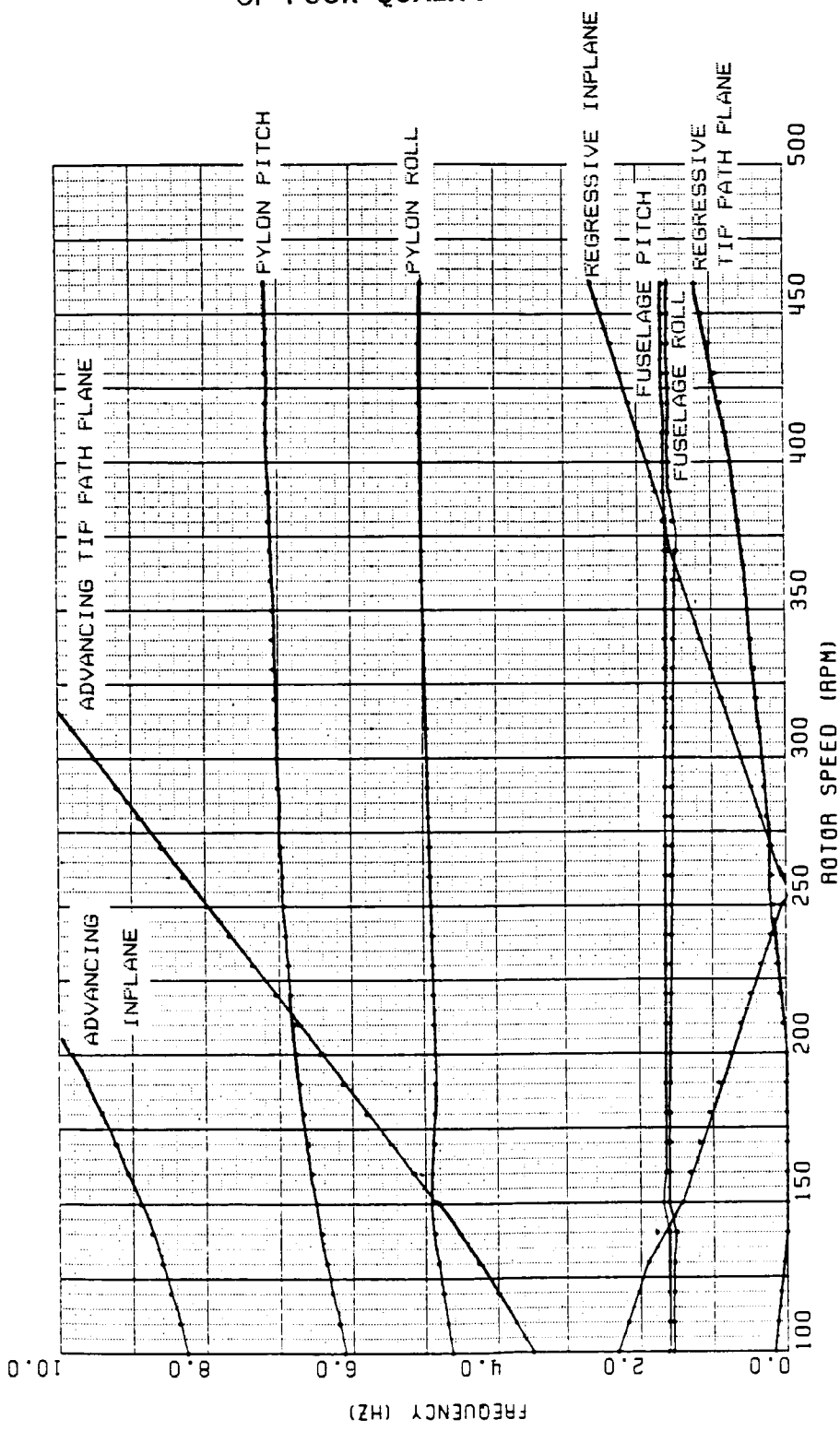

Figure 40. Ground Resonance Frequency Analysis Using Shake Test Frequencies and Damping

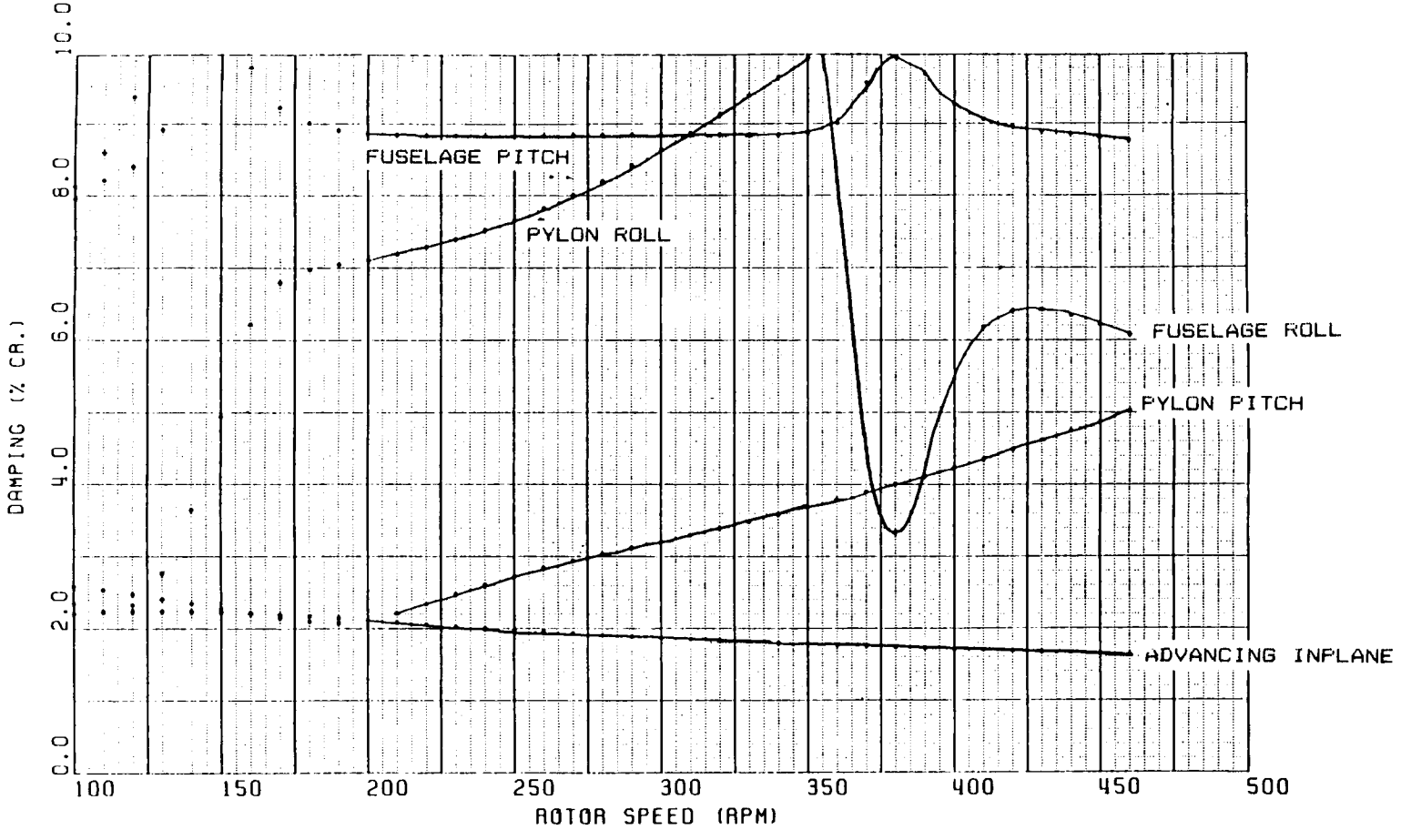

Figure 41. Ground Resonance Damping Analysis Using Shake Test Frequencies and Damping

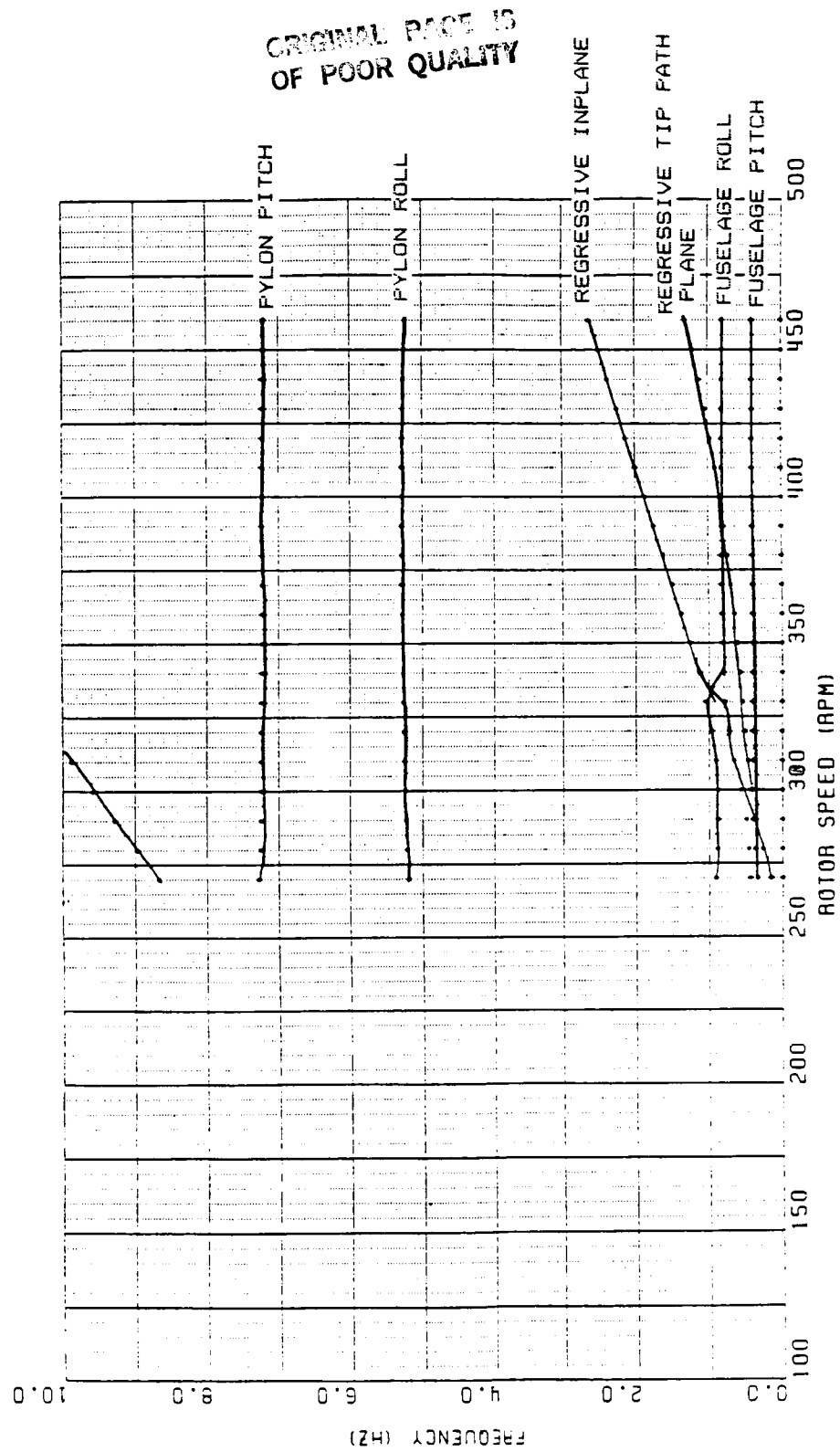

Figure 42. Air Resonance Frequency Analysis Using Shake Test Frequencies and Damping

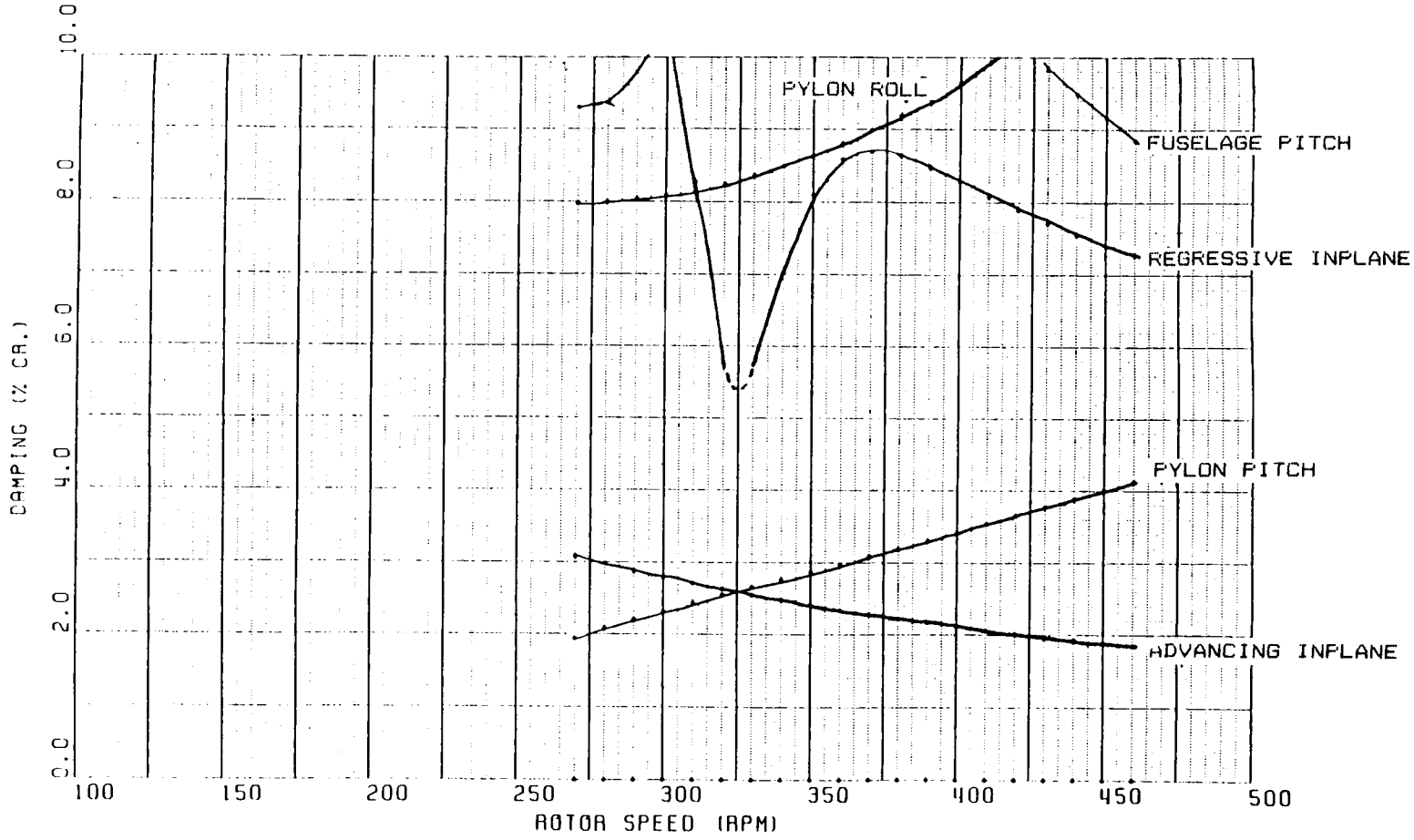

Figure 43. Air Resonance Damping Analysis Using Shake Test Frequencies and Damping

intersected (or are focused) on the mast centerline. This geometry of the control tubes (see Figure 44) results in no control coupling when the pylon pitches or rolls about this focal point. If excited at a pylon natural frequency then, there would be no instability due to control coupling. This approach results in simple design and does not complicate the standard 206L control system. The resulting control coupling was measured and is shown in Table VI.

Input Drive Shaft

A measurement of the maximum input drive shaft misalignment angles was made. This test was performed by rocking the pylon to all extremes of allowable motion until it contacted the pylon stops. At each extreme, the drive shaft angle was measured. The results are shown in Figure 45. The allowable angle for the coupling is 3.5° continuous and 5° transient.

GROUND RUN AND FLIGHT TESTS

Instrumentation

There were two different instrumentation lists used for the ground and flight tests. The first list (Table VII, column 1) was used for all safety of flight items during ground run and the envelope expansion phase of the flight test. At the completion of the envelope expansion, the instrumentation was switched to those items (Table VII, column 2) necessary to fully document the performance of the isolation system.

The instrumentation package used during this program consisted of an on-board 4-track tape recorder, voltage conditioning amplifiers, AM to FM converters, multiplexing system, and a telemetering system. Three of the four tracks were multiplexed, 13 channels of data per track, giving 39 data channels. The other track was used for voice, tape time code, level code, and record number. The TM system was used to send data to the Ground Data Center

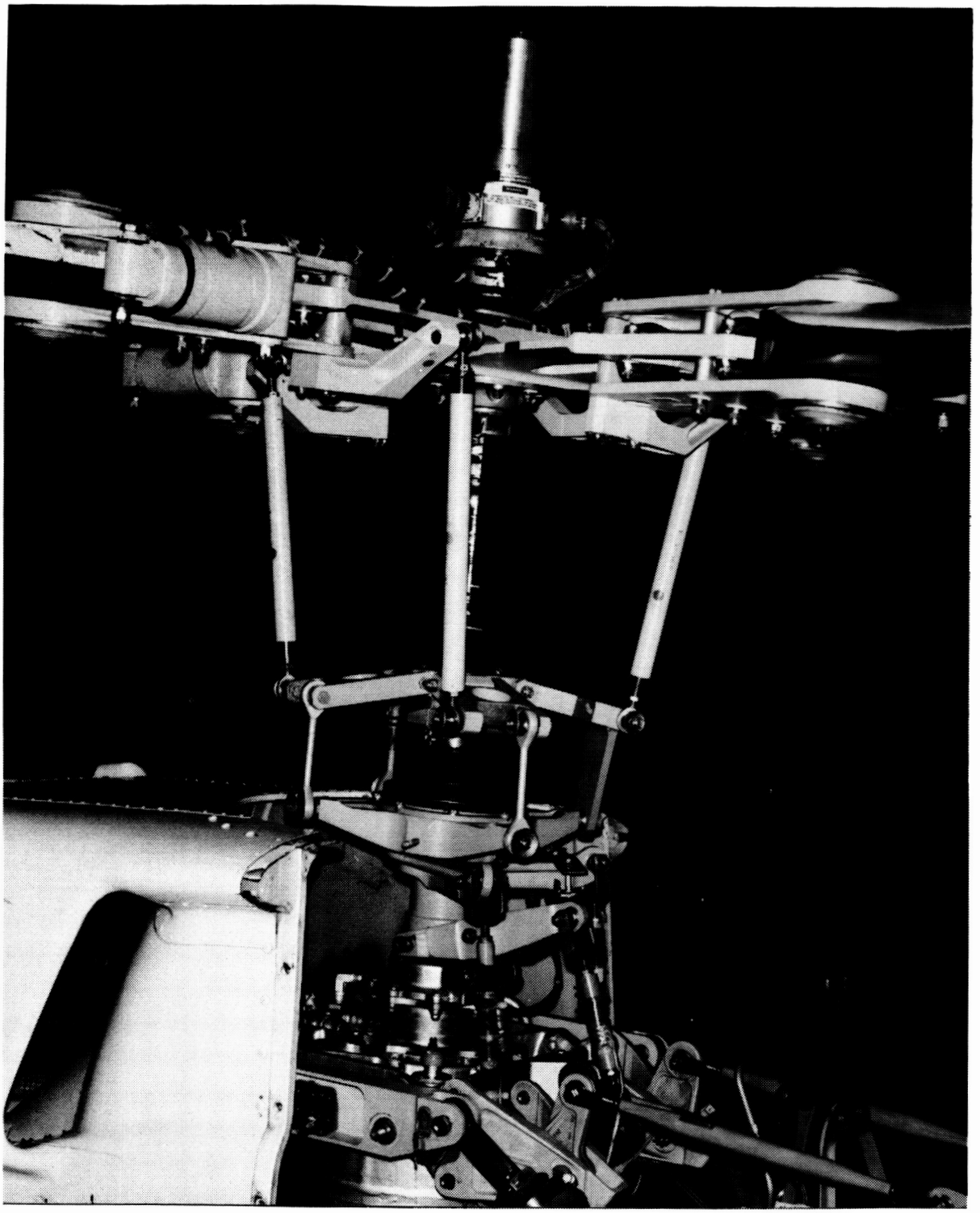

Figure 44. Model 206LM Main Rotor and Control Tube Installation

Table VI. Measured Main Rotor Control Coupling to Pylon Motion

PYLON MOTION	COLLECTIVE	PITCH	ROLL
PITCH PENDULUM MODE	-8.8'/deg	-2.8'/deg	+8.5'/deg
ROLL PENDULUM MODE	-2.2'/deg	-4.5'/deg	-2.8'/deg
T/B VERTICAL (IN AIR)	+46'/in	-1°22'/in	+3°50'/deg

+COLLECTIVE = THRUST UP
+ PITCH = HUB AFT
+ ROLL = HUB RIGHT

NOTE: Maximum Pitch Angle equals 1.8°, Roll Angle = 2.6°, Vertical Travel = 0.875 inches (0.25 inches/g).

POSITION	FWD COUPLING α
1. REFERENCE	1.812°
2. HUB FWD.	1.686°
3. HUB AFT	3.669°
4. HUB RIGHT	3.739°
5. HUB LEFT	1.590°
6. 1.0 G	1.729°

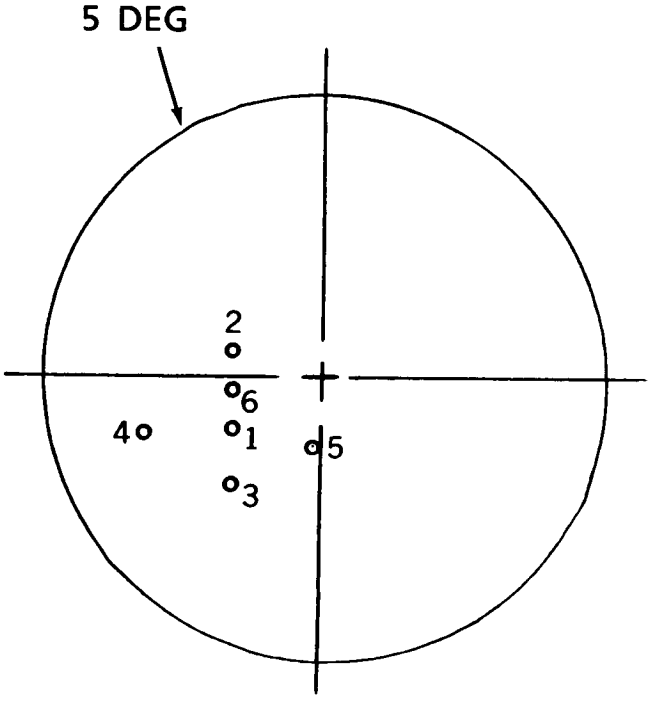

Figure 45. Measured Drive Shaft Angles from Ground Test

Table VII. Instrumentation List for Flight Test

DESCRIPTION	SAFETY OF FLIGHT	VIBRATION PERFORMANCE TESTS
F/A CYCLIC STICK POSITION	X	
PITCH RATE GYRO	X	
LATERAL CYCLIC STICK	X	
ROLL RATE GYRO	X	
MAIN ROTOR RED YOKE BEAM MB STATION 3.5	X	X
MAIN ROTOR MAST TORQUE	X	X
MAIN ROTOR MAST PERPENDICULAR BENDING STATION 16.0	X	X
MAIN ROTOR MAST PARALLEL BENDING STATION 16.0	X	X
RIGHT HAND PYLON F/A POSITION	X	X
LATERAL PYLON POSITION	X	X
MAIN ROTOR RED PITCH LINK LOWER AXIAL	X	X
MAIN ROTOR RED YOKE CHORD MB STATION 3.5	X	X
MAIN ROTOR RED BLADE LEAD-LAG POSITION	X	X
LEFT HAND PYLON POSITION - F/A	X	X
MAIN ROTOR RED BLADE ANGLE	X	
LATERAL ACCELERATION AT AFT HAT RACK	X	X
YAW RATE GYRO	X	
YAW ATTITUDE GYRO	X	
PITCH ATTITUDE GYRO	X	
ROLL ATTITUDE GYRO	X	
COLLECTIVE STICK POSITION	X	
PEDAL POSITION	X	
RIGHT HAND FORWARD PYLON POSITION - VERTICAL	X	X
RIGHT HAND AFT PYLON POSITION - VERTICAL	X	
LEFT HAND FORWARD PYLON POSITION - VERTICAL	X	X
LEFT HAND AFT PYLON POSITION - VERTICAL	X	X
ANGLE OF ATTACK	X	
ANGLE OF SIDE-SLIP	X	
PILOT SEAT VERTICAL ACCELERATION	X	X

Table VII. Instrumentation List for Flight Test (Continued)

DESCRIPTION	SAFETY OF FLIGHT	VIBRATION PERFORMANCE TESTS
PILOT SEAT LATERAL ACCELERATION	X	
CO-PILOT SEAT VERTICAL ACCELERATION	X	X
VERTICAL ACCELERATION LEFT HAND PASSENGER SEAT	X	
VERTICAL ACCELERATION RIGHT HAND PASSENGER SEAT	X	
MAIN ROTOR MAST PARALLEL BENDING STATION 29.7	X	
AIRSPEED	X	
CG LOAD FACTOR	X	X
F/A ACCELERATION AT AFT PASSENGER SEAT CENTERLINE		X
LEFT HAND CYCLIC BOOST TUBE AXIAL		X
RIGHT HAND CYCLIC BOOST TUBE AXIAL		X
MAIN ROTOR HUB LATERAL ACCELERATION		X
MAIN ROTOR HUB F/A ACCELERATION		X
LATERAL ACCELERATION AT AFT PASSENGER SEAT ARM		X
RIGHT HAND FORWARD LIVE ISOLATOR AXIAL POSITION		X
RIGHT HAND AFT LIVE ISOLATOR AXIAL POSITION		X
LEFT HAND FORWARD LIVE ISOLATOR AXIAL POSITION		X
LEFT HAND AFT LIVE ISOLATOR AXIAL POSITION		X
RIGHT HAND F/A LIVE ISOLATOR AXIAL POSITION		X
LEFT HAND F/A LIVE ISOLATOR AXIAL POSITION		X
RIGHT HAND LATERAL PYLON POSITION - VERTICAL		X
MAIN ROTOR HUB VERTICAL ACCELERATION		X
RIGHT HAND TRANSMISSION LATERAL ACCELERATION		X
FORWARD TRANSMISSION F/A ACCELERATION		X
90 DEGREE GEARBOX VERTICAL ACCELERATION		X
90 DEGREE GEARBOX LATERAL ACCELERATION		X
ELEVATOR CENTERLINE VERTICAL ACCELERATION		X
ELEVATOR CENTERLINE LATERAL ACCELERATION		X
CG F/A ACCELERATION		X

for on-line monitoring of the one track of data (13 channels) that was considered the most critical for safety of flight. Additional flight instruments were added to the instrument panel for control position indication and load factor meter for maneuvers. These instruments are shown in Figure 46.

PROCEDURE

Ground runs and flight runs were performed to evaluate ground and air resonance, isolation system performance, handling qualities, and demonstration rides. A flight log of all runs is given in Table VIII.

Ground Run

The ground run was performed to verify that the aircraft would be free from any aeromechanical instability throughout all operational conditions on the ground. For this test the following procedure was followed to determine stability margins. For each rpm tested, the following sequence of excitations of the rotor was performed starting at flat pitch:

a. A longitudinal pulse at the cyclic stick.

b. A lateral pulse at the cyclic stick.

c. A counterclockwise stir of the cyclic stick at the best frequency to excite the first in-plane rotor mode.

d. An increase in collective to 40% and a repetition of steps 1 through 3.

Each record was analyzed by a complex exponential solution algorithm in Bell's VIBRATEC Data Analysis System to determine the rotor response frequency and the percentage of critical damping from the yoke chord bending strain gage.

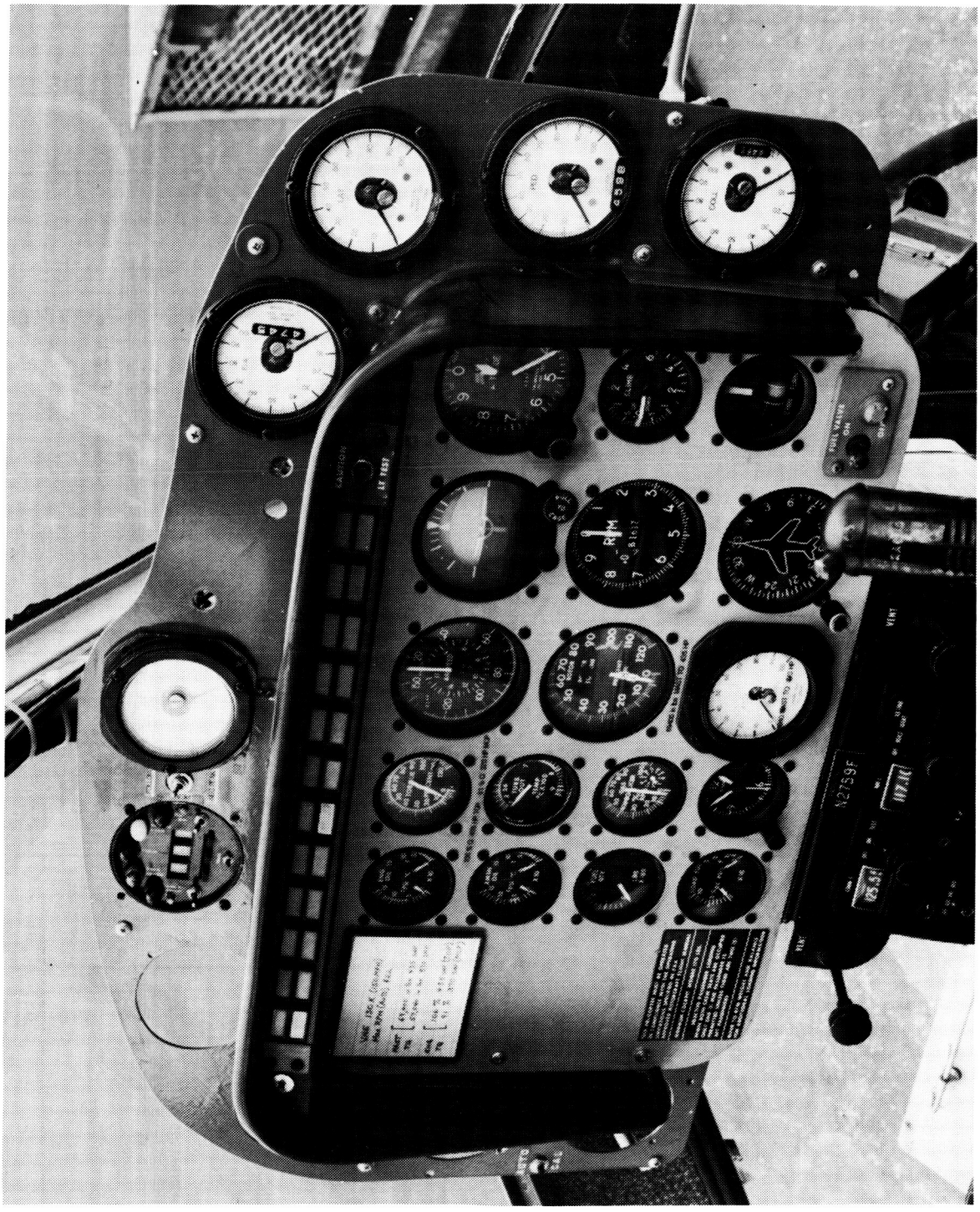

Figure 46. Flight Test Instrument Panel

Table VIII. Log of Flights

G.R. NO.	FLIGHT NO.	1985 DATE	TIME (HR)	G.W. (LB)	C.G. STA.	PURPOSE
1		6-26	0.6	3448	124.9	Initial G.R. Begin Ground Resonance Investigation
2A		6-27	1.0	3400	124.5	Continue Ground Resonance Evaluation
2B		6-27	0.6	3400	124.5	Complete Ground Resonance Evaluation
2C		6-27	0.5	3400	124.5	Main Rotor Balance
	1	6-28	0.9	3448	124.9	Begin Air Resonance Evaluation
	2A	7-16	0.8	3523	123.7	Continue Air Resonance thru 130 Knots V_{Cal}
	2B-2F	7-16	1.0	3523	123.7	Main Rotor Track and Balance
	3A	7-17	0.6	3523	123.7	Airspeed Calibration
	3B	7-17	0.6	3523	123.7	Vibration Survey - Level Flight Sweeps
	4A	7-18	0.2	3523	123.7	Hover Step Inputs to Verify Rotor Phasing
	4B	7-18	0.8	3523	123.7	Envelope Expansion thru 130 Knots/2.5 g turns/Boost-off Evaluation
	4C	7-18	1.0	3523	123.7	Demonstration of Flying Qualities to Chief Experimental Pilot
	5A	7-19	0.8	3523	123.7	IGE Sideward/Rearward Flight for Vibrations and Handling Qualities
	5B	7-19	0.8	3523	123.7	Power vs Control Positions at Constant Airspeed/Static Longitudinal Stability
	6A	7-22	0.8	3523	123.7	Install and Test 206-001-526-1 R/H Bellcrank. Static Longitudinal Stability, Apparent Speed Stability. Control Position vs Power at Constant Airspeed.
	6B	7-22	0.8	3523	123.66	Demonstration Flight to Chief Pilot
	6C	7-22	0.4	3523	123.66	Vibration Survey Speed Sweeps
	7A	7-23	0.7	3523	123.66	Removed 206-801-301 Cyclic Bellcrank. Installed Standard 206 Cyclic Bellcrank. Static Longitudinal Stability. Power vs Control Positions at Constant Airspeed.
	7B	7-23	0.4	4100	123.4	IGE Low Speed Vibration Data at Heavier GW

Table VIII. Log of Flights (Continued)

G.R. NO.	FLIGHT NO.	1985 DATE	TIME (HR)	G.W. (LB)	C.G. STA.	PURPOSE
	8A	7-24	1.1	4100	123.4	Loads and Vibrations, Turns to 2.5 g's, Airspeeds to 130 V_{Cal}
	8B	7-24	0.8	3000	127.4	Loads and Vibrations, Turns to 2.5 g's, Airspeeds to 130 V_{Cal}
	8C	7-24	0.7	4100	121.0	Loads and Vibrations, Turns to 2.5 g's, Airspeeds to 130 V_{Cal}
	8D	7-24	2.4	3500	123.6	Prepare Aircraft for Demonstrations
	9A	7-25	0.7	4100	121.0	Repeat of Flight 8C Due to Instrumentation Failure
	9B-10B	7/25-26		3500	123.6	Demonstration Flights to Program Engineers and Pilots
	11A	8-13	0.5	4100	121.0	Instrumentation Shakedown Following Instrumentation Buildup for Dynamic Handling Qualities Evaluation
	11B	8-13	1.3	4100	121.0	Step Inputs (100 Knots V_{Cal} and Hover)
	12A	8-14	1.0	4100	121.0	Step Inputs (Cyclic and Pedals) Hover, 60 Knots, 100 Knots V_{Cal} Level Flight
	12B	8-14	1.0	4100	121.0	Control Pulses (Cyclic and Pedals) 60 Knots, 100 Knots, Level, Climbs, Descents
	13A	8-15	1.1	3450	128.0	Static Longitudinal Stability (0.9 VH Trim, 60 Knots Trim)
	13B	8-15	1.2	3500	128.0	Step Inputs (Cyclic and Pedals) Hover, Level Flight, Climbs, Descents
	13C	8-15	0.5	3500	128.0	Rough Air Handling Qualities Evaluation
	14-15	8/20-21	3.0	3500	123.0	Demonstration Flights
	16A	8/23	0.9	4100	121.0	Hover Step Inputs. Static Lateral Directional Stability
	16B	8/23	0.8	3500	127.5	Hover Step Inputs. Static Lateral Directional Stability

Air Stability

At the completion of the ground stability testing no test conditions were found that exhibited damping of less than 3.4% critical. After reviewing the data, a safety of flight release was granted and the air stability testing commenced. The aircraft was ballasted to 3500 lb GW and neutral cg for the initial air resonance testing. A similar test procedure to the ground resonance tests was followed for the air resonance testing, and listed below, starting in hover.

a. Excite the rotor with a longitudinal cyclic pulse.

b. Excite the rotor with a lateral cyclic pulse.

c. Excite the rotor at its first inplane natural frequency with a counterclockwise cyclic stir.

d. Repeat step c with a higher magnitude input.

If the rotor response showed over 2% critical damping in steps a through c and greater damping with the higher magnitude input of step d, then the airspeed was increased 10 kn and steps a through d were repeated.

This process was repeated until V_{ne} airspeed was achieved. During each step of this testing, the critical track of data was telemetered to the Ground Data Center and monitored on-line for either load or stability problems. Bell's Data Analysis Computer Program VIBRATEC was used to monitor the rotor stability. This program enabled the test director to determine the percentage of critical damping in the rotor system within approximately 10 seconds of the completion of each record, and progress to the next condition with very little delay. At the completion of the airspeed sweep to Vne, various maneuvers were investigated using the same procedure. These maneuvers included: right and left turns to 2.5g at 60, 100, and 120 kn; autorotation at 60 and 80 kn; max power climbs at 60, 80, and 100 kn; and pushovers and pullups at 60, 80, and

100 kn. At the completion of these tests, there were no flight conditions found that exhibited less than 4% critical damping. Therefore, the instrumentation was changed from the safety of flight instrumentation to the isolation system performance list shown in Table VII , Column 2.

Isolation System Performance Flights

To determine the performance of the isolation system, the list of flight conditions shown in Table IX was flown for the following gross-weight/cg combinations:

Gross Weight	Center of Gravity
3,500	124
4,100	121
3,000	127
4,100	124

Figure 47 shows the gross weight, center of gravity envelope for the 206LM and the relationship of the flight conditions flown to the allowable GW/cg envelope. From Table VIII, flights 6C, 8A, 8B, and 9A were the flight conditions flown for the isolator performance investigation.

FLIGHT TEST RESULTS

The results of the flight test have been presented in a number of formats. Plots of 4/rev vibration level vs. airspeed for each seat and main rotor hub accelerometer are presented in Figure B1 of Appendix B. These plots include hover and dive flight conditions. Plots of 4/rev vibration level for forward, rearward, right sideward, and left sideward flight up to 30 kn are presented in Figure B2 . Plots of 4/rev vibration levels vs mean cg g's for right and left turns, pushups and pushovers are presented in Figures B3 through B5.

These data show that for all GW/cg loadings, the pilot and copilot seat

Table IX. Flight Conditions Flown for the Vibration Performance Flights

FLIGHT CONDITION	AIRSPEED	G's
HOVER	0	1.0
LEVEL FLIGHT (PACED ON RUNWAY)	5	1.0
LEVEL FLIGHT (PACED ON RUNWAY)	10	1.0
LEVEL FLIGHT (PACED ON RUNWAY)	15	1.0
LEVEL FLIGHT (PACED ON RUNWAY)	20	1.0
LEVEL FLIGHT (PACED ON RUNWAY)	25	1.0
LEVEL FLIGHT (PACED ON RUNWAY)	30	1.0
LEVEL FLIGHT (1500 FT. ALT.)	40	1.0
LEVEL FLIGHT (1500 FT. ALT.)	50	1.0
LEVEL FLIGHT (1500 FT. ALT.)	60	1.0
LEVEL FLIGHT (1500 FT. ALT.)	70	1.0
LEVEL FLIGHT (1500 FT. ALT.)	80	1.0
LEVEL FLIGHT (1500 FT. ALT.)	90	1.0
LEVEL FLIGHT (1500 FT. ALT.)	100	1.0
LEVEL FLIGHT (1500 FT. ALT.)	110	1.0
LEVEL FLIGHT (1500 FT. ALT.)	120	1.0
LEVEL FLIGHT (1500 FT. ALT.)	V_H	1.0
LEVEL FLIGHT (1500 FT. ALT.)	V_{NE}	1.0
TURNS (RIGHT AND LEFT)	60	1.5
TURNS (RIGHT AND LEFT)	60	2.0
TURNS (RIGHT AND LEFT)	60	2.5
TURNS (RIGHT AND LEFT)	95	1.5
TURNS (RIGHT AND LEFT)	95	2.0
TURNS (RIGHT AND LEFT)	95	2.5
TURNS (RIGHT AND LEFT)	V_H	1.5
TURNS (RIGHT AND LEFT)	V_H	2.0
TURNS (RIGHT AND LEFT)	V_H	2.5
PULLUP	V_{NE}	1.5
PULLUP	V_{NE}	2.0
PUSHOVER	95	0.5
PUSHOVER	95	0.75
AUTOROTATION	60	1.0
AUTOROTATION	80	1.0

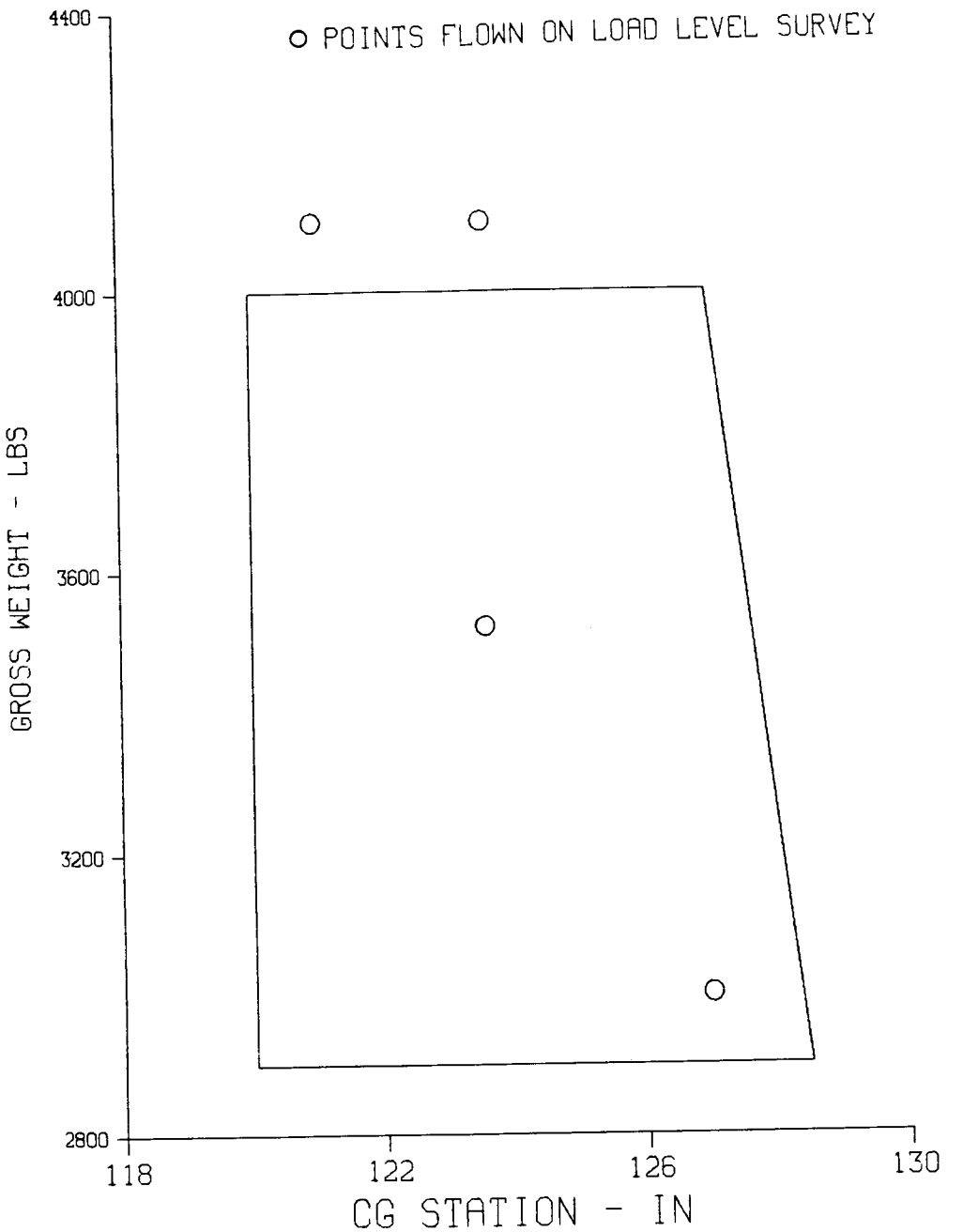

Figure 47. Model 206LM Center of Gravity-Gross Weight Envelope

4/rev vibration levels in the transition region (15 to 25 kn), which is traditionally the highest vibration level, did not exceed 0.056g in any direction.

Similarly, the aft seats show no 4/rev levels above 0.10g. A comparison of the hub 4/rev levels (Figure B1) shows that the highest rotor input vibration levels are in the transition region, and that the highest 4/rev cabin levels are at high speed. This effect is explained later in this section.

The plots of 4/rev vibration level vs cg mean g's for the maneuvers show essentially the same levels at different mean g's as are achieved at 1.0 g, except when the maneuver approaches 2.5g's. The isolation system was originally designed for -0.5g to 3.0g's. However, during the final turning phase of the individual isolators (Reference 1), the spring rate of the isolators had to be reduced to achieve optimum tuning. This spring rate reduction resulted in two isolators bottoming at approximately 2.5g's instead of 3.0g's as initially designed. The two isolators that bottom out at 2.5g's are the right forward and left aft units. These two units bottom as a result of the combination of torque and lift, which adds a steady strain in the same direction on these two isolators. Torque subtracts from lift on the right aft and left forward isolators. The result of this bottoming at 2.5g's is an increase in vibration levels in the cabin up to 0.17g at the aft seat fore-and-aft accelerometer. Although these vibration levels were high enough to be perceived by the crew, the levels were still significantly below the levels on the baseline helicopter. Additionally, this bottoming resulted in no audible sounds to the crew and only by detailed investigation of the data after the flight test was completed was this bottoming detected.

The TRIS proof-of-concept vibration surveys demonstrated a significant improvement in ride quality throughout the flight envelope investigated. Favorable comments were received from all who flew or rode in the aircraft.

Non-Main Rotor Hub Induced Vibration

Due to the nature of the helicopter, there are other sources of main rotor 4/rev besides the main rotor hub loads. These other sources include: main rotor downwash on the cabin roof, elevator and tail boom causing vertical vibration, and rotor downwash on the elevator endplates, vertical fin, and tail rotor disc causing lateral vibration.

In order to determine the true performance of the pylon isolation system in a flight test program, it is necessary to separate the cabin vibration level produced by the main rotor hub loads from the vibration produced from these other sources. This is a difficult task and is beyond the scope of this project. However, careful study of the shake test and flight test data reveals a reliable conclusion as to the magnitude and effect of the other sources.

By comparing the level flight airspeed plots (Figure B1) it can be seen that the three main rotor hub vibration levels all peak at approximately 20 kn during transitional flight. The hub vibration levels are 3 to 4 times the levels at the maximum level flight airspeed. Since the transfer functions from shake test show that the cabin vibration levels are all much less than 10% of the hub g's for all 6 degrees-of-freedom, it would follow that this relationship would hold true also in flight test. This does hold true in transitional flight where the hub vibration levels are over 1.0g in all directions and all the cabin seat accelerometers are under 0.1g, showing better than 90% isolation. At 20 kn, the aircraft is not moving fast enough to cause rotor downwash to impinge on the fin and tailrotor. Therefore, very little additional cabin vibration is produced from airloads on the tail. However, this is not true at high speed.

An examination of the V_H and V_{ne} data show that although the hub vibration levels are much lower at high speed than at 20 kn, this is not true with the cabin vibration levels. A review of the 90° gearbox vertical and lateral accelerometers (Figure B1) show the cause of this effect. The 90°

gearbox accelerometers show a sudden increase in main rotor 4/rev vibration levels starting at about 120 kn, increasing to over 0.5g vertical and almost 1.0g lateral. This sudden increase in vibration level is caused by main rotor downwash on the elevator, tailrotor and fin. The sudden increase in the 90° gearbox lateral causes the pilot seat lateral acceleration to increase proportionally and the increase in the 90° gearbox vertical causes the cabin vertical accelerometers to increase. Since there are no downwash effects that cause F/A vibration, the cabin cg F/A acceleration responds directly and proportionally to the main rotor hub accelerations through the isolation system.

Isolation System Performance

It can be seen from the analysis above that the isolation system performance during flight test can only be directly determined in the transition airspeed region where 4/rev excitations from other sources are small, since the cabin vibrations are dominated at high speed by excitations from sources other than the pylon isolation system.

In the transition region (shown in the airspeed sweep plots, Figure B1 and the rearward and sideward flight plots, Figure B2), it can be seen that all the crew accelerometers are below 0.05g for all GW/cg's flown showing over 95% isolation. For the same conditions, the aft seats are below 0.10g, showing approximately 90% isolation.

Handling Qualities

During the initial test flight with the six degree-of-freedom configured aircraft, the pilot reported significantly improved handling characteristics in the TRIS configured Model 206LM compared with any previous Model 206LM configuration. The improvement in handling characteristics was due in part to the standard Model 206L-1 focused pylon flight controls installation, which differed from the previous 206LM coupled main rotor control installation. Quantitative handling qualities information was acquired under separate IR&D

funding in an attempt to document the excellent handling characteristics of this light four-bladed configured helicopter. Following completion of the TRIS contracted effort vibration survey flights, additional testing was begun for purposes of acquiring static and dynamic handling qualities data.

Handling qualities evaluations were conducted at both heavy gross weight/forward cg and light gross weight/aft cg. Cyclic and pedal step inputs and pulses were both conducted during level flight (at 60 and 100 knots), descents (60 knots), and climbs (60 knots). In addition, step inputs were conducted in hover. Static lateral directional stability was quantified in level flight (60 and 100 knots). The aircraft static longitudinal stability was conducted with trim airspeeds of 106 knots in level flight and 60 knots in climb and autorotation.

Handling qualities of the 206LM helicopter, serial number 45269, as configured during the TRIS program were excellent. This improvement compared to previous 206LM configurations is due in part to the fixed control geometry of the cyclic and collective controls as they relate to the TRIS pylon motion.

Aircraft response to control step inputs and pulses reflected neutral to slightly positive damping of the longitudinal phugoid at 100 knots and time to double amplitude in excess of 20 seconds at 60 knots at aft cg/light gross weight. Lateral aircraft response to step inputs was generally a slow rolling spiral. Static longitudinal and static lateral directional stick gradients were slightly positive at aft cg. Dihedral was slighty positive at aft cg as well.

The TRIS proof-of-concept demonstration was an excellent example of a light four-bladed helicopter with low vibration levels and improved handling qualities. Although the reasons for the reduced vibration levels are understood, the reasons for the improved handling qualities are not fully understood. The mechanics of the improved handling qualities should be pursued for purposes of applying the technology to current model helicopters. The TRIS flight test program demonstrated that a non-SCAS four-blade

helicopter with IFR handling qualities and low vibration levels is within existing technology.

BASELINE HELICOPTER COMPARISON

A comparison between the TRIS installed helicopter and the same helicopter with its baseline isolation system installed was performed. It should be understood that the latest configuration of the baseline helicopter had a softly sprung (soft rubber springs) pylon isolation system called SAVITAD (Reference 2) that was developed in the late 1970s to achieve a good ride quality. Tests of this soft system are shown in Figures B6 and B7.

A comparison of the data from both the soft system flights and the TRIS data in the low speed transition region (where cabin vibration is not influenced by rotor downwash on the empennage surfaces) shows that the TRIS approach reduces vibration by a factor of 3 or more over the SAVITAD System.

The high speed cabin vibration data of the SAVITAD system shows the same effect of the rotor downwash on the fin, elevator, and tail rotor as was shown with the TRIS System. Both systems show that the higher vibration levels at V_H are dominated by rotor downwash effects and not hub loads.

By comparing the transition airspeed region shown in Figure B2 for the TRIS installation and Figure B7 for the baseline configuration, it can be seen that the greatest improvement in ride achieved by the TRIS installation occurs at the airspeed that produces the highest hub loads. For example, the pilot seat lateral vibration levels for rearward flight at 20 kn are reduced from 0.24g on the baseline aircraft to only 0.023g on the TRIS installation. Similar reductions are seen in the copilots seat data. The aft seat vibration levels are not reduced as dramatically, but still they are reduced by a factor of two.

Comparison to Focal Pylon

Many BHTI helicopters incorporate a Focal Pylon (Reference 3) isolation system to achieve isolation of inplane rotor hub loads; therefore, a second comparison was also made to the baseline helicopter when it was first flown with a Focal Pylon isolation system. The Focal Pylon installation only isolates hub pitch and roll moments and does not isolate vertical hub shears at all.

Although limited test data were available, a comparison between the Focal Pylon isolation system (two degrees-of-freedom) and the TRIS installation (six degrees-of-freedom) shows the real potential of total rotor isolations. Figure B8 shows the comparison at the pilot seat vertical, and the comparison of the right aft seat vertical. These comparisons show a reduction at 20 kn of 77% at the pilot seat and 67% at the right aft seat.

RELIABILITY AND MAINTAINABILITY ANALYSIS

The baseline for the reliability and maintainability analysis was an imaginary rigid link mount between the transmission case and the helicopter roof mounting plane. The reliability of the LIVE isolation system was then calculated and compared to this baseline rigid mount.

The analysis was hindered by the following limitations:

a. There were no field data available on the LIVE system.

b. There were only limited data available on the Model 206LM flight test helicopter.

c. There were no production isolators available for analysis. Test unit design drawings were used, in conjunction with verbal descriptions of what the production unit would look like.

The prediction was therefore tested against standard designs as a comparison check to ensure validity of the results and to guide the accuracy of the starting assumptions.

Methodology

A top-down approach was used to obtain the overall system reliability prediction. Several helicopter models were examined to determine what correlation existed between failure rates, maintenance man-hours per flight-hour (MMH/FH), and rotor head type (semirigid or fully articulated). The results are shown in Table X.

TABLE X. COMPARISON OF SYSTEM RELIABILITY OF DIFFERENT HELICOPTER MODELS

	Max Weight	Pylon Isolation		Total - Main Rotor	
Model	(lb)	Failure Rate	MMH/FH	Failure Rate	MMH/FH
CH-53E	69,700	N/A	N/A	138,179	1.616
CH-53D	40,174	N/A	N/A	58,909	1.597
CH-46D	21,000	N/A	N/A	63,432*	0.88
UH-1N	11,200	5,827	0.558	37,999	0.344
TH57A	3,200	399	0.00171	6,105	0.0222
TH57B	3,200	117	0.000438	3,073	0.008589
OH-58D†	4,500	637	0.000050	11,362	0.010353

*126,865÷2 for two main rotor systems.
†Prediction from Bell Report 406-949-111.
N/A - Not applicable on these aircraft

A bottom-up analysis using piece-part predictions previously used in a calculation of OH-58D reliability was utilized to determine reliability of the LIVE and rigid-mount systems. The results obtained were then compared to the system reliability prediction using a top-down approach as a test of the correlations. Details of the bottom-up analysis are presented in Table XI. Failure modes of the LIVE and solid link systems are listed in Table XII.

TABLE XI. BOTTOM-UP RELIABILITY ANALYSIS

Qty	Item	Failure Rate †
6	LIVE isolator	
	Outer cylinder	10
	Inner cylinder	12
	Inner/outer attaching bolts (2)	4
	Elastomer rubber insert	10
	Mercury fluid	10
	Attaching bearings (one at each end)	2
	Attaching nuts/bolts (one set at each end)	2
	Outer wrap bag	30
	Bag clamps (one at each end)	8
	Bag fluid detector windowglass (or comparable device)	40
		128
		6 × 128 = 768
9	Mounting brackets and hardware* (transmission and roof)	16
		784
	LIVE Isolator System: $\lambda = 784 \times 10^{-6}$	
6	Solid link mount	22
	Attaching bearings (2)	2
	Attaching hardware	2
		26
		6 × 26 = 156
9	Mounting brackets and hardware* (transmission and roof)	16
		172
	Solid Link Mounting System: $\lambda = 172 \times 10^{-6}$	

*Same for LIVE and solid link systems.
†Failures per million flight hours.

TABLE XII. FAILURE MODES

Item	Failure Mode
LIVE System	
Attaching bolts	Loose, missing
Elastomer rubber insert	Damaged by overheating, contamination, etc.
Inner/outer cylinder	Damaged by dents, cracks, breaking, etc.
Mercury fluid	Incorrect fluid level (overhaul or factory defect), fluid leak
Outer wrap (bag)	Damaged or deteriorated by ripping, contamination, drying out, etc.
Outer bag clamps	Loose, missing, damaged
Outer bag fluid detector	Broken, damaged, etc.
Mounting brackets	Broken, cracked, corroded, or otherwise damaged
Attaching bolts/bearings (mounting hardware)	Loose, missing
Solid Link System	
Links	Bent, broken, etc.
Attaching bearings & hardware	Loose, broken, etc.
Mounting brackets	Broken, cracked, corroded, or otherwise damaged

The MMH/FH for the two systems is as follows:

	Organizational	Depot
Solid link system	0.000038	-
LIVE isolator system	0.000450	0.000759

The organizational level for the LIVE system includes an allowance for rotor vibration isolation troubleshooting. The depot level covers maintenance to overhaul LIVE units. The result was $\lambda = 784 \times 10^{-6}$ for reliability of the LIVE isolation system and $\lambda = 172 \times 10^{-6}$ for the baseline rigid mount. The LIVE isolation system reliability prediction is fairly compatible with that for the state-of-the-art impedance controlled isolation system used on the OH-58D. The overall rotor head reliability is significantly better than a rigid-mounted, complex, fully articulated rotor system using hub absorbers to achieve a compatible low-vibration ride.

CONCLUSIONS

The following conclusions are apparent from the analysis of the ground vibration test and the flight test of the TRIS installation on the Model 206LM.

a. A six degree-of-freedom pylon isolation system can be made to isolate well over 90% of the main rotor hub loads.

b. The resulting levels of vibration at the crew stations (from the remaining percent of hub shears and moments that are not isolated) are below human perception levels.

c. With the TRIS installed, there are 4/rev vibration sources other than hub loads that dominate the resulting cabin 4/rev levels at high speed and they must be reduced before any additional reductions in cabin vibration levels can be achieved at these speeds.

d. The highest vibration levels at the crew stations during transitional flight measured less than 0.06g, and were imperceptible by the crew. Vibration criteria this low must be re-evaluated with respect to cost, weight, and mission efficiency.

e. This TRIS installation had a weight penalty of 69.57 lb, (see Reference 1) less than 1.7% of the maximum gross weight of 4100 lb. This installation was designed to be very adjustable and therefore much heavier than a production system need be. By manufacturing the LIVE units without adjustability and using light weight materials, (stainless steel was used for the test units) less than 1.0% weight penalty is easily achievable.

f. The objective of this program (6 degrees-of-freedom isolated over 90% in flight) has been met with the TRIS installation. However, the desired goal of less than 0.05g throughout the level flight envelope was not met due to other airframe excitations that dominate the vibrations at high speed.

g. By providing proper main rotor control coupling, a non-SCAS four-bladed helicopter with excellent handling qualities can be achieved.

h. Although yaw isolation was provided with the TRIS approach, analysis and laboratory tests indicate that on a helicopter with a torsionally soft mast an excellent ride could be obtained without yaw isolation.

APPENDIX A

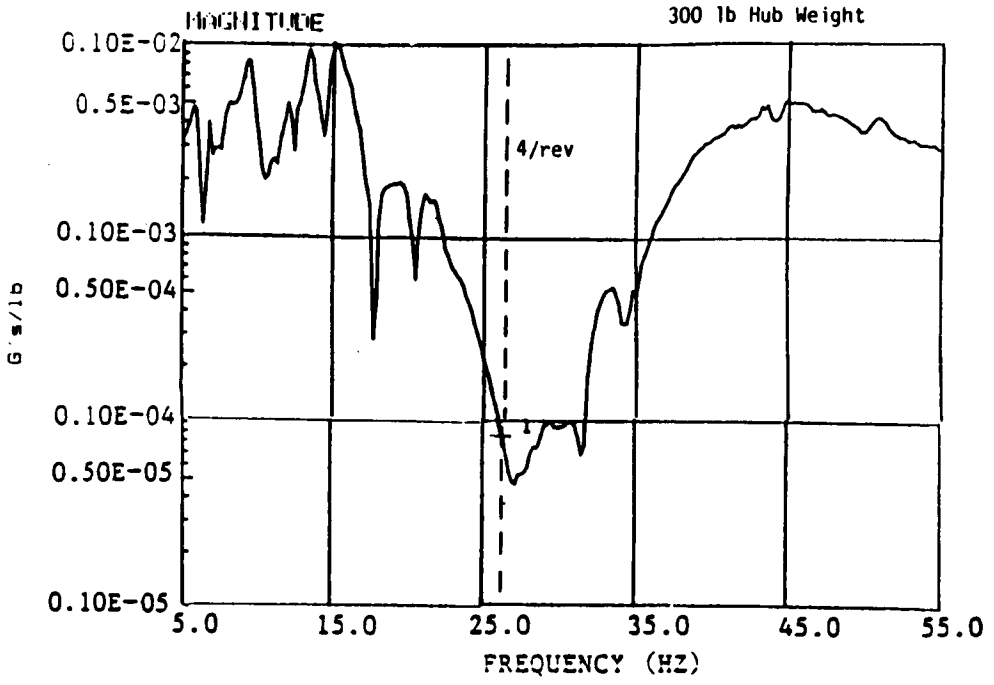

Figure A1. Pilot Seat Vertical Response to Vertical Shear Force

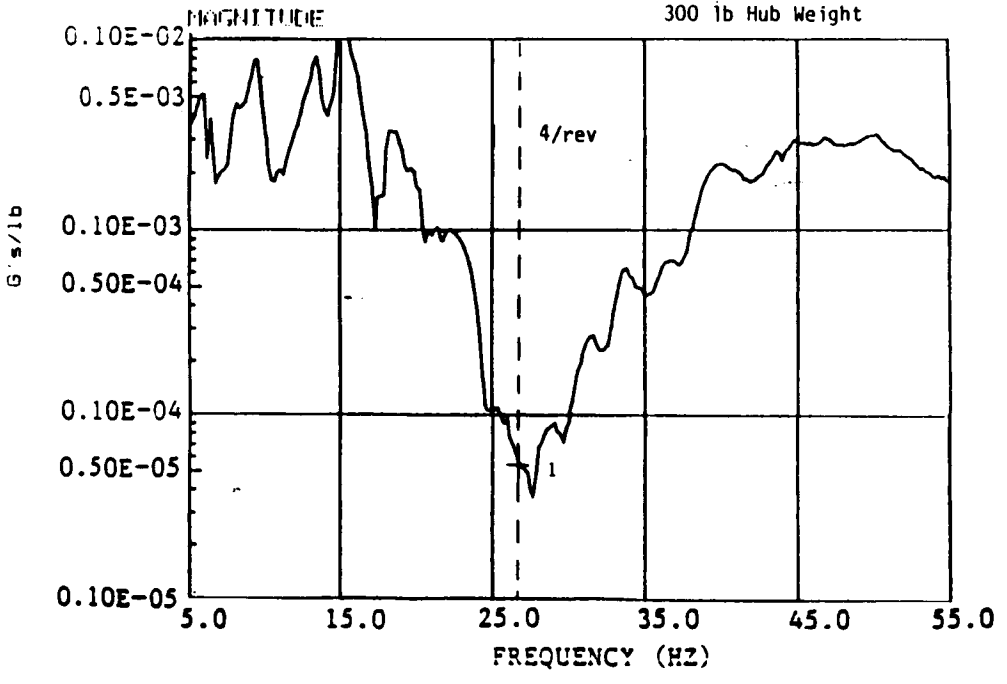

Figure A2. Co-pilot Seat Vertical Response to Vertical Shear Force

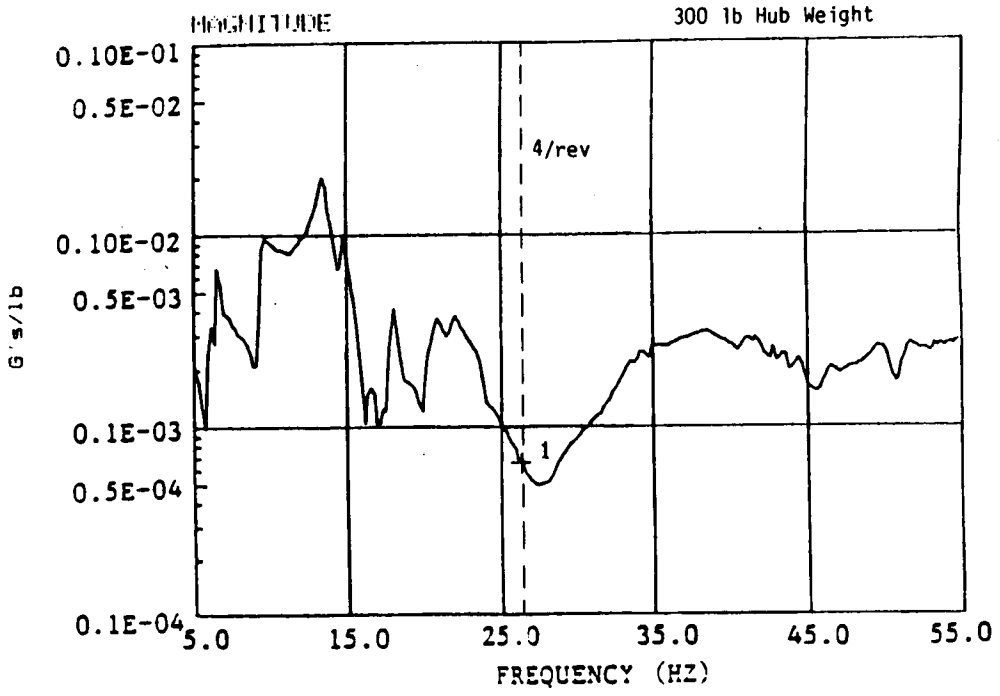

Figure A3. Right Aft Seat Back Vertical Response to Vertical Shear Force

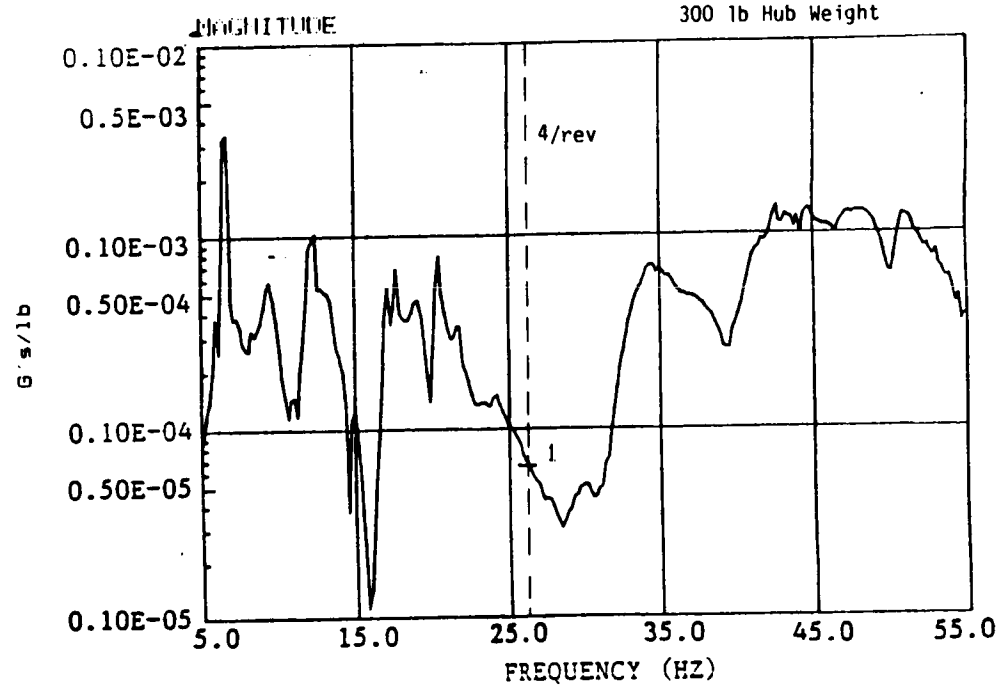

Figure A4. Right Aft Seat Back Lateral Response to Vertical Shear Force

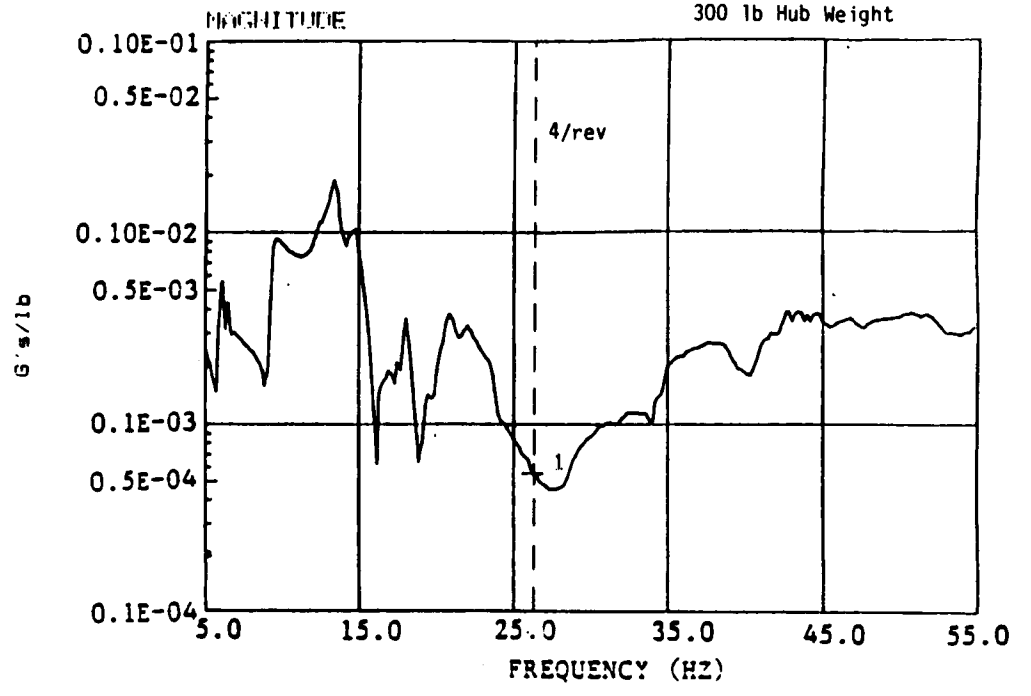

Figure A5. Left Aft Seat Back Vertical Response to Vertical Shear Force

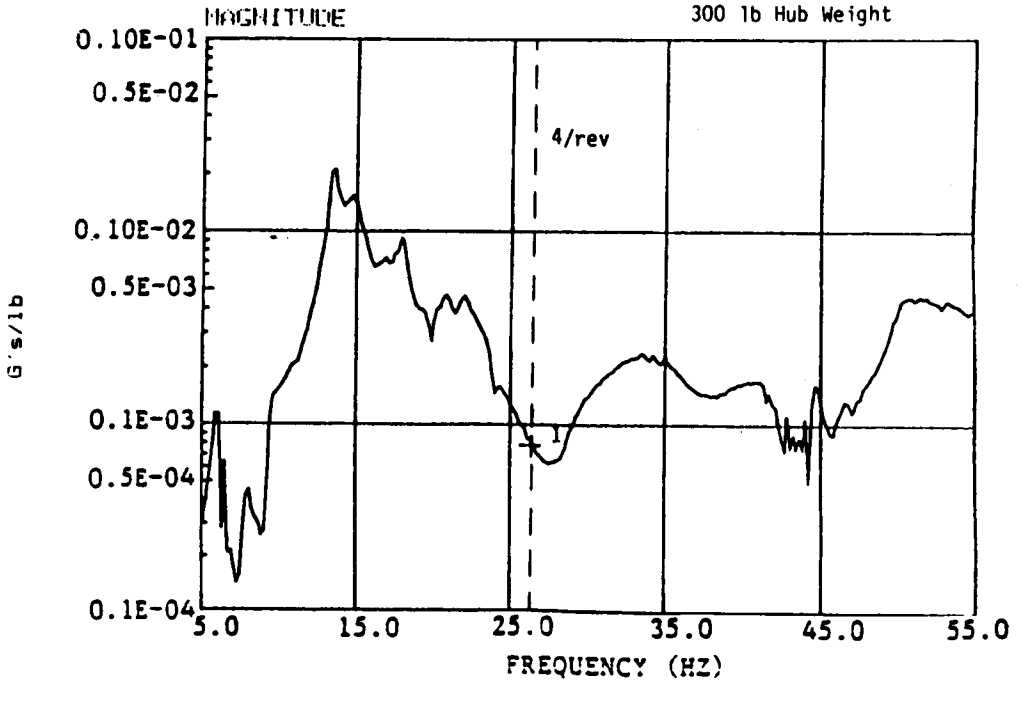

Figure A6. Left Aft Seat Back F/A Response to Vertical Shear Force

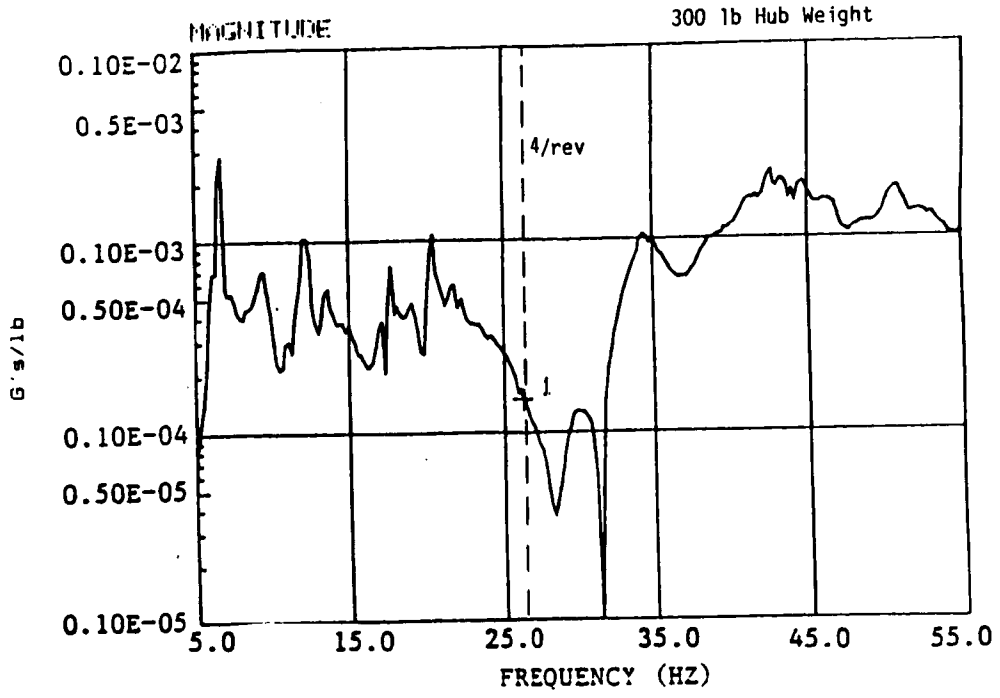

Figure A7. CG Lateral Response to Vertical Shear Force

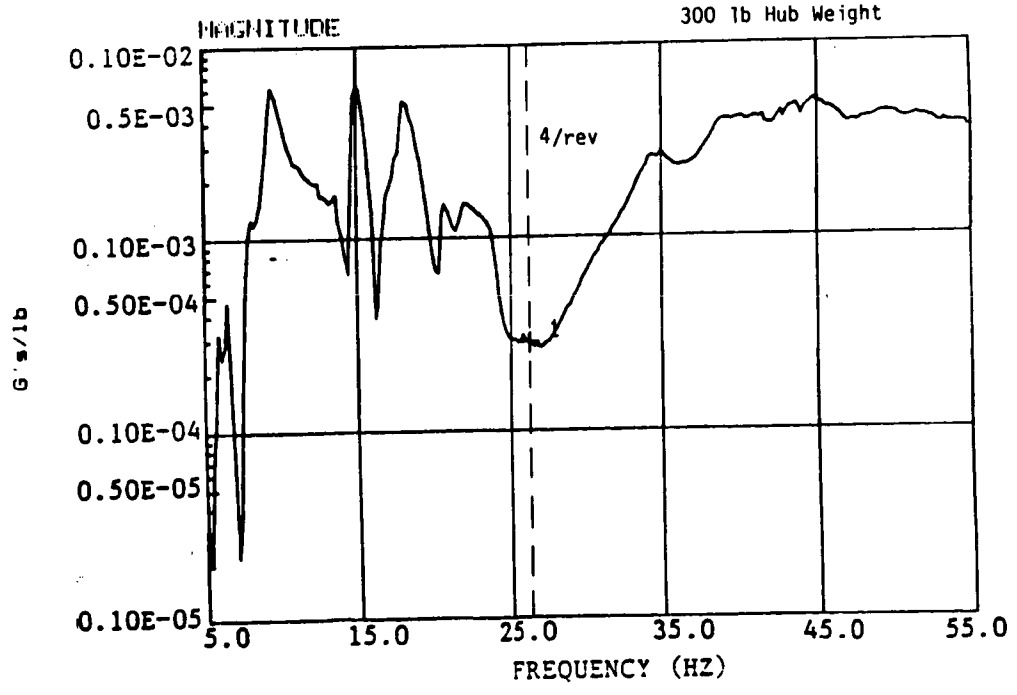

Figure A8. CG F/A Response to Vertical Shear Force

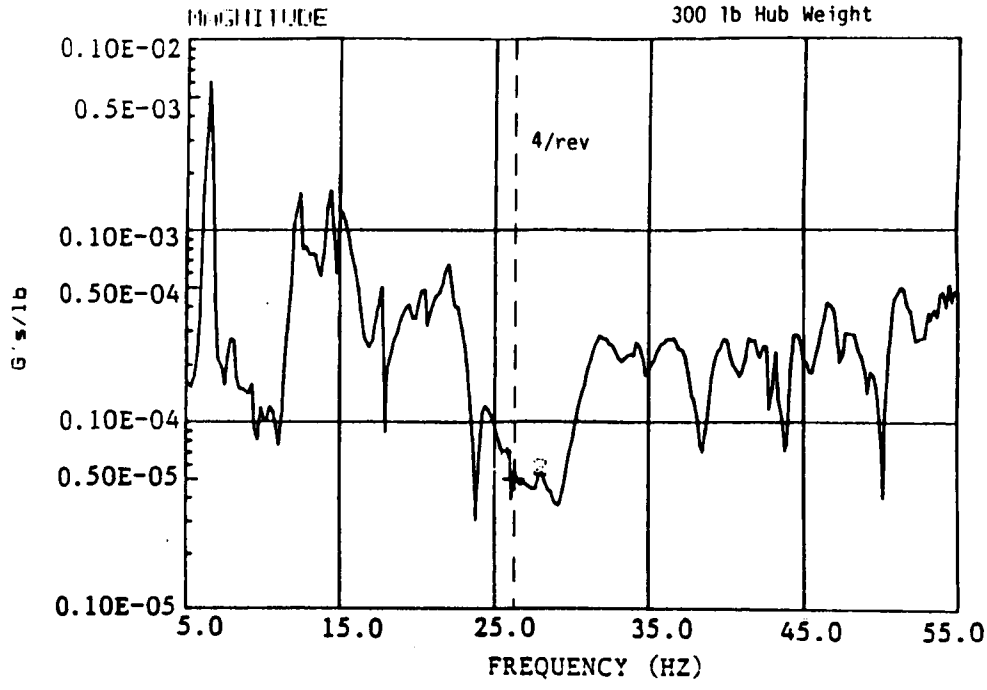

Figure A9. Pilot Seat Lateral Response to Vertical Shear Force

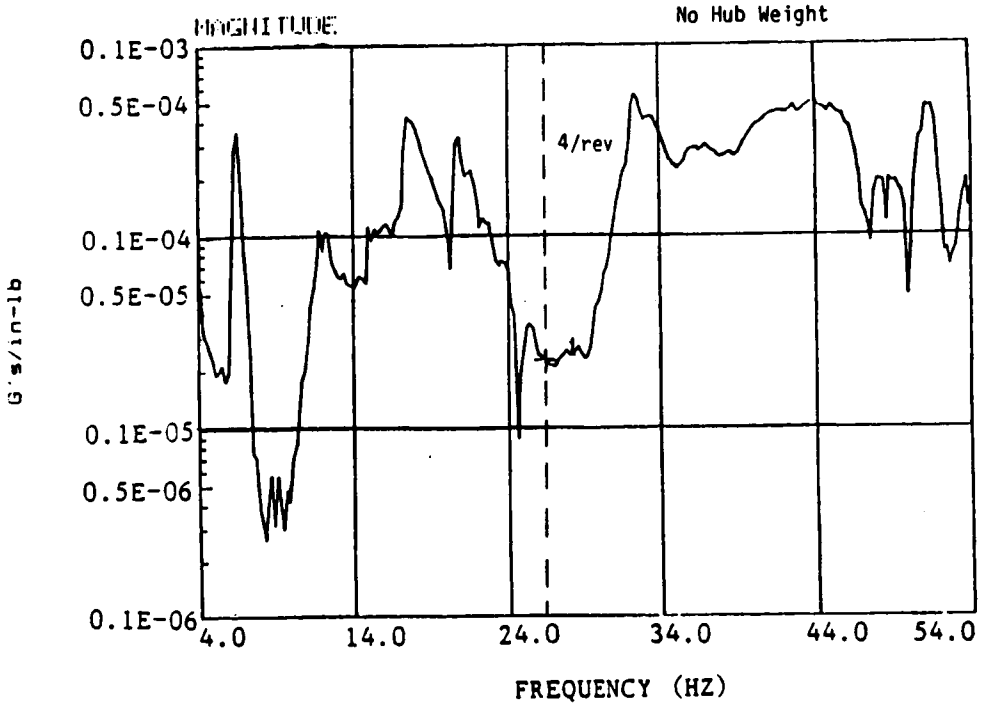

Figure A10. Pilot Seat Vertical Response to Yaw Moment

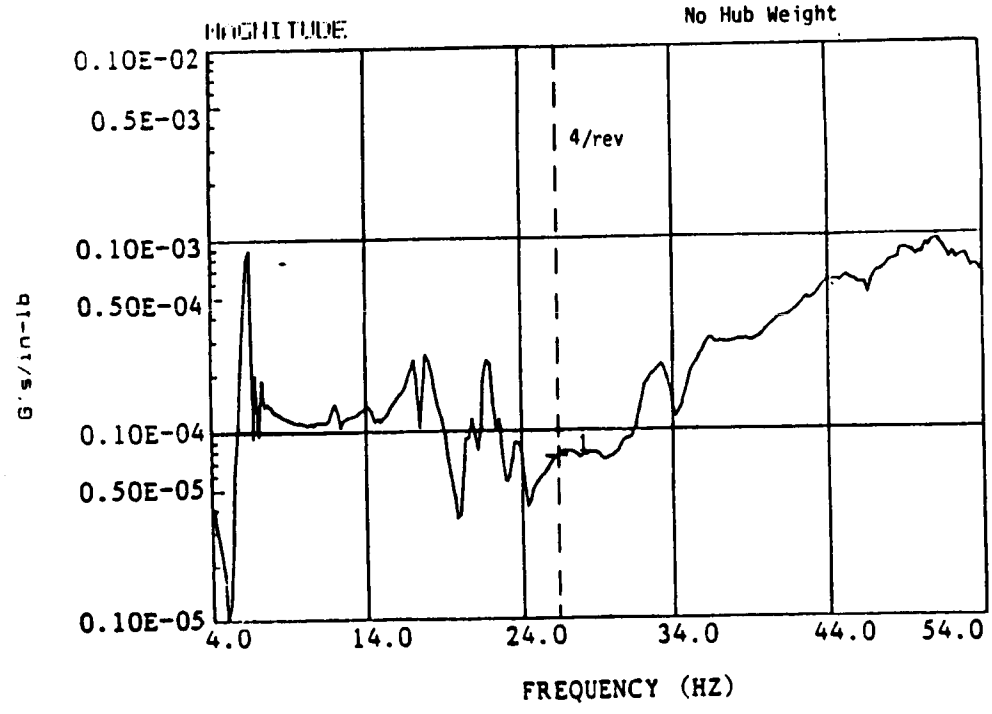

Figure A11. Pilot Seat Lateral Response to Yaw Moment

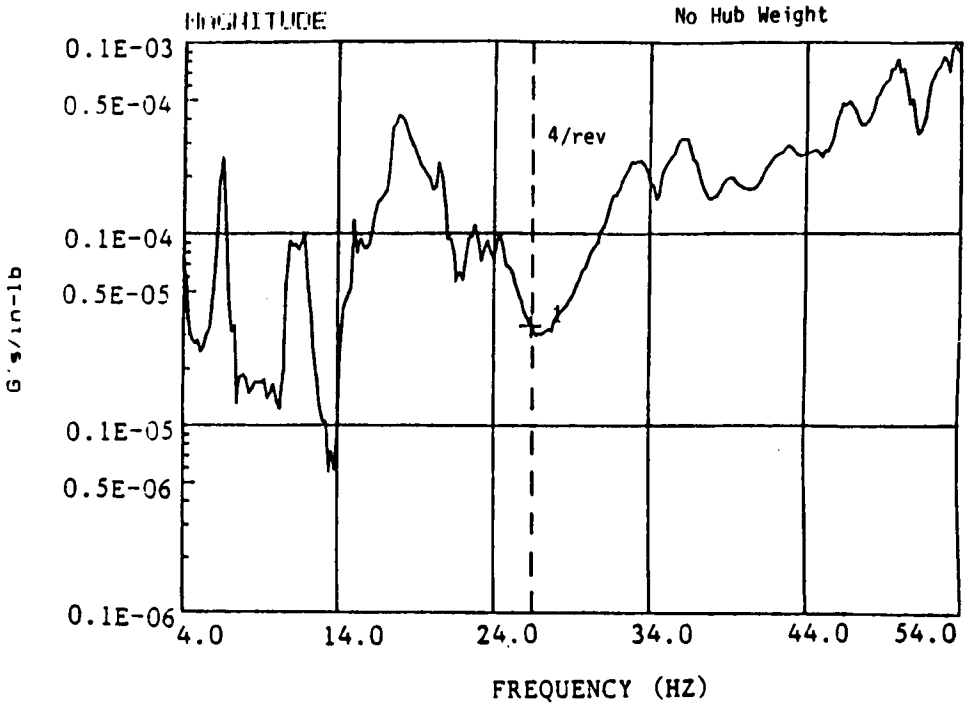

Figure A12. Right Aft Seat Back Vertical Response to Yaw Moment

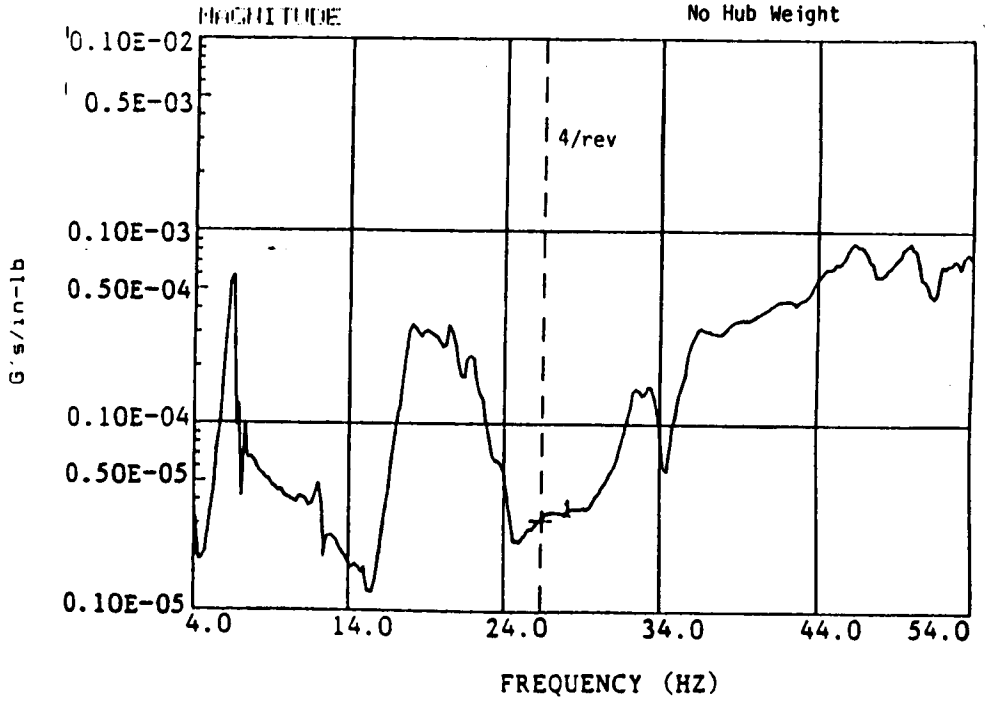

Figure A13. Right Aft Seat Back Lateral Response to Yaw Moment

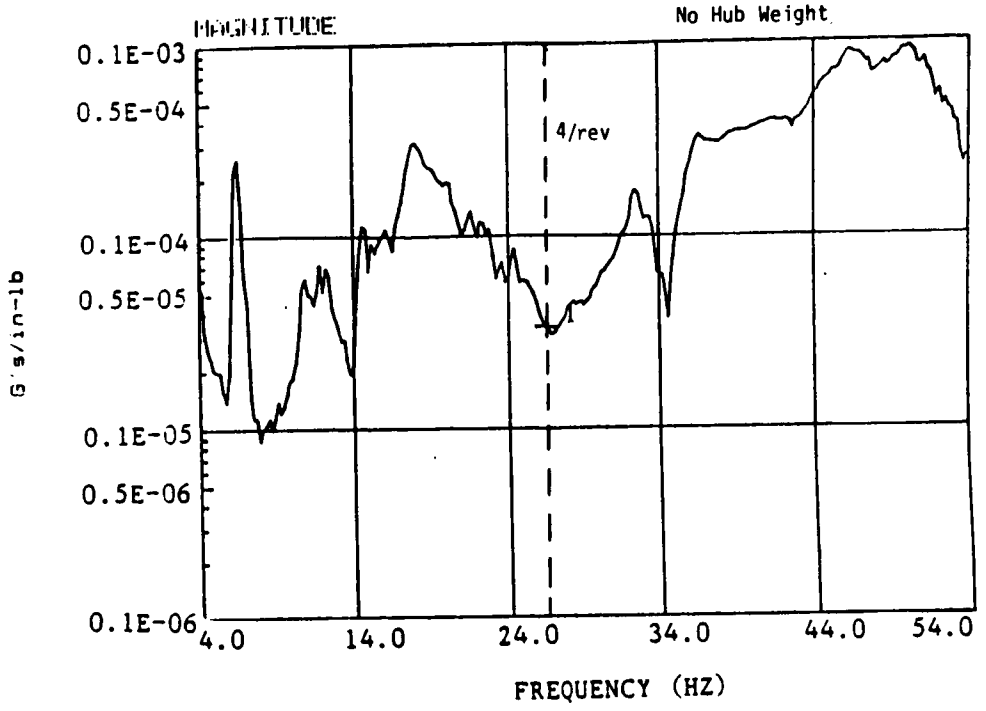

Figure A14. Left Aft Seat Back Vertical Response to Yaw Moment

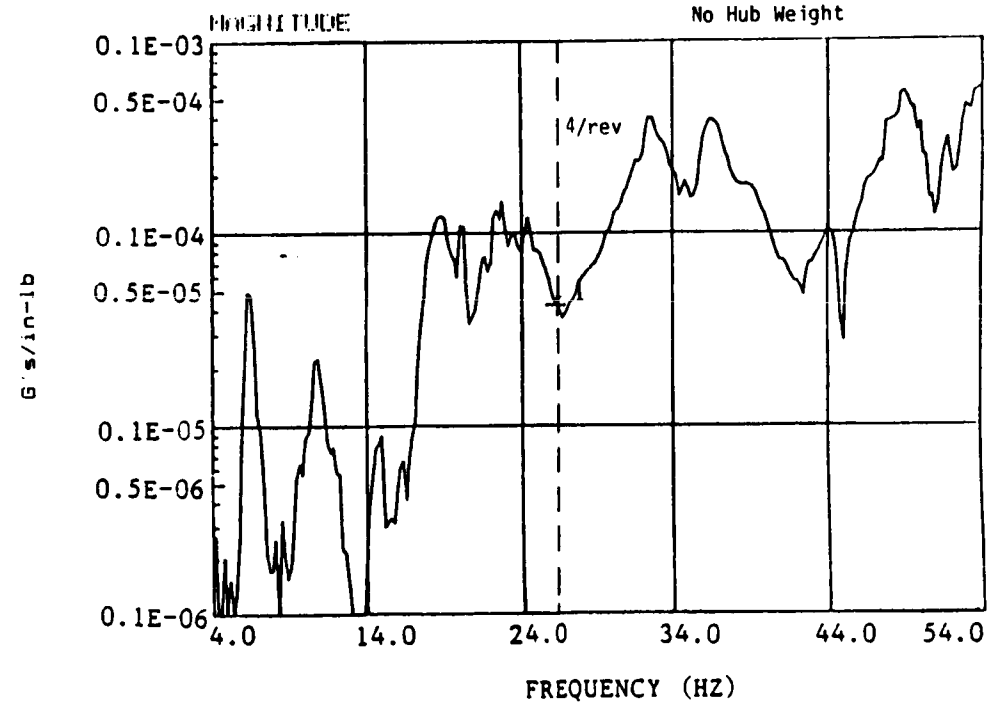

Figure A15. Left Aft Seat Back F/A Response to Yaw Moment

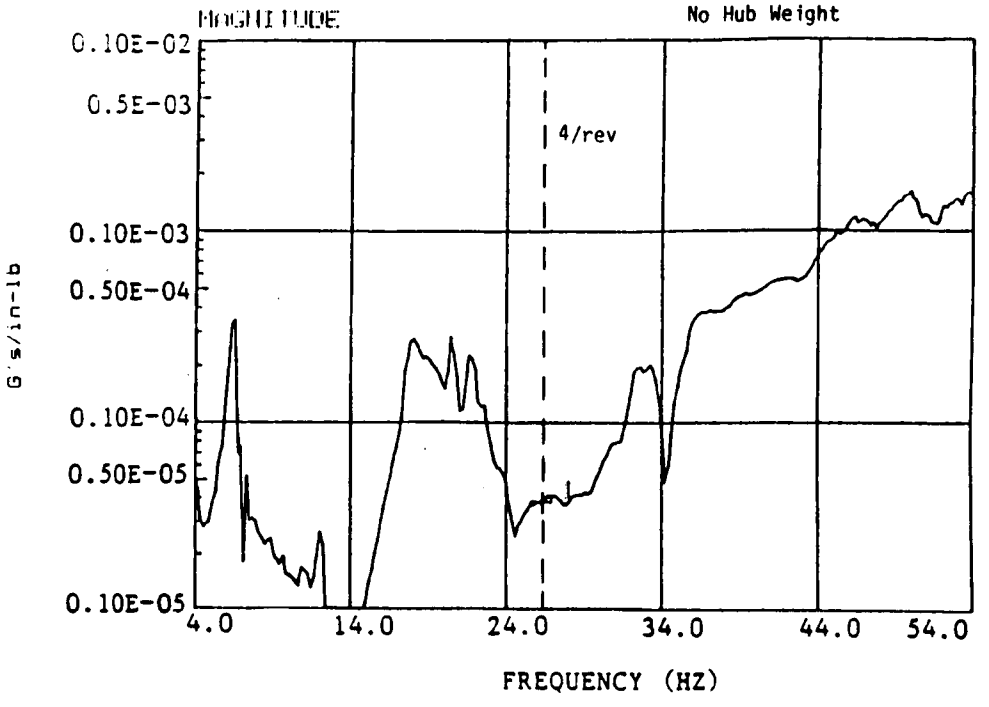

Figure A16. CG Lateral Response to Yaw Moment

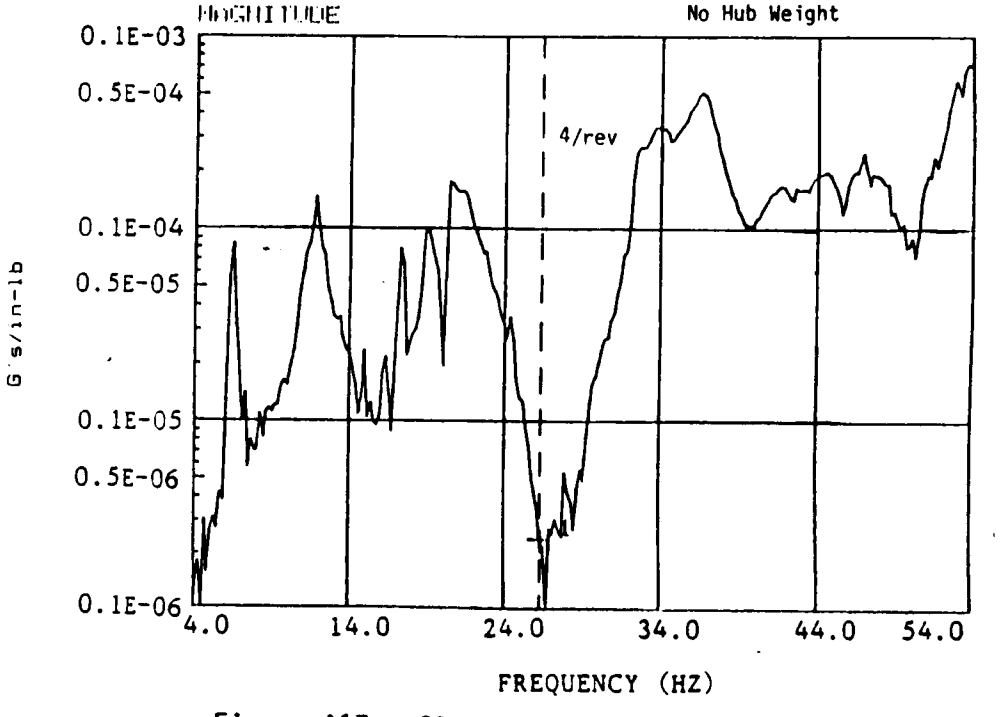

Figure A17. CG F/A Response to Yaw Moment

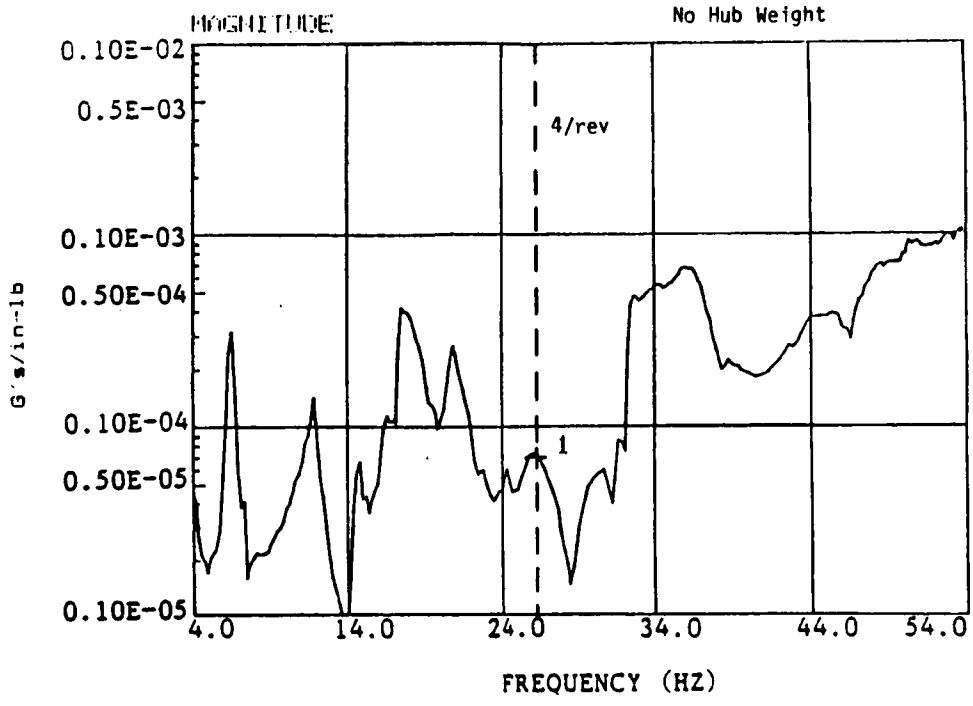

Figure A18. Co-pilot Seat Vertical Response to Yaw Moment

C-2

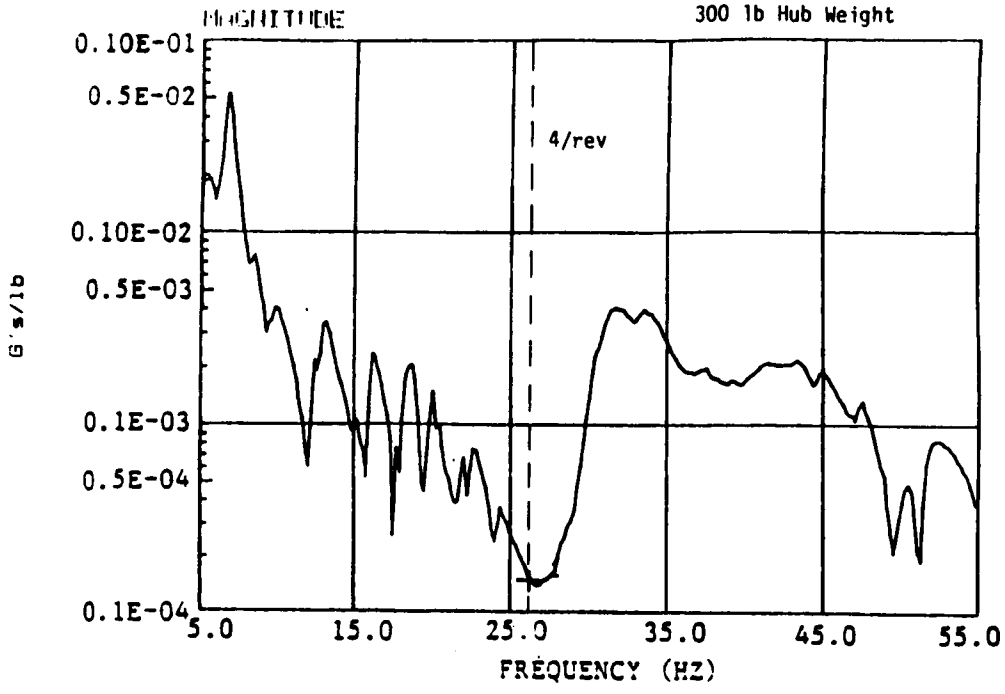

Figure A19. Pilot Seat Vertical Response to Longitudinal Shear Force

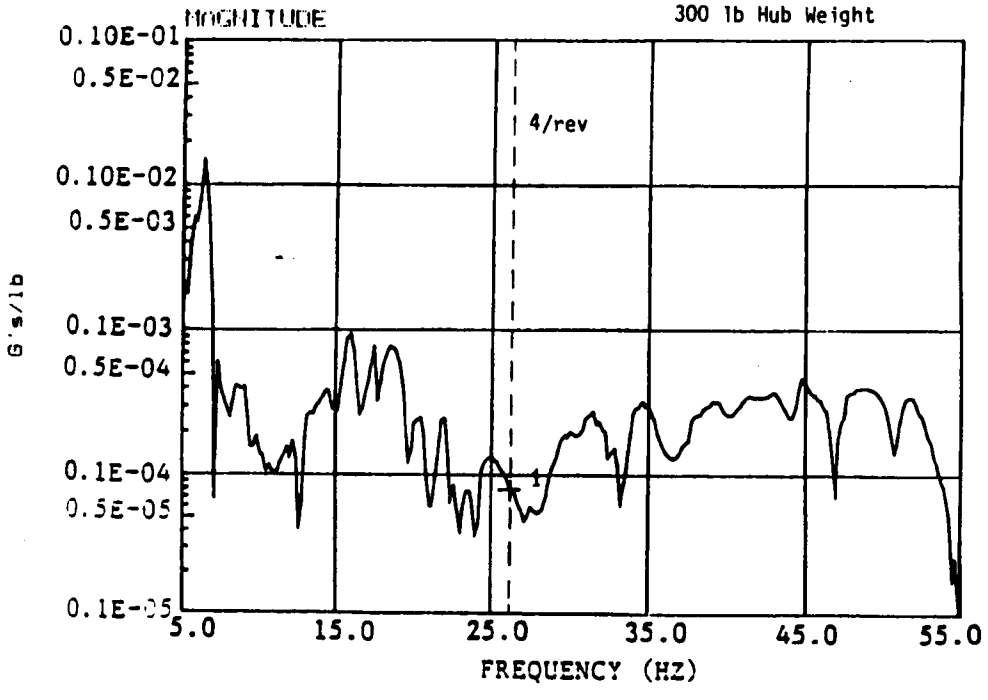

Figure A20. Pilot Seat Lateral Response to Longitudinal Shear Force

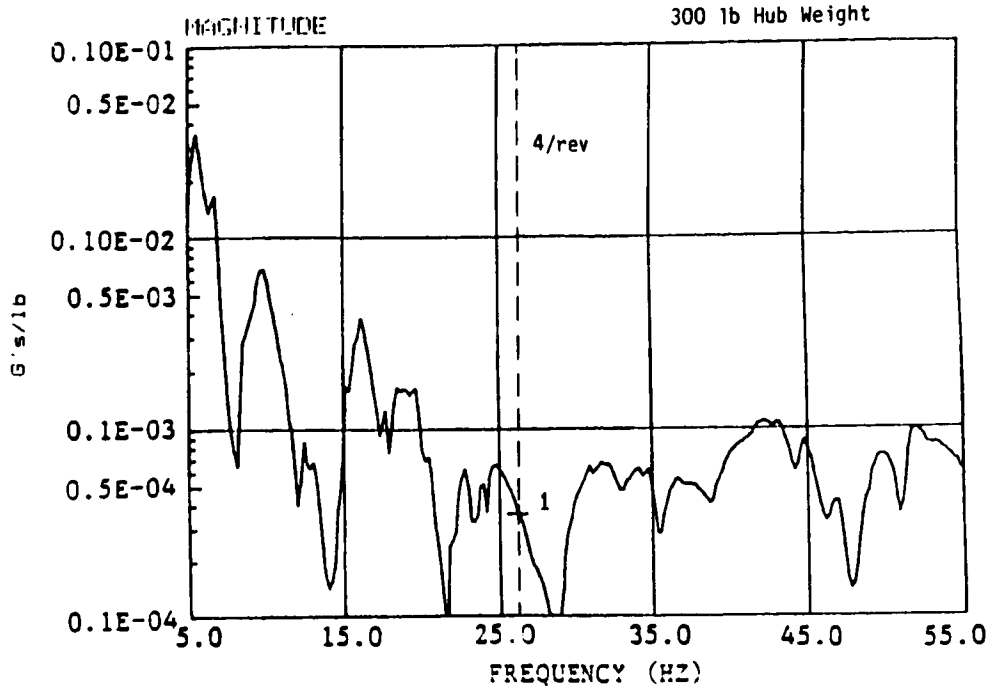

Figure A21. Right Aft Seat Back Vertical Response to Longitudinal Shear Force

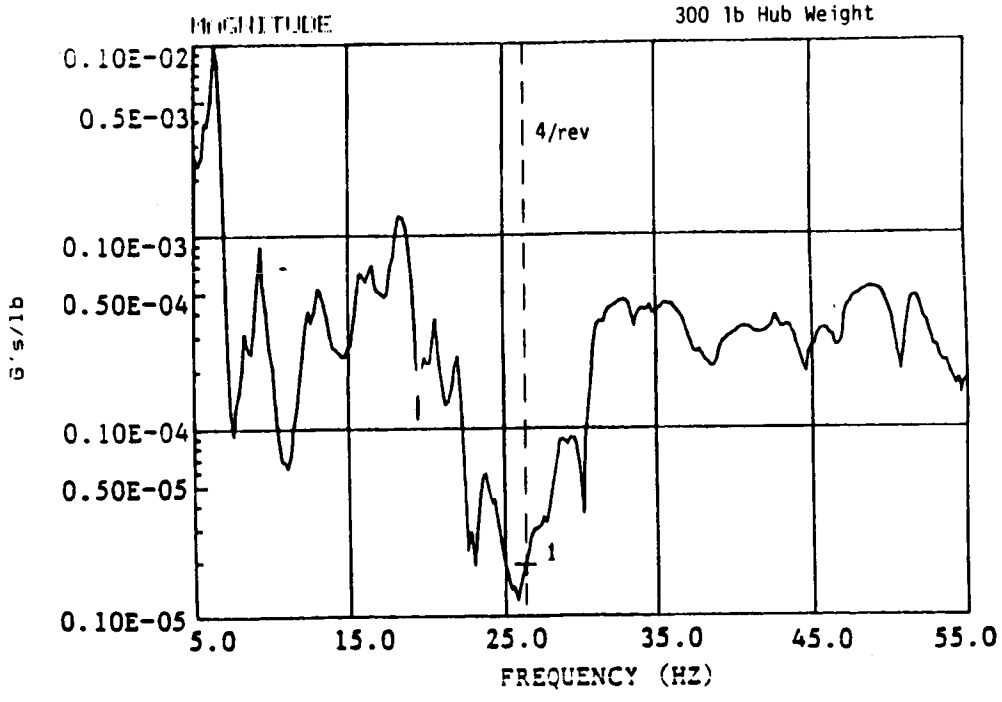

Figure A22. Right Aft Seat Back Lateral Response to Longitudinal Shear Force

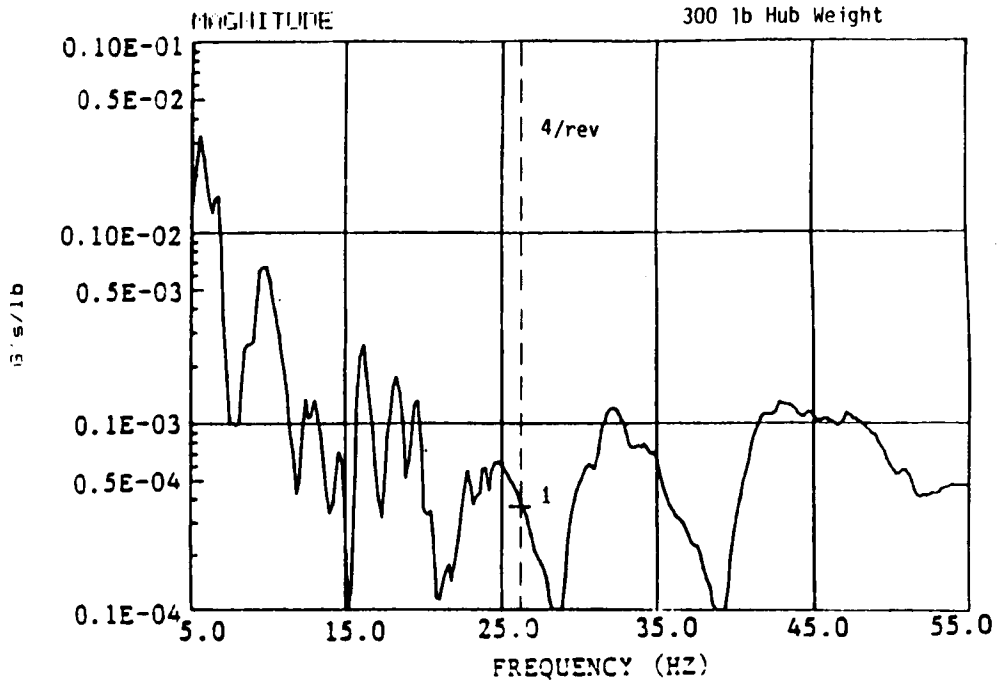

Figure A23. Aft Seat Back Vertical Response to Longitudinal Shear Force

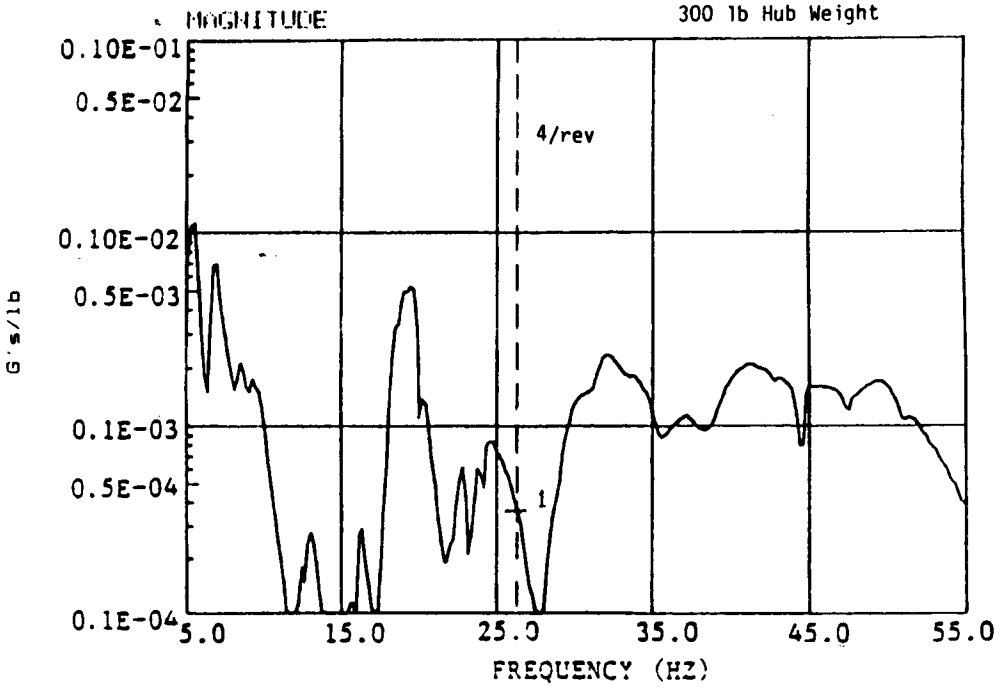

Figure A24. Aft Seat Back F/A Response to Longitudinal Shear Force

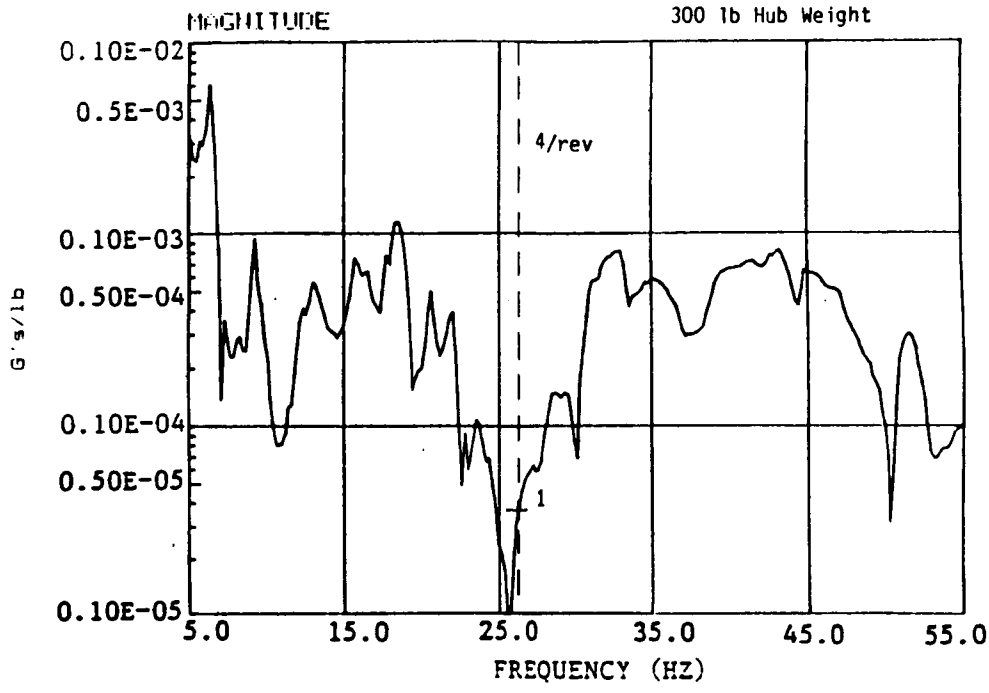

Figure A25. CG Lateral Response to Longitudinal Shear Force

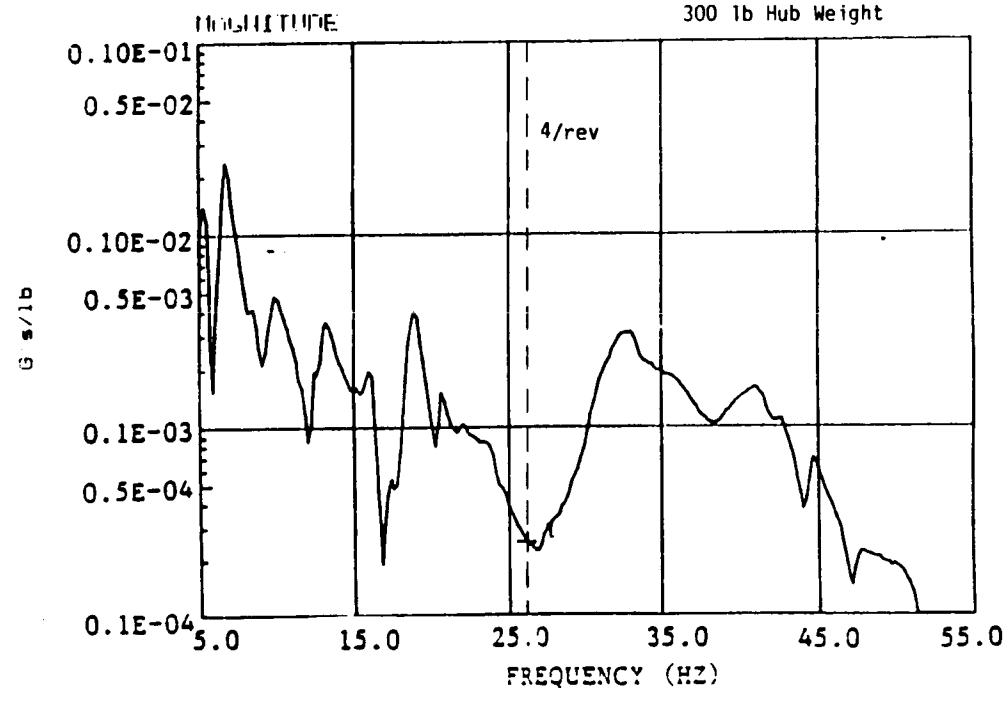

Figure A26. CG F/A Response to Longitudinal Shear Force

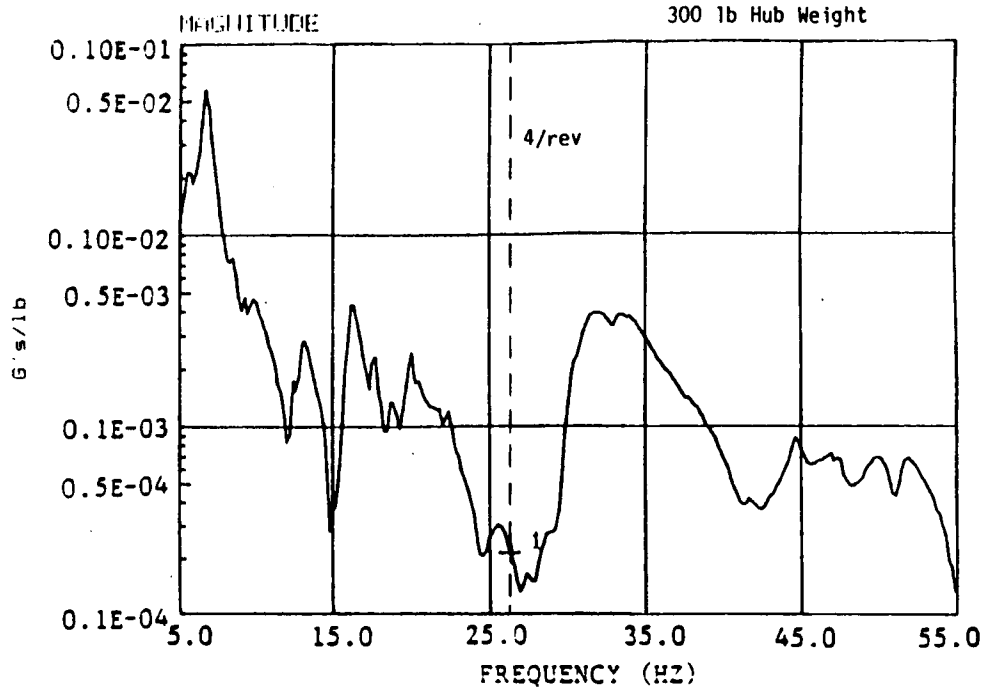

Figure A27. Co-pilot Seat Vertical Response to Longitudinal Shear Force

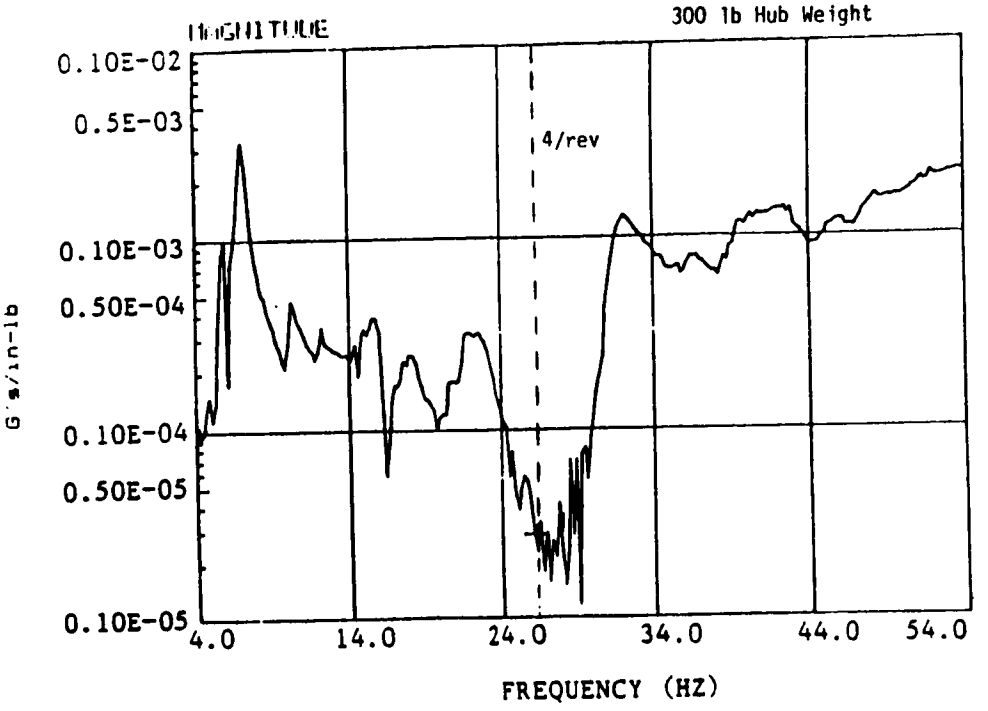

Figure A28. Pilot Seat Vertical Response to Pitching Moment

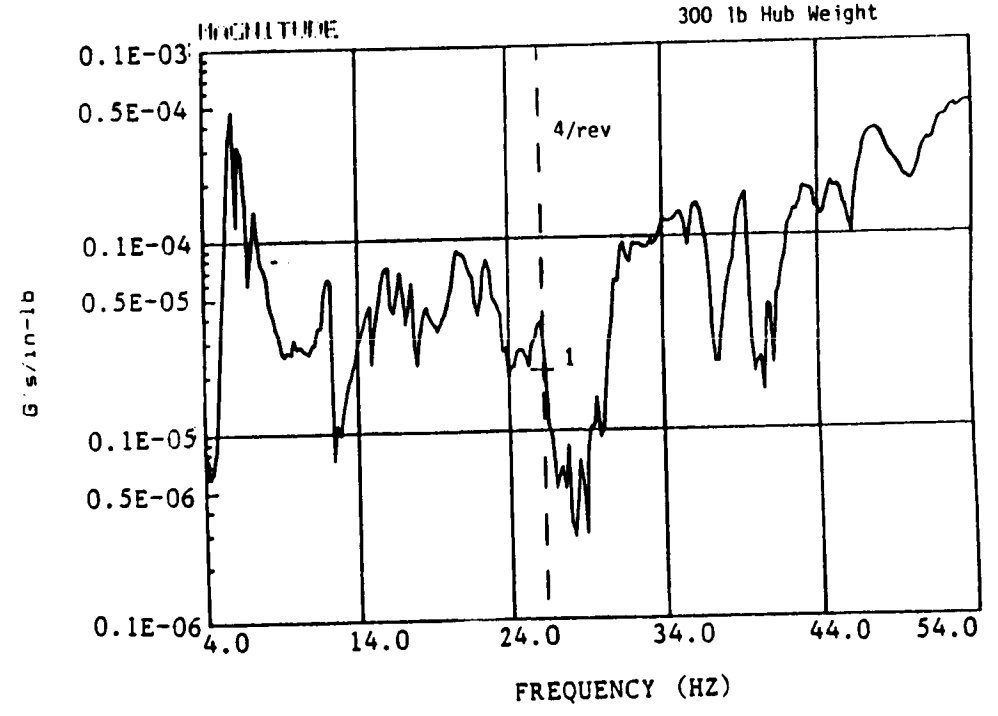

Figure A29. Pilot Seat Lateral Response to Pitching Moment

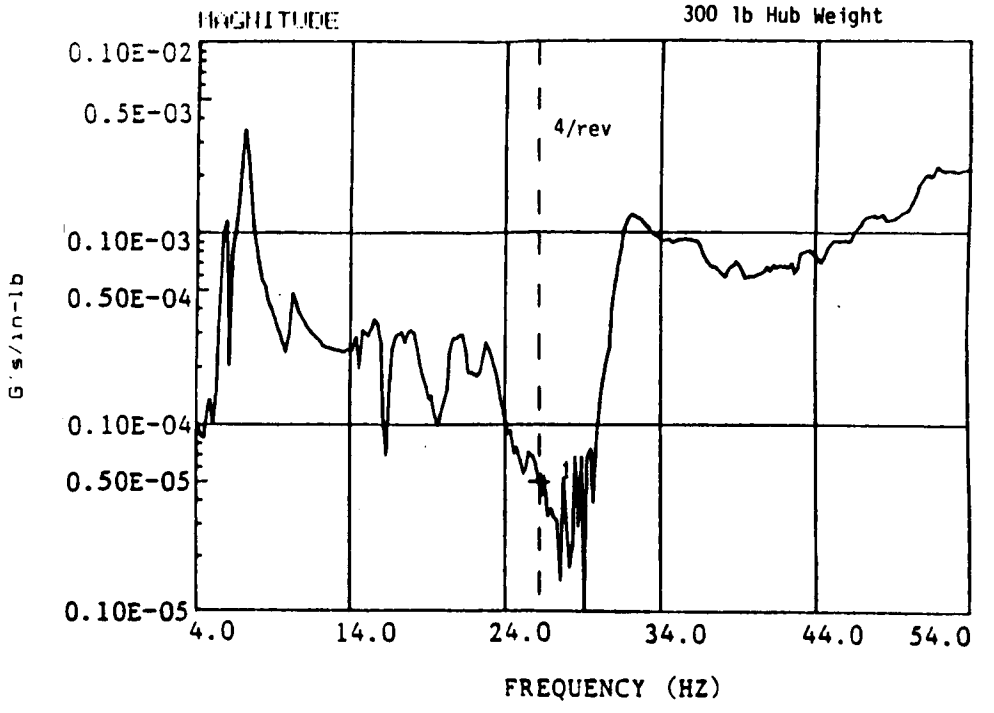

Figure A30. Co-pilot Seat Vertical Response to Pitching Moment

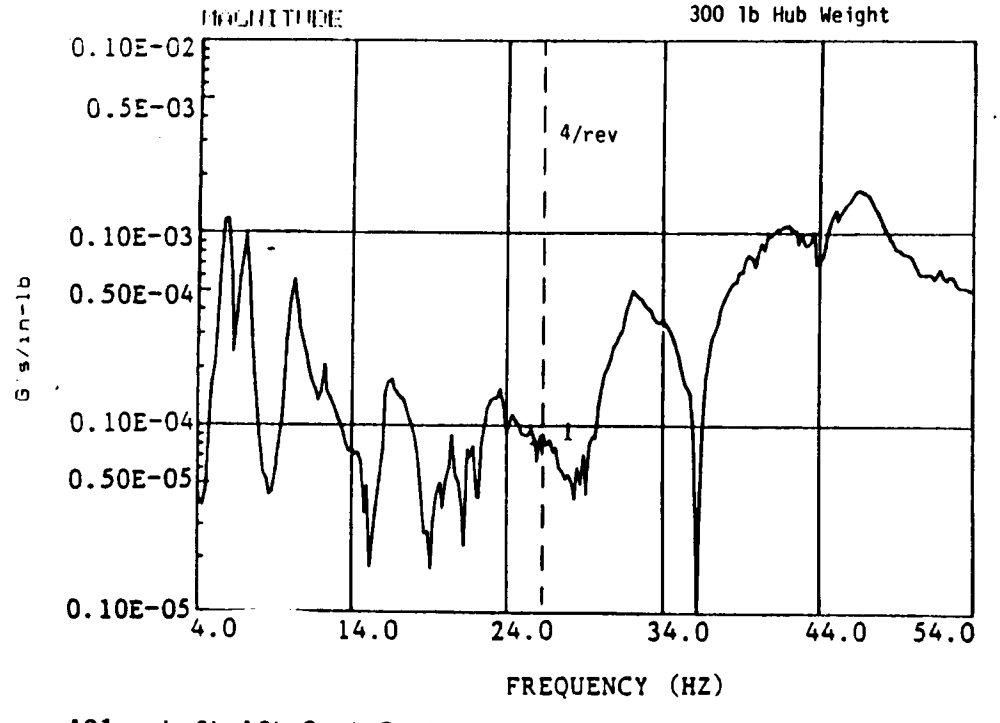

Figure A31. Left Aft Seat Back Vertical Response to Pitching Moment

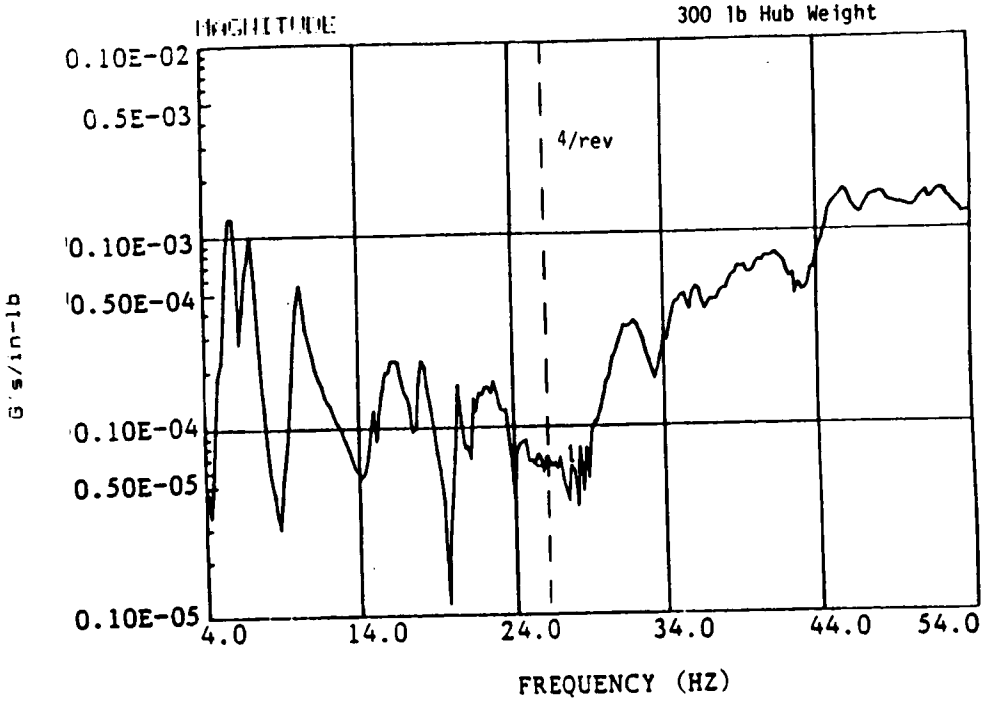

Figure A32. Right Aft Seat Back Vertical Response to Pitching Moment

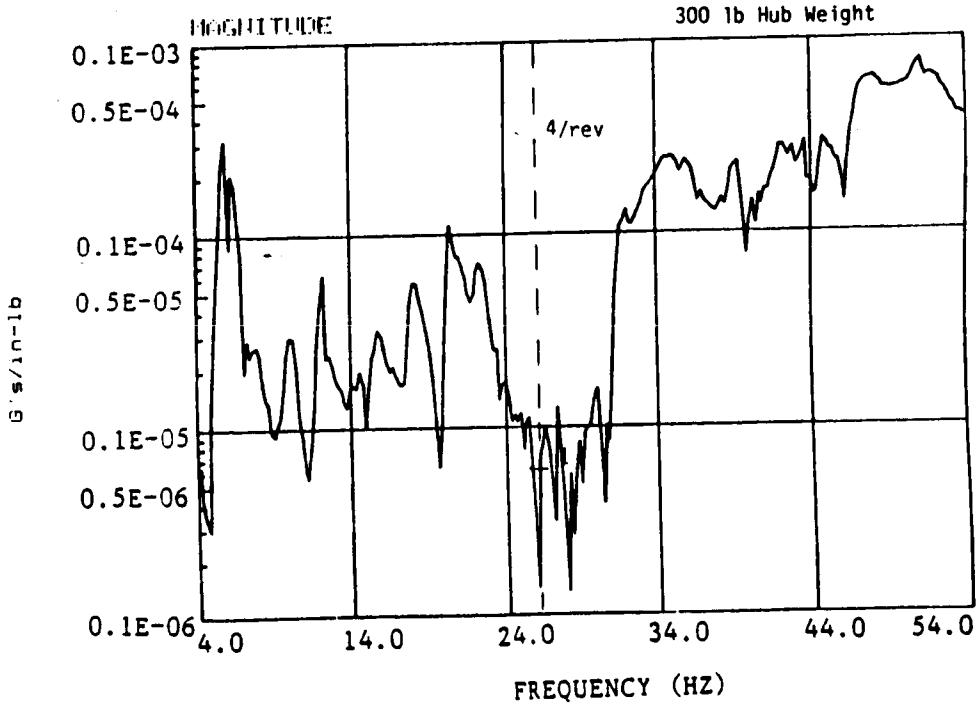

Figure A33. Right Aft Seat Back Lateral Response to Pitching Moment

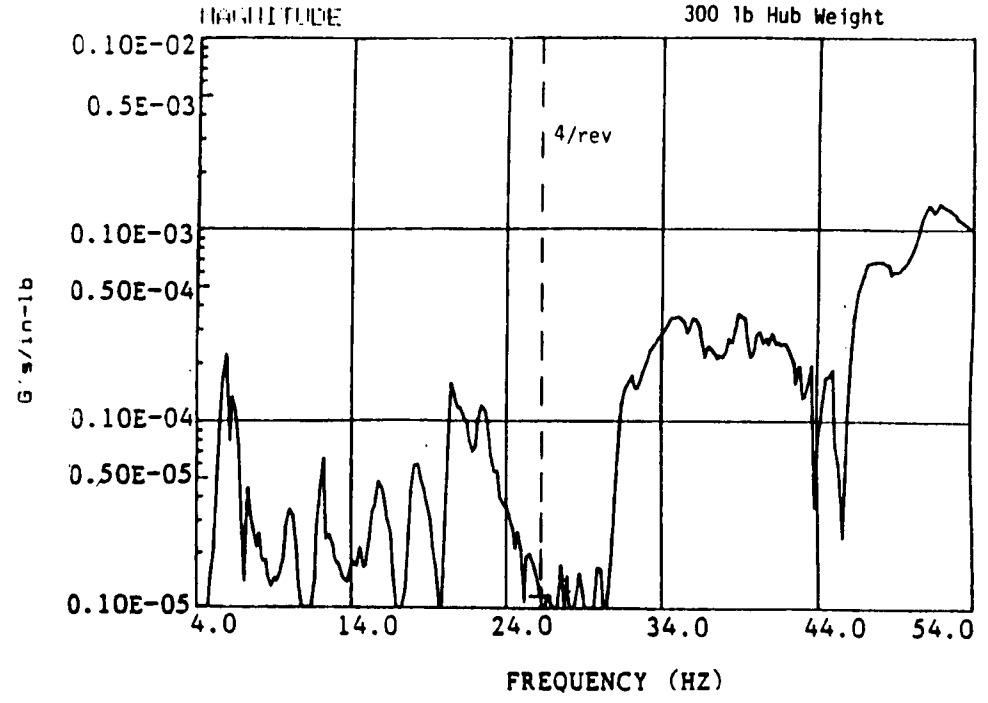

Figure A34. CG Lateral Response to Pitching Moment

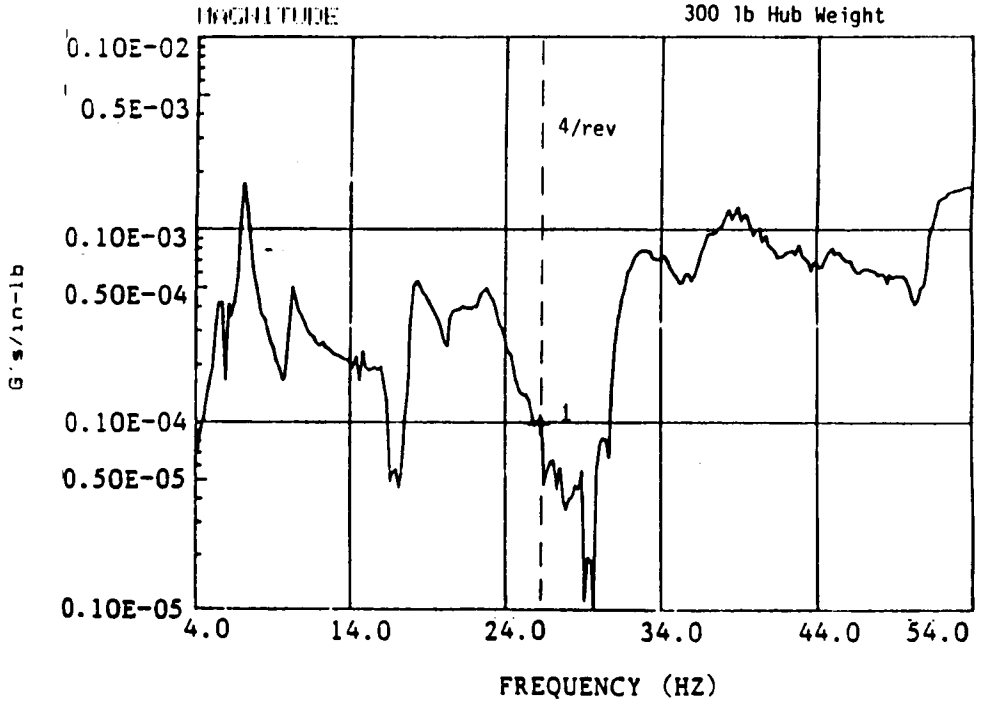

Figure A35. CG F/A Response to Pitching Moment

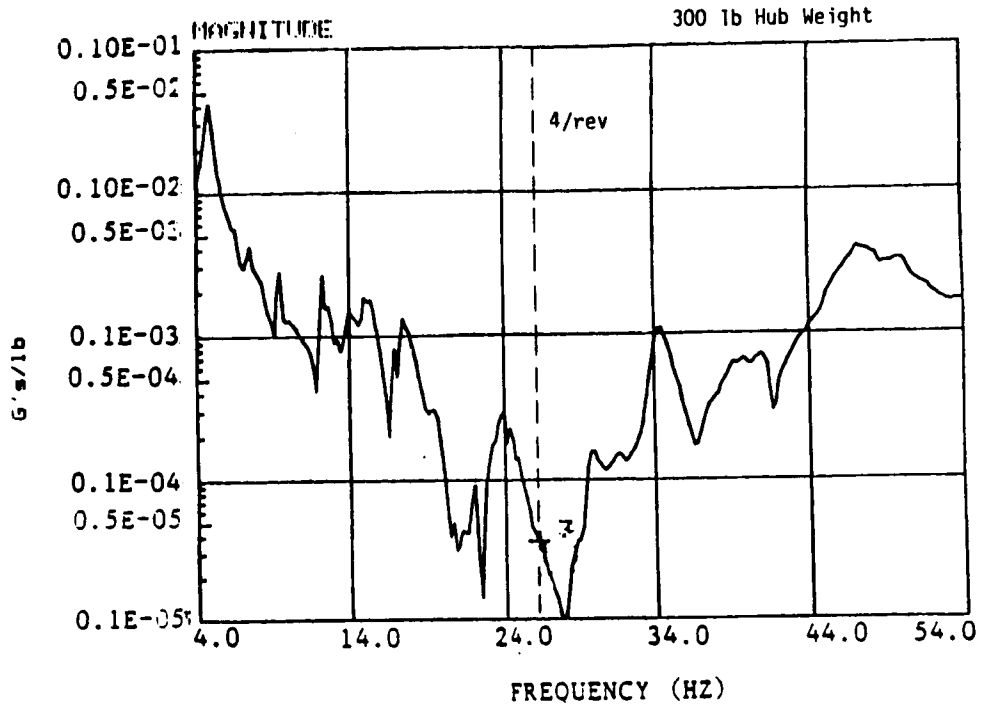

Figure A36. Pilot Seat Vertical Response to Lateral Shear Force

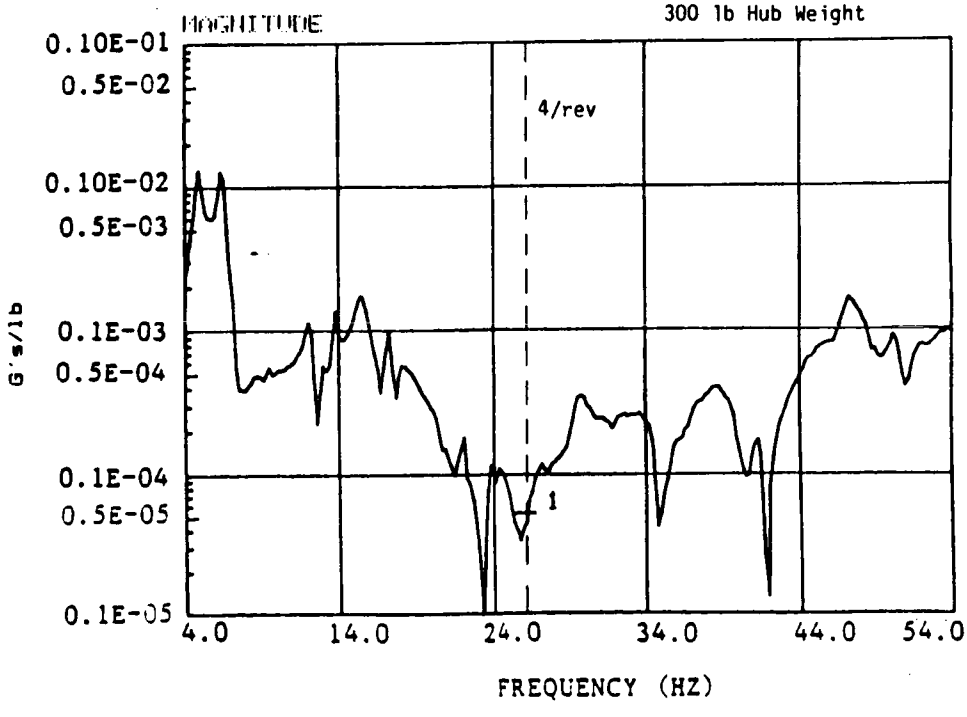

Figure A37. Pilot Seat Lateral Response to Lateral Shear Force

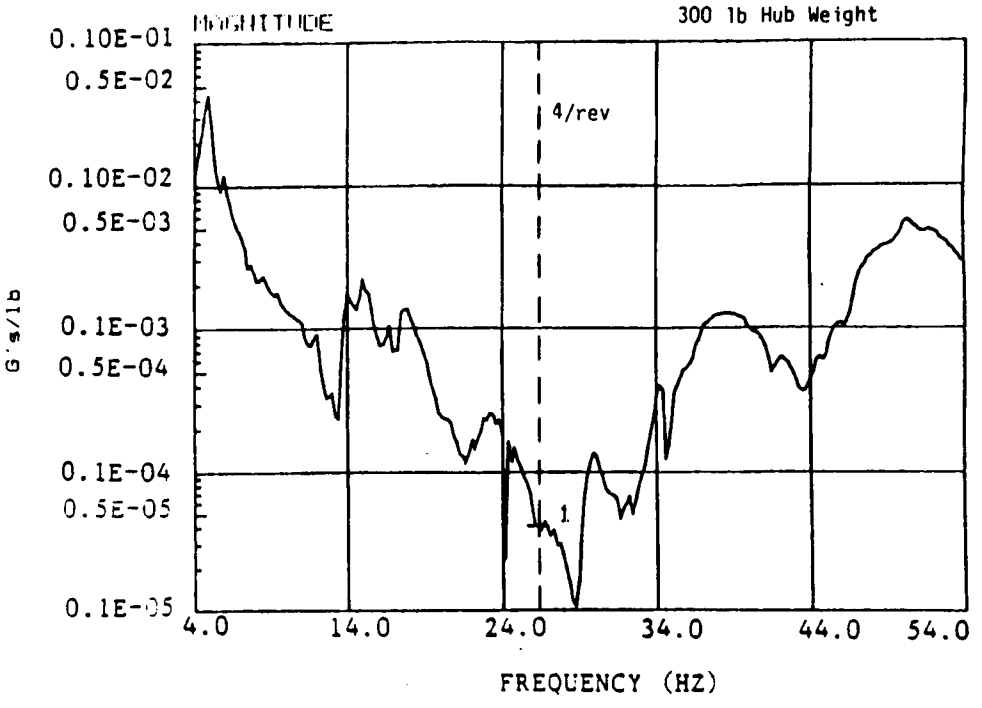

Figure A38. Right Aft Seat Back Vertical Response to Lateral Shear Force

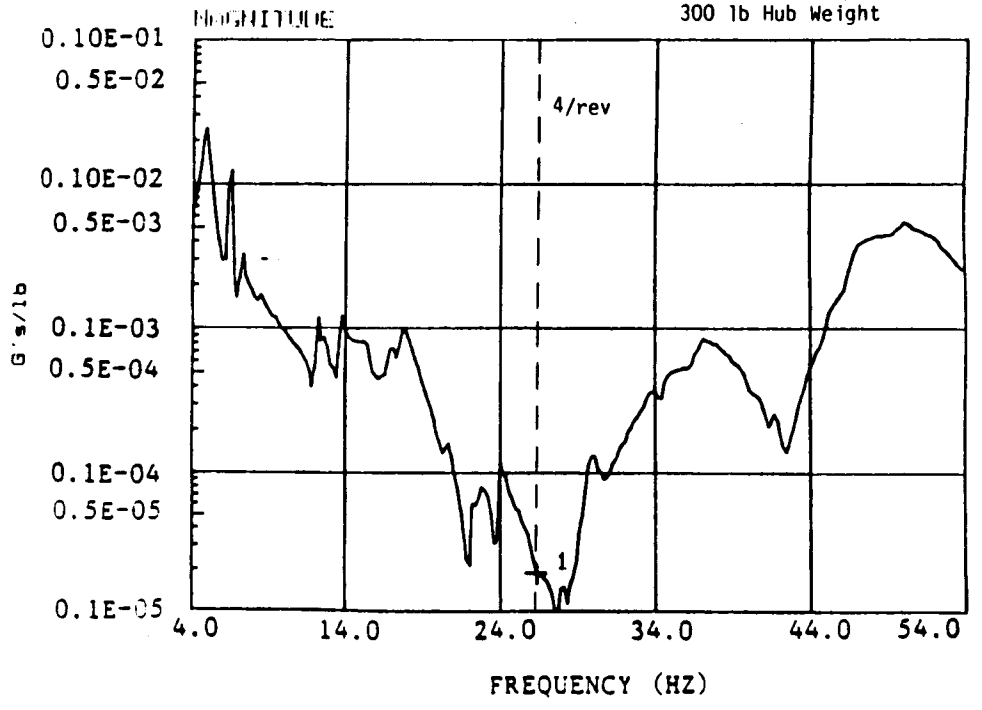

Figure A39. Right Aft Seat Back Lateral Response to Lateral Shear Force

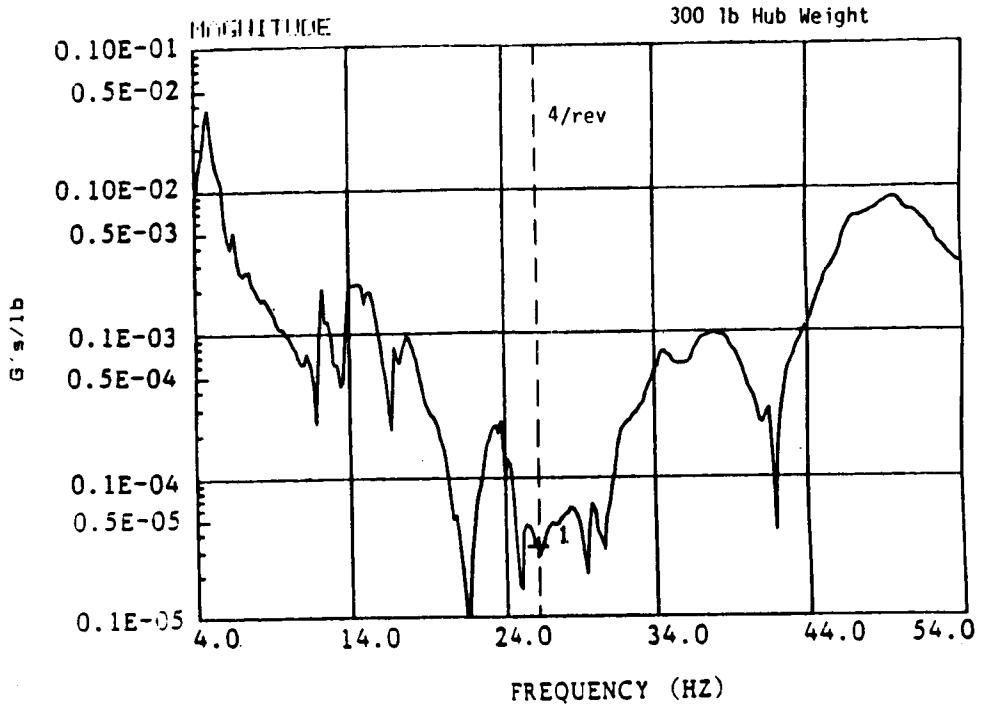

Figure A40. Left Aft Seat Back Vertical Response to Lateral Shear Force

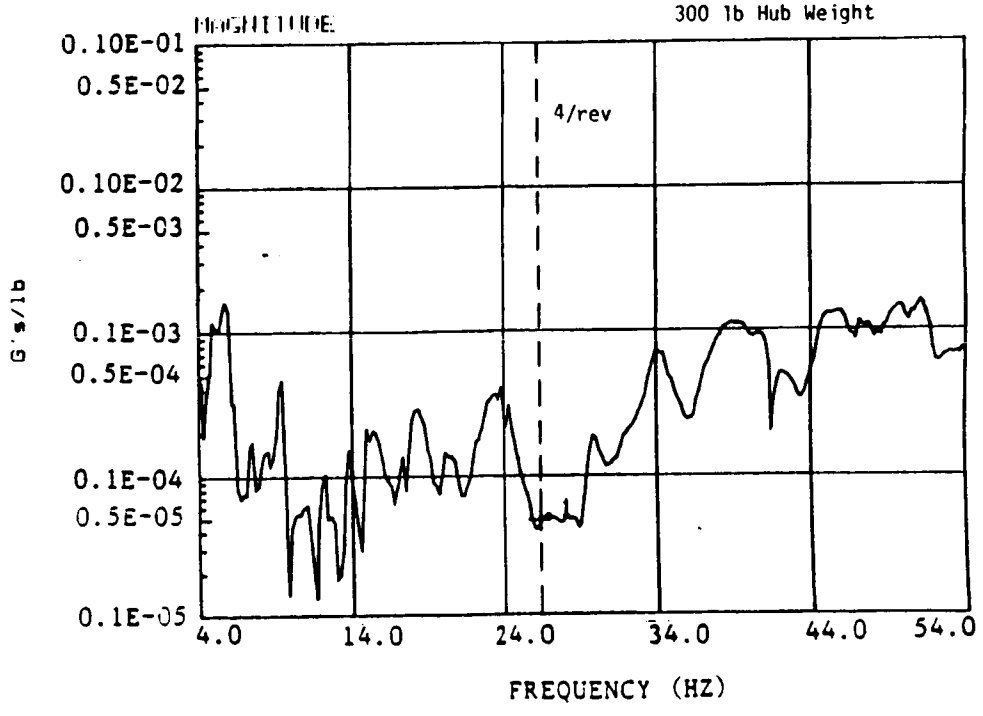

Figure A41. Left Aft Seat Back F/A Response to Lateral Shear Force

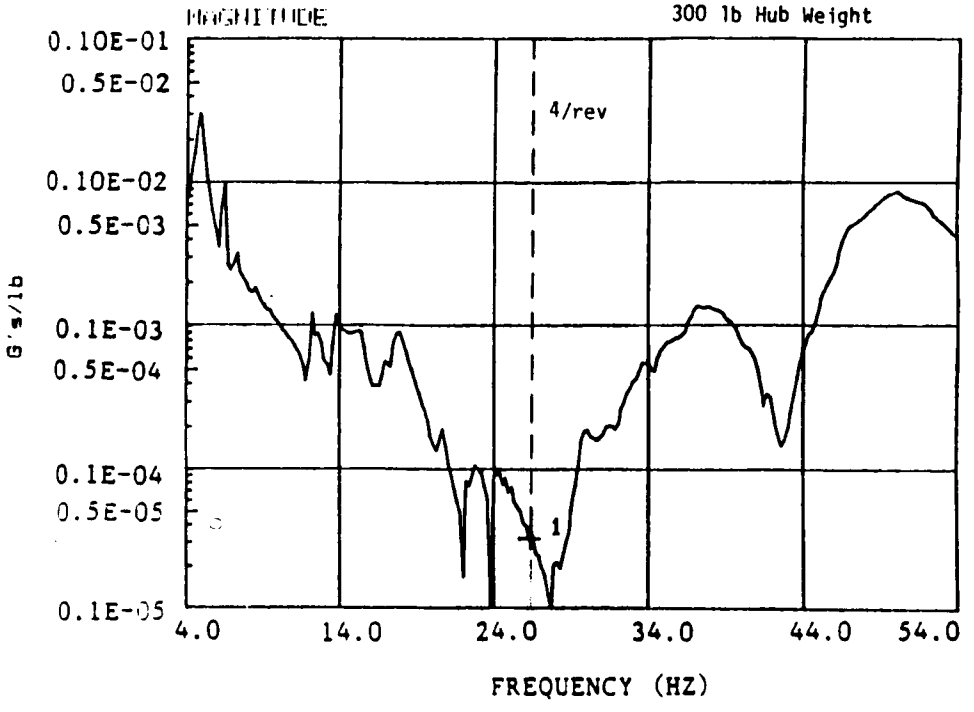

Figure A42. CG Lateral Response to Lateral Shear Force

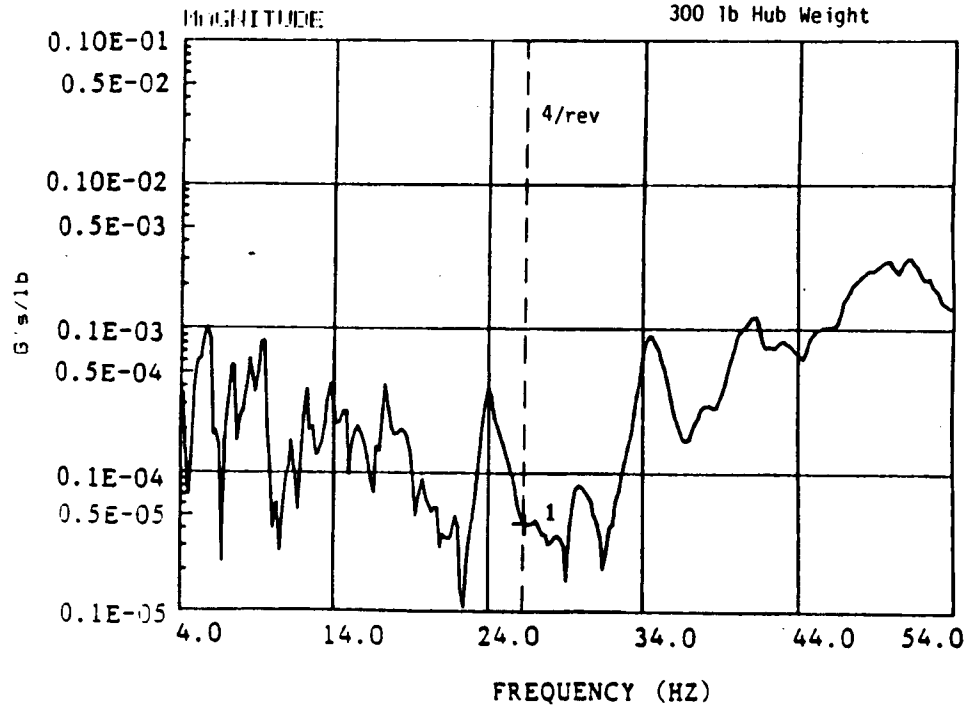

Figure A43. CG F/A Response to Lateral Shear Force

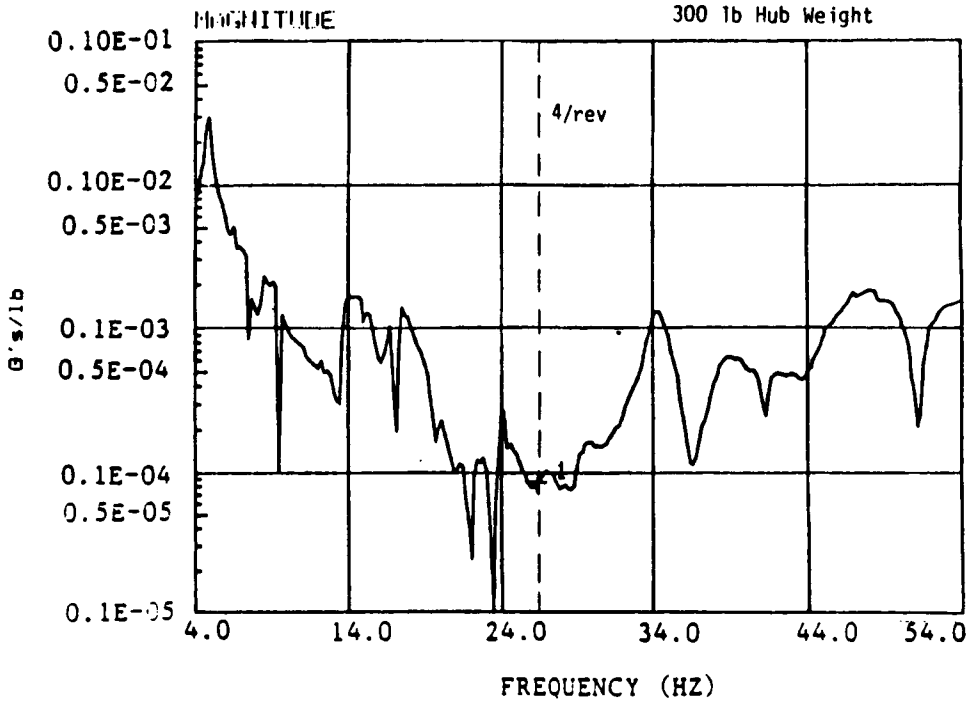

Figure A44. Co-pilot Seat Vertical Response to Lateral Shear Force

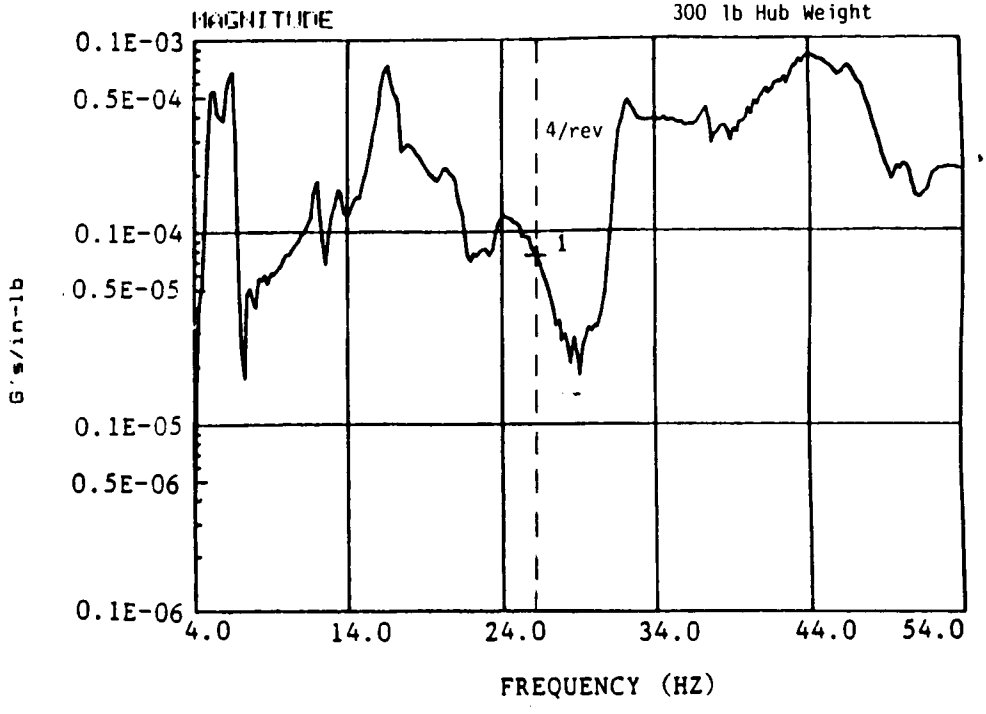

Figure A45. Pilot Seat Lateral Response to Roll Moment

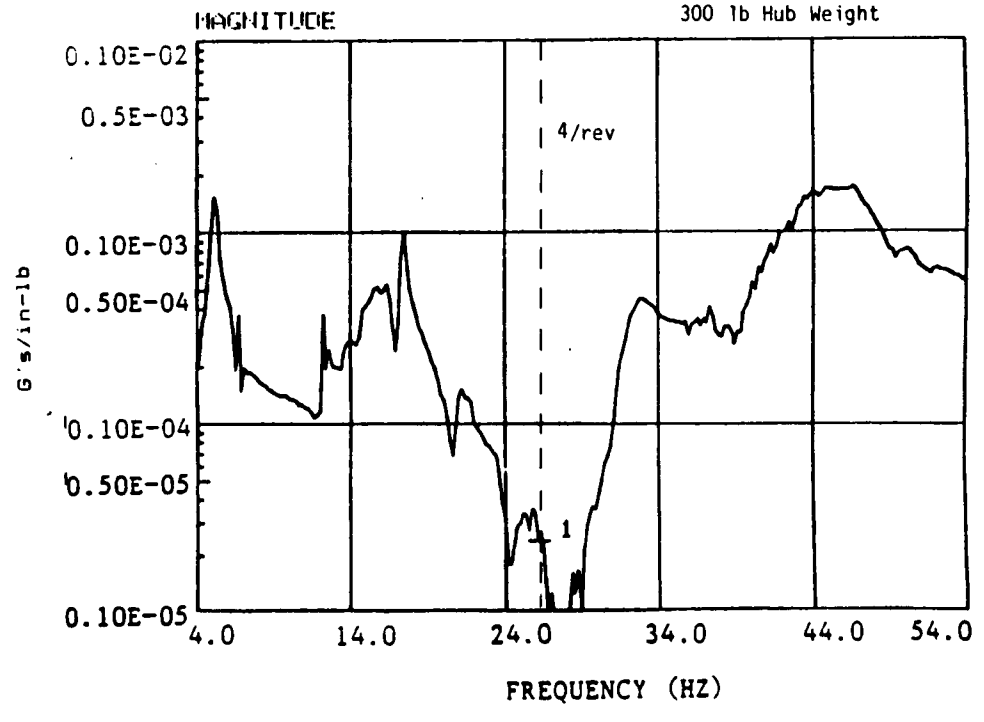

Figure A46. Pilot Seat Vertical Response to Roll Moment

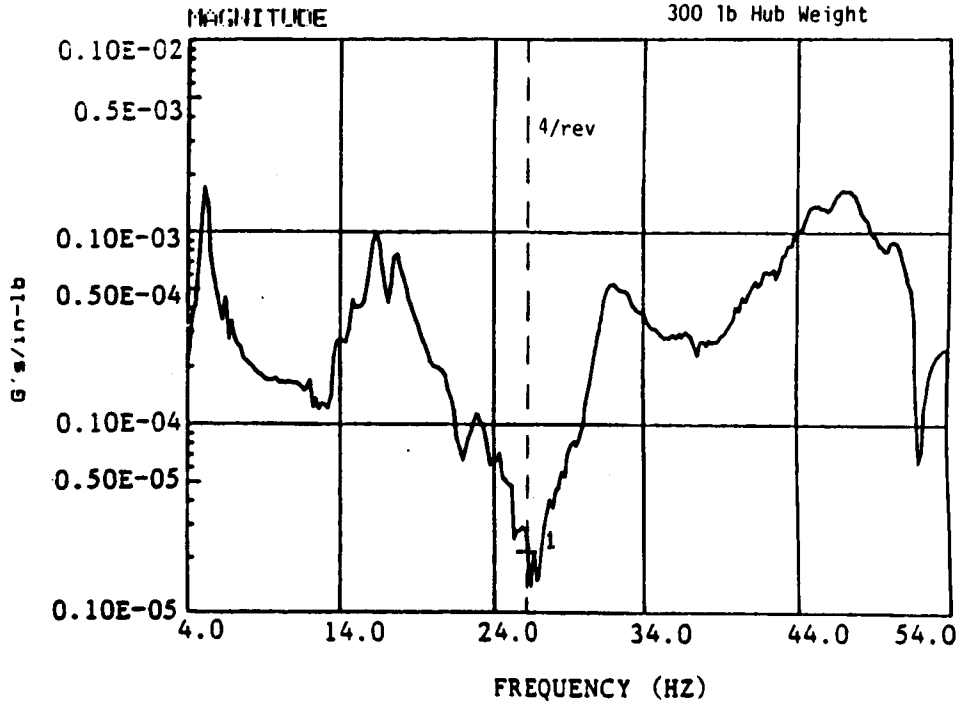

Figure A47. Right Aft Seat Back Vertical Response to Roll Moment

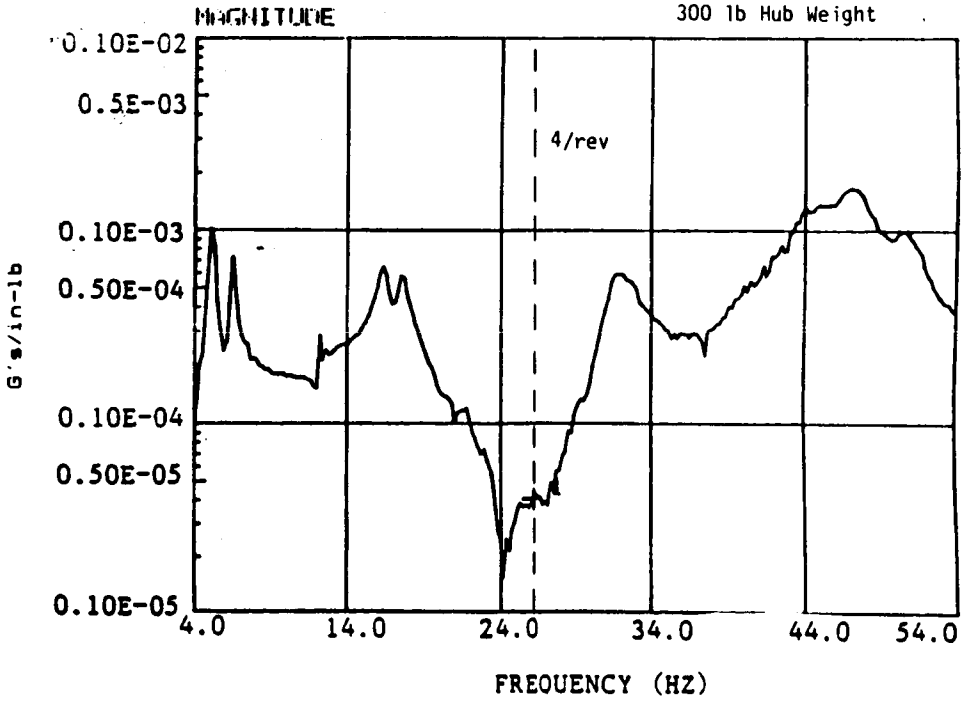

Figure A48. Right Aft Seat Back Lateral Response to Roll Moment

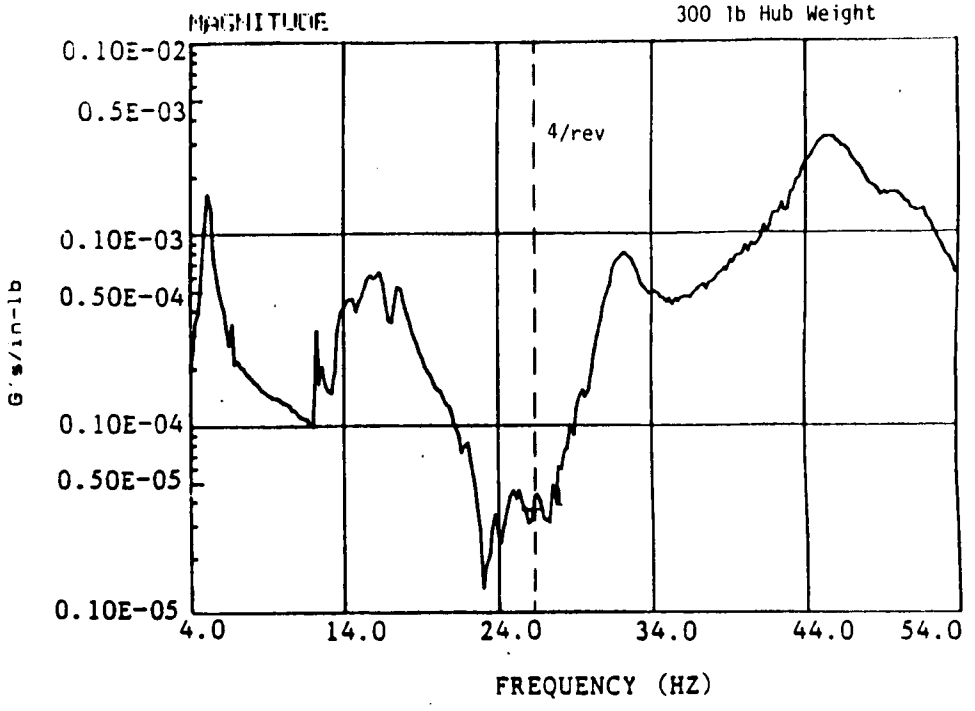

Figure A49. Left Aft Seat Back Vertical Response to Roll Moment

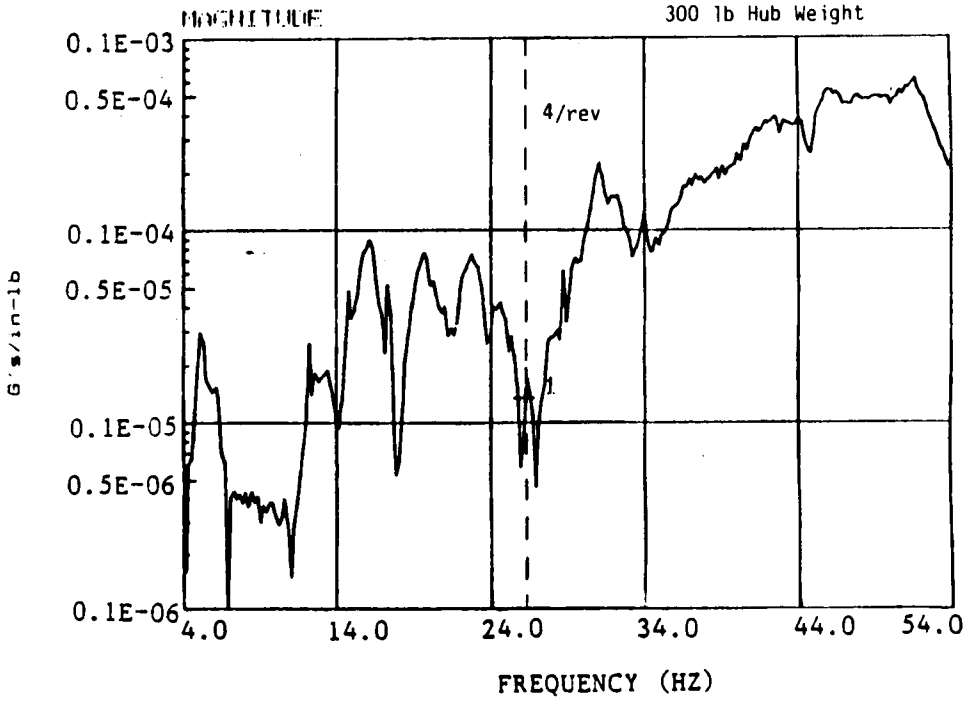

Figure A50. Left Aft Seat Back F/A Response to Roll Moment

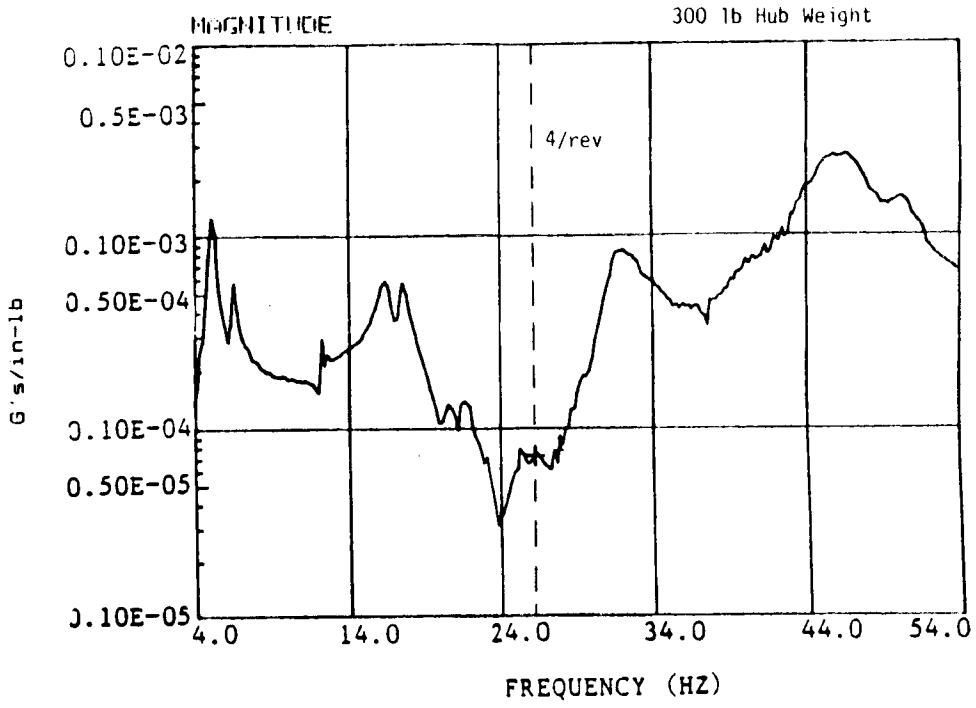

Figure A51. CG Lateral Response to Roll Moment

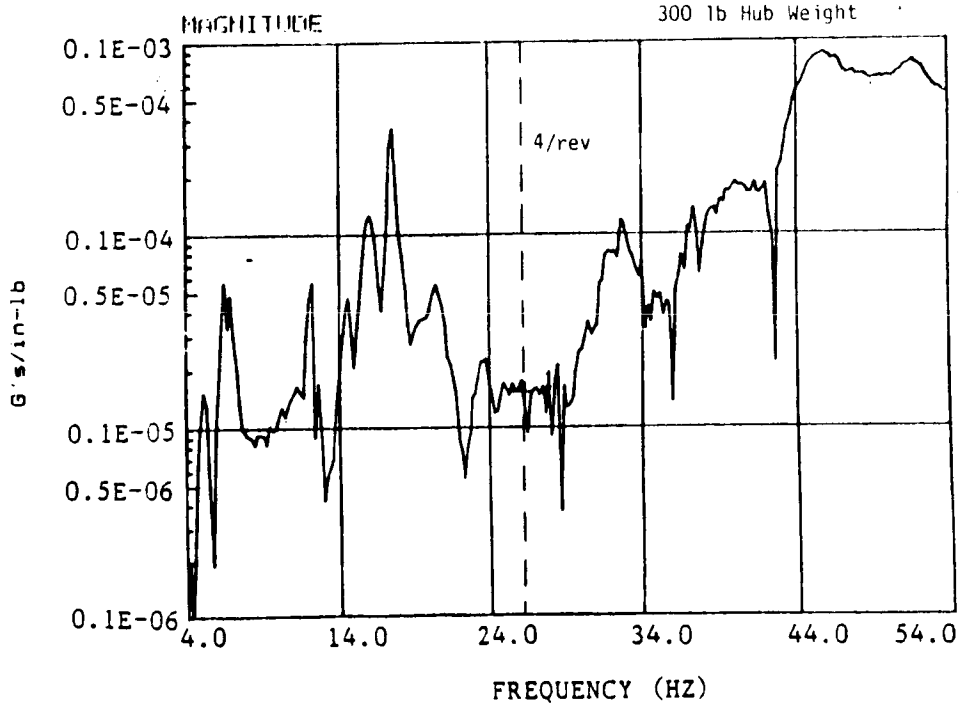

Figure A52. CG F/A Response to Roll Moment

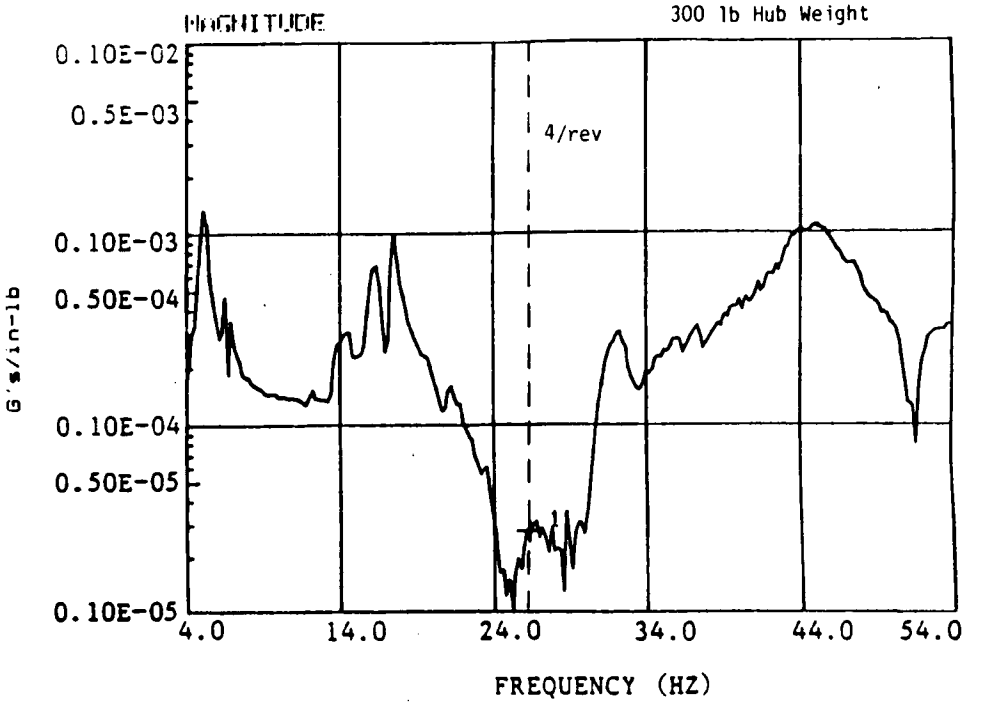

Figure A53. Co-pilot Seat Vertical Response to Roll Moment

APPENDIX B

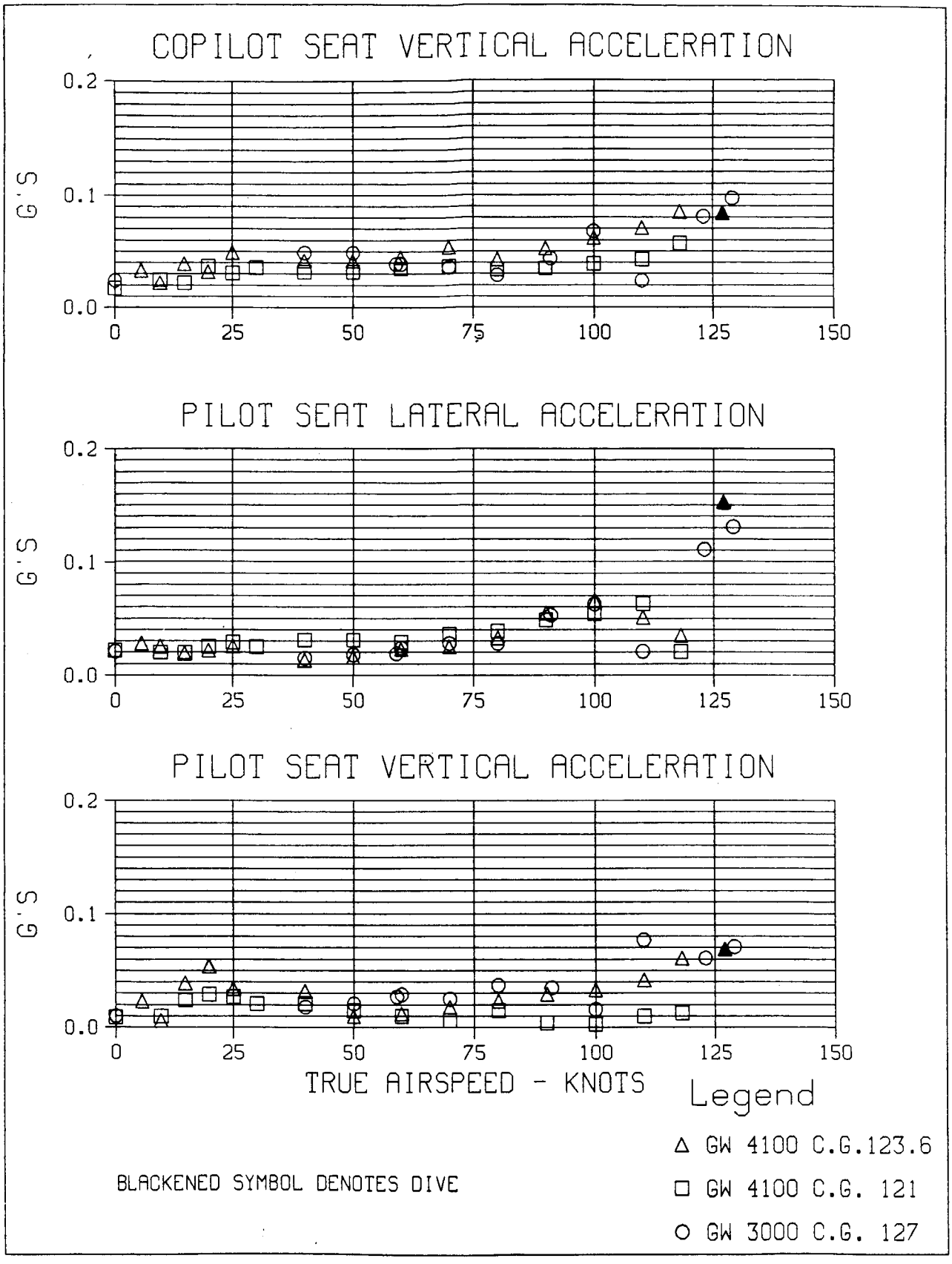

Figure B1. 4/Rev Vibration Level vs Airspeed

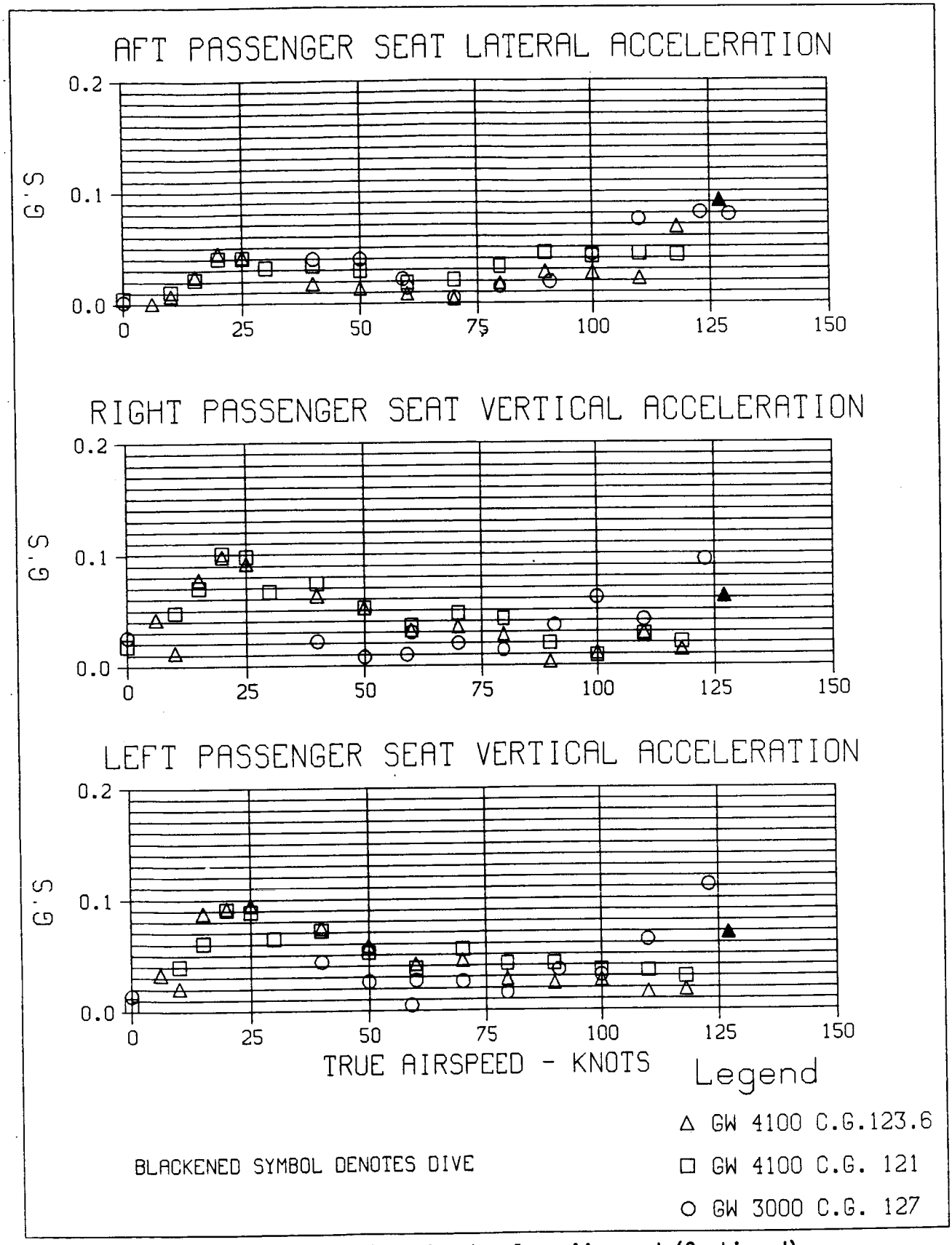

Figure B1. 4/Rev Vibration Level vs Airspeed (Continued)

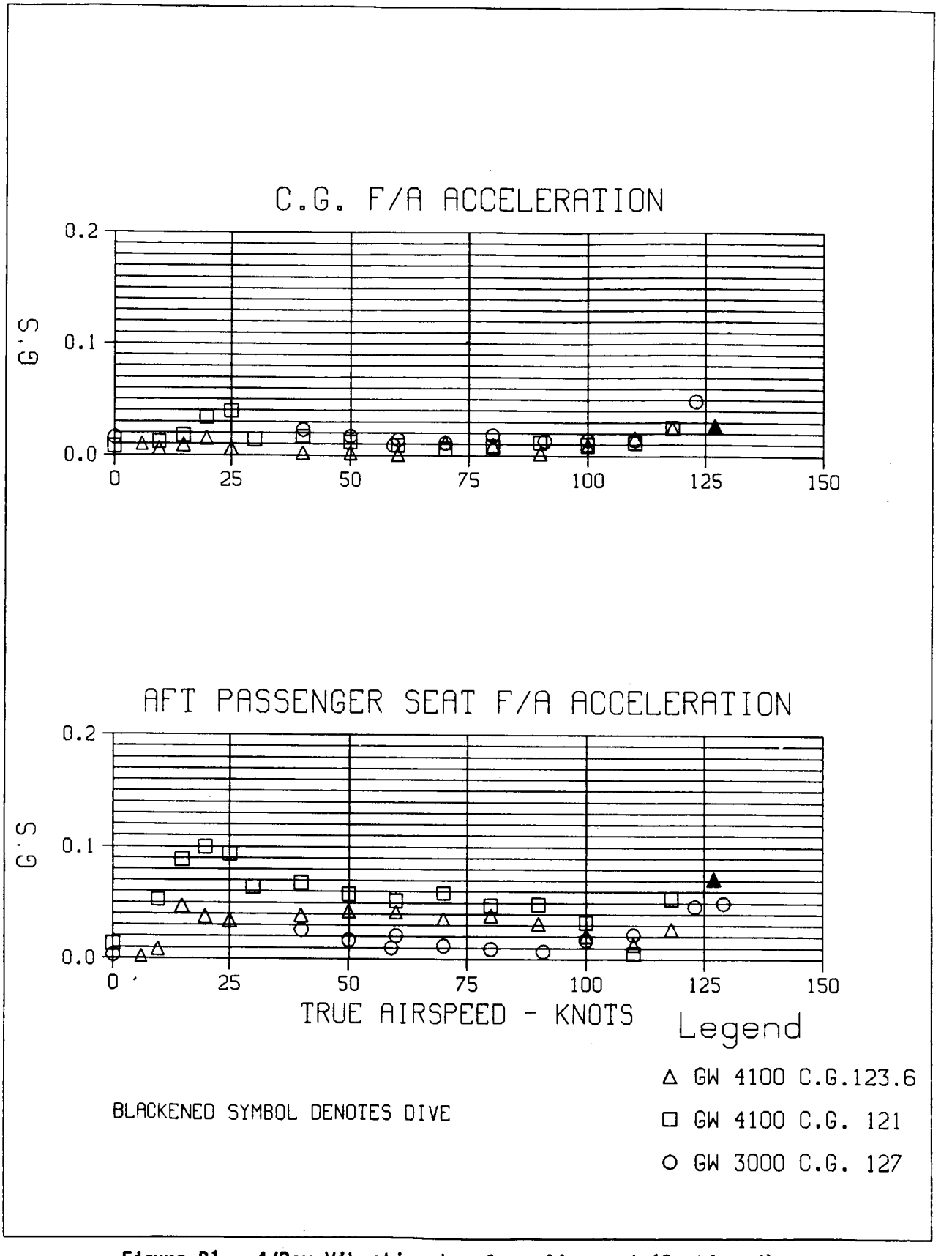

Figure B1. 4/Rev Vibration Level vs Airspeed (Continued)

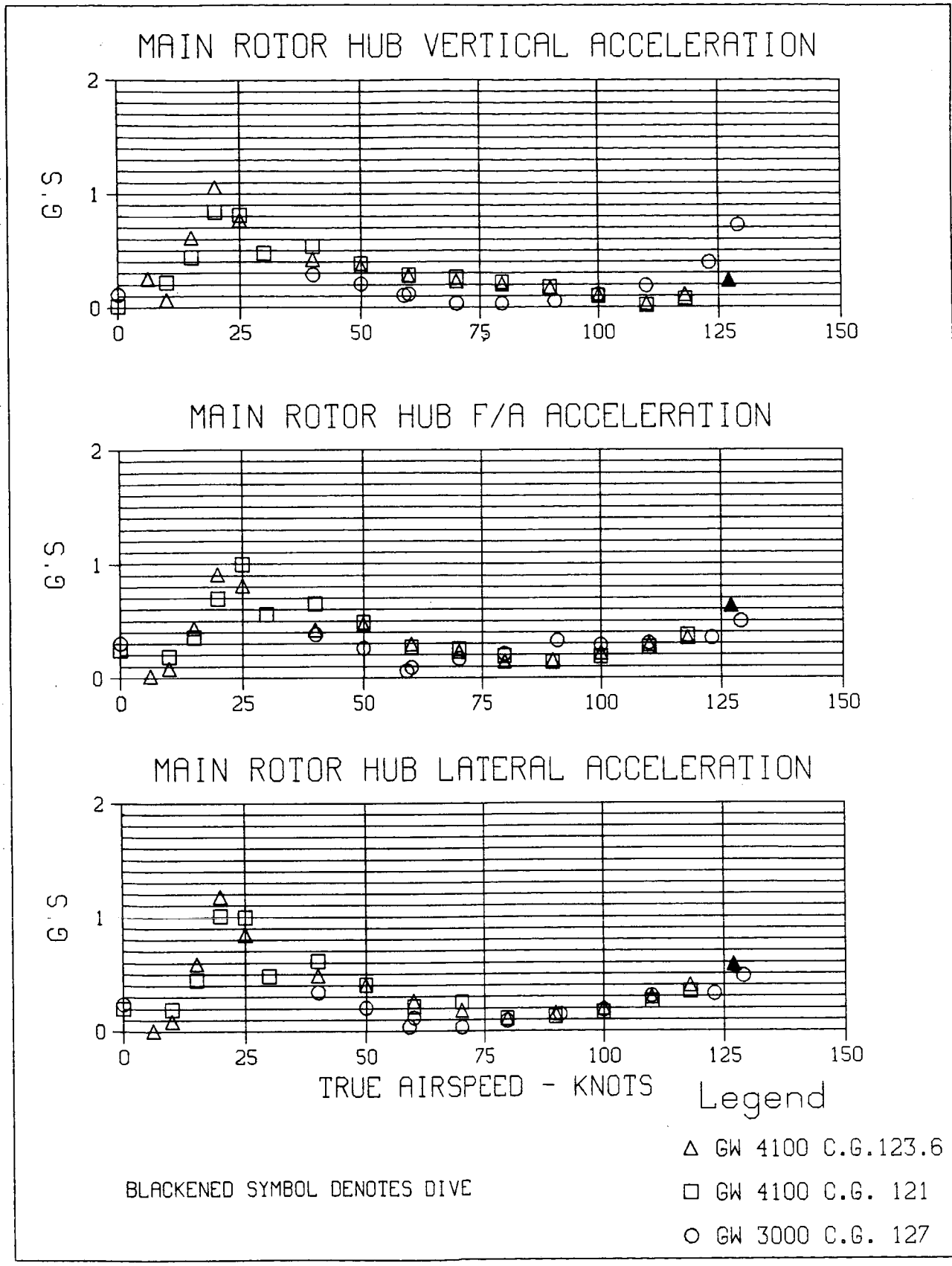

Figure B1. 4/Rev Vibration Level vs Airspeed (Continued)

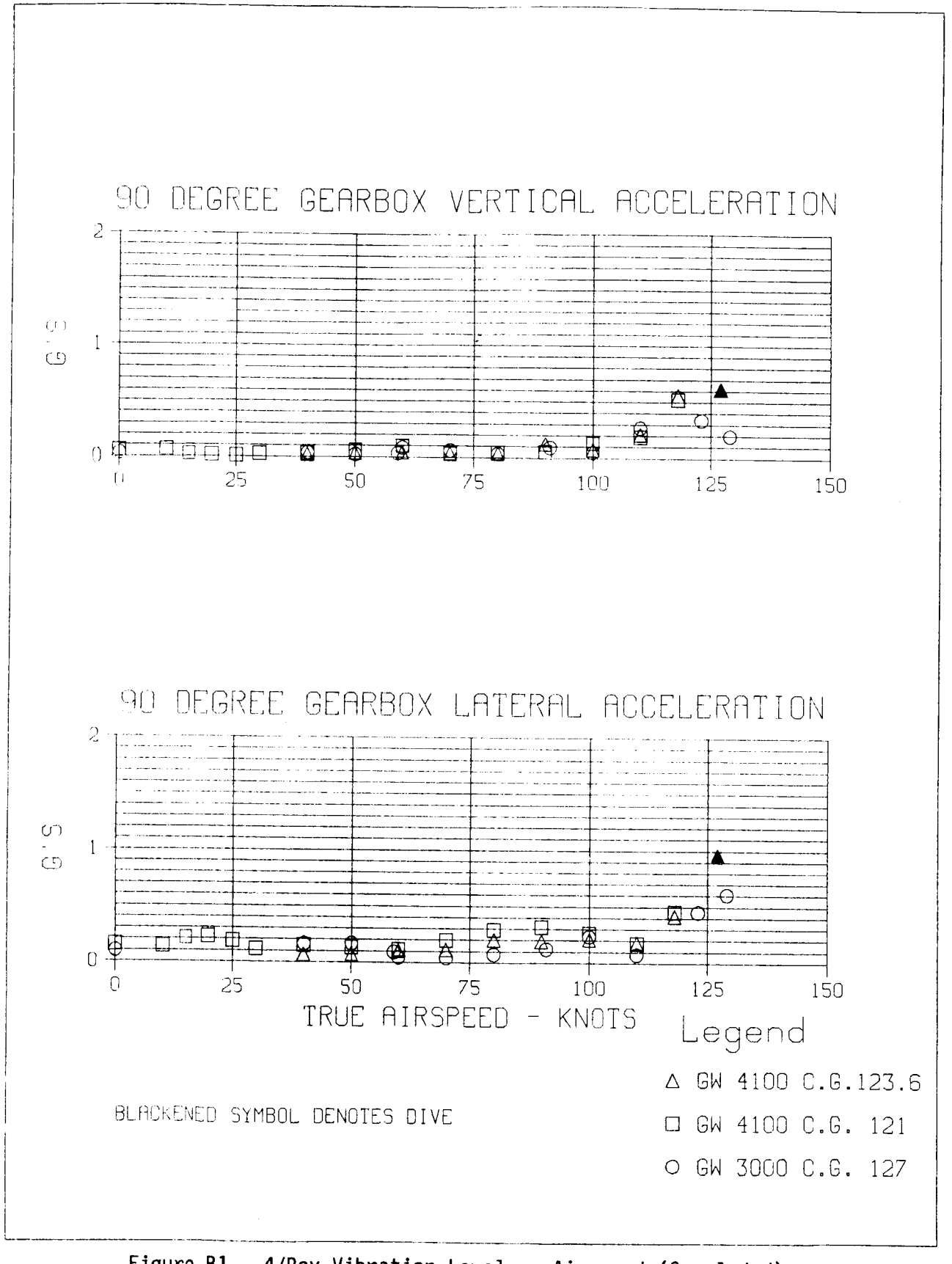

Figure B1. 4/Rev Vibration Level vs Airspeed (Concluded)

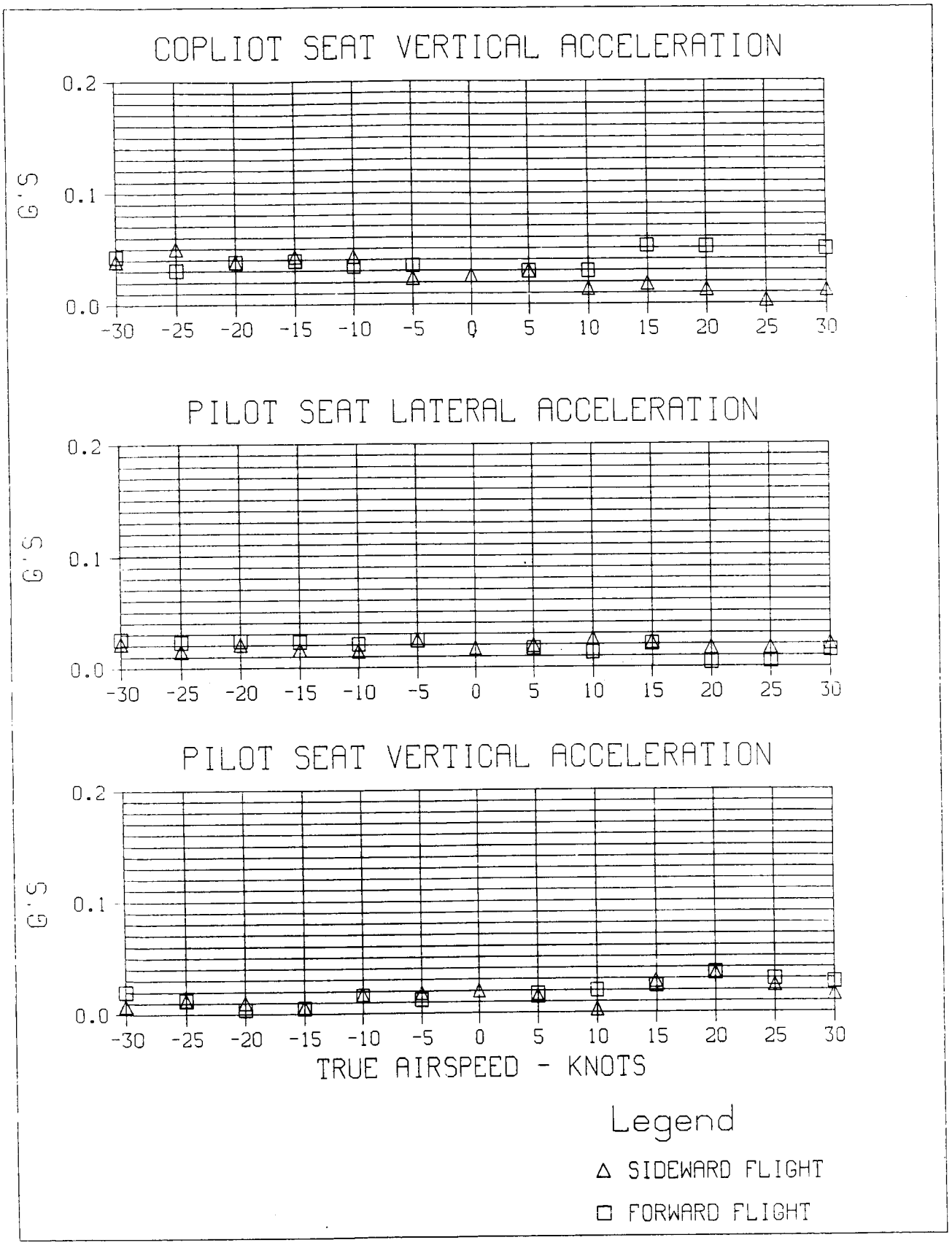

Figure B2. 4/Rev Vibration Level vs Airspeed for Transitional Flight Speed Range

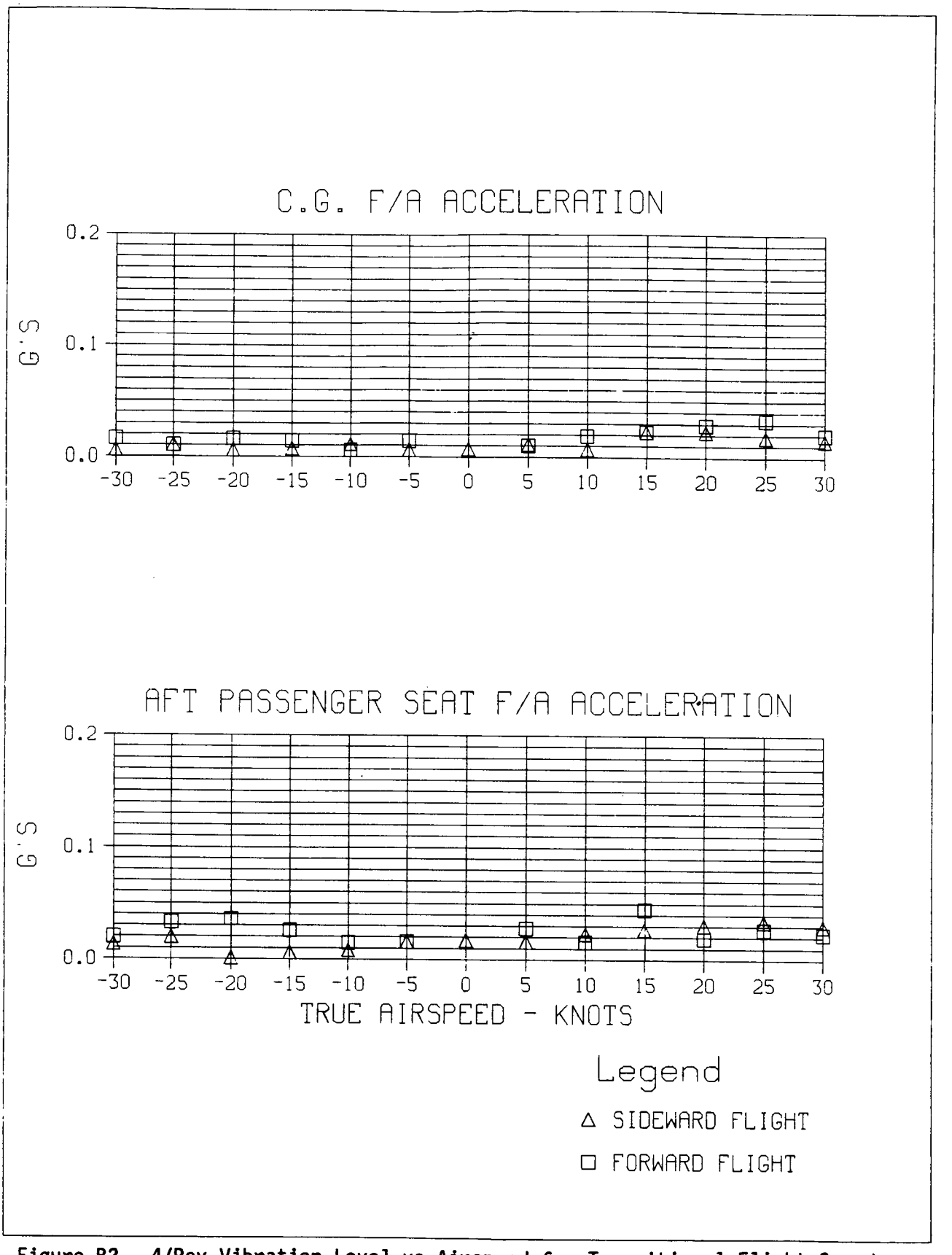

Figure B2. 4/Rev Vibration Level vs Airspeed for Transitional Flight Speed Range (Continued)

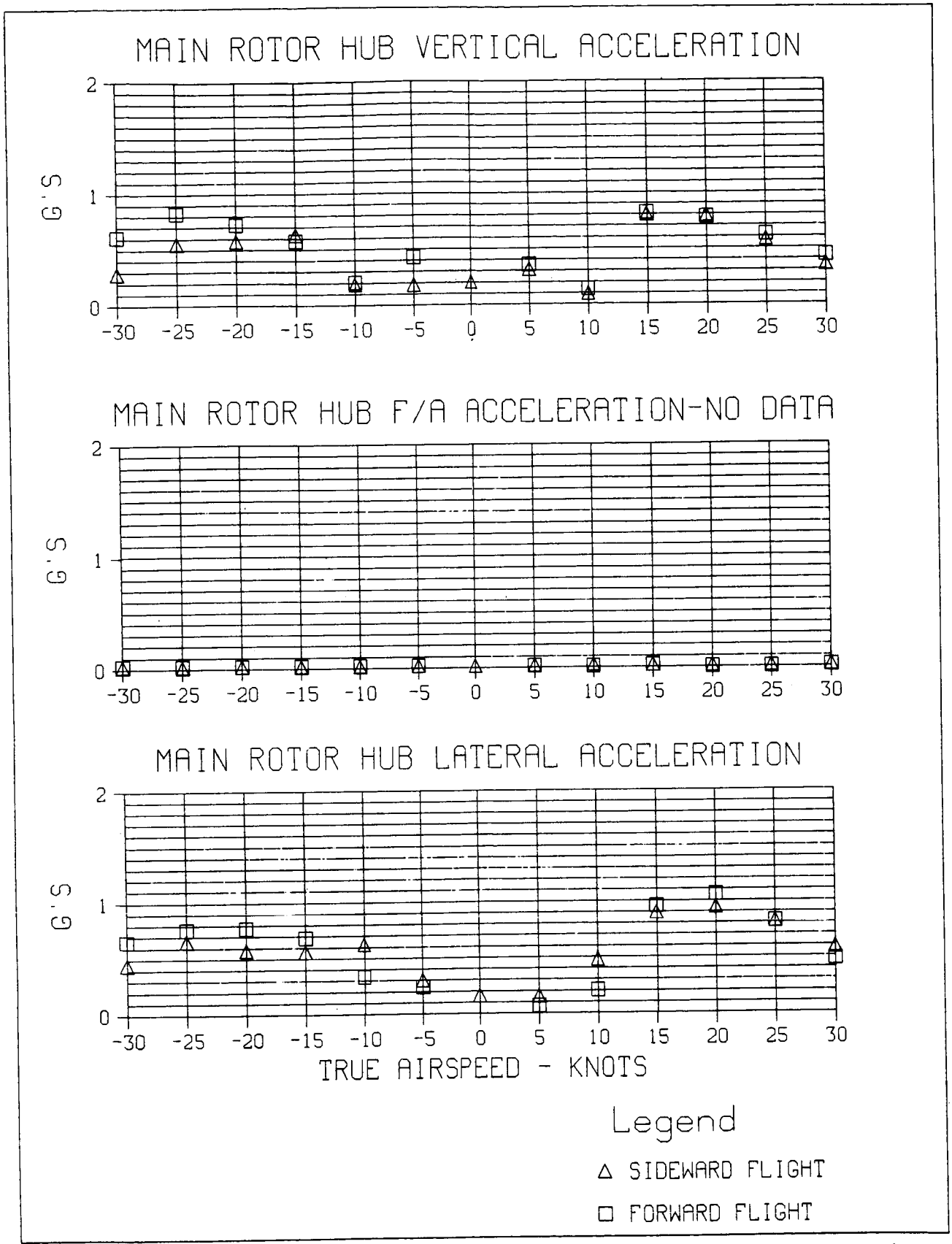

Figure B2. 4/Rev Vibration Level vs Airspeed for Transitional Flight Speed Range (Continued)

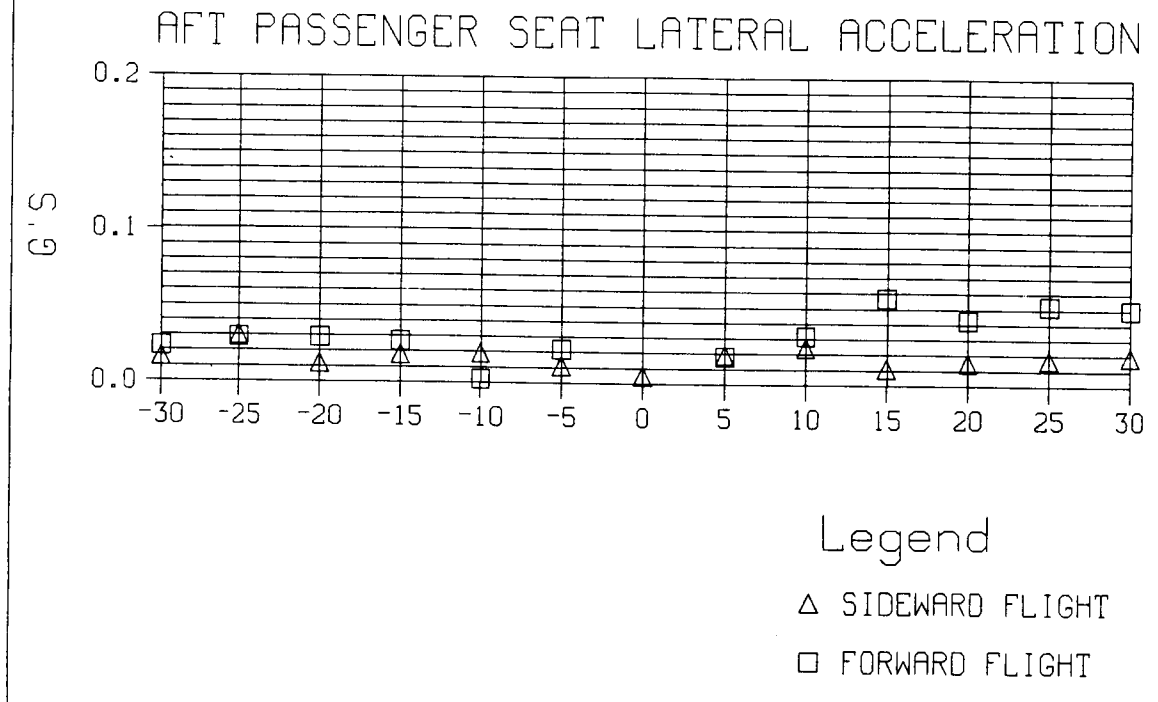

Figure B2. 4/Rev Vibration Level vs Airspeed for Transitional Flight Speed Range (Concluded)

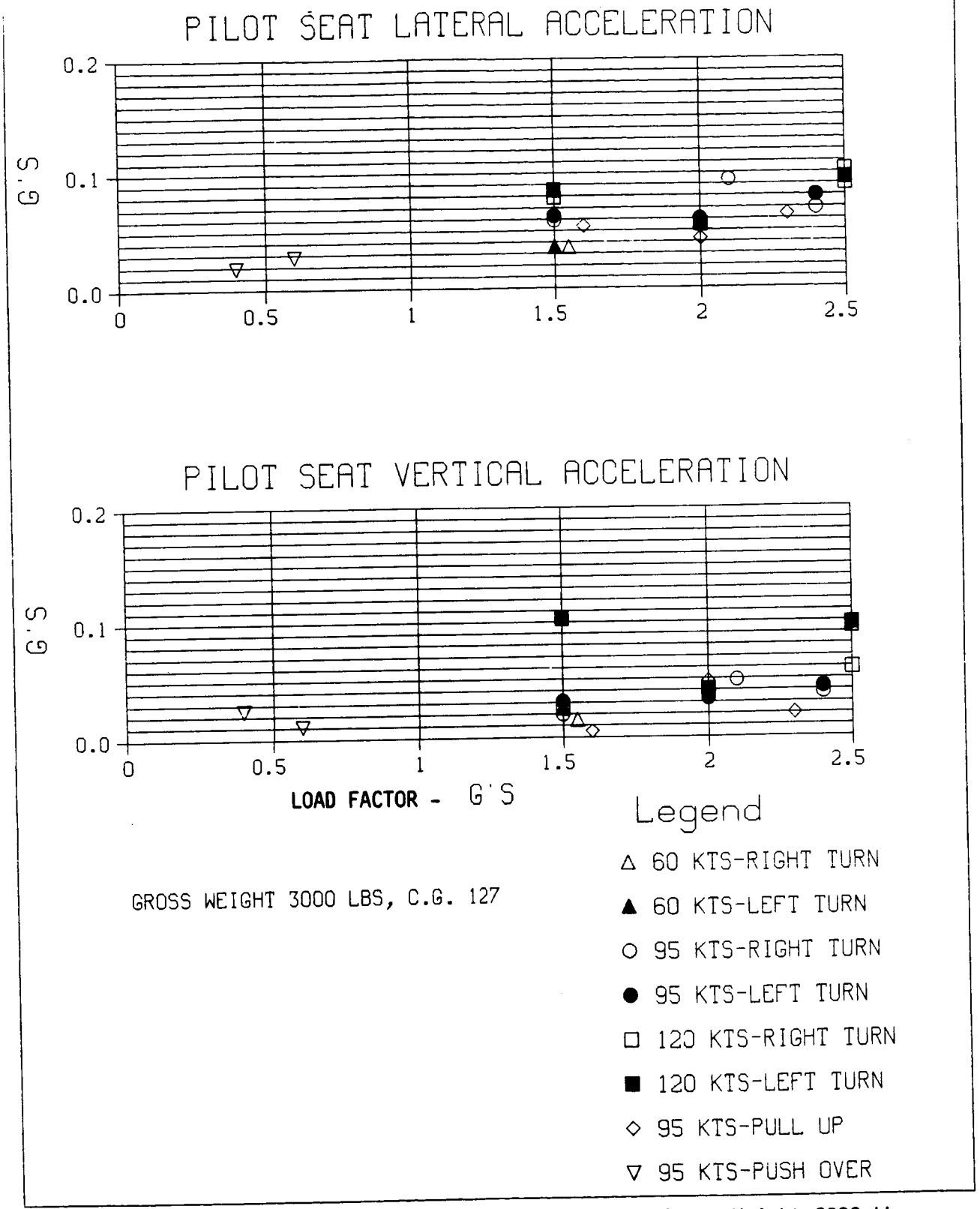

Figure B3. 4/Rev Vibration Level vs Load Factor for Gross Weight 3000 Lbs., CG 127

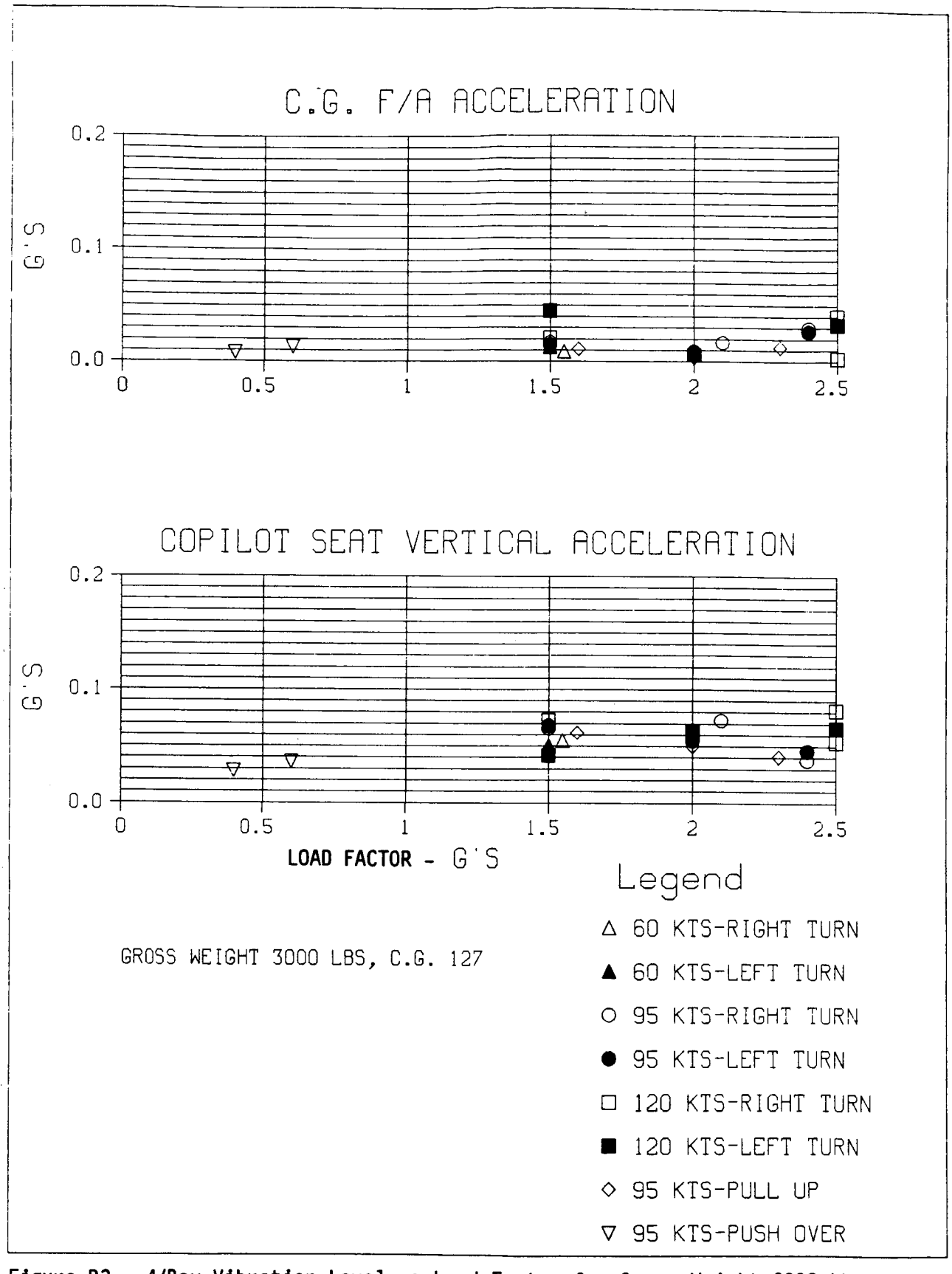

Figure B3. 4/Rev Vibration Level vs Load Factor for Gross Weight 3000 Lbs., CG 127 (Continued)

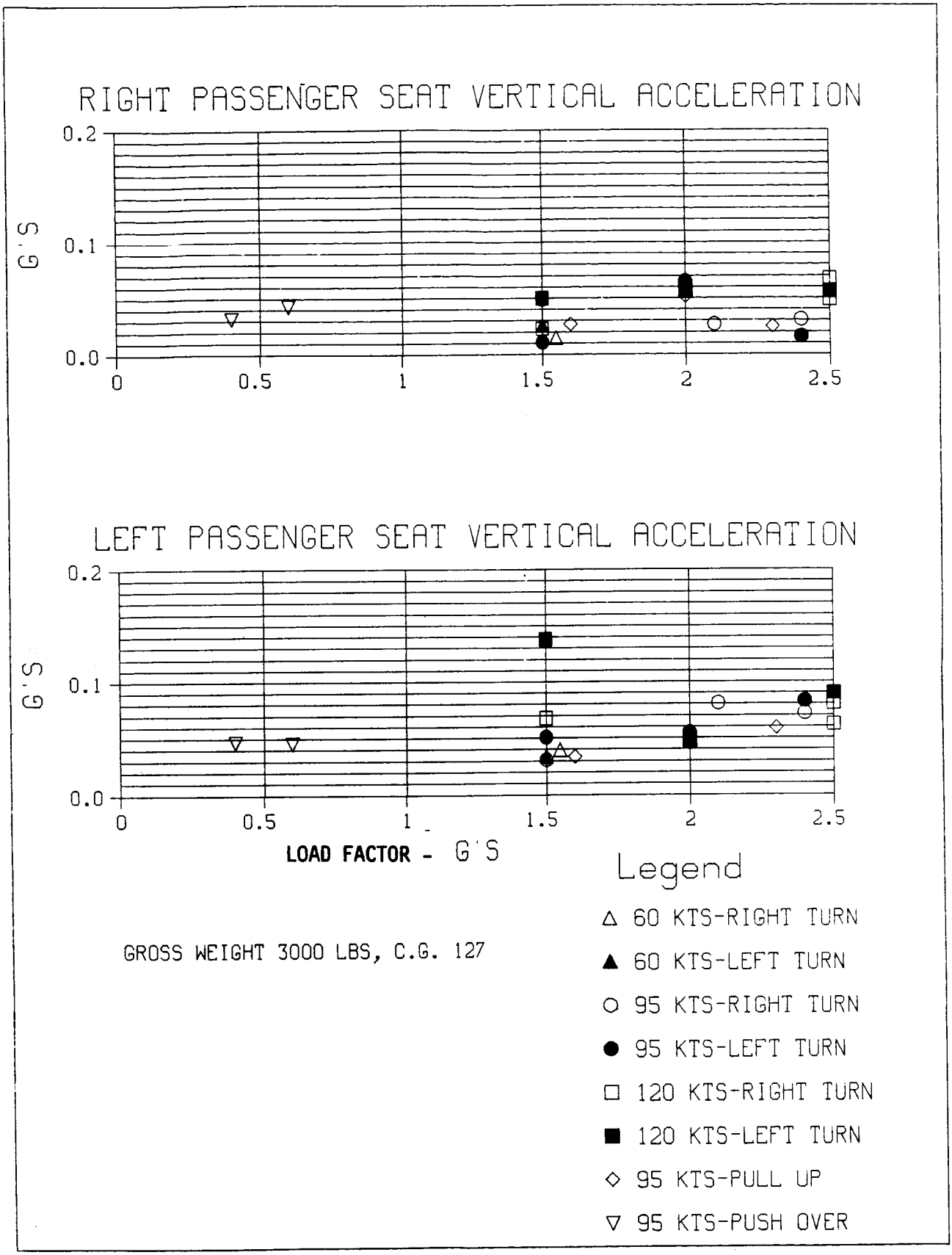

Figure B3. 4/Rev Vibration Level vs Load Factor for Gross Weight 3000 Lbs., CG 127 (Continued)

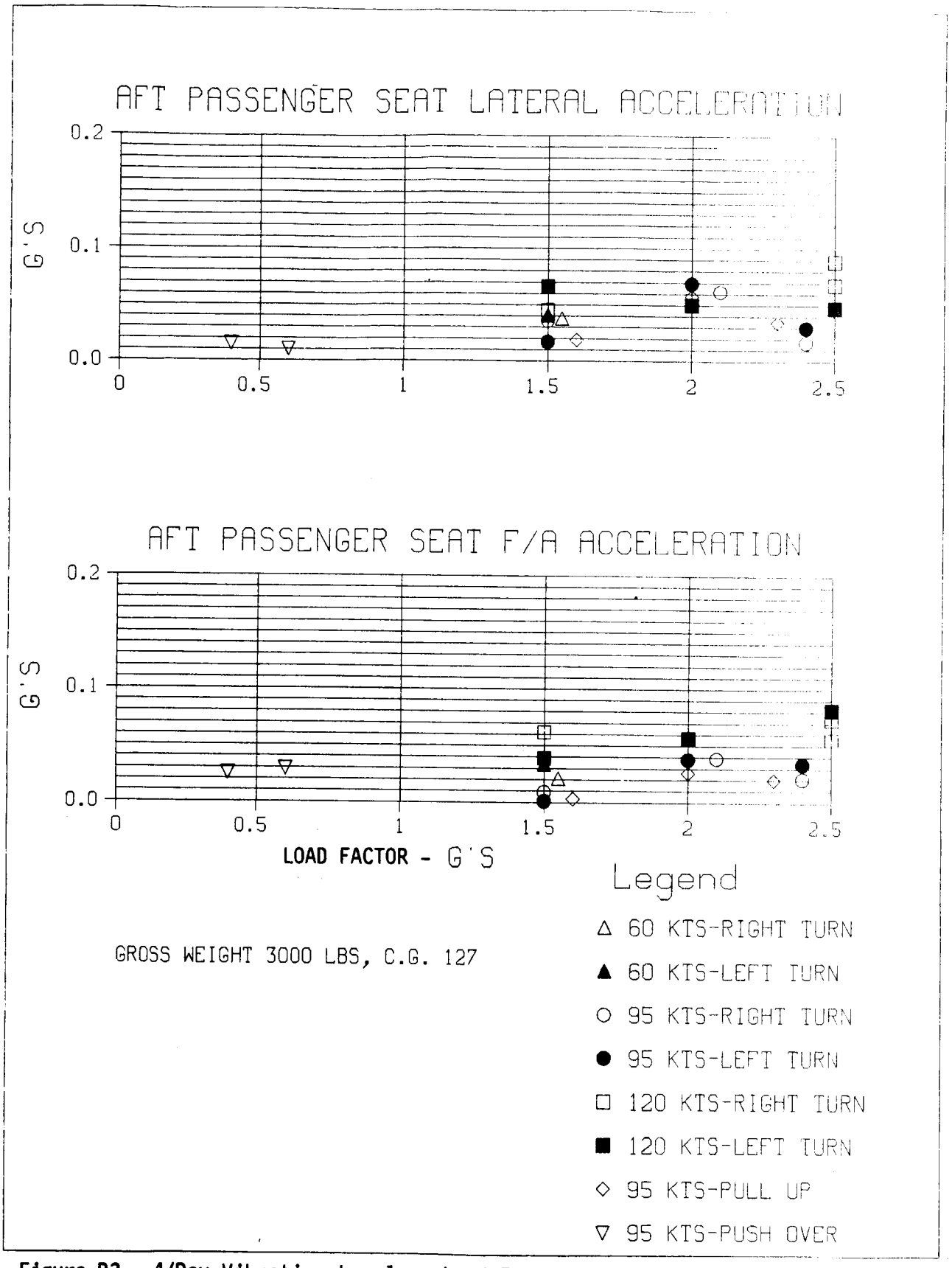

Figure B3. 4/Rev Vibration Level vs Load Factor for Gross Weight 3000 Lbs., CG 127 (Continued)

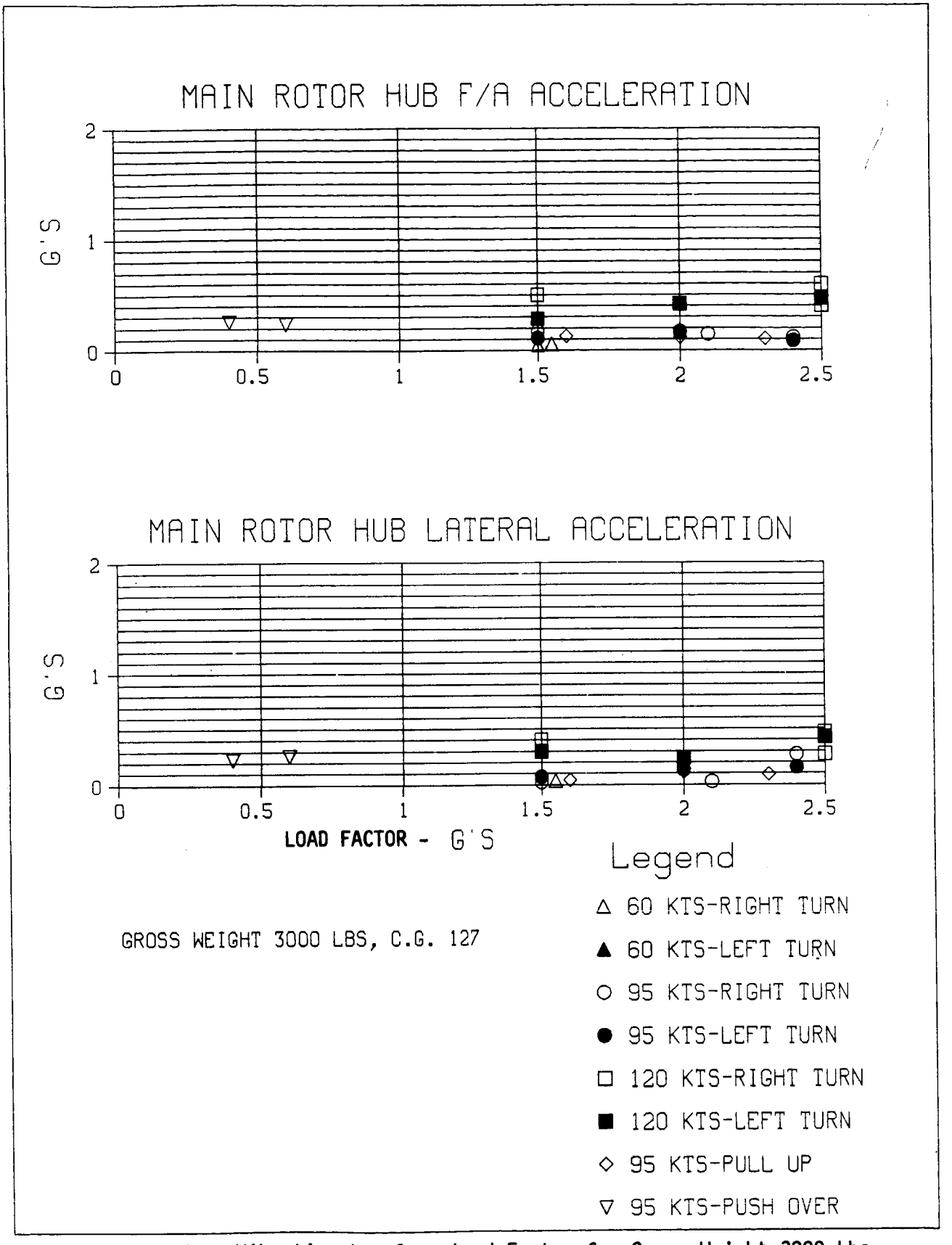

Figure B3. 4/Rev Vibration Level vs Load Factor for Gross Weight 3000 Lbs., CG 127 (Continued)

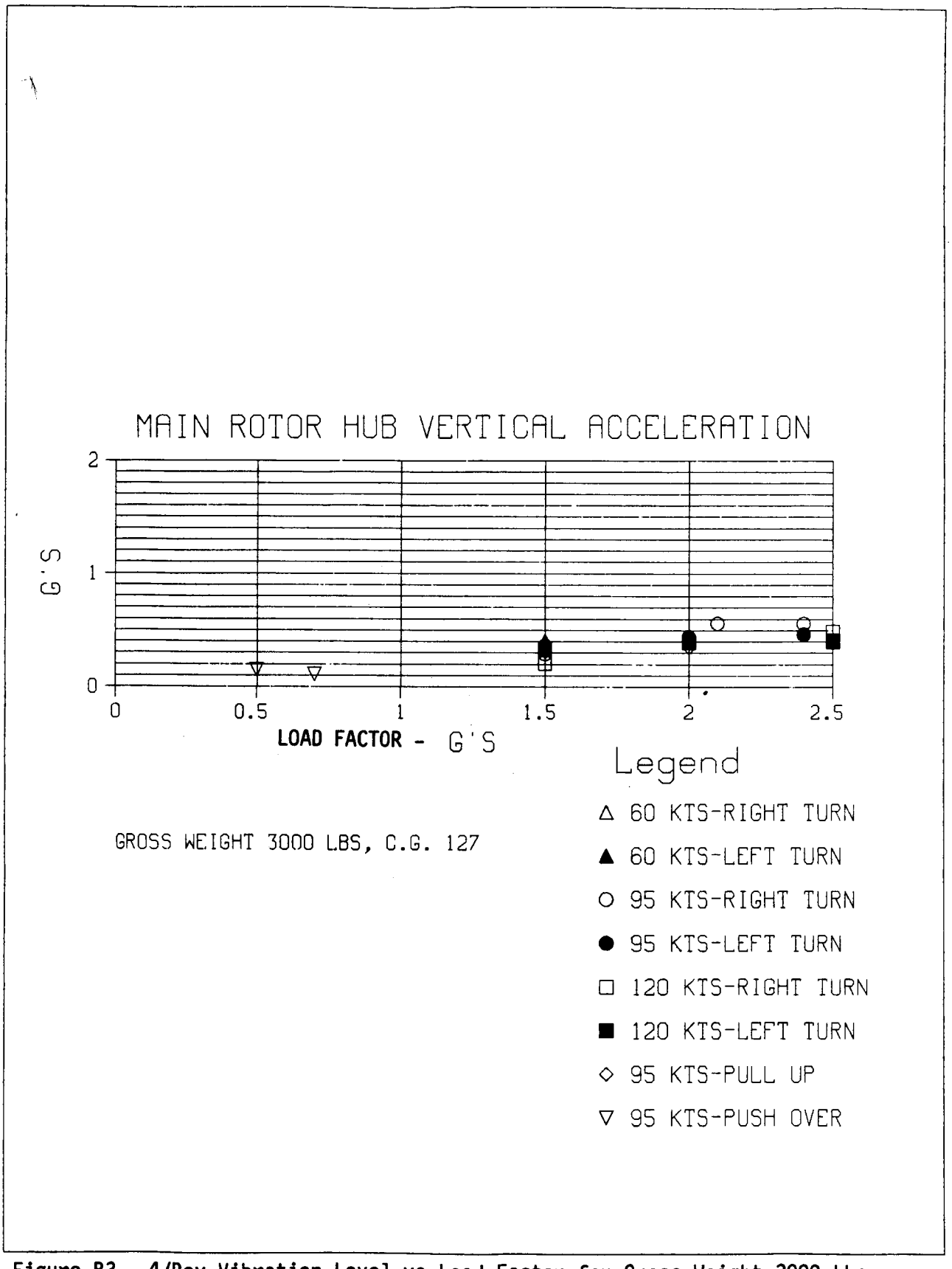

Figure B3. 4/Rev Vibration Level vs Load Factor for Gross Weight 3000 Lbs., CG 127 (Concluded)

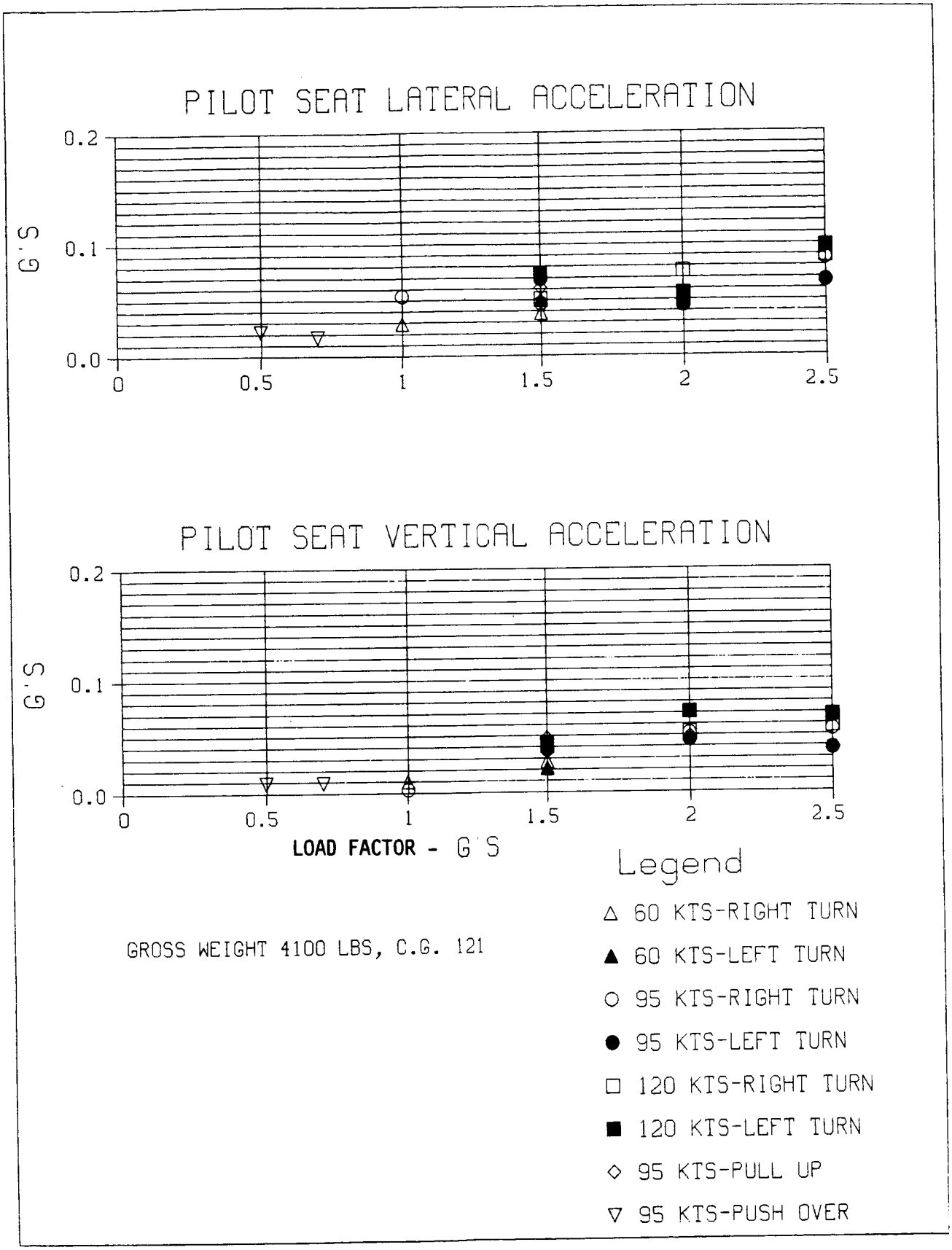

Figure B4. 4/Rev Vibration Level vs Load Factor for Gross Weight 4100 Lbs., CG 121

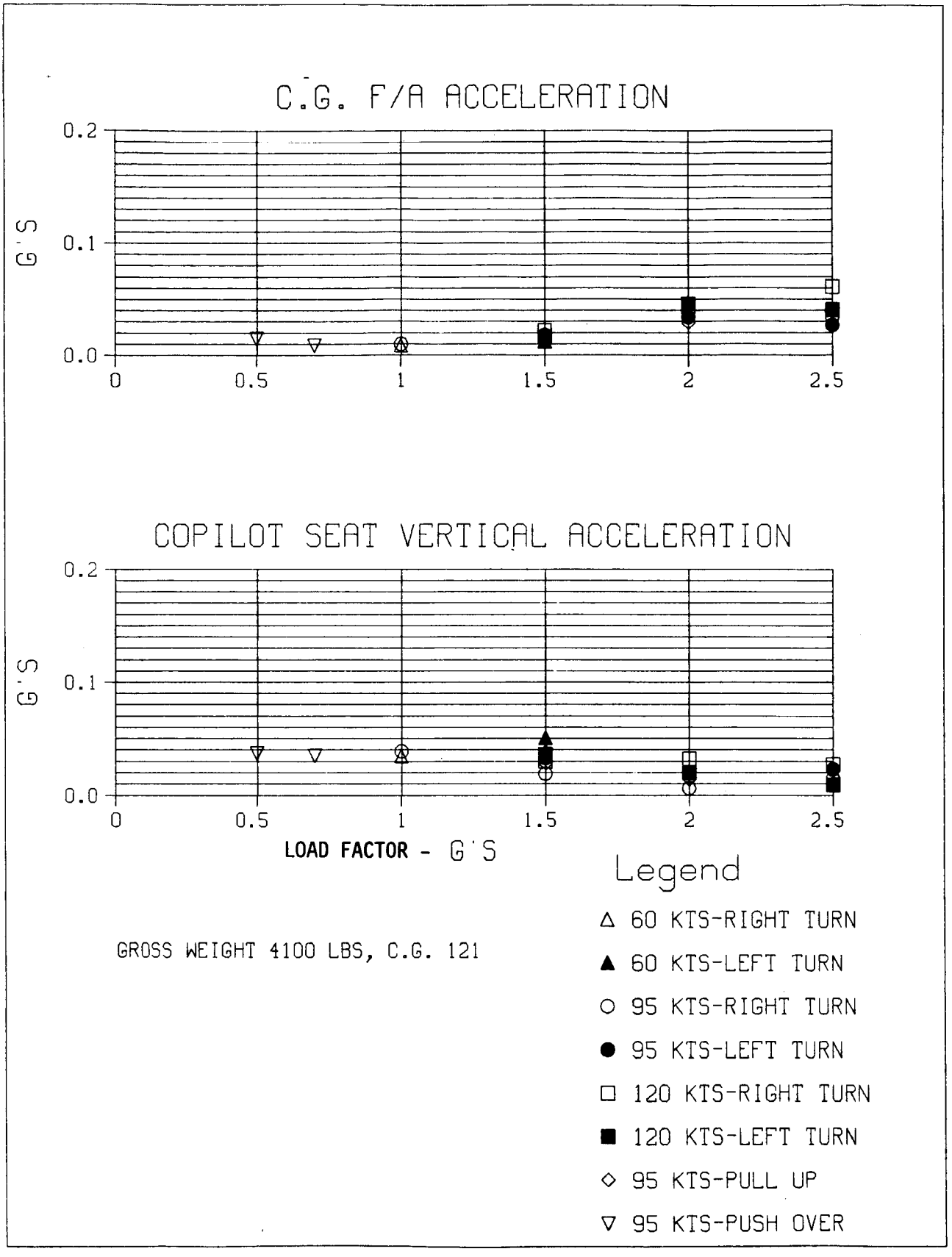

Figure B4. 4/Rev Vibration Level vs Load Factor for Gross Weight 4100 Lbs., CG 121 (Continued)

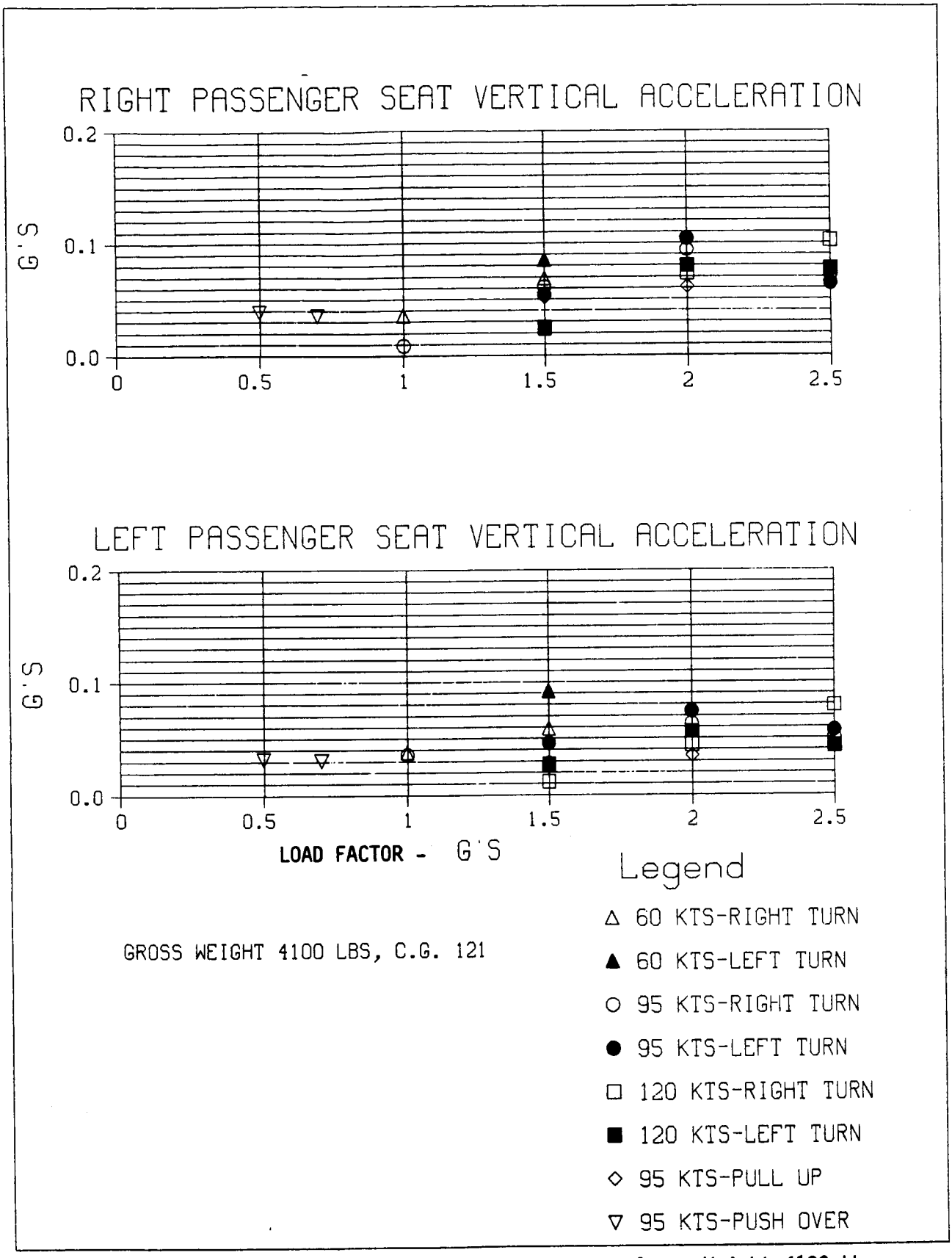

Figure B4. 4/Rev Vibration Level vs Load Factor for Gross Weight 4100 Lbs., CG 121 (Continued)

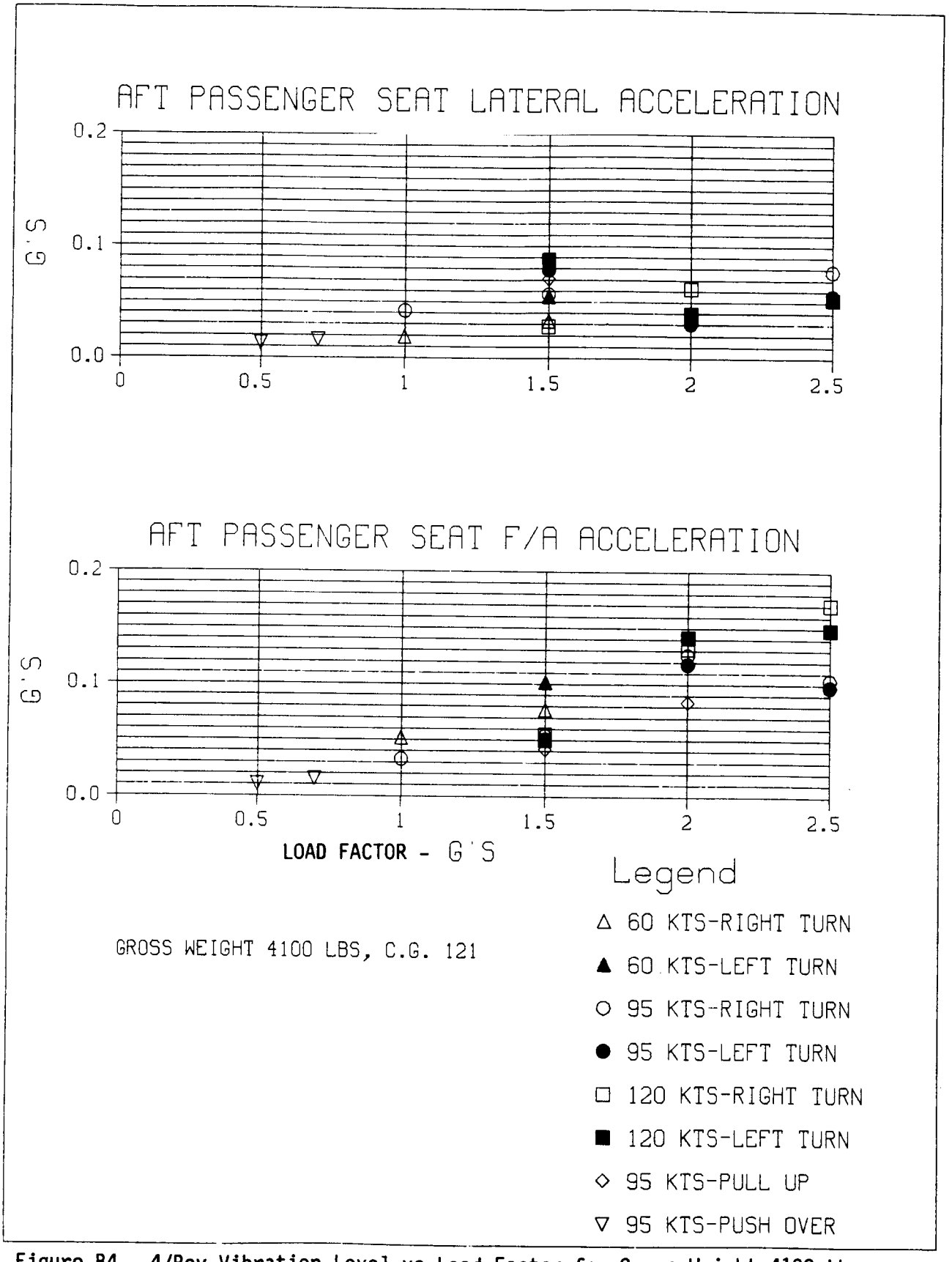

Figure B4. 4/Rev Vibration Level vs Load Factor for Gross Weight 4100 Lbs., CG 121 (Continued)

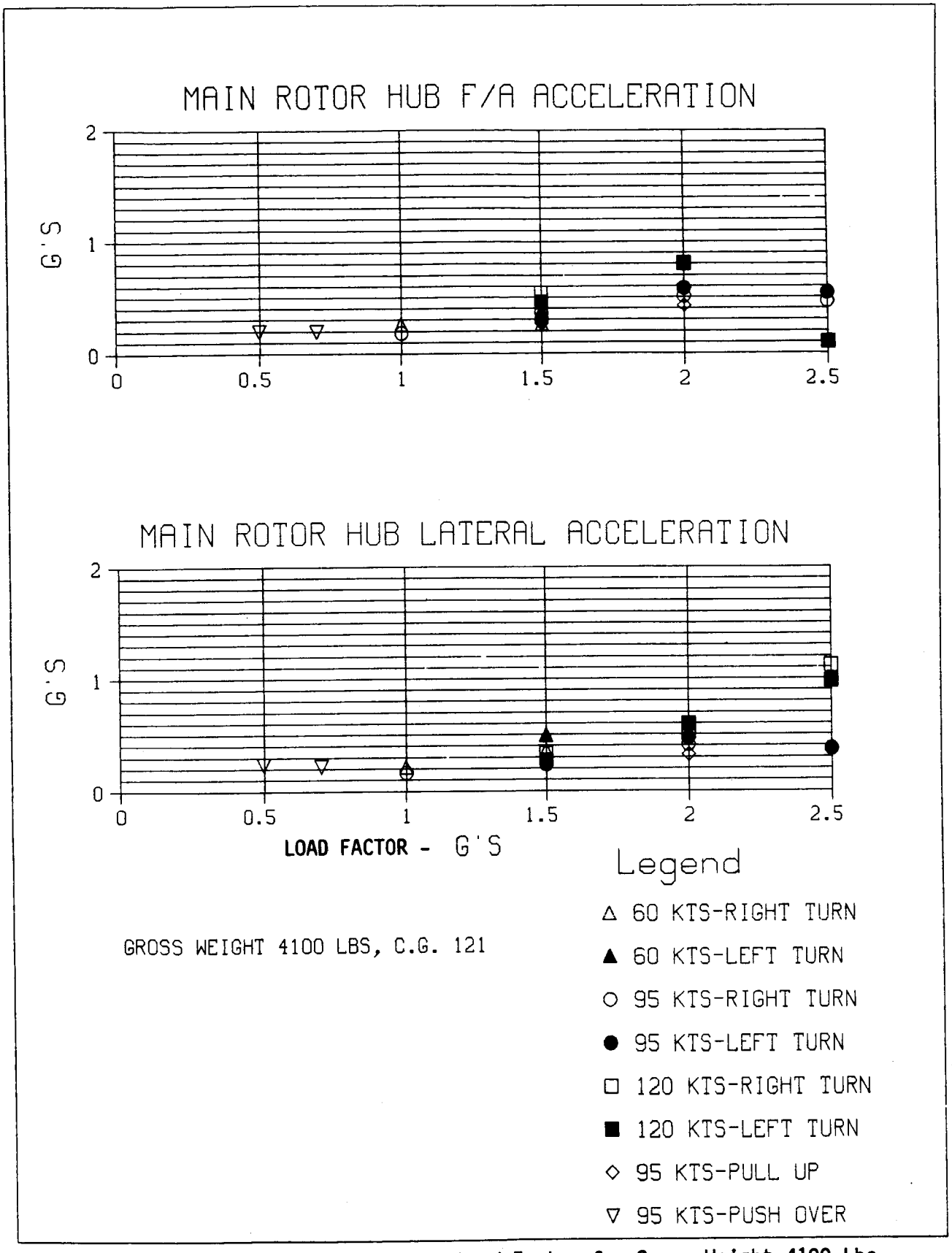

Figure B4. 4/Rev Vibration Level vs Load Factor for Gross Weight 4100 Lbs., CG 121 (Continued)

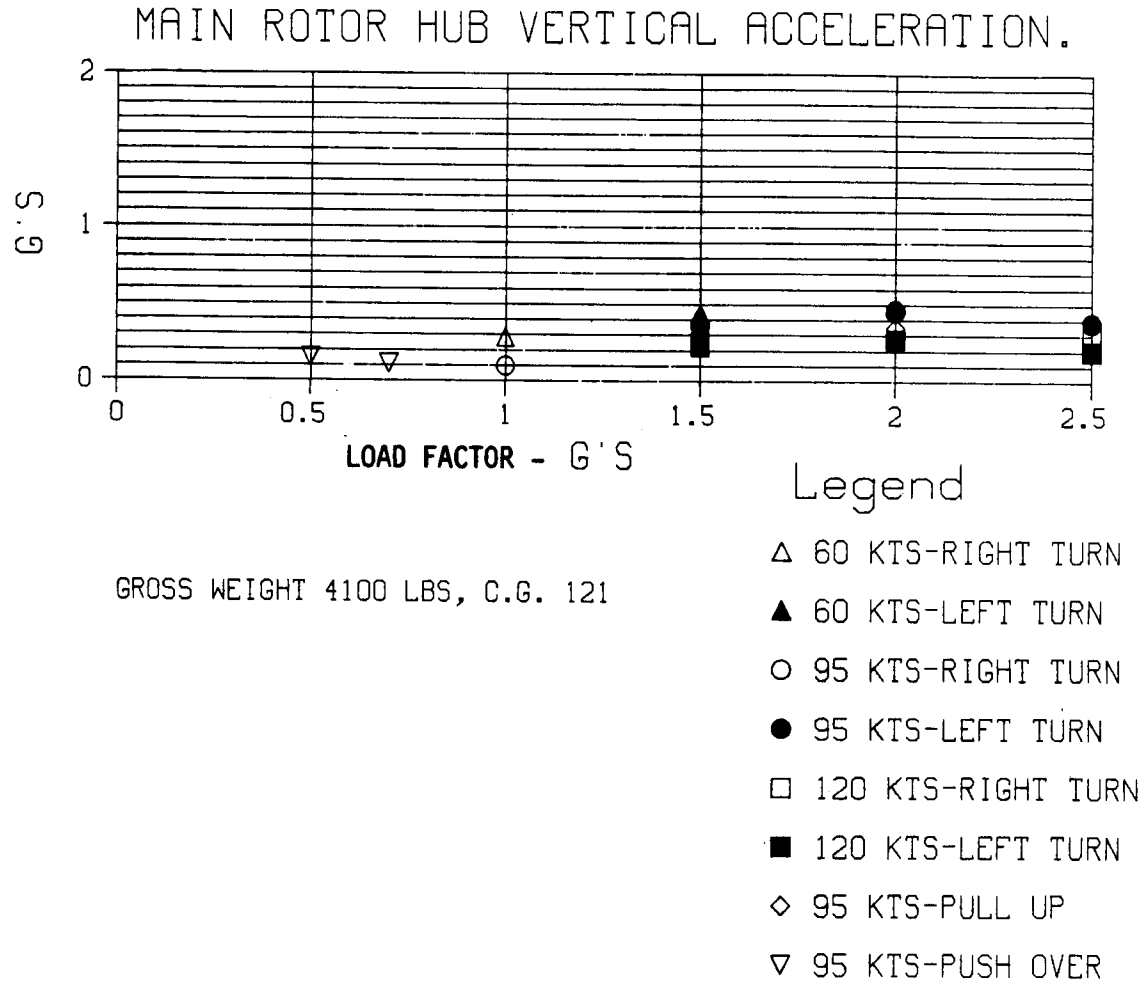

Figure B4. 4/Rev Vibration Level vs Load Factor for Gross Weight 4100 Lbs., CG 121 (Concluded)

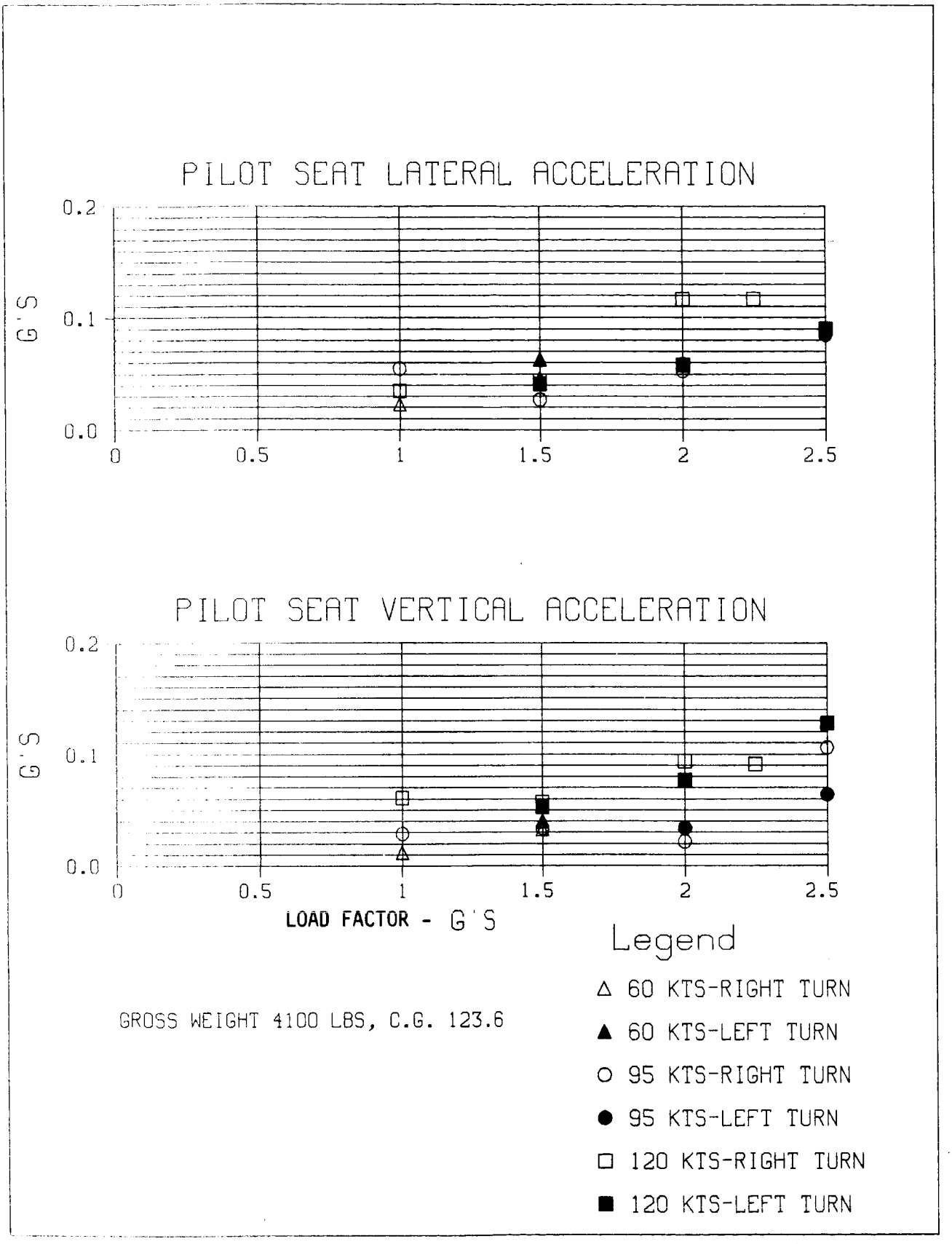

Figure B5. 4/Rev Vibration Level vs Load Factor for Gross Weight 4100 Lbs., CG 123.6

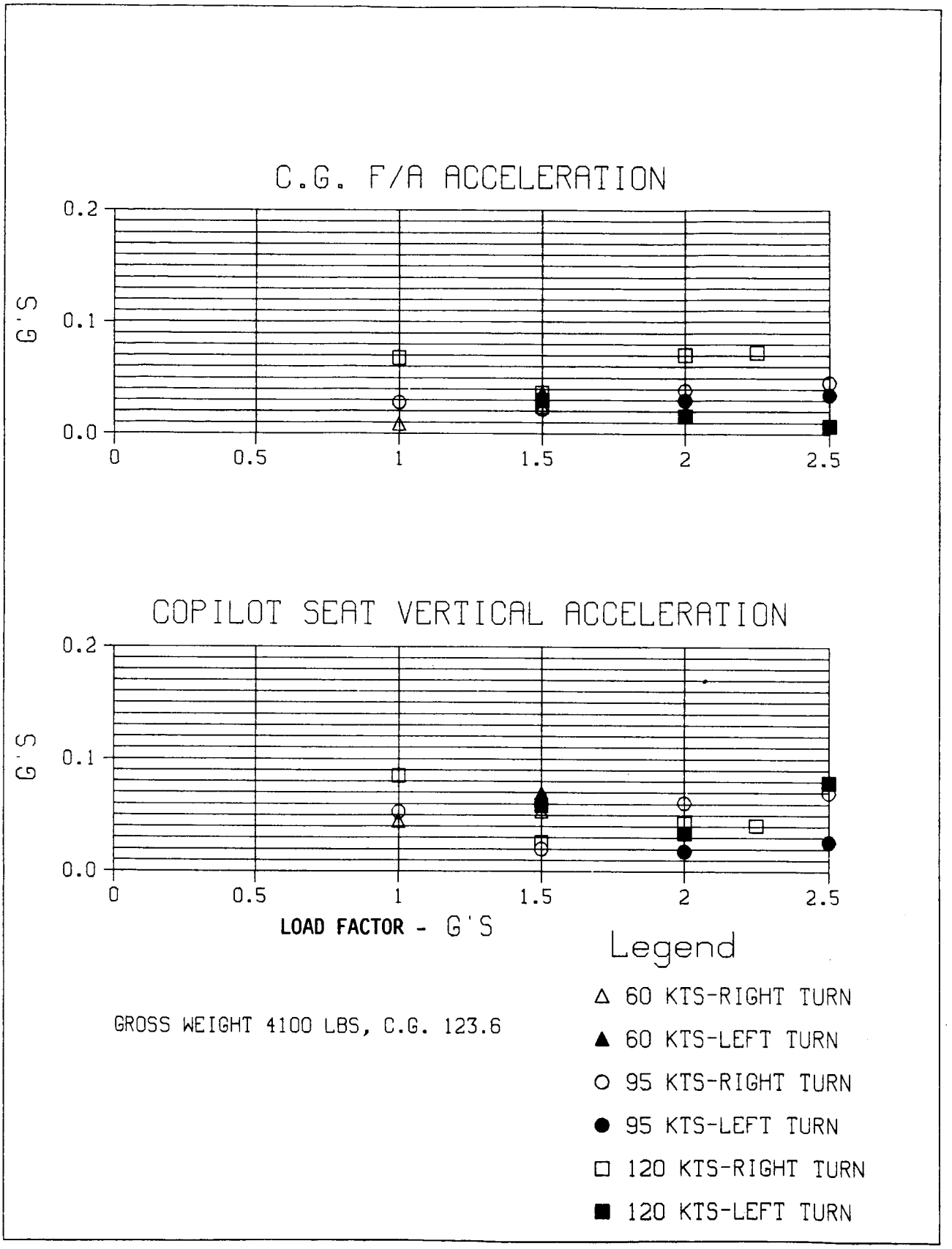

Figure B5. 4/Rev Vibration Level vs Load Factor for Gross Weight 4100 Lbs., CG 123.6 (Continued)

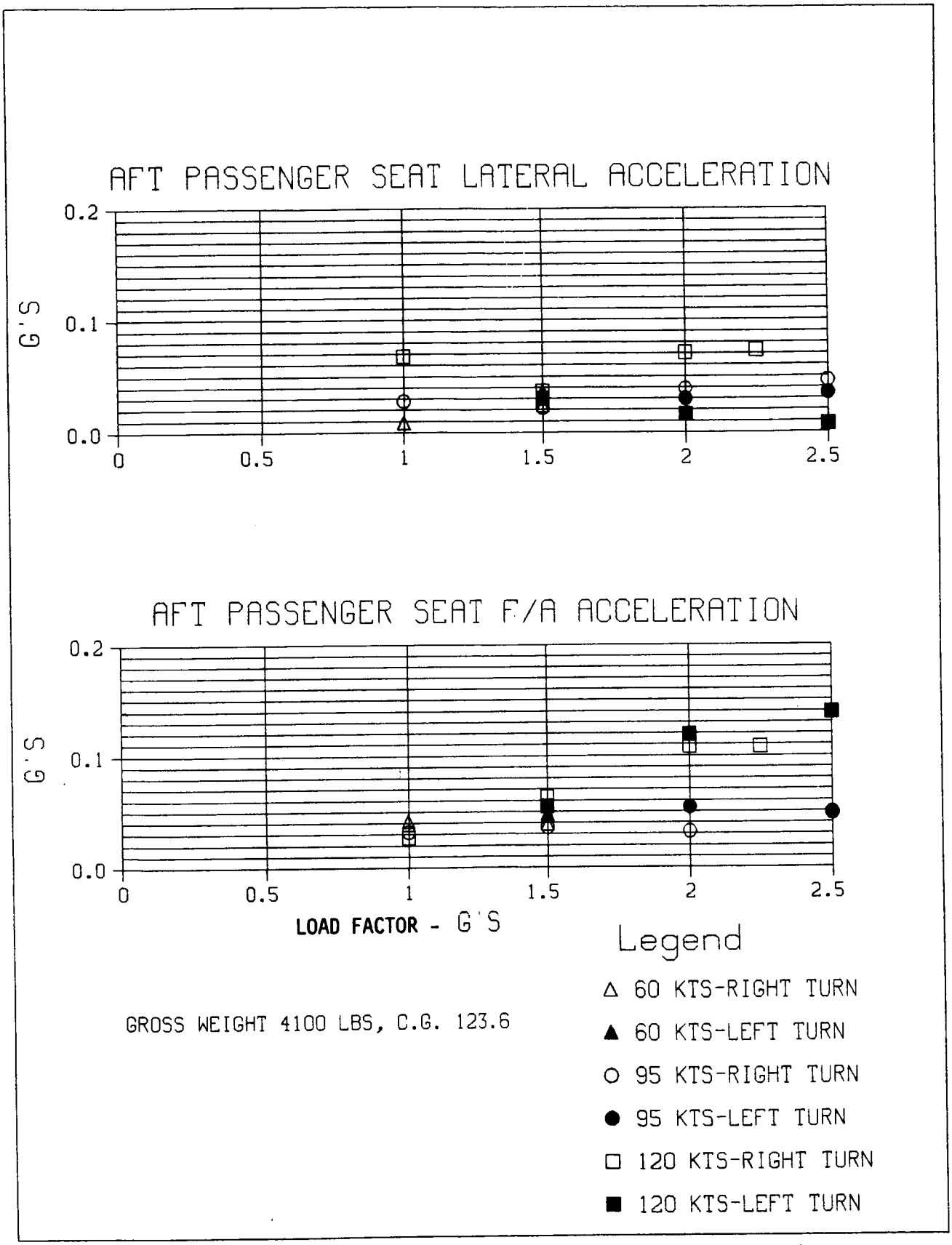

Figure B5. 4/Rev Vibration Level vs Load Factor for Gross Weight 4100 Lbs., CG 123.6 (Continued)

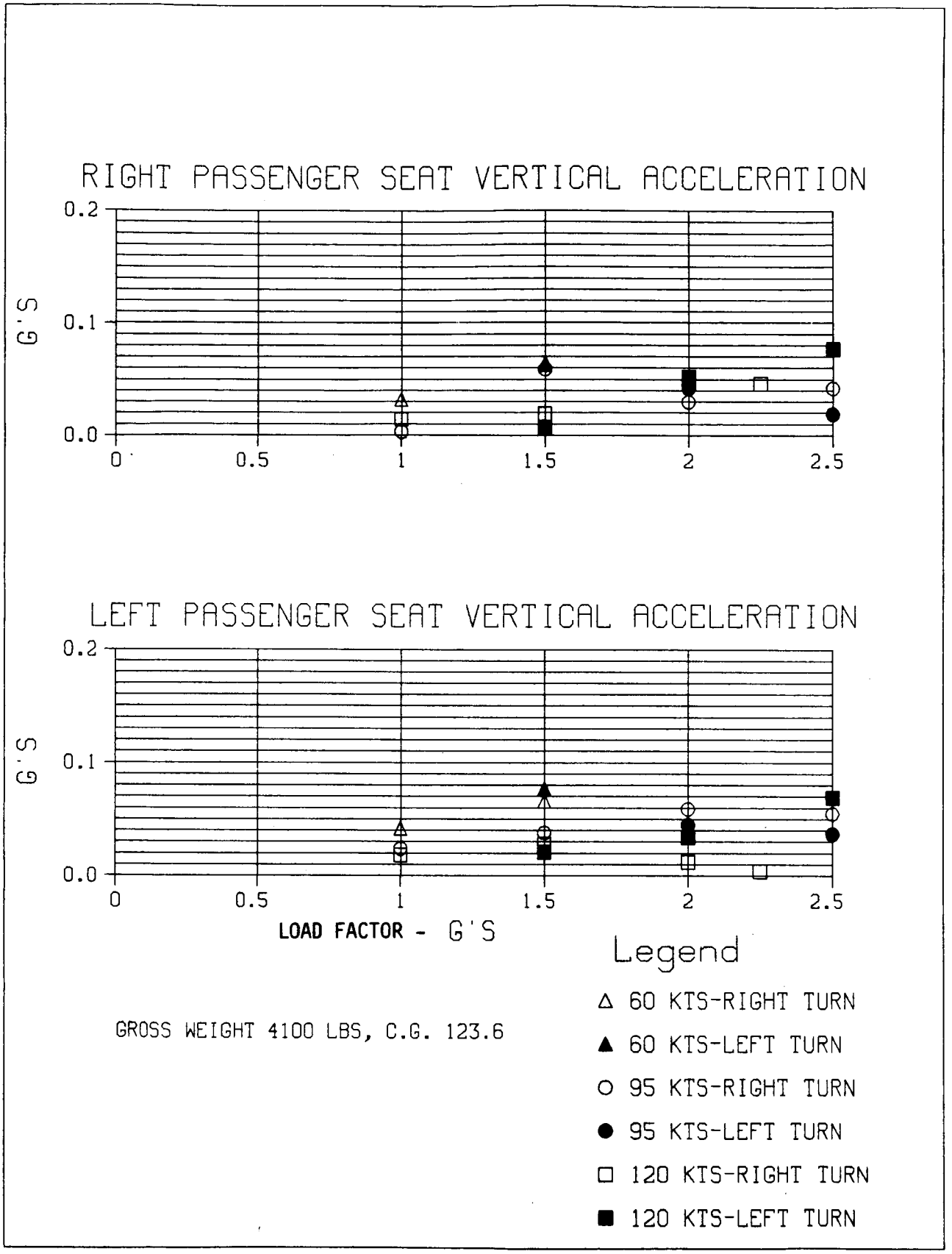

Figure B5. 4/Rev Vibration Level vs Load Factor for Gross Weight 4100 Lbs., CG 123.6 (Continued)

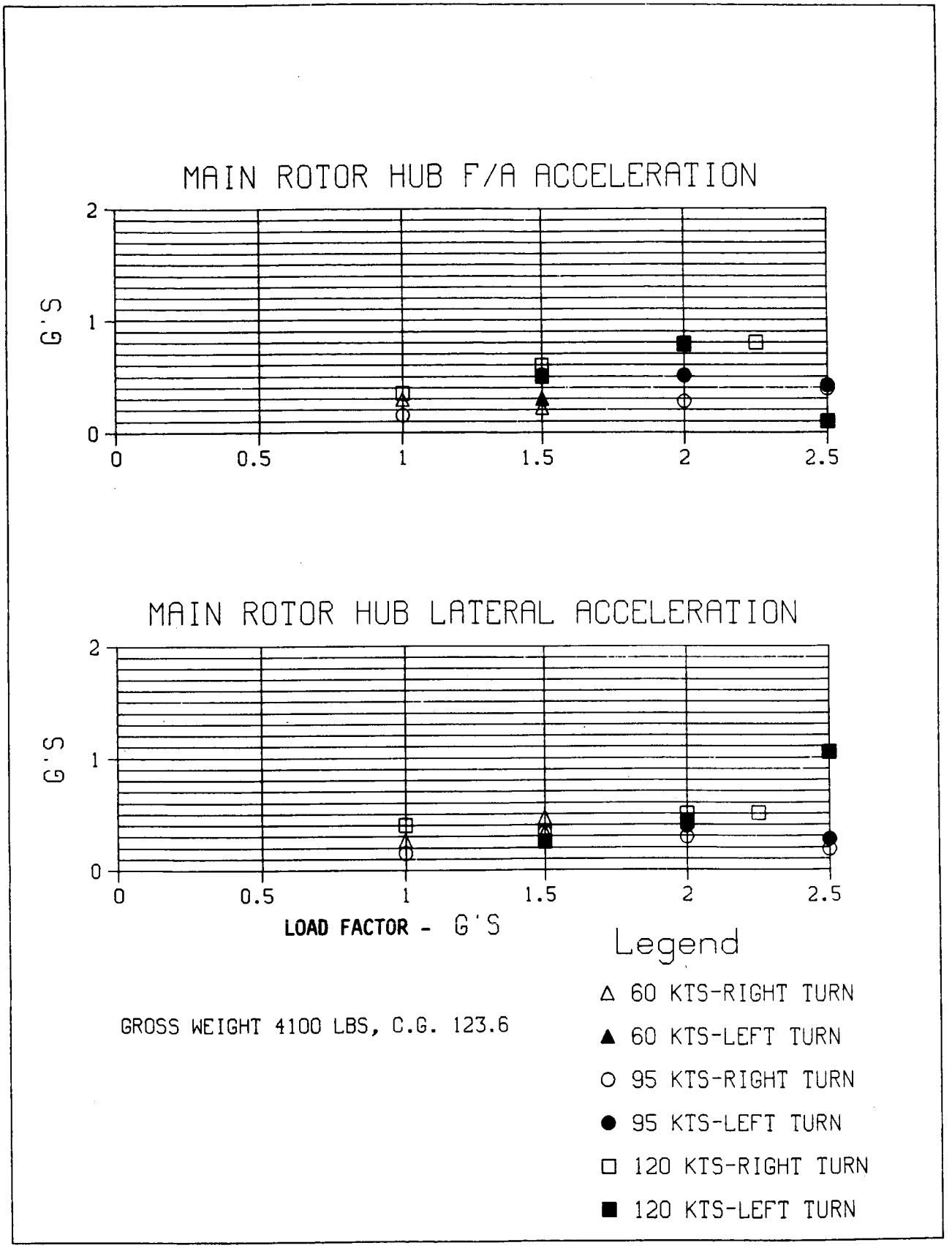

Figure B5. 4/Rev Vibration Level vs Load Factor for Gross Weight 4100 Lbs., CG 123.6 (Continued)

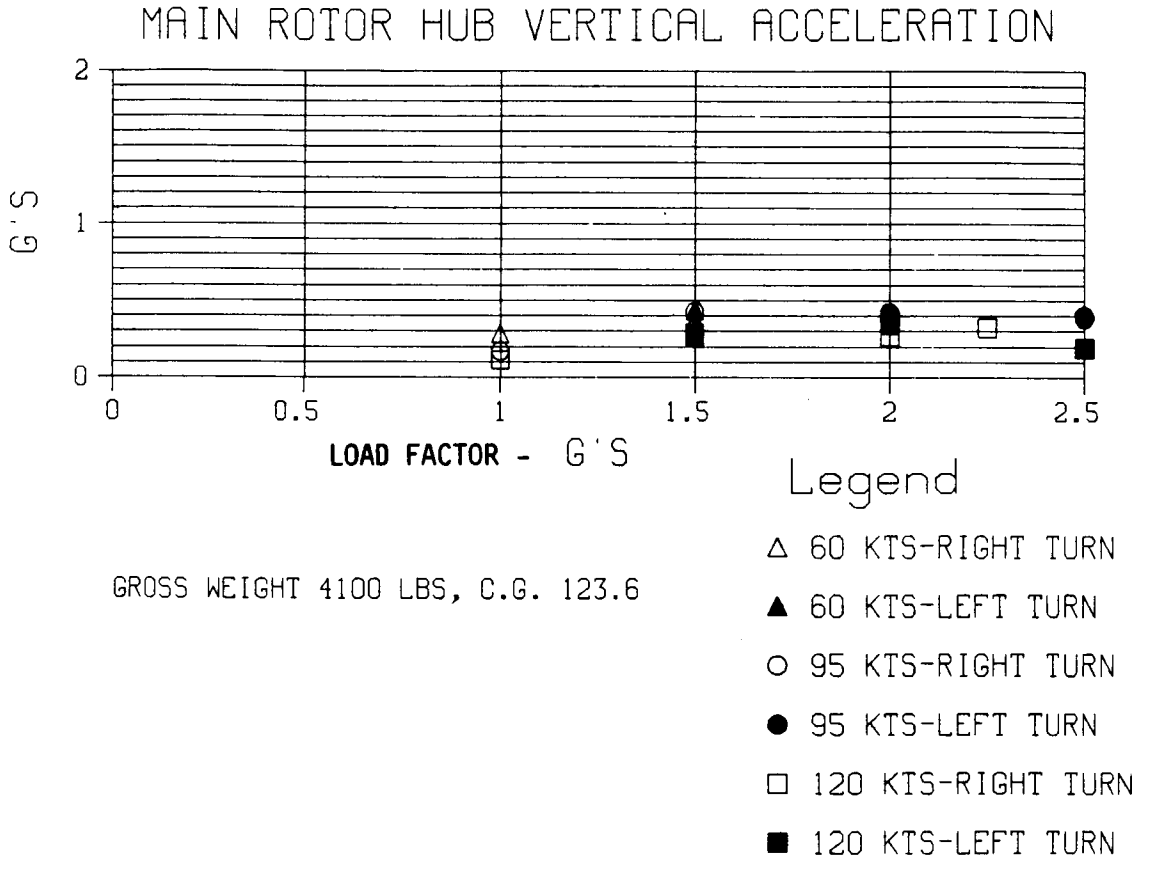

Figure B5. 4/Rev Vibration Level vs Load Factor for Gross Weight 4100 Lbs., CG 123.6 (Concluded)

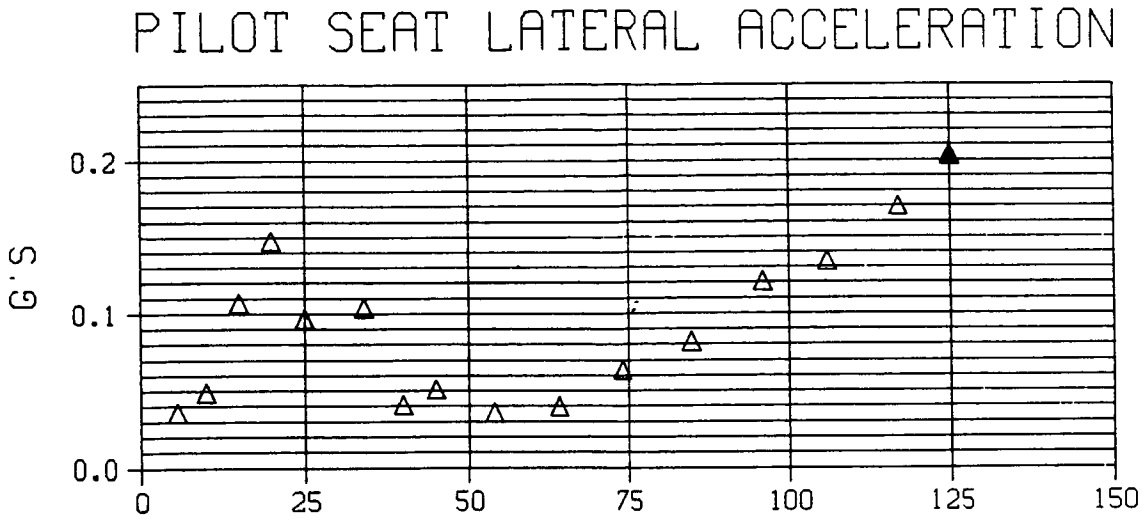

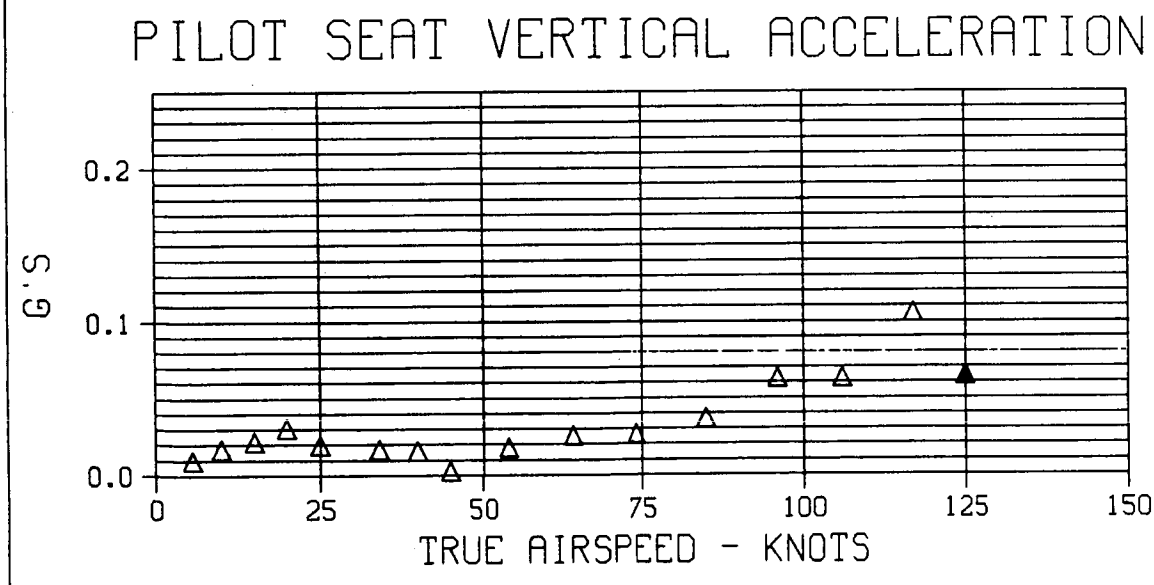

BLACKENED SYMBOL DENOTES DIVE

Figure B6. 4/Rev Vibration Level vs Airspeed for Baseline Helicopter with Soft Pylon

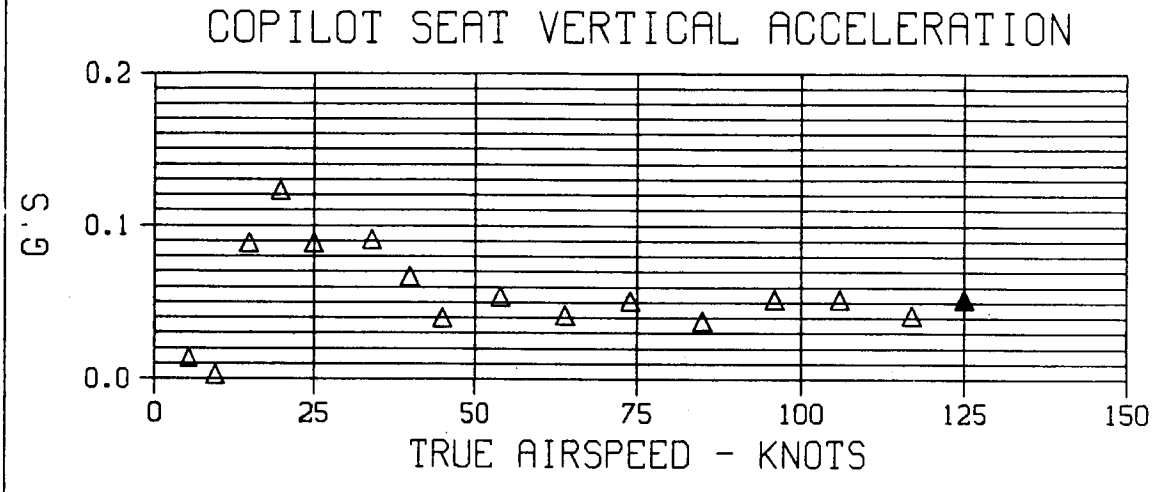

BLACKENED SYMBOL DENOTES DIVE

Figure B6. 4/Rev Vibration Level vs Airspeed for Baseline Helicopter with Soft Pylon (Continued)

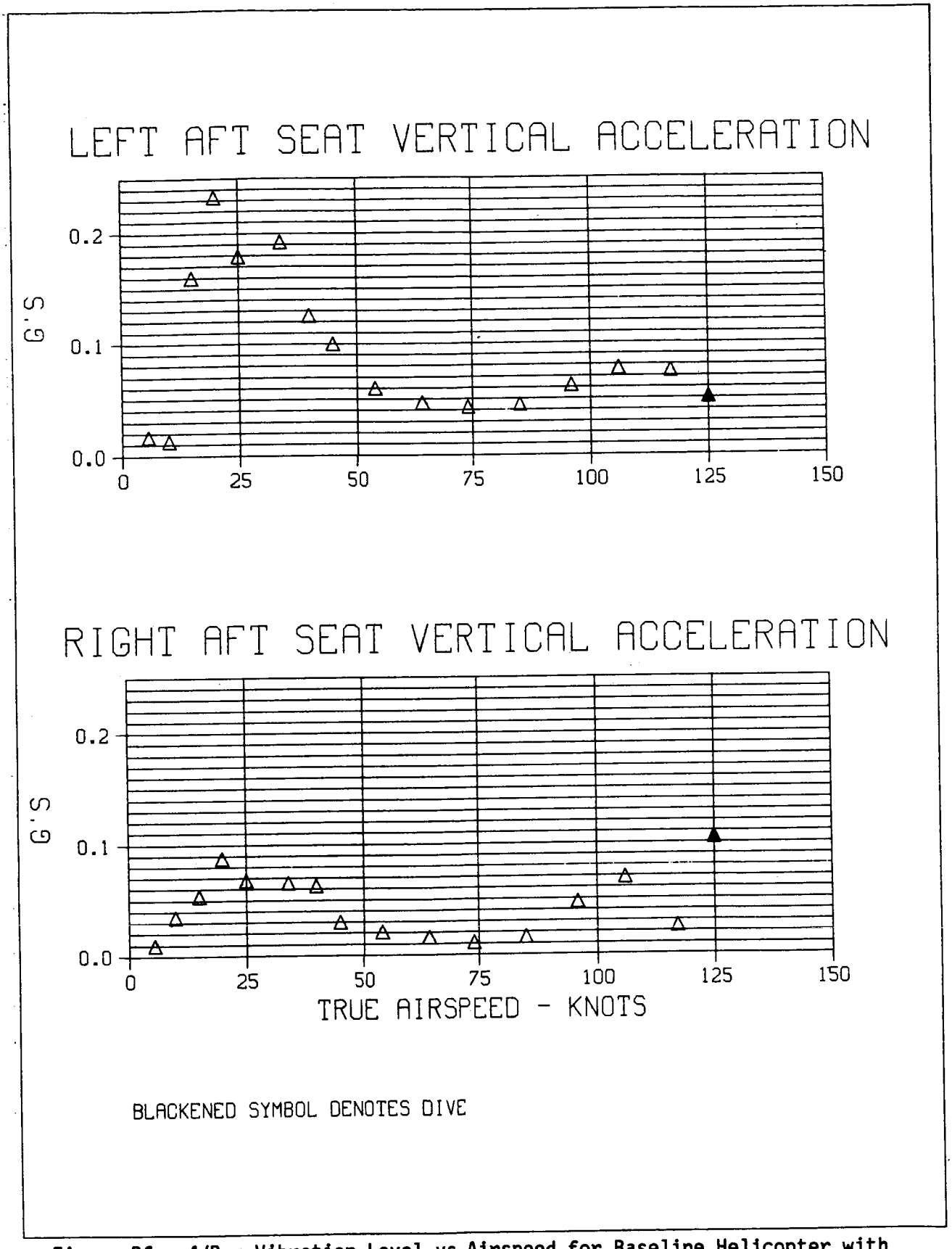

Figure B6. 4/Rev Vibration Level vs Airspeed for Baseline Helicopter with Soft Pylon (Concluded)

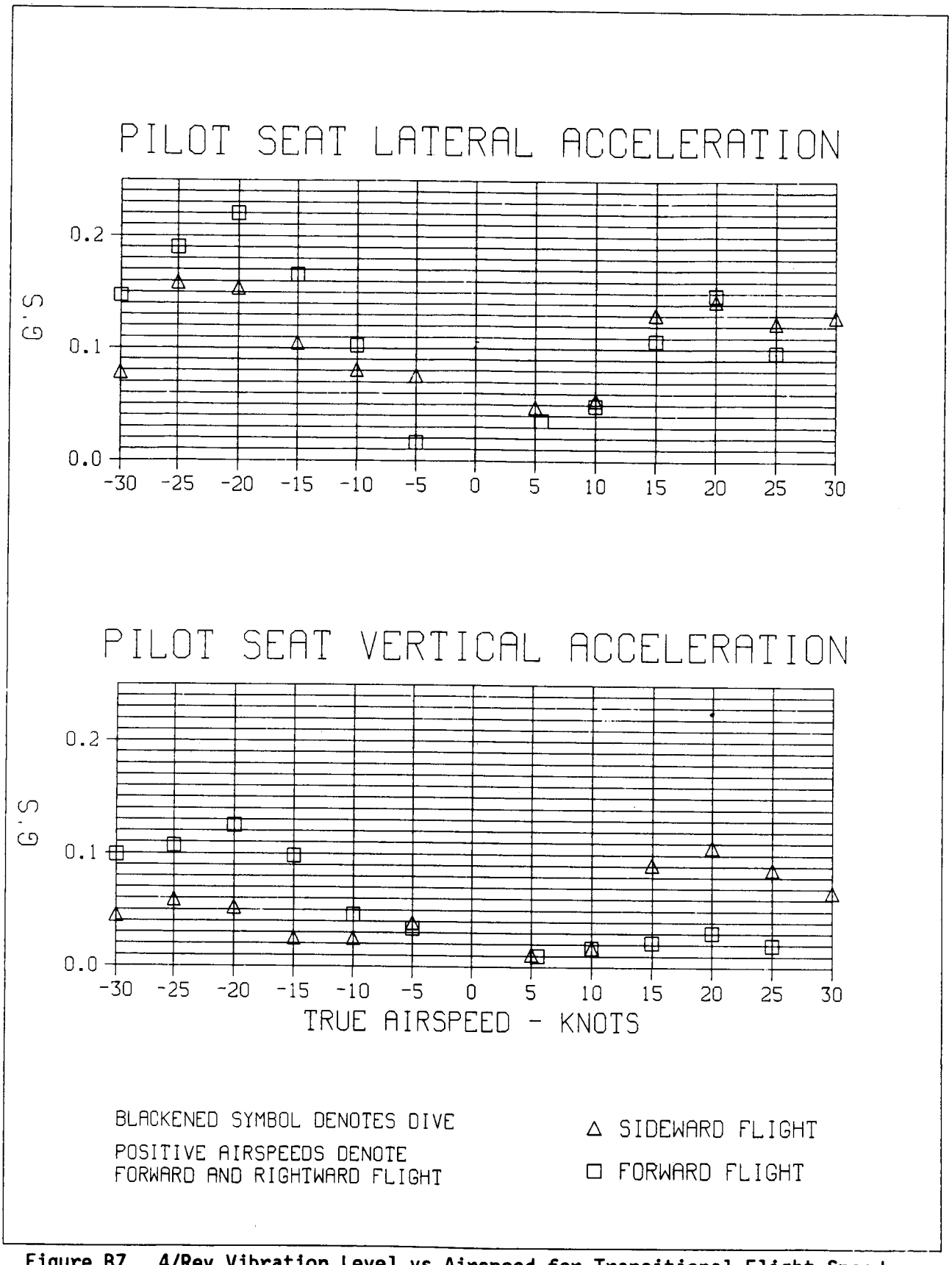

Figure B7. 4/Rev Vibration Level vs Airspeed for Transitional Flight Speed Range on Baseline Helicopter with Soft Pylon

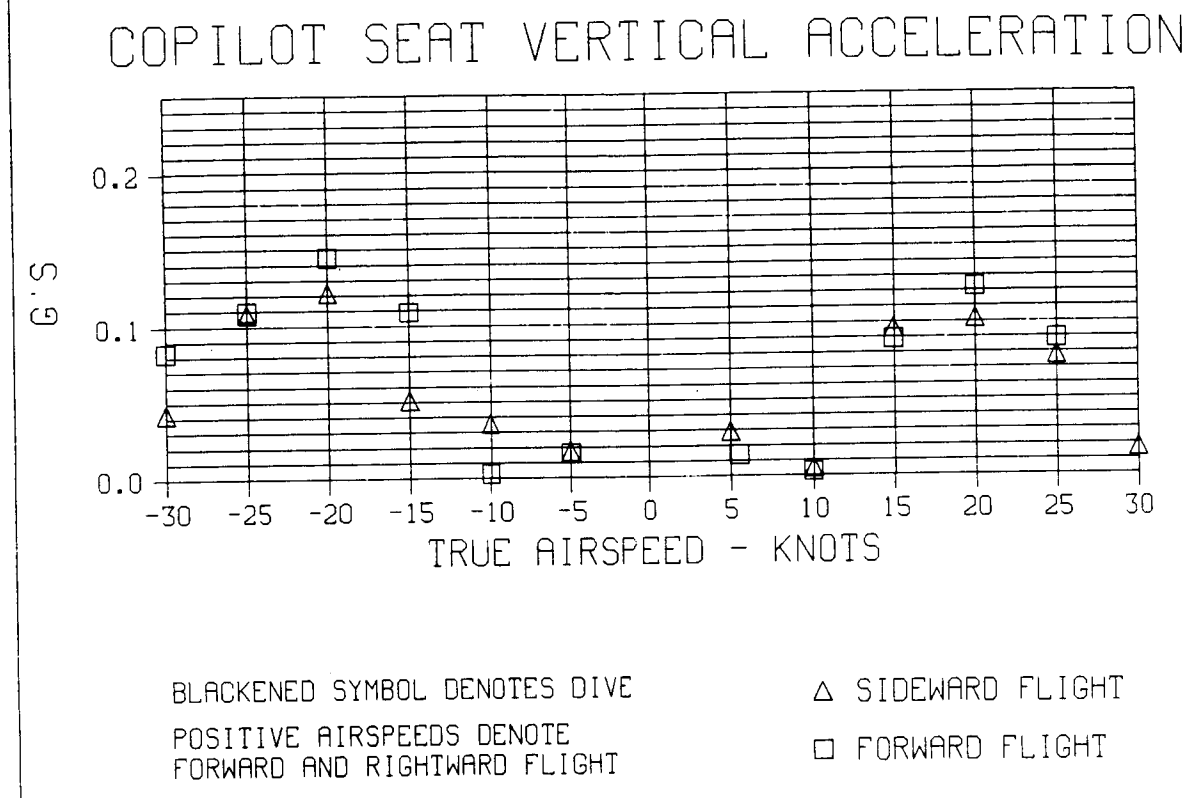

Figure B7. 4/Rev Vibration Level vs Airspeed for Transitional Flight Speed Range on Baseline Helicopter with Soft Pylon (Continued)

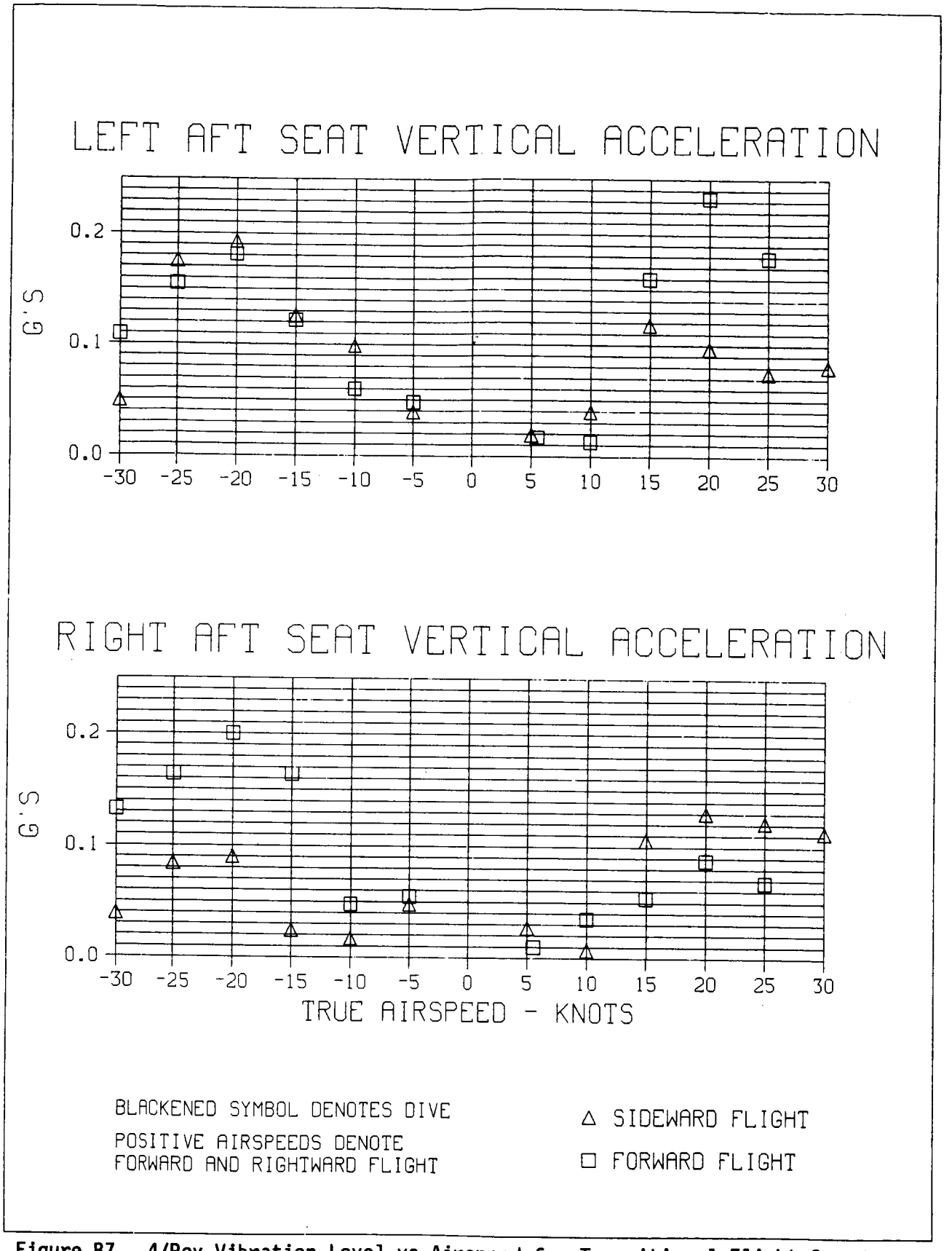

Figure B7. 4/Rev Vibration Level vs Airspeed for Transitional Flight Speed Range on Baseline Helicopter with Soft Pylon (Concluded)

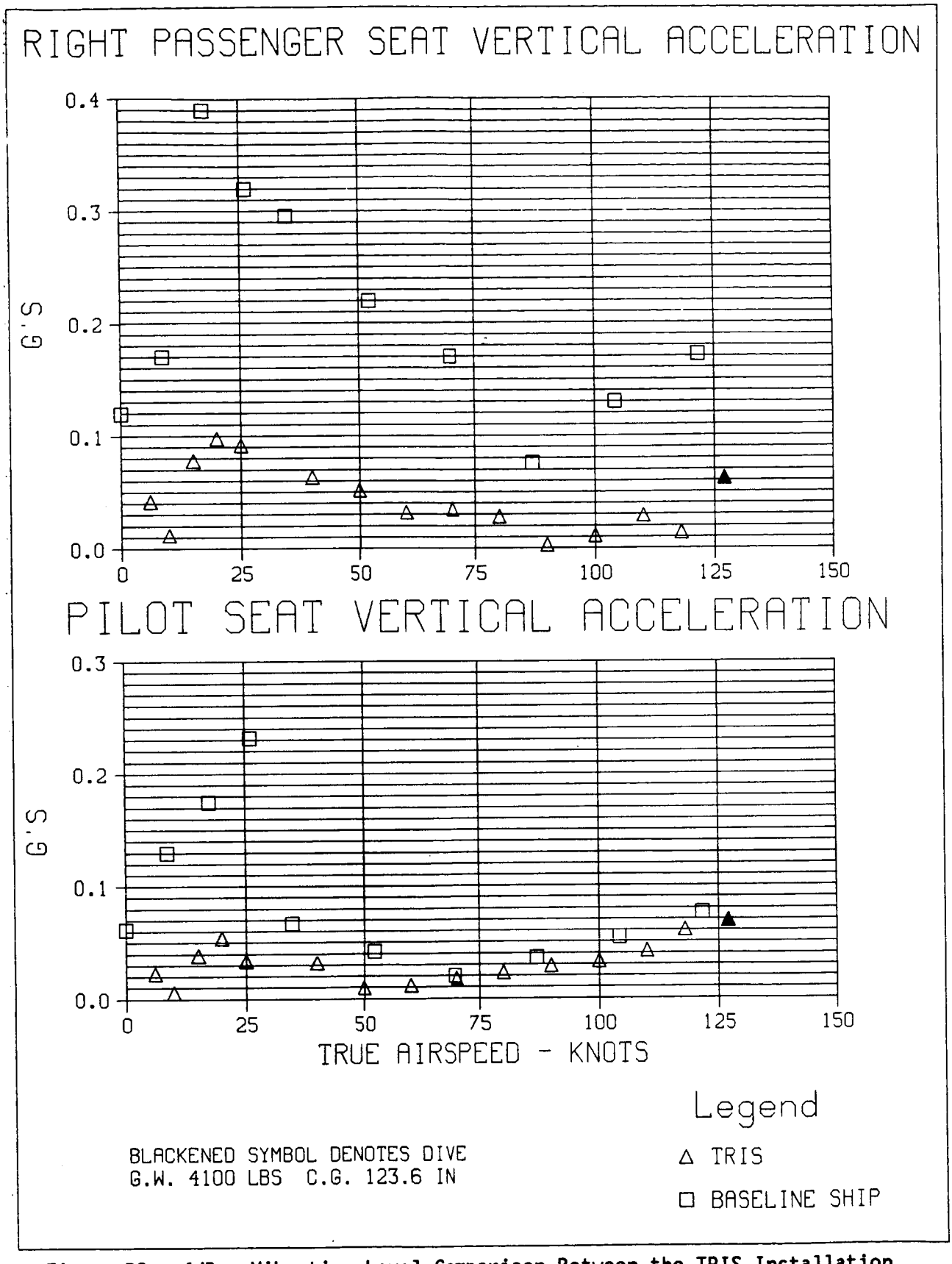

Figure B8. 4/Rev Vibration Level Comparison Between the TRIS Installation and the Baseline Helicopter with the Focus Pylon Installation

REFERENCES

References

1. Halwes, Dennis R.; and Nicks, Colby O.: "Six Degree-of-Freedom 'LIVE' Isolation System Tests, Part I: Interim Report," NASA Contractor Report 177928, 1986.

2. Viswanathan, Sathy P.; and Myers, Alan W.: "Reduction of Helicopter Vibration through Control of Hub-Impedance," Journal of the American Helicopter Society, Vol. 25 - No. 4, 1980, pp. 3-12.

3. Balke, Rodney W.: "Development of the Kinematic Focal Isolation System for Helicopter Rotors," Presented at the 38th Shock and Vibration Symposium, St. Louis, Missouri, 1968.

Standard Bibliographic Page

1. Report No.	2. Government Accession No.	3. Recipient's Catalog No.
NASA CR-4082		

4. Title and Subtitle	5. Report Date
Ground and Flight Test Results of a Total Main Rotor Isolation System	July 1987
	6. Performing Organization Code
7. Author(s)	8. Performing Organization Report No.
Dennis R. Halwes	699-099-055
9. Performing Organization Name and Address	10. Work Unit No.
Bell Helicopter Textron Inc. P.O. Box 482 Fort Worth, TX 76101	505-61-51
	11. Contract or Grant No.
	NAS1-16969
12. Sponsoring Agency Name and Address	13. Type of Report and Period Covered
National Aeronautics and Space Administration Washington, DC 20546	Contractor Report
	14. Sponsoring Agency Code

15. Supplementary Notes

Technical Monitor: John H. Cline, U.S. Army Aerostructures Directorate, USAARTA-AVSCOM, Langley Research Center, Hampton, Virginia.
Final Report - The contract research effort which led to the results in this report was funded by the U.S. Army Aerostructures Directorate.

16. Abstract

A six degree-of-freedom (DOF) isolation system using six LIVE units has been installed under an Army/NASA contract on a Bell 206LM helicopter. This system has been named the Total Rotor Isolation System, or TRIS. To determine the effectiveness of TRIS in reducing helicopter vibration, a flight verification study was conducted at Bell's Flight Research Center in Arlington, Texas. The flight test data indicate that the 4/rev vibration level at the pilot's seat were suppressed below the 0.04g level throughout the transition envelope. Flight tests indicate over 95% suppression of vibration level from the rotor hub to the pilot's seat. The TRIS installation was designed with a decoupled control system and has shown a significant improvement in aircraft flying qualities, such that it permitted the trimmed aircraft to be flown "hands-off" for a significant period of time, over 90 seconds. TRIS flight test program has demonstrated a system that greatly reduces vibration levels of a current-generation helicopter, while significantly improving the flying qualities to a point where stability augmentation is no longer a requirement.

17. Key Words (Suggested by Authors(s))	18. Distribution Statement
Vibration Isolation Handling Qualities Isolation System Isolator Attenuation	Unclassified-Unlimited Subject Category 02

19. Security Classif.(of this report)	20. Security Classif.(of this page)	21. No. of Pages	22. Price
Unclassified	Unclassified	84	A05

For sale by the National Technical Information Service, Springfield, Virginia 22161

NASA Langley Form 63 (June 1985)

*U.S. GOVERNMENT PRINTING OFFICE:1987 -726 -123/ 61801